

Alma Mater Studiorum – Università di Bologna

DOTTORATO DI RICERCA IN

Scienze Biotecnologiche e Farmaceutiche

Ciclo XXXI

**Settore Concorsuale: 03/D1**

**Settore Scientifico Disciplinare: CHIM/08**

*Novel Antitumoral Strategies  
Inducing Membrane Lipid and DNA Damage:  
Artificial Chemical Nucleases & the 'ClickGene' Project*

**Presentata da:** Georgia Menounou

**Coordinatore Dottorato**  
Prof. Santi Mario Spampinato

**Supervisore:** Prof. Marinella Roberti &  
Dr. Carla Ferreri

**Esame finale anno 2019**

# Contents

<b>Abstract</b> .....	- 5 -
<b>Abbreviations and Acronyms</b> .....	- 9 -
<b>Chapter 1: Membrane Lipidomics – A Novel Approach in Antitumoral Strategies</b> .....	- 14 -
1.1. Introduction .....	- 14 -
1.2. Cell Membrane Lipids .....	- 18 -
1.3. Oxidative - Free Radical Chemistry and Fatty Acid Moieties.....	- 22 -
1.4. Transition Metal-Based Drugs.....	- 24 -
1.5. Lipid Geometry .....	- 28 -
1.5.1. Cis-trans Isomerization.....	- 30 -
1.5.2. Lipid Peroxidation .....	- 34 -
1.6. Cell Membrane and Lipidomic Analysis .....	- 37 -
1.7. Liposomes: a Simulation of Cell Membranes .....	- 38 -
1.8. Thesis Overall Objectives.....	- 41 -
<b>Chapter 2: Model Studies of Cu-TPMA-Phen-Induced Lipid Damage in Liposome Membranes</b> .....	- 42 -
2.1. Materials and Methods .....	- 44 -
2.1.1. Liposome Experiments.....	- 44 -
2.1.2. GC Analysis .....	- 45 -
2.2. Results and Discussion .....	- 46 -
2.2.1. Building-up a Membrane Biomimetic Model.....	- 46 -
2.2.2. MUFA-containing Vesicles .....	- 48 -
2.2.3. MUFA- and PUFA-containing Vesicles.....	- 59 -
2.3. Conclusions .....	- 64 -
<b>Chapter 3: Trans Lipid Library; Synthesis of Docosahexaenoic Acid (DHA) Monotrans Isomers - Regioisomer Identification &amp; Model Studies in DHA-Containing Liposomes</b> .....	- 65 -
3.1. Materials and Methods .....	- 70 -
3.2. Epoxidation of Methyl All-(Z)-4,7,10,13,16,19-docosahexaenoate .....	- 72 -
3.2.1. Synthesis of Epoxydocosapentaenoic Acid Methyl Ester (EDP-Me) Regioisomers.....	- 72 -

3.2.2.	Transformation of EDP-Me Regioisomers to Monotrans DHA-Me Isomers .....	- 75 -
3.3.	Synthesis of Monotrans DHA-Me Isomers by Photolysis .....	- 77 -
3.4.	Isomerization of Fish Oil by Photolysis .....	- 78 -
3.5.	Analysis of Monotrans DHA Isomers from Commercially Available Supplements .....	- 78 -
3.6.	LUVET Preparation.....	- 79 -
3.6.1.	Isomerisation vs Peroxidation of PC in LUVET .....	- 79 -
3.7.	Results and Discussion .....	- 81 -
3.7.1.	Dual Synthetic Approach for DHA Transformation and Monotrans DHA Isomer Identification .....	- 81 -
3.7.2.	NMR Study of the EDP Isomers and the Monotrans DHA Isomers .....	- 85 -
3.7.3.	Isomerization of DHA-Containing Fish Oil and Determination of the Monotrans DHA Isomer Content in Commercially Available Supplements .....	- 88 -
3.7.4.	Model Studies in DHA-Containing Liposomes and Cu-TPMA-Phen-Induced Lipid Damage.....	- 91 -
3.8.	Conclusions .....	- 96 -
<b>Chapter 4: Novel Artificial Chemical Nucleases Induce DNA Cleavage .....</b>		<b>- 97 -</b>
4.1.	Introduction .....	- 97 -
4.2.	Copper Complexes as Intercalators with Endonuclease Reactivity.....	- 100 -
4.3.	AMN's Reactivity and Formation of Lesions.....	- 102 -
4.4.	Materials and Methods .....	- 105 -
4.4.1.	DNA Binding Studies.....	- 105 -
4.4.2.	DNA Damage Studies .....	- 105 -
4.4.3.	Identification and Quantification of 8-oxo-Pus and cdPus Lesions In The Presence of AMNs .....	- 107 -
4.5.	Results and Discussion .....	- 110 -
4.5.1.	DNA Binding Studies - Topoisomerase I-Mediated Relaxation. ....	- 110 -
4.5.2.	Artificial Chemical Nuclease Activity.....	- 114 -
4.5.3.	Oxidative DNA Cleavage in the Presence of Non-Covalent DNA Binding Agents .....	- 116 -
4.5.4.	DNA Damage Mechanism.....	- 117 -
4.5.5.	DNA Repair Enzyme Recognition .....	- 119 -
4.5.6.	AMNs-induced Oxidative Cleavage in Supercoiled Plasmid DNA .....	- 124 -
4.6.	Conclusions .....	- 129 -
<b>Appendix.....</b>		<b>- 131 -</b>
<b>Part I – Studies on Lipid Damage .....</b>		<b>- 131 -</b>
5.1.	UV-VIS Spectra .....	- 131 -
5.2.	Gas Chromatography (GC).....	- 132 -
5.3.	Thin Layer Chromatography (T.L.C.) .....	- 134 -

5.4.	NMR Assignments of EDP Isomers Methyl Esters .....	- 135 -
5.5.	Ag-Thin Layer Chromatography .....	- 153 -
5.6.	Gas Chromatographic Analysis of DHA Isomers.....	- 155 -
5.7.	Gas Chromatography Mass Spectrometry (GC-MS).....	- 157 -
5.8.	<sup>13</sup> C – NMR Spectra.....	- 161 -
5.9.	Analysis of Omega-3 Containing Supplements.....	- 163 -
5.10.	Gas Chromatographic Identification of FAMES in 20 % 18:0-22:6 PC/16:0-18:1 PC Composition of Vesicles -	167 -
<b>Part II – Studies on DNA Damage .....</b>		<b>- 168 -</b>
5.11.	Agarose Gel Electrophoresis .....	- 168 -
5.12.	High Pressure Liquid Chromatography (H.P.L.C.) .....	- 170 -
5.13.	Liquid Chromatography Tandem–mass Spectrometry (LC-MS/MS) .....	- 171 -
<b>Acknowledgements .....</b>		<b>- 197 -</b>

## **Abstract**

This PhD project was carried out within the frame of a Marie Curie Network with the acronym 'ClickGene', which focuses on the development of next-generation gene silencing therapeutics. The 'ClickGene' project studies the gene knockout mechanism induced by new synthesized materials, such as the artificial metallo-nucleases (AMNs). These nucleases offer a unique mechanism for inducing DNA damages by oxidative cleavage, which can be associated to a specific DNA binding site through an oligonucleotide sequence as shown in **Figure 1**.

Nowadays, the design of therapeutics that interact specifically with DNA represents a paradigm shift for modern medicine due to the fact that this approach allows precise genetic modifications in order to correct the underlying causes of many human diseases. The concept of aiming at DNA as a target for anticancer drugs inspired the development of numerous compounds with DNA-damaging reactivity. Among these novel compounds are included metal-containing agents that directly modify DNA bases, intercalate between bases, or form crosslinks in DNA. So far, the molecular basis of the drugs mechanism has focused primarily on DNA damage, but recently the novel antitumoral strategies highlighted the cell membranes as a relevant site of the drug's multitarget reactivity. The design of effective treatments against cancer pointed in understanding the role of membranes, particularly the changes induced in the unsaturated lipids, which are important for cell membrane properties and functions.

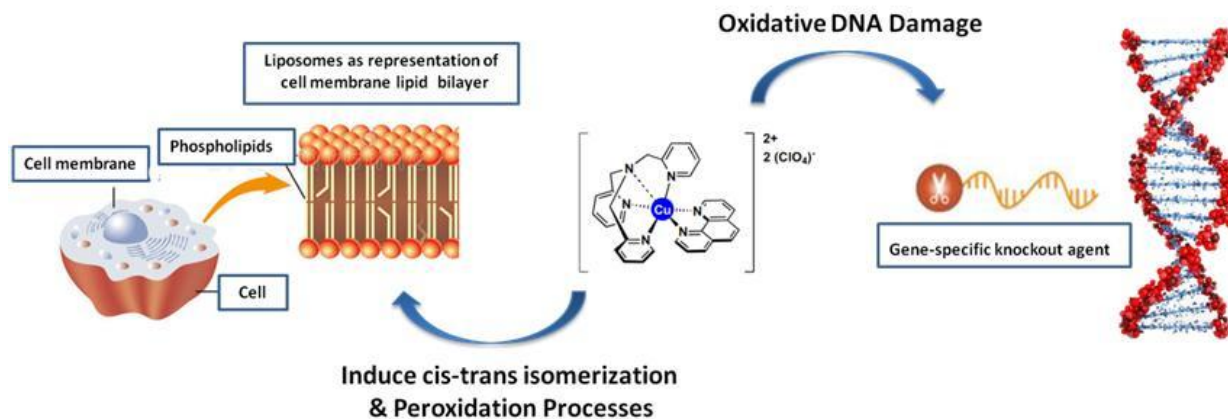


**Figure 1.** Artificial chemical nucleases induce lipid modifications and targeted oxidative DNA scission *via* oxidative/free radical mechanisms.

The project carried out in this PhD thesis, in the frame of the activities as Early Stage Researcher in the ‘ClickGene’ network, was devoted to the study of the oxidation mechanisms of both lipids and nucleic acids induced by free radicals in the presence of one representative member of these metallo-nucleases.

The project was carried out in the ‘Bio Free Radicals’ Group at the Institute of Organic Synthesis and Photoreactivity at the National Council of Research in Bologna (‘ClickGene’ partner) under the supervision of Dr. Carla Ferreri in collaboration with the Department of Pharmacy and Biotechnology of the University of Bologna under the supervision of Professor Marinella Roberti. The work first aimed to investigate the lipid reactivity in the presence of a metallo-drug. In particular, to simulate the cell membrane a biomimetic model of liposomes was designed by different mono- and poly-unsaturated fatty acid moieties in order to examine the reactivity in the presence of the novel synthesized metallodrug Cu-TPMA-Phen and a reducing agent. A variety of conditions was tested and the liposome work-up with isolation and characterization of the fatty acid components gave an interesting mechanistic picture of the membrane-drug interaction.

Connected with the fatty acid transformations, the thesis includes the synthesis and the full analytical characterization of the six mono-trans isomers of docosahexaenoic acid (DHA), which is a semi-essential  $\omega$ -3 polyunsaturated fatty acid. Two different synthetic approaches

were combined to obtain a full identification of the six mono-trans isomers and the analysis was based on gas chromatography (GC) and nuclear magnetic resonance (NMR). The characterization was novel and essential for building-up a molecular reference library. The usefulness of such library was tested in an analytical application to identify trans content in nutraceutical formulas.

The second part of the project was carried out at Dublin City University (a 'ClickGene' partner) in the National Institute for Cellular Biotechnology under the supervision of Professor Andrew Kellett. The work focused on artificial metallo-nuclease (AMN) activity and their ability for precise cleavage of DNA. The cleavage occurs by DNA oxidation, mediated by reactive oxygen species (ROS) and contributes toward therapeutic utility by damaging the genome of cancer cells to impede faithful cell replication. In these experiments, the damage profiles were studied using major groove recognition elements, spin-trapping scavengers of reactive oxygen species (ROS), and DNA repair enzymes with glycosylase and/or endonuclease activity. Finally, the DNA damage fragments produced in DCU were isolated, purified and enzymatically digested to single nucleosides. The analytical protocol, previously defined by the CNR group, was applied to identify the drug effect regarding the formation of oxidative lesions, such as 8-oxo-dA, 8-oxo-dG, 5'*R*-cdA, 5'*S*-cdA, 5'*R*-cdG and 5'*S*-cdG, in double strand DNA fragments.

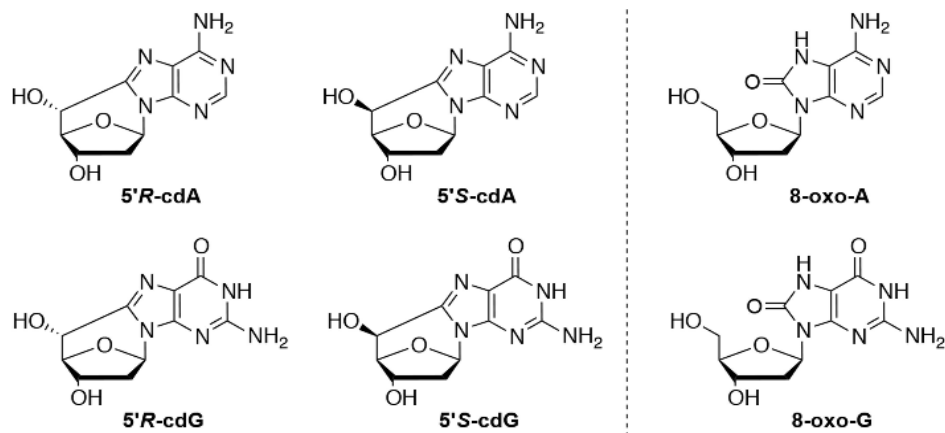


**Figure 2.** Oxidatively induced DNA purine lesions.

The work carried out in this PhD thesis is multidisciplinary, providing novel insights in antitumoral strategies and highlighting the dual effect of the drug towards membrane lipids and DNA. In-depth knowledge of several disciplines was acquired related to cutting-edge research in liposome formulations, membrane lipidomic approach, nucleic acid chemistry, gene therapy and diagnostics. Finally, the results contribute in the fields of free radicals in chemistry, bioinorganic chemistry, biology, pharmacology and medicine.

## Abbreviations and Acronyms

<b>A</b>	Adenine
<b>AB</b>	Abasic Site
<b>AcONa</b>	Sodium Acetate
<b>Ag-TLC</b>	Silver Ion Thin Layer Chromatography
<b>AgNO<sub>3</sub></b>	Silver Nitrate
<b>ALA</b>	$\alpha$ -linolenic Acid
<b>ARA</b>	Arachidonic Acid
<b>AMN</b>	Artificial Metallo-Nuclease
<b>AP</b>	Apurine / Apyrimidine
<b>BER</b>	Base Excision Repair
<b>BHT</b>	Butylated Hydroxytoluene
<b>Bipy</b>	Bipyridine
<b>BSA</b>	Bovine Serum Albumin
<b>C<sub>6</sub>D<sub>6</sub></b>	Deuterated Benzene
<b>cdA</b>	5',8-Cyclo-2'-Deoxyadenosine
<b>cdG</b>	5',8-Cyclo-2'-Deoxyguanosine
<b>CDCl<sub>3</sub></b>	Deuterated Chloroform
<b>Chol</b>	Cholesterol
<b>cPu</b>	Cyclopurine Lesions
<b>Cu-Oda</b>	Copper-octanedioate
<b>Cu-TPMA-Bipy</b>	Copper-tris-(2-pyridylmethyl)amine-2,2'-bipyridine

<b>Cu-TPMA-DPQ</b>	Copper-tris-(2-pyridylmethyl)amine-dipyrido[3,2-f:2',3'h]quinoxaline
<b>Cu-TPMA-DPPZ</b>	Copper-tris-(2-pyridylmethyl)amine- dipyrido[3,2-a:2',3'-c]phenazine
<b>Cu-TPMA-Phen</b>	Copper-tris-(2-pyridylmethyl)amine-1,10-phenanthroline
<b>C</b>	Cytosine
<b>DGLA</b>	Dihomo- $\gamma$ -linolelic Acid
<b>DHA</b>	Docosahexanoic Acid
<b>DHA-Me</b>	Docosahexanoic Acid Methyl Ester
<b>dI</b>	Deoxyinosine
<b>DLS</b>	Dynamic Light Scattering
<b>DMF</b>	Dimethylformamide
<b>DMPO</b>	5,5-Dimethyl-1-Pyrroline N-Oxide
<b>DMSO</b>	Dimethyl Sulfoxide
<b>DNA</b>	Deoxyribonucleic Acid
<b>DSB</b>	Double-Strand Break
<b>dU</b>	Deoxyuracil
<b>EDTA</b>	Ethylenediamine Tetraacetic Acid
<b>EDP</b>	Epoxy-Docosapentaenoic Acid
<b>ET</b>	Electron Transfer
<b>Endo</b>	Endonuclease
<b>ESI</b>	Electrospray Ionisation
<b>EtBr</b>	Ethidium Bromide
<b>FA</b>	Fatty Acid
<b>FAME</b>	Fatty Acid Methyl Ester

<b>FaPy</b>	Formamidopyrimidine
<b>FDA</b>	Food and Drug Administration
<b>FID</b>	Flame Ionization Detector
<b>Fpg</b>	Formamidopyrimidine DNA Glycosylase
<b>GC</b>	Gas Chromatography
<b>GC-MS</b>	Gas Chromatography – Mass Spectrometry
<b>G</b>	Guanine
<b>GUV</b>	Giant Unilamellar Vesicle
<b>hAAG</b>	Human Alkyladenine DNA Glycosylase
<b>HMBC</b>	Heteronuclear Multiple Bond Correlation
<b>HEPES</b>	4-(2-Hydroxyethyl)-1-Piperazineethanesulfonic Acid
<b>HPLC</b>	High Pressure Liquid Chromatography
<b>HSQC</b>	Heteronuclear Single-Quantum Coherence
<b>KOH</b>	Potassium Hydroxide
<b>L</b>	Linear
<b>LA</b>	Linoleic Acid
<b>LC/MS</b>	Liquid Chromatography–Mass Spectrometry
<b>LC-PUFA</b>	Long Chain Polyunsaturated Fatty Acid
<b>LUV</b>	Large Unilamellar Vesicle
<b>LUVET</b>	Large Unilamellar Vesicle by Extrusion Technique
<b>2-ME</b>	2-Mercaptoethanol
<b>Me-Tar-U</b>	Methyltartronylurea
<b>Me</b>	Methyl

<b><i>m</i>-CPBA</b>	<i>Meta</i> -Chloroperoxybenzoic Acid
<b>MeOH</b>	Methanol
<b>MG</b>	Methyl Green
<b>MgCl</b>	Magnesium Chloride
<b>MLV</b>	Multilamellar Vesicle
<b>MRM</b>	Multiple-Reaction Monitoring
<b>MUFA</b>	Monounsaturated Fatty Acid
<b>m/z</b>	Mass-to-charge Ratio
<b>Na<sub>2</sub>SO<sub>4</sub></b>	Sodium Sulphate
<b>NaCl</b>	Sodium Chloride
<b>NaHCO<sub>3</sub></b>	Sodium Bicarbonate
<b>NEB</b>	New England Biolabs
<b>NH<sub>4</sub>OH</b>	Ammonium Hydroxide
<b>NMR</b>	Nuclear Magnetic Resonance
<b>OH</b>	Hydroxy
<b>OC</b>	Open Circular
<b>8-oxo-dA</b>	8-oxo-2'-deoxyadenosine
<b>8-oxo-dG</b>	8-oxo-2'-deoxyguanosine
<b>18:0-22:6 PC</b>	1-stearoyl-2-docosahexaenoyl-sn-glycero-3-phosphocholine
<b>PC</b>	Phosphatidylcholine
<b>PD</b>	Phendione
<b>PDA</b>	Photometric Diode Array
<b>PDE</b>	Phosphodiesterase

<b>POPC</b>	1-palmitoyl-2-oleoylphosphatidylcholine
<b>Pu</b>	Purines
<b>pUC19</b>	Plasmid DNA
<b>Py</b>	Pyrimidines
<b>Rf</b>	Retention Factor
<b>ROS</b>	Reactive Oxygen Species
<b>RSS</b>	Reactive Sulfur Species
<b>SC</b>	Supercoiled
<b>SDS</b>	Sodium Dodecyl Sulfate
<b>SSB</b>	Single-Strand Break
<b>SUV</b>	Small Unilamellar Vesicle
<b>TAE</b>	Tris/Acetate/EDTA
<b>TBE</b>	Tris/Borate/EDTA
<b>TFA</b>	Trans Fatty Acid
<b>T</b>	Thymine
<b>TLC</b>	Thin Layer Chromatography
<b>UFA</b>	Unsaturated Fatty Acid
<b>U</b>	Uracil
<b>UV</b>	Ultraviolet
<b>V</b>	Volt
<b>WHO</b>	World Health Organization
<b>ZnCl<sub>2</sub></b>	Zinc Chloride

# Chapter 1: Membrane Lipidomics – A Novel Approach in Antitumoral Strategies

## 1.1. Introduction

Cancer is the name given to a genetic disease in which some of the body's cells begin to divide without stopping and spread into surrounding tissues in an uncontrolled way.<sup>1</sup>

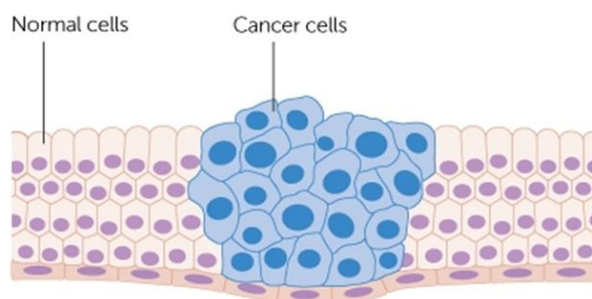


**Figure 3.** Cancer starts when cells change abnormally.<sup>2</sup>

Cancer has been affecting people for centuries and a variety of treatments has been developed through the years. Billions of money has been raised, invested and spent on cancer research over many decades, however due to the fact that cancer is a collection of highly complex diseases characterized by unregulated cell proliferation that can arise from numerous different factors, the therapeutic challenge is remarkable complexed and not yet achieved. The World Health Organization (WHO) names cancer as a leading cause of death worldwide, accounting for 7.6 million deaths (around 13% of all deaths) in 2008 and projected to rise above 13.1 million deaths in 2030.

If we consider the fact that the human body is consisted by trillions of cells, cancer can initiate almost anywhere. The human cells grow and divide to form new cells regarding to the body's requirements. The cells, which grow old or become damaged, die and new cells

are formed. This physiological process might be disrupted when cancer is developed and new cells form when they are not needed. In particular, the moment of the cell division which requires not only chromosome duplication but also membrane phospholipid recruitment is nowadays looked at with attention, since it is evident that in the tumor replication both DNA and membrane lipids are necessary.

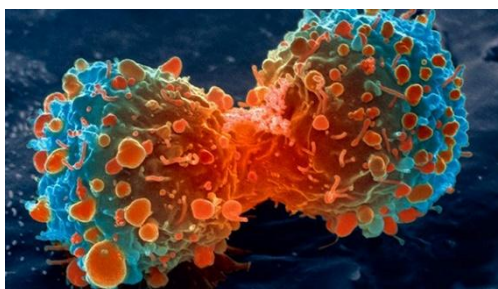


**Figure 4.** A dividing lung cancer cell.<sup>3</sup>

Genetic changes that cause cancer can arise during a person's lifetime, as a result of errors that occur not only as cells divide, but also due to DNA damage caused by certain environmental exposures. Normally, DNA contain four canonical nucleobases, however is possibly to occur chemical alterations on the bases of DNA or the sugar-phosphodiester backbone may also suffer various damages. Lesions may be spontaneous, induced endogenously (i.e. by reactive oxygen species), by radiations (UV light, X-rays) or by chemicals.<sup>4,5</sup> The lesions in DNA are efficiently repaired by action of numerous repair systems. Cell-cycle checkpoint proteins, whose activation induces cell-cycle arrest to prevent the transmission of damaged DNA during mitosis, detect high levels of damage to DNA.<sup>6</sup> However, is possible some of these lesions to escape the repair mechanisms, therefore they are present when DNA is being replicated. In this case, the risk is the generation of mutations at high frequency,<sup>7</sup> which are able to transform normal cells into rapidly proliferating, cancer-type cells.

Cancer cells have relaxed DNA damage-sensing/repair capabilities and this information generated the concept of aiming at DNA as a target of action for the drug.<sup>8</sup> Therefore, a

variety of anticancer drugs were inspired and the development of compounds, such as cisplatin,<sup>9</sup> doxorubicin,<sup>10</sup> 5-fluorouracil,<sup>11</sup> etoposide,<sup>12</sup> and gemcitabine<sup>13</sup> that react chemically with DNA is growing constantly.<sup>14</sup> Among them, the most common metallodrug is cisplatin with clinical application as chemotherapeutic agent. However, this compound is severely limited by its toxic side effects such as kidney damage, increased risk of getting an infection, tiredness, weakness and hair loss.<sup>15,16,17</sup> This has spurred chemists to employ different strategies in the development of new metal-based anticancer agents with different mechanisms of action. The research interest was aimed towards compounds able to directly modify DNA bases, intercalate between bases, or form crosslinks in DNA leading to stalled replication, fork progression and subsequent cell death via apoptosis.<sup>18,19,20</sup>

In addition, the scientific advancements revealed the deleterious effects of metal-catalyzed reactive oxygen species (ROS) in biological systems and relate them with various pathological conditions, such as cancer. The ROS-dependent activation of apoptotic cell death, highlight the potential use of ROS as an antitumor agent. This valuable information led in the development of the next generation therapeutic compounds with ability in a targeted ROS production in the vicinity of nucleic acids. Complexes of redox active metals, principally copper and iron, represent an important group of metallodrugs, such as the artificial chemical nucleases.<sup>21</sup> The ligand environment in these complexes allows for the tuning of charge, redox potential, chirality and geometry to optimize DNA binding. Under aerobic conditions, or in the presence of appropriate intracellular oxidants, these compounds can undergo Fenton or Haber–Weiss chemistry to generate reactive oxygen species (ROS). If the complex is bound to DNA, then there is a high probability that ROS will oxidize DNA, leading to strand breakages.<sup>19</sup> A well-studied example of ROS-active chemotherapeutic drugs is the metal-activated bleomycin, which is able to induce DNA single- and double-strand scission via formation of an intermediate metal-complex, requiring a metal cofactor such as copper or iron.<sup>22,23</sup> Due to these properties bleomycin is used in cancer treatments and Hodgkin's lymphoma. This *in cellulo* catalytic production of ROS by copper(II) and iron(II) complexes is recognized as a major mechanistic model in design of effective inorganic formulated drugs, giving rise in the development of such promising materials.

The idea of a unique anticancer strategy named “oxidation therapy” has been developed by inducing oxidative and free radical chemistry for cytotoxic oxystress as cancer treatment.<sup>24</sup> Overproduction of highly reactive oxygen metabolites can initiate lethal chain reactions, which involve oxidation and damage to every structure that is present and is able to be modified within the cell. Therefore, both DNA and unsaturated lipid components of cell membranes, which are crucial for cellular integrity and survival, can be damaged giving rise to senescent, degenerative or fatal lesions in cells offering a powerful therapeutic modality for future anticancer therapy.<sup>25</sup>

In fact, the novel antitumoral strategies examine the chemotherapeutic drug’s reactivity as a synergic effect towards DNA and cell membrane lipids. Recent studies by our group, both in cell cultures and liposomes as representation of the cell membrane, with the anticancer drug bleomycin report the formation of a bleomycin-iron complex, highlighting that the free radical reactivity does not concern only DNA cleavage mechanism, but involves also the moiety of unsaturated lipids, which are present in membranes.<sup>26,27</sup> Cell membrane plays a crucial role in several biological processes and stress situations can enhance the production of free radicals.. As described previously, among antitumor active metallodrugs copper(II) complexes are particularly interesting due to the redox behavior of  $\text{Cu}^{+2} \rightarrow \text{Cu}^{+1}$ .<sup>28</sup> This *in situ* electron transfer can give rise in the formation of other radical species. The presence of thiols, as biologically relevant reducing agents lead in generation of thiyl radicals, which are able to cause damages involving among others the membrane lipids.<sup>29</sup> These highly active species are able to trigger a cascade of reactions, leading in permanent modifications on the structure of the membrane constituents.<sup>30</sup> The monounsaturated fatty acids (MUFAs) and the polyunsaturated fatty acids (PUFAs) are highly abundant and essential structural components of the cell membrane with important effects on the structure and physical properties of localized membrane domains. MUFA and PUFA moieties contain one or more double bonds respectively, with *cis* geometry in their backbone. In the presence of sulfur-centered radicals, the intraconversion of the *cis* geometry of unsaturated fatty acids moieties is possible to occur and as a result, the corresponding *trans* lipids are formed. This change in membrane architecture is possible to reduce the membrane permeability and fluidity, affect the membrane-associated enzymes and altered the ion transport. In addition, the PUFA moieties can be partitioned in oxidative and lipid peroxidation pathways leading in a

decreased PUFA content in the membrane.<sup>31</sup> The structural differences in the fatty acid moieties result in alterations and direct the cell to an apoptotic pathway. The changes in the membrane lipid compositions can be monitored by fatty acid-based lipidomics.<sup>32</sup> This type of analysis in the research field of lipid structures and functions represents a powerful diagnostic tool for detection of membrane impairments and correlate them with pathological conditions.

Finally, model studies using liposomes as a simpler representation of the cell membrane allow the lipid damage evaluation on the monounsaturated fatty acids (MUFA) and polyunsaturated fatty acids (PUFA)-containing phospholipids, under biologically related free radical and oxidative conditions.<sup>33</sup> This approach allows an insight of the metallodrug's chemical reactivity that mediates ROS damage to the moieties of phospholipids, in the presence of reductant in order to achieve the electron transfer and the generation of radicals. By building up biomimetic models, the radical and oxidative processes can be followed up using a variety of reaction conditions, thereby providing a molecular basis to observe and study these processes.<sup>34</sup>

## 1.2. Cell Membrane Lipids

The membranes constitute the cell boundaries, as well as the boundaries of organelles within the cell. Membranes are consisted by a hydrophobic matrix, formed by an oriented double layer of phospholipids to which proteins are bound in different forms. In 1935, Danielli and Davson proposed as representation, the model of a double layer of phospholipids as the basic structural element of membranes.<sup>35</sup> It was assumed that all membranes had a uniform thickness and a constant lipid-protein ratio with symmetrical internal – external surfaces. Due to limitations of this model in 1972 Singer and Nicolson proposed the structure and dynamics of biological membranes with the view of a 'fluid mosaic' model as framed in **Figure 5**.<sup>36</sup>

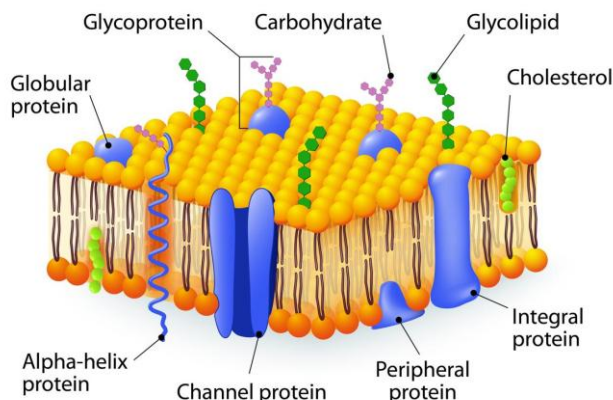


**Figure 5.** Cartoon representation of cell membranes as ‘fluid mosaic’.<sup>37</sup>

Cell membrane is a mixture of fluid state lipids, which are organized in a double layer or bilayer, along with proteins and other molecules. As far as concerns the membrane lipids, they are amphipathic and they possess both a hydrophobic and a hydrophilic moiety. This occurs in phospholipids, glycolipids and sterols.<sup>38</sup> Because of this amphipathic character, in an aqueous medium they can organize themselves on both sides of an imaginary plane, with the hydrophobic portions facing each other and the polar moieties oriented to the outer, aqueous space.<sup>39</sup> Both lipids and proteins are in constant motion (hence the fluid mosaic name mentioned above) and they rotate around their long axis, under physiological condition. The most abundant lipid components are the phospholipids consisting of a L-glycerol molecule, in which the hydroxyl groups in positions 1 and 2 are esterified with two fatty acids and the hydroxyl group in position 3 is esterified with a phosphate group that is bound to small polar molecules such as choline, serine, ethanolamine or inositol. As presented in **Figure 6**, in the phospholipid structure the hydrophobic tails are consisted by fatty acid residues with different lengths of aliphatic chain, which can be either saturated or unsaturated.<sup>40</sup> Taking into account the structure of the hydrocarbon chain the fatty acids can be distinguished in:

- Saturated fatty acids (SFAs), when the aliphatic chain contains no double bond
- Monounsaturated fatty acids (MUFAs), which have one double bond in the fatty acid chain with all of the remained carbon atoms being single-bonded and
- Polyunsaturated fatty acids (PUFAs), in which the constituent hydrocarbon chain possesses two or more carbon–carbon double bonds.<sup>41</sup>

In fact, depending on the position of the double bonds, PUFAs are either omega-3 or -6 methylene-interrupted fatty acids.<sup>42</sup> It is important to mention that this classification of PUFAs in two different families reflects the fact that they are synthesized starting from a common precursor for each family. The precursor for the series of omega-3 linoleic acid (LA, 9c, 12c, 18:2) and for the omega-6 series is  $\alpha$ -linolenic acid (ALA, 9c, 12c, 15c, 18:3). Both fatty acids, linoleic and  $\alpha$ -linolenic, are considered essentials, which means that they cannot be produced via enzymatic pathways, but need to be taken by the diet.<sup>43,44</sup>

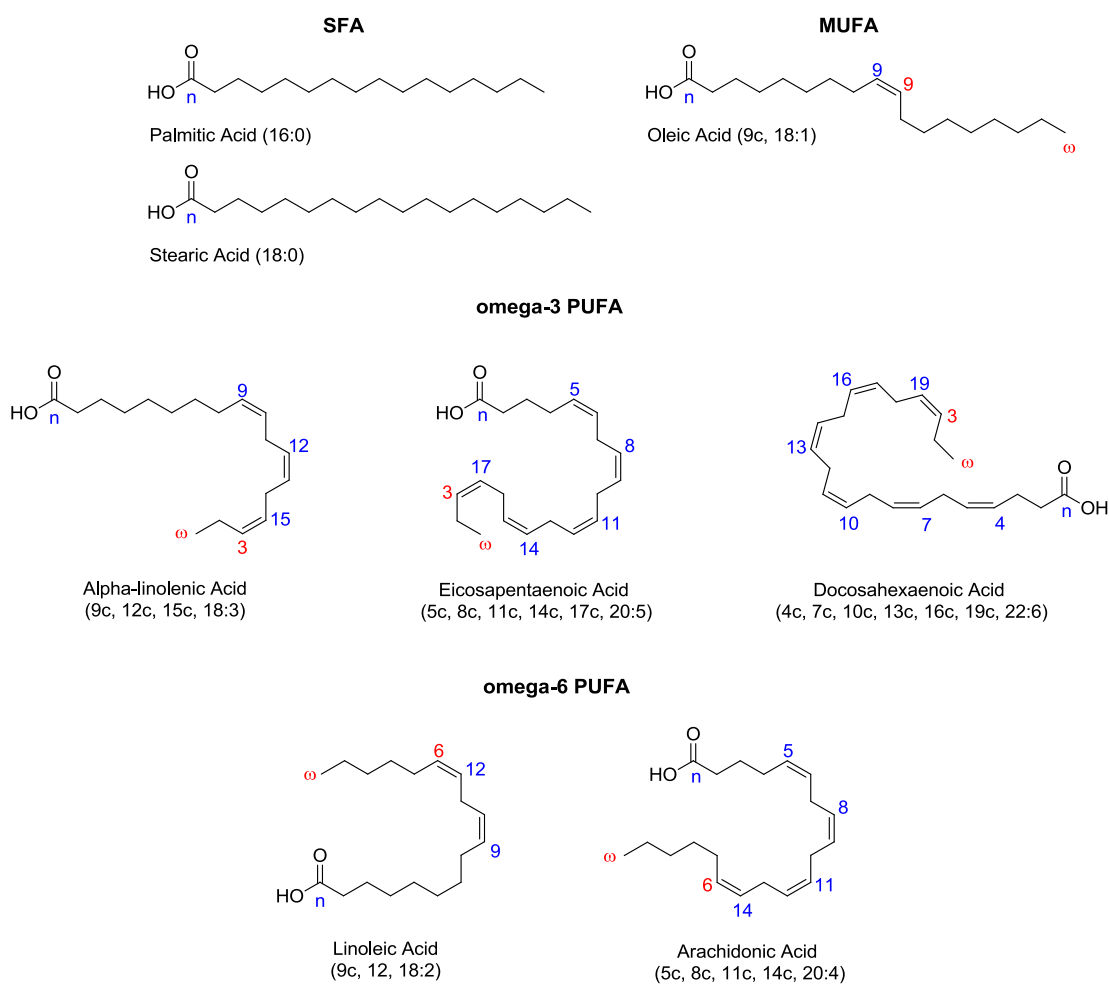
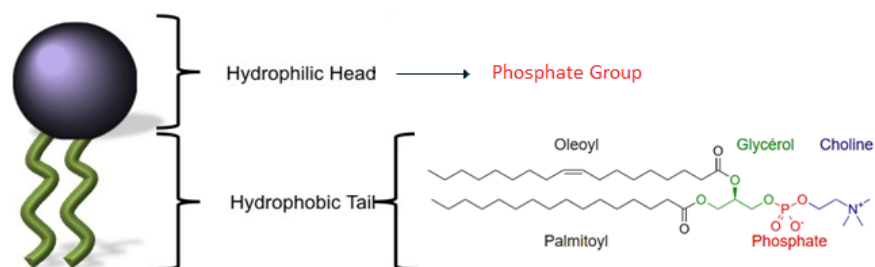


**Figure 6.** Cartoon representation of phospholipid structure and molecular structures of the most important components of the main fatty acid families.

### 1.3. Oxidative - Free Radical Chemistry and Fatty Acid Moieties

There are several definitions of 'free radical', as well as debates about whether the word 'free' is superfluous. A simple definition is that a free radical is any specie capable of independent existence (hence the term 'free') that contains one or more unpaired electrons. The presence of one or more unpaired electrons usually causes free radicals to be attracted slightly to a magnetic field (i.e. to be paramagnetic) and sometimes makes them highly reactive, although the chemical reactivity of radicals varies widely. Many free radicals exist in living systems, although most molecules *in vivo* are non-radicals. If the above rule is taken into account then the diatomic oxygen molecule can be considered itself a free radical since it has two unpaired electrons, each located in a different  $\pi^*$  antibonding orbital. This is the most stable state or ground state of  $O_2$  and is the form it takes in the air around us. If one electron is added to the ground-state  $O_2$  molecule, it enters one of the  $\pi^*$  antibonding orbitals and the product is superoxide radical,  $O_2^{\bullet-}$ . Addition of another electron to  $O_2^{\bullet-}$  will give  $O_2^{-2}$  the peroxide ion, a non-radical. Species, like the ones described previously, that derived from molecular oxygen and they are more reactive than  $O_2$  itself, are well known as reactive oxygen species (ROS).<sup>45</sup> The term includes not only superoxide and some other oxygen radicals, but also some non-radical derivatives of  $O_2$ , such as  $H_2O_2$  and hypochlorous acid (HOCl). Hence, all oxygen radicals are ROS, but not all ROS are oxygen radicals. 'Reactive' is a relative term;  $O_2^{\bullet-}$  and  $H_2O_2$  are selective in their reactions with biological molecules, leaving most of them unscathed, whereas  $OH^{\bullet}$  attacks everything around it.<sup>46</sup> The term reactive species has been expanded to include reactive nitrogen, chlorine, bromine, iron and sulphur species.

Oxidative stress occurs when the production of reactive oxygen species (ROS) is greater than the body's ability to detoxify the reactive intermediates.<sup>47</sup> This imbalance leads to oxidative damage to DNA, lipids, proteins, molecules and genes within the body.<sup>48</sup> Since the body is incapable of keeping up with the detoxification of the free radicals, the damage continues to spread. The body naturally produces antioxidants like superoxide dismutase, catalase and an assortment of peroxidase enzymes, as a means of defending itself against free radicals.<sup>49</sup> The antioxidants neutralize the free radicals, thereby rendering them harmless to other cells. Antioxidants have the remarkable ability to repair damaged molecules by donating hydrogen atoms to the molecules. Some antioxidants even have a chelating effect decreasing the free radical production that is catalyzed by metals.<sup>50</sup> In this situation, the antioxidant contains the

metal molecules so strongly that the chemical reaction necessary to create a free radical never occurs.

Production of  $O_2^{\bullet-}$  in the presence of NADH or NADPH can occur for the presence of an NADPH oxidase enzyme. The  $O_2^{\bullet-}/H_2O_2$  produced have the potential to damage nuclear components, in particular by conversion into  $OH\bullet$  the damage to DNA and consequent mutation can occur.<sup>51,52</sup> Plasma membranes contain redox systems that transfer electrons from NADH to external electron acceptors, such as ascorbate but there are cases that also the cell membranes suffer from permanent modifications of their components. The above data evidenced the necessity to apply a novel strategy when considering the oxidative – free radical chemistry within the cell, since targets of the produced radicals is probable to be both DNA and membrane lipids each one resulting in a modification leading in pathologic conditions or in the case of cancer tumors to induce an apoptotic response.<sup>53,54</sup>

## 1.4. Transition Metal-Based Drugs

Metal ions play important roles in biological processes, and the field of knowledge concerned with the application of inorganic chemistry to therapy or diagnosis of disease appeals very promising. The introduction of metal ions or metal ion binding components into a biological system for the treatment of diseases is growing faster, next to general strategies and challenges of metallodrug research and development. The metallodrug–DNA adducts, together with cellular pathways activated in response to the drug, lead to replication arrest, transcription inhibition, cell-cycle arrests, and apoptosis.<sup>55</sup>

Transition metal ions are of particular interest, because they are qualified as free radicals under the definition given previously. Most of the metals in the first row of the d-block in the periodic table contain unpaired electrons in its atoms and/or ions and are thus free radicals. Indeed, it is appropriate to classify most transition metal ions as radicals, since many of their biological effects, whether beneficial or deleterious involve the ability to accept or donate single electrons, since the single-electron transfers they promote can overcome the spin restriction on direct reaction of O<sub>2</sub> with non-radicals. The reduction potentials of transition metal ions depend on the ligands to the metal, and thus can be altered in different enzymes to allow the same metal to catalyze different reactions.<sup>56</sup> The danger is that, unless their availability is carefully controlled, transition metals will catalyze unwanted free-radical reactions such as autoxidation and OH<sup>•</sup> formation.<sup>57</sup> Copper has two common oxidation numbers, copper (I) and copper (II), as shown below.

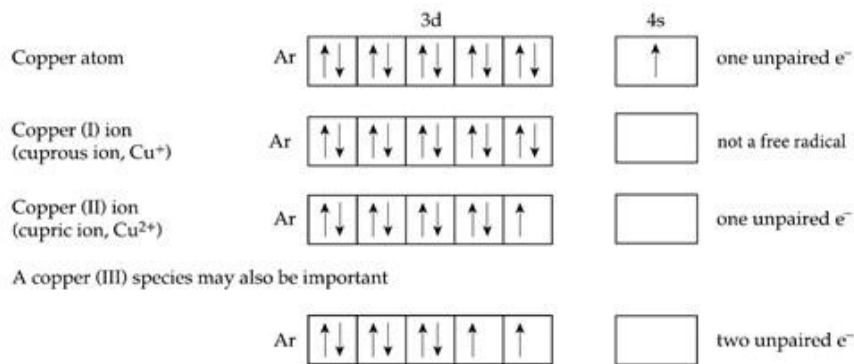
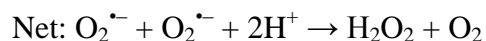
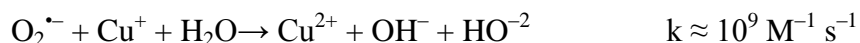


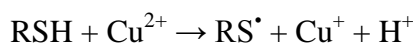
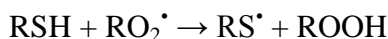
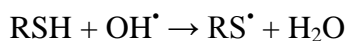
**Figure 7.** Electron configuration of copper atom and kations in orbitals.

Copper (I) readily undergoes self-reaction if it accumulates;  $\text{Cu}^+ + \text{Cu}^+ \rightarrow \text{Cu} + \text{Cu}^{2+}$ .

The one-electron difference between  $\text{Cu}^+$  and  $\text{Cu}^{2+}$ , or  $\text{Cu}^{2+}$  and Cu (III), allows copper to promote radical reactions. Under appropriate conditions, for example, copper ions interact rapidly with  $\text{O}_2^{\bullet-}$ .



The copper, by changing its oxidation number, is catalyzing the conversion of two  $\text{O}_2^{\bullet-}$  radicals and two  $\text{H}^+$  ions to  $\text{H}_2\text{O}_2$  and  $\text{O}_2$ . It is known, that several copper ions chelate - react with biological molecules. Among these bioactive molecules are the thiols, which act as antioxidants. It is highly probable for thiols to react with copper *in vivo*, leading in formation of free radicals. Thiyl radicals are formed when thiols react with carbon-centered radicals, with transition metal ions or with several oxygen radicals, including  $\text{OH}^{\bullet}$ ,  $\text{RO}^{\bullet}$ ,  $\text{CO}_3^{\bullet-}$ ,  $\text{RO}_2^{\bullet}$ .<sup>58</sup> For example,



Once the thiyl radical in the presence of copper (II) is generated, is often assumed that  $\text{RS}^{\bullet}$  radical is essentially inert and disappear by dimerization,<sup>59</sup> e.g. for the glutathione thiyl radical,



Copper can participate in oxidative or free radical pathways giving rise in formation of ROS, which are able to initiate lipid and DNA damage.<sup>60</sup> Due to these properties, a variety of

copper-coordination complexes with nuclease reactivity and site-directed DNA cleavage has been developed. Artificial chemical nucleases are biomimetic and rely on simple systems, which incorporate well-known enzymatic properties, such as metal coordination, general acid-base catalysis, and nucleophilic attack to hydrolyze activated phosphodiester. A well-studied chemical nuclease is 1,10-phenanthroline-copper, and the ability of this redox-active coordination complex to cleave DNA has been established. One of the striking features of the reaction was the specificity of 1,10-phenanthroline ligand and the absolute requirement for copper ion. In fact, both the redox chemistry of the copper ion as well as the extrinsic stereoelectronic and steric properties of phenanthroline copper complexes are of equal importance in the mechanism.<sup>61</sup>

This new generation of drugs does not concern only copper, a wide range of redox metallodrugs has been established in anticancer therapies. Among them, the most popular is cisplatin due to the ability to crosslink with the purine bases on the DNA, interfering with DNA repair mechanisms, causing DNA damage, and subsequently inducing apoptosis in cancer cells.<sup>62</sup> Nowadays, cisplatin is used as a chemotherapy medication to treat a number of cancers.

Finally yet importantly, bleomycin is another drug that is used and it has a unique mechanism of antitumor activity. Bleomycin has both metal binding and DNA binding sites and its activity to generate radical species, such as hydroxyl radicals, in the presence of ferrous or copper(I) ions and molecular oxygen, is known since long time. The mechanism of its action includes the production of oxidative DNA strand scission via formation of OH radicals. The mechanism includes the binding of five nitrogen atoms with divalent metals such as iron. Molecular oxygen, bound by the iron, can produce highly reactive free radicals and Fe(III). The free radicals produce DNA single-strand breaks at 3'-4' bonds in deoxyribose.<sup>63</sup>

In conclusion, platinum-based drugs such as cisplatin are powerful anticancer agents, they have undesirable side effects and are effective against only a few kinds of cancers.<sup>64</sup> There is, therefore, a need for new drugs with an improved spectrum of efficacy and lower toxicity. Complexes of copper, gold and silver (coinage metals) are potential candidates to fulfill this need.<sup>65</sup> Although metallodrugs are used in antitumoral therapies, the mechanism of reactivity is not yet fully explored in many cases. A precise understanding of both the DNA binding properties and the chemical reactivity of any scission reagent is essential for site selectivity

potential application of more synthetic restriction endonucleases. Needless to be mentioned, the development of anticancer drugs based on these metals is currently a very active field.

## 1.5. Lipid Geometry

Double bonds in unsaturated fatty acids, like any alkene, are present in two different geometrical configurations; with two of the substituent groups on the same side of the double bond plane, called 'cis' isomer or on the opposite side, called the 'trans' isomer (**Figure 8**).

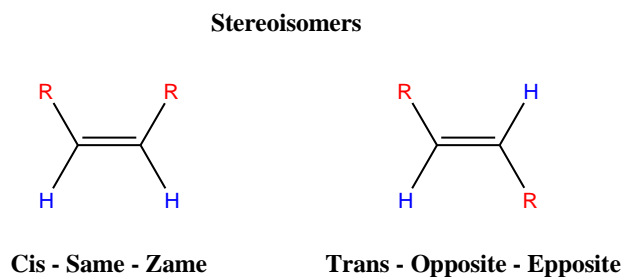


**Figure 8.** Cis and trans configuration of double bonds.

Most of the monounsaturated fatty acid (MUFA) residues present in plants and animals display cis geometry of the double bond. Double bonds with cis configuration are generated during the biosynthesis of MUFAs and PUFAs by the regioselective and stereospecific activity of desaturase enzymes, which act only in specific positions of the aliphatic chain and always mediate the formation of cis double bonds.<sup>66</sup> The significance of the ubiquitous cis structural feature of the unsaturated lipid double bond is based on its contribution to the organization of phospholipids in one of the most important units of living organisms: the cell membrane. Indeed, life needs the compartmentalization given by the phospholipid bilayer that surrounds the cell, the cis fatty acid is necessary to provide the hydrophobic part with favorable properties to organize proteins and other components, rendering membranes active components with several functionalities rather than being merely a wall.<sup>67</sup> The bend corresponding to the cis double bond gives quite typical physical characteristics, such as melting points or phase transition temperatures, as well as biophysical and biochemical properties.<sup>68,69</sup> It is intriguing that the trans geometry, despite its thermodynamic stability, is almost excluded from most of the unsaturated fatty acid structures involved in cellular compartments of living organisms. The presence of trans double bonds in fatty acid residues

produces a dramatic change of the molecular shape from a bent to a linear structure as reported in **Figure 9**.<sup>70</sup>

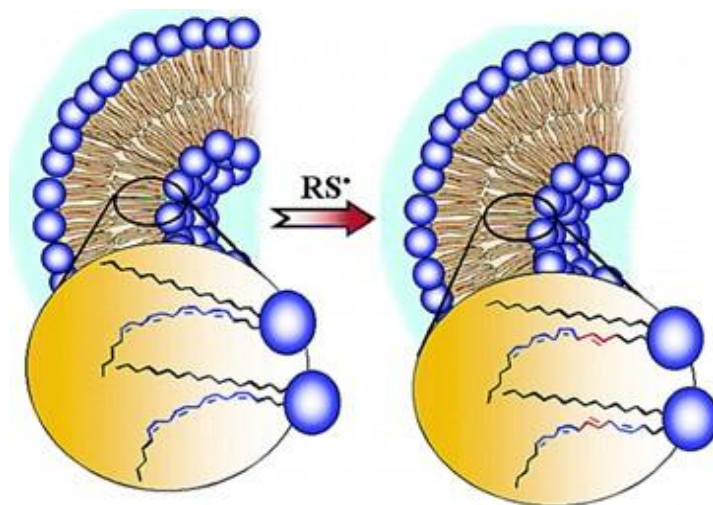


**Figure 9.** Structural differences of membranes composed by cis PUFA and trans PUFA.<sup>71</sup>

Phospholipids are the main components of the cell membranes, therefore their structure regulates the supramolecular organization and the properties of the double layer. Considering the degree of unsaturation a general rule on lipid assembly is that the lowest the number of double bonds, the higher the packing order of lipids. The lipids are assembled with increasing rigidity according to the order: saturated > trans unsaturated > cis unsaturated aliphatic chain. Modification of lipid composition affects both the physical and chemical properties of the membrane and hence allows a fine-tuning of membrane micro viscosity and molecular mobility.<sup>72</sup>

In the last two decades, free radical stress was one of the topics of integrated multidisciplinary research directed towards health and aging. These studies led to the individualization of the importance of cell membranes in stress management and highlighted how crucial is the retention of configuration in the lipid geometry.<sup>73</sup>

### 1.5.1. *Cis-trans Isomerization*

As described previously, the unsaturated fatty acids are important hydrophobic constituents of phospholipids present in the cell membrane and are essential for the control of physical properties of the lipid bilayer. Under normal conditions in eukaryotic cells most of unsaturations are in a *cis* conformation, which does not introduce perturbation in the relative alkyl chain arrangement inside the lipid bilayer. However, there are some prokaryotic cells, such as the bacteria *Pseudomonas Aeruginosa* and *Vibrio Cholera*, in which under stress conditions an enzyme called isomerase can convert the *cis* double bonds to *trans* in the phospholipid residues geometry.<sup>74,75</sup> This transformation plays an essential role in adaptation responses and the number and geometry of unsaturations are correlated with thermotolerance and to adjust in toxic substances. The energy difference between esterified *cis* and *trans* fatty acids is low (about  $-1 \text{ kcal mol}^{-1}$ ), and all-*trans*-fatty acids readily isomerize upon  $\gamma$ -irradiation of tert-butanol solutions, or photolysis of di-tert-butyl ketone. Experimental evidence was also presented for the *cis-trans* isomerization occurring at 90–120°C without adding initiator, the initiation step being a complex reaction between thiol and alkene through molecule-assisted homolysis of the S–H bond. *Trans*-fatty acids are also produced by aborted catalytic hydrogenation and free radicals, in particular thiyl radicals that act as catalysts both in homogeneous solution and lipid vesicles and provoke permanent modifications.<sup>76</sup> Thiyl radicals result from sulfur-containing molecules and these species are able to initiate a *cis-trans* isomerization type of reaction the mechanism of which is presented in the **figure 10** below.<sup>77,78</sup> Herein, is reported as an example the addition of 2-mercaptoethanol to methyl oleate and the isomerization catalyzed by the corresponding  $\text{HOCH}_2\text{CH}_2\text{S}^\bullet$  radical.

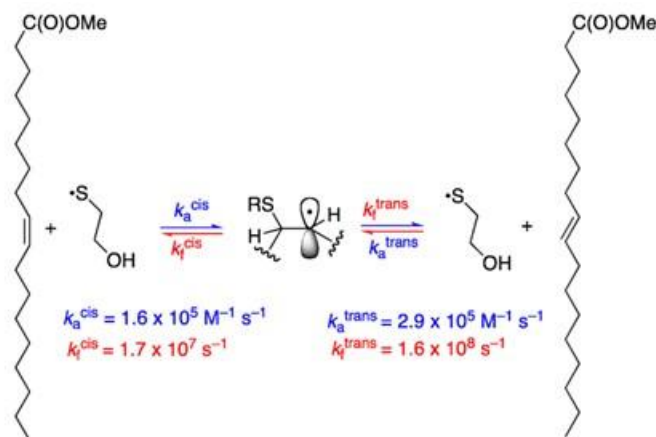


**Figure 10.** HOCH<sub>2</sub>CH<sub>2</sub>S<sup>•</sup> radical-catalyzed isomerization of methyl oleate.<sup>[62]</sup>

The mechanism is an addition-elimination type reaction, which leads to the conversion of stereochemistry. The initial step is the generation of a S-centered radical that is added to the double bond. As a result, an unstable radical intermediate is formed, followed by an elimination reaction that leads to the formation of the most thermodynamically favorable trans isomer. The MUFA isomerization is widely studied and the overall picture is complete, however regarding the analogous reaction with PUFA, the reaction is more complexed. Using identical reaction conditions with regard to MUFA the time profiles of linoleic acid methyl ester (9cis,12cis-C18:2; LAME) disappearance and formation of mono-trans and di-trans isomers in these experiments indicated that the cis–trans isomerization occurs stepwise. The reaction figure shows the equilibrium situation for a dienoic unsaturated fatty acid structure.<sup>79</sup>

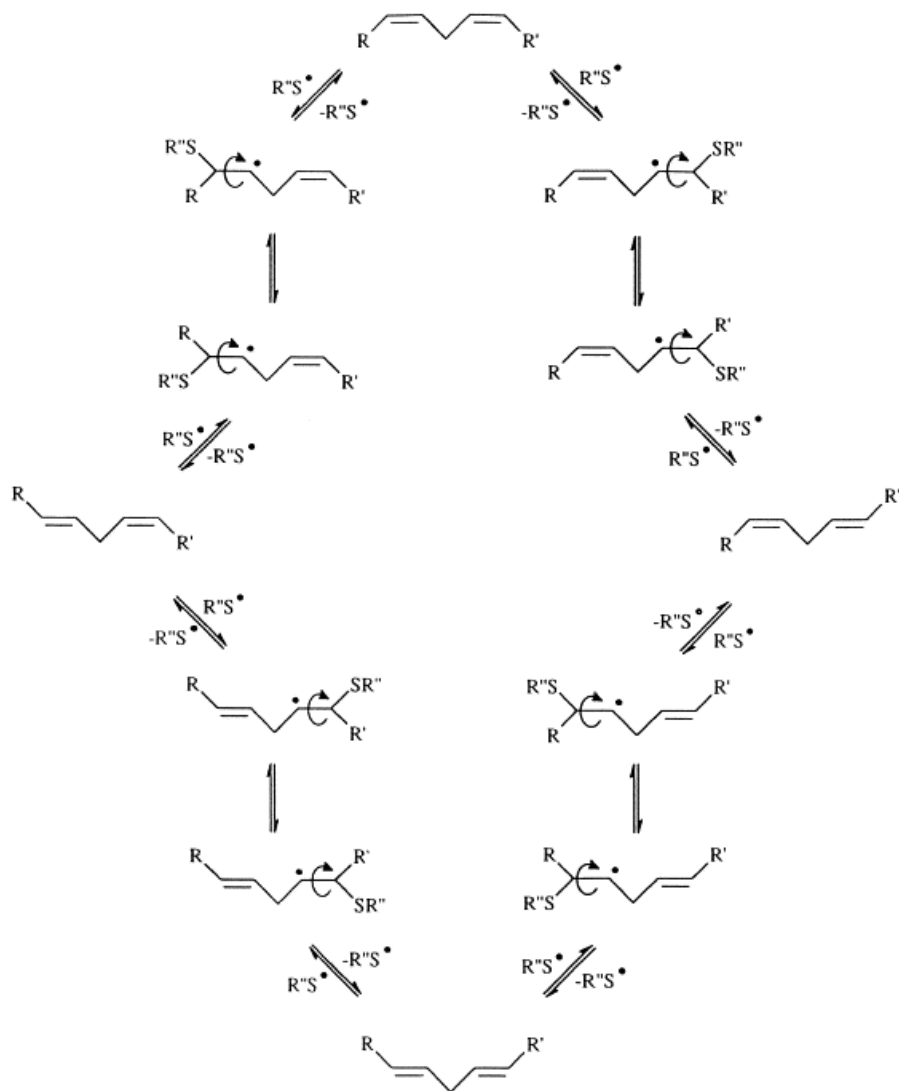


**Figure 11.** Addition of thiols to dienes.<sup>80</sup>

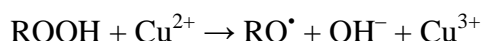
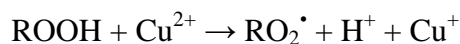
It must be pointed out that in the biological environment, the cis-trans isomerization of the fatty acid moieties is influenced by the supramolecular organization of the phospholipids in the bilayer. All the double bonds in the structure of fatty acid residues are not exposed at the same way and the thiyl radicals should be diffused in order to approach them. This provide evidence that the double bonds are not equivalently reactive and is expected that the ones closer to the polar head are easier to be attacked by the radicals, rather than the double bonds located in the hydrophobic bilayer.<sup>81,82</sup>

Trans fatty acids are correlated with a series of harmful effects in human health such as inhibition of enzymatic processes, increase plasma concentrations of low-density-lipoprotein

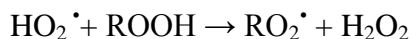
cholesterol and reduce concentrations of high-density-lipoprotein, which results in relation between the blood lipid concentrations and the risk of coronary artery disease.<sup>83</sup>

### 1.5.2. Lipid Peroxidation

In recent years, it has become apparent that the oxidation of lipids, or lipid peroxidation, is associated with pathogenesis of several disease states in adult and infant patients.<sup>84</sup> Lipid peroxidation is a process generated naturally in small amounts in the body, mainly by the effect of several reactive oxygen species (hydroxyl radical, hydrogen peroxide etc.). Many of these free radicals can be generated *in vivo*, such as carbon-centered radicals, which are intermediates in a process called lipid peroxidation. Carbon-centered radicals usually react quickly with O<sub>2</sub> (rate constants often > 10<sup>9</sup> M<sup>-1</sup>s<sup>-1</sup>) to form RO<sub>2</sub><sup>•</sup> radicals. Decomposition of organic peroxides (ROOH) generates both RO<sub>2</sub><sup>•</sup> and RO<sup>•</sup>. Most peroxides are stable at room temperature, but they can be decomposed by heating, exposure to UV light (in some cases), or by addition of transition metal ions, such as copper.<sup>85</sup>



These reactions are important in copper ion-stimulated lipid peroxidation. Lipid peroxides might also react with HO<sub>2</sub><sup>•</sup> to form RO<sub>2</sub><sup>•</sup>,



The pro-oxidant effects of ascorbate/Cu<sup>2+</sup> mixtures have been studied, also for their ability to inactivate many enzymes, probably by formation of OH<sup>•</sup> and/or oxo-copper species and is possible to induce lipid peroxidation and other oxidative damage within the cell, a crucial capability in antitumoral strategies.<sup>86</sup>

These reactive oxygen species are readily to attack the polyunsaturated fatty acids of the cell membrane, initiating a self-propagating chain reaction. As far as PUFA reactivity is concerned, it must be noted that PUFAs have methylene-interrupted double bonds and bisallylic positions with a low C–H bond dissociation enthalpy.



This reactivity attracted immediate interest for its connection with the role of thiols as active biomolecules. Cysteine and glutathione are quite efficient hydrogen donors toward carbon-centered radicals generated by various pathways of damage in vivo and they are able to react with PUFA bisallylic positions via two different pathways. In the literature is suggested that thiyl radicals abstract the bisallylic hydrogen, whereas the remaining  $RS^{\bullet}$  attack the double bond to form a radical adduct.<sup>87</sup> Because of possible competitive pathways between hydrogen abstraction and the reversible thiyl radical addition to the double bonds, it is clear that the specific conditions and reactant concentrations are important for the outcome. In presence of molecular oxygen, carbon-centered radicals react with it leading to peroxy radicals that then propagate the oxidative chain.

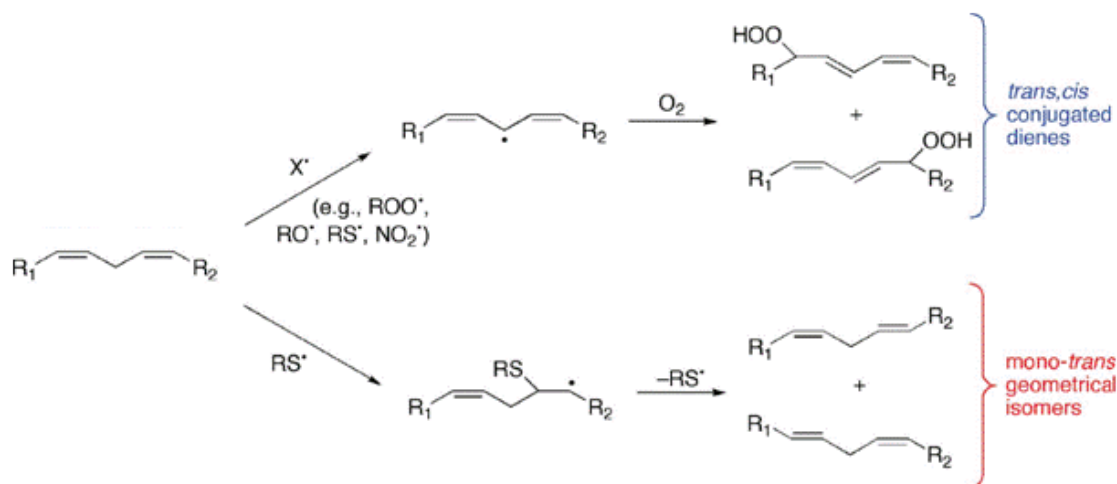


**Figure 12.** Mechanisms for the radical-based peroxidation and isomerization processes in unsaturated fatty acids.

Alteration of membrane lipids and the occurrence of lipid peroxidation reactions compromise the viability of cells and tissue functioning. Enzymatic (catalase, superoxide dismutase) and nonenzymatic (vitamins A and E) natural antioxidant defense mechanisms exist; however, these mechanisms may be overcome, causing lipid peroxidation to proceed with a more damaging

effect.<sup>88</sup> Since lipid peroxidation is a self-propagating chain-reaction, the initial oxidation of only a few lipid molecules can result in significant tissue damage.<sup>89</sup> Extensive research in the field of lipid peroxidation determined the alteration of the physiological functions in cell membranes and the important role in cellular membrane damage.<sup>90</sup> Lipid peroxidation has been implicated in disease states such as atherosclerosis, asthma, Parkinson's disease, kidney damage and others.<sup>91</sup> Beyond ROS involvement in carcinogenesis, increased ROS level can inhibit tumor cell growth via formation of their products which are also the lipid peroxides. Indeed, in tumors in advanced stages, a further increase of oxidative stress, such as that occurs when using several anticancer drugs and radiation therapy, can overcome the antioxidant defenses of cancer cells and drive them to apoptosis.<sup>92</sup>

## 1.6. Cell Membrane and Lipidomic Analysis

The healthcare approach has improved a lot in the last decades due to the understanding of signaling and response pathways at the cellular level. As described previously, it is of high importance the fatty acid residues of phospholipids to maintain their natural assembly and structural integrity. Membranes are necessary to not only divide and form the living cell, but represent also a crucial site for regulating exchange of nutrients, oxygen and stimuli inside the cell or even between different cells.<sup>93,94</sup> The cell membrane is a relevant site for receiving and emitting signals, inducing an adaptive response in the lipid constituents. The division of lipids into lipid classes reinforce the knowledge regarding the membrane composition and its regulation by the appropriate mix of fatty acid residues. The total mapping of the membrane components allowed a different perspective for understanding the relationship between structures and functions, as well as their connection to the status of the organism in a more dynamic and functional way. The new technological advancements gave birth in 'Lipidomics' that took the place of the "old" lipidology with a suffix "-omics," in order to express the correlation with other "-omics" technologies, such as genomics and proteomics.<sup>95</sup> Lipidomics address the lipid diversity needed for life by analyzing lipid molecules in a 'dynamic' context, following up the changes that occur to lipids in a cell compartment or in whole organism, under physiological or pathological conditions. The fatty acid monitoring opened new frontiers to health prevention and disease treatment. To date, the lipidomic analytical strategies are applied to a wide variety of biological samples such as blood, plasma, serum, urine and biological tissues derived from animal models or clinical patients. This powerful diagnostic tool provides information on quantification and qualification of fatty acid constituents for monitoring the membrane remodeling under different conditions.<sup>96</sup> The lipidomic approach is very promising due to a very important achievement that includes the contribution in the field of biomarker discovery.<sup>97</sup> Finally, lipidomics enhance the understanding of the increase or decrease of a lipid level and its combination with the development of a disease and in fact, can play a key role in risk prediction and therapeutic monitoring for several pathologies.<sup>98</sup>

## 1.7. Liposomes: a Simulation of Cell Membranes

All the scientific achievements in the field of lipidomics pointed out the importance of cell membrane and its components. Once it was clear that fatty acid residues represent important vectors of free radicals reactivity with all the harmful consequences mentioned above, the study of the lipid behavior under various conditions became a necessity. A simpler representation is the liposomes, which serve as excellent model membranes.<sup>99</sup> Liposomes were first described in the mid-60s, they are self-closed structures composed of amphiphilic lipids that form a bilayer encompassing an aqueous compartment and have been extensively used as cell membrane models.<sup>100,101</sup> Liposomes composed of phospholipids present a membrane structure similar to the cellular one, in which the lipophilic hydrocarbon region is sandwiched between two ordered polar head group regions. Phospholipids are amphipathic molecules, many of which form liposomal structures spontaneously when confronted with excess water. Research on liposome technology has progressed from conventional vesicles to 'second-generation liposomes', in which long-circulating liposomes are obtained by modulating the lipid composition, size, and charge of the vesicle.<sup>102,103</sup> Generally, liposomes are definite as spherical vesicles with particle sizes ranging from 30 nm to several micrometers,. The liposome size can vary from very small (0.025  $\mu\text{m}$ ) to large (2.5  $\mu\text{m}$ ) vesicles. Moreover, liposomes may have one or bilayer membranes. Based on their size and number of bilayers, liposomes can also be classified into one of two categories: (1) multilamellar vesicles (MLV) and (2) unilamellar vesicles. Unilamellar vesicles can also be classified into two categories: (1) large unilamellar vesicles (LUV) and (2) small unilamellar vesicles (SUV), as depicted in **Figure 13**. In unilamellar liposomes, the vesicle has a single phospholipid bilayer as a sphere enclosing the aqueous solution. Multilamellar liposomes have a multilayered, onion-like structure. Classically, several unilamellar vesicles will form on the inside of the other with smaller size, making a multilamellar structure of concentric phospholipid spheres separated by layers of water.

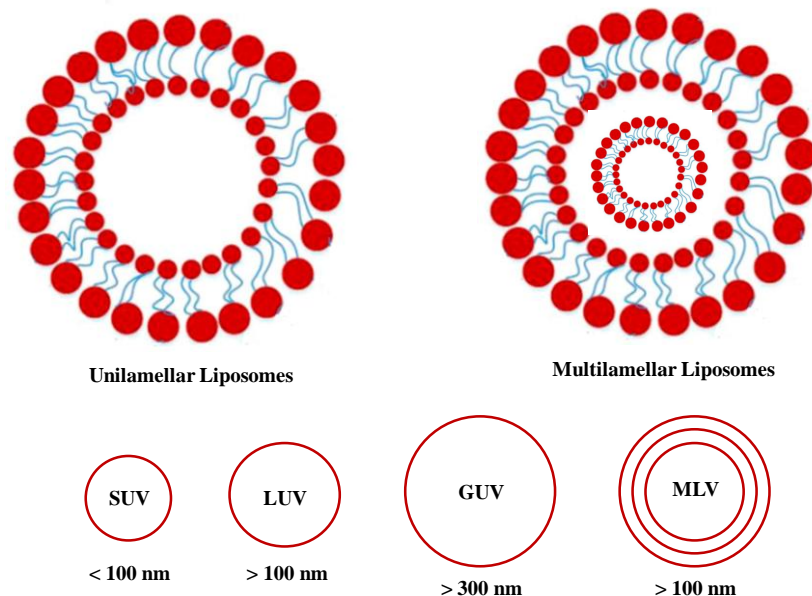


**Figure 13.** Liposome classification and diameter sizes. (SUV = small unilamellar vesicle; LUV = large unilamellar vesicle; GUV = giant unilamellar vesicle; MLV = multilamellar vesicle)

There is a variety of methods for liposome preparation such as sonication,<sup>104</sup> french pressure cell: extrusion,<sup>105</sup> freeze-thawed liposomes,<sup>106</sup> lipid film hydration by hand shaking,<sup>107</sup> non-hand shaking or freeze drying,<sup>108</sup> micro-emulsification,<sup>109</sup> membrane extrusion<sup>110</sup> etc, all methods have four common stages:<sup>111</sup>

1. Drying down lipids from organic solvent.
2. Dispersing the lipid in aqueous media.
3. Purifying the resultant liposome.
4. Analyzing the final product.

Liposomes have been used in a broad range of pharmaceutical applications showing particular promise as intracellular delivery systems for anti-sense molecules, ribosomes, proteins/peptides, and DNA.<sup>112</sup> However, despite the liposomes primary use as drug deliverable systems this is not their only application.<sup>113</sup> Liposome models can be used in studies of lipid peroxidation or cis-trans isomerization due to the fact that they are a stimulation of the cell membrane, in order to avoid the

complication of possible interference of cell components other than the membrane lipids.<sup>114,115</sup> They exhibit ion discrimination, osmotic swelling, and response to a variety of agents that accelerate or retard loss of ions or molecules from the spherules in a way that at least qualitatively mimics their action on natural membrane-bounded structures. Among others, cell membranes act as a physiological barrier for a drug in its path to reach the site of action. The diffusion through cell membrane phospholipid bilayer, is a key step in the absorption and distribution of a drug as well as, ultimately, its action in the organism. The molecule must enter the membrane within the polar head group region, diffuse through the lipophilic hydrocarbon double layer and emerge throughout the head group region on the inner side. Even in cases where a specific transporter is involved, the drug's ability to interact with the membrane is often highly correlated with structural changes in her components. This ability depends on the drug's hydrophilic/lipophilic equilibrium. The study of the interaction between a drug and the membrane lipids of unilamellar liposomes is a novel aspect in antitumoral treatments. Nowadays, this aspect is highlighted more and more, providing many distinct advantages and bringing out several important features regarding the reaction mechanism and the consequent membrane damage under free radical conditions. Applications of liposomes in medicine and pharmacology can be divided into diagnostic and therapeutic applications; liposomes containing various markers or drugs, and their use as a tool, a model, or reagent in the basic studies of cell interactions, recognition processes, and mode of action of certain substances.<sup>116,117,118,119</sup>

## 1.8. Thesis Overall Objectives

The overall objective of this PhD thesis was to explore the oxidative/free radical damage mechanism induced by my novel synthesized metallodrugs using biomimetic models in order to simulate the biological system and exploring mechanistic scenarios with targeted experiments of lipid cis-trans isomerization and DNA damages.

The damage mechanism is mediated by ROS, which are able to lead in permanent oxidative modifications in cellular components. Due to this reason the research achievements presented in this thesis focused on the two most important targets of the antitumoral metallodrug's reactivity; membrane lipids and DNA. Therefore, the experimental work can be divided in two parts according to the aspect that is studied.

- Evaluation of the lipid damage in the presence of the artificial metallo-nucleases  $[\text{Cu}(\text{TPMA})(N,N')]^{2+}$ . For the purposes of these studies, liposome models were employed as representation of the cell membranes. Alterations in the chemical structure of fatty acid moieties in the presence of a novel metallodrug and a reducing agent are discussed in **Chapter 2** as well as, in **Chapter 3**. In addition, in **Chapter 3** is presented the first complete synthetic strategy and analytical characterization of the most electron rich fatty acid; the docosahexaenoic acid (DHA) which was essential for further investigation regarding DHA's reactivity in lipid damage.
- Evaluation of the DNA oxidation profiles and damage mechanism induced by a novel type of  $[\text{Cu}(\text{TPMA})(N,N')]^{2+}$  artificial metallo-nucleases. The detailed examination regarding the DNA binding, cleavage ability as well as radical trapping experiments to identify the dominant free radical(s) giving rise to SSBs and DSBs of AMNs was determined with supercoiled DNA. The results obtained during the course this analysis are discussed in **Chapter 4**.

## Chapter 2: Model Studies of Cu-TPMA-Phen-Induced Lipid Damage in Liposome Membranes

Among metal complexes of therapeutic use as antitumor drugs, copper(II) complexes have a particular place due to the fact that they can undergo redox activity with in vivo formation of Cu(I) and, together with DNA binding properties to cause DNA cleavage.<sup>120</sup> The increased requirement of copper in cancer cells for redox metabolism and its oxidative properties to generate reactive oxygen species (ROS) are the biological and chemical basis, respectively, for the anticancer activity of these metallodrugs acting as artificial nucleases for the sequence specific disruption of gene function.<sup>121</sup> The artificial chemical nuclease Cu-TPMA-Phen of the novel series  $[\text{Cu}(\text{TPMA})(\text{N},\text{N}') ]^2$  that was used for the studies on lipid damage was synthesized, purified and fully characterized by ESR Nicolo Fantoni in Dublin City University a 'ClickGene' partner, under the supervision of Professor Andrew Kellett.

As mentioned above, an important aspect of the Cu-TPMA-Phen chemical reactivity is the fact that it has a redox behavior of  $\text{Cu}^{+2} \rightarrow \text{Cu}^{+1}$  and this *in situ* electron transfer can give rise in the formation of radical species.<sup>122</sup> In the presence of thiols, which are active biomolecules, this redox potential of the copper(II) complex can generate S-centered radicals, able to cause biological damages involving among others the membrane lipids.<sup>123,124</sup> The outcome of the generation of thiyl radicals, is that these species can either catalyse a cis-trans isomerisation of double bonds and/or initiate a peroxidation process involving the unsaturated fatty acid residues of phospholipids.<sup>124</sup> Phospholipids are a large family of compounds, they are considered as building blocks of the membrane and naturally in eukaryotic cells, the double bond geometry of unsaturated fatty acid residues is cis.<sup>125</sup> However, the intervention of sulfur-centered radicals, can lead in a cis-trans isomerization, giving rise to the formation of the more thermodynamically stable trans isomer.<sup>126</sup> The free radical-based drug effect inspired biomimetic studies in membrane models, composed of liposomes containing monounsaturated fatty acid residues (such as oleic acid, 18:1 cis-9) in the presence of the potential drug  $[\text{Cu}(\text{TPMA})(\text{Phenanthroline})](\text{ClO}_4)_2$  and different thiols as reducing agents to cause the recycling of the redox state of the complex and

incubation at 37°C. In our experiments, we were interested in studying the transformation of cis geometry into trans, under a variety of different conditions. The study of the biomimetic model in a radical-catalyzed cis-trans isomerization is of high importance, since the trans lipid geometry resembles that of saturated lipids and is possible to lead in a permanent modification of the membrane and formation of a more rigid bilayer packing.<sup>127,70</sup>

On the other hand, it is known that the monounsaturated fatty acid moieties are less prone to a radical-based oxidative degradation compared with the polyunsaturated fatty acids.<sup>128</sup> In order to evaluate the peroxidation pathway, liposomes formed by soybean lecithin containing different percentages of SFA, MUFA and PUFA fatty acids were tested in the presence of the copper complex and thiol. These vesicles offer the advantage of studying the competition of free radical transformations towards peroxidation and isomerization processes, since the polyunsaturated fatty acids can partition in both pathways.<sup>129</sup> Comparing the results we obtained by the use of these two different liposomal compositions under a variety of conditions concerning the effect of concentration both for the copper(II) complex and the thiol, the different thiols used, the addition of well known antioxidants and the presence or absence of oxygen an interesting scenario of this potential metallodrug reactivity was furnished.

The biomimetic model of liposomes was designed to follow the fatty acid fate after reaction with thiyl radicals, formed in the presence of the Cu-TPMA-Phen and a thiol compound. The model studies underlined the crucial role of membranes in antitumoral treatments and the fact that membranes are not just spectators but important vectors of the antitumoral's drug reactivity.<sup>130,131</sup>

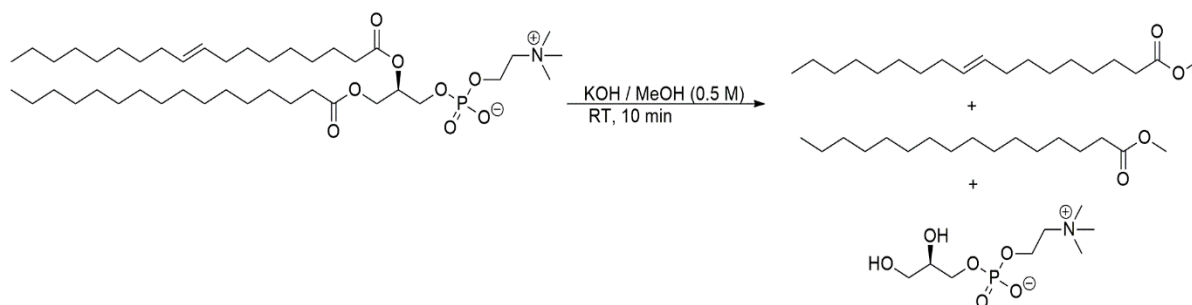
## 2.1. Materials and Methods

### 2.1.1. Liposome Experiments

The first step in our experimental procedure is the addition of POPC in chloroform (53 mg dissolved in 3 mL), followed by evaporation in a test tube under argon stream. The thin film that is formed, remains under vacuum until it is completely free of solvent and then 1 mL tridistilled water is added, in order to obtain a final concentration of 70 mM phospholipid content.<sup>132</sup> The solution is vortexed vigorously under argon stream for 7 min and this procedure yields at large, multilamellar liposomes (LMV). Our next step is downsizing LMV dispersions in unilamellar vesicles (LUV) with a mean diameter of 156-158 nm using the extrusion technique (LUVET) and a 200 nm polycarbonate membrane filter.<sup>133</sup> This method is chosen since not only it helps prevent the membranes from fouling and improves the homogeneity of the size distribution of the final suspension, but also because this membrane model represents in the closest way the membrane bilayer. The size of the liposomes is measured using DLS and the LUVET stock suspensions are transferred into a vial and stored at 4°C for a maximum of 2 weeks.

The total volume of every reaction is 1 mL with phospholipid concentration of 1 mM. More specifically an aliquot of 14.5  $\mu$ L fatty acid content from the stock solution is added in tridistilled water in the reaction vessel. To the liposome suspension, the copper complex is transferred (0.15 mM) and the reaction remains under stirring for 2 min. From stock solutions in tridistilled water and final concentration in the reaction 10 mM, the thiol (2-mercaptoethanol or l-cysteine or reduced glutathione) is added drop wise (0.5 mm/min) using a syringe pump. Each reaction vessel is incubated at 37°C and in order to follow the formation of trans fatty acid residues, samples are analyzed at different times, as reported in **Tables 1-9**.

The work-up of the vesicles is made with 2:1 chloroform/methanol, extracting and collecting the organic phases dried over anhydrous sodium sulfate and evaporating the solvent under vacuum at room temperature. The phospholipids are treated with 0.5 M KOH/MeOH, in a transesterification type of reaction for 10 min at room temperature, as shown in **Scheme 1**.<sup>134</sup>



**Scheme 1.** Mechanism of transesterification reaction in which the phosphoryl group of phospholipids is exchanged with the methyl group of methanol under alkaline conditions.

The reaction is quenched with addition of tridistilled water and an extraction with *n*-hexane follows. The organic layers containing the corresponding fatty acid methyl esters are analyzed by GC for the examination of the FAME content.<sup>135</sup> For the experiments under anaerobic conditions, all the solutions are degassed with argon for 15 min and the addition of all reagents take place under argon. The anaerobic conditions are maintained during the incubation period by creating pressure of argon inside the reaction vial.

### 2.1.2. GC Analysis

Fatty acid methyl esters were analyzed by gas chromatograph (Agilent 6850, Milan) equipped with a 60 m X 0.25 mm X 0.25  $\mu$ m (50%-cyanopropyl)-methylpolysiloxane column (DB23, Agilent, U.S.A.). The instrument has a flame ionization detector (FID) that requires air (450 mL/min) and hydrogen (40 mL/min) and is maintained at a temperature of 250 °C and applying injection temperature at 230 °C. From an initial temperature of 165 °C held for 3 min, followed by an increase of 1 °C/min up to 195 °C, held for 40 min. A final ramp, with a temperature increase of 10 °C/min up to a maximum temperature of 240 °C, was maintained for 10 min for column purge. A constant pressure mode (29 psi) was chosen with helium as carrier gas. Methyl esters were identified by comparison with the retention times of commercially available standards or trans fatty acid references.

## 2.2. Results and Discussion

### 2.2.1. Building-up a Membrane Biomimetic Model

In order to simulate the cell membrane phospholipid behavior, large unilamellar vesicles were formed by extrusion technique (LUVET). In our experiments, two different lipid compositions were used at concentration of phospholipid content 1 mM. Firstly, the synthetic phospholipid 1-palmitoyl-2-oleoyl phosphatidyl choline (POPC) was chosen due to the fact that it represents the simplest biomimetic model, containing only two different phospholipid moieties of saturated and monounsaturated fatty acids. Moreover, the preparation of vesicles from soybean lecithin was made, containing different percentages of SFA, MUFA and PUFA fatty acids residues.

POPC vesicles are proved ideal for the study of cis-trans isomerization since they are consisted of the MUFA moiety of oleic acid (9 cis-18:1). Oleic acid can react with sulfur centered radicals and be transformed into its trans geometrical isomer (see Appendix **Figure S2**), which is elaidic acid (9 trans-18:1).<sup>136</sup> For the best estimation of the copper complex contribution to lipid isomerization, also control experiments were carried out in the presence of the potential drug, without addition of thiol, in which case no transformation was observed. In addition, the efficiency of different thiols, such as 2-mercaptoethanol, l-cysteine and glutathione (reduced) was evaluated, under anaerobic and aerobic conditions. Due to its amphiphilic character and the ability to diffuse freely in the membrane bilayer, 2-mercaptoethanol gave the highest yields of isomerization in every condition tested.

In the experiments with lecithin liposomes the transformations of MUFA (oleic acid, 9 cis-18:1) and PUFA (linoleic acid, 9cis,12cis-18:2) residues to their corresponding geometrical isomers, as well as the PUFA consumption by oxidative degradation were evaluated. Depending from the reaction conditions, isomerization and peroxidation processes were examined and compared. The yield of isomerization for each fatty acid MUFA or PUFA, along with the consumption of PUFA was based on the peak areas obtained by GC analysis. Gas chromatography is proved to be a valuable analytical tool for the identification of each geometrical isomer providing a clear separation (see Appendix **Figure S3**). The estimation of PUFA peroxidation, it is based on the fact that lecithin is composed, among others, by the saturated fatty acid residue of palmitic acid (16:0). Due to the lack of double bonds in its moiety, palmitic acid is unreactive under free

radical conditions and can play the role of internal standard. The quantification of consumption is possible using the GC calibration curves made for each fatty acid that was analyzed vs the palmitic acid residue.

In order to understand the mechanism of this metallodrug, it is crucial to gain an insight to the electron transfer that occurs between the metal and the thiol compound. For this reason, the UV-VIS spectra of the Cu-TPMA-Phen, before and after addition of different concentrations of thiol were obtained, as presented in Appendix in **Figure S1**.

### 2.2.2. MUFA-containing Vesicles

Our first aim was to study if the lipid isomerization is possible to occur on MUFA liposomes, in the presence of the copper complex with addition of thiol and incubation at 37 °C.

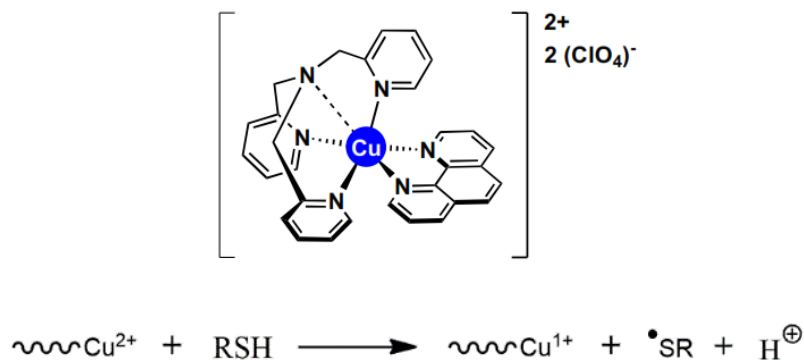
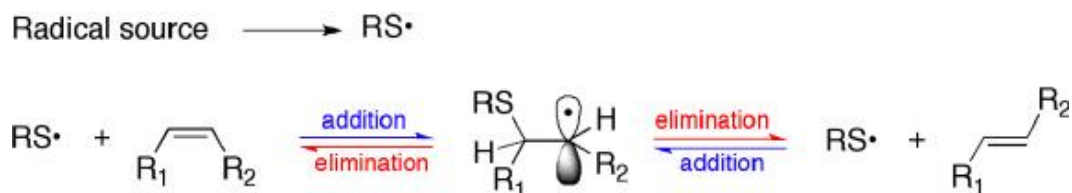


**Figure 14.** In the presence of redox-based antioxidants, such as thiols, the reduction of Cu(II) to Cu(I) occurs with the formation of thiyl radicals.<sup>137</sup>

It is known that sulfur-centered radicals are responsible for the transformation of fatty acid residues from the natural cis-configuration to trans, via an addition-elimination type of reaction.<sup>138</sup>



**Scheme 2.** Reaction mechanism for the cis-trans isomerization catalyzed by thiyl radicals.

A variety of conditions was tested in order to achieve the formation of trans isomer of oleic acid in POPC liposomes. As presented in the **Table 1** below, from our experiments we discovered that is essential to make the addition of thiol drop wise, since excess of thiol leads in reaction between two molecules of thiol and formation of the corresponding disulfide.<sup>139</sup>

**Table 1.** Addition of thiol with two different ways in the presence of 0.15 mM Cu-TPMA-Phen and incubation for 240 min at 37 °C, leads to various % formation yields of trans 18:1 isomer in POPC liposomes.

<b>2-Mercaptoethanol (10 mM)</b>			
<i>Aerobic Conditions</i>		<i>Anaerobic Conditions</i>	
Quick Addition	Drop wise Addition	Quick Addition	Drop wise Addition
0.154	16.296	0.246	18.883

In liposomes containing MUFA after addition of the copper complex, the effect of the thiol concentration was also tested, in the presence and absence of oxygen (**Table 2**) and the results are reported in **Figures 15,16**. Moreover, the effect of different concentrations of the copper complex was also studied in a specific concentration of thiol (**Table 3**) as shown in **Figures 17,18**.

**Table 2.** The concentration effect of 2-ME on the % formation of trans 18:1 isomer in POPC liposomes after incubation for 240 min at 37 °C.

<b>Cu-TPMA-Phen (0.15 mM)</b>		
<b>2-Mercaptoethanol (mM)</b>	<i>Aerobic Conditions</i>	<i>Anaerobic Conditions</i>
2.5	0.785	2.163
5.0	3.425	4.520
10	16.296	18.883

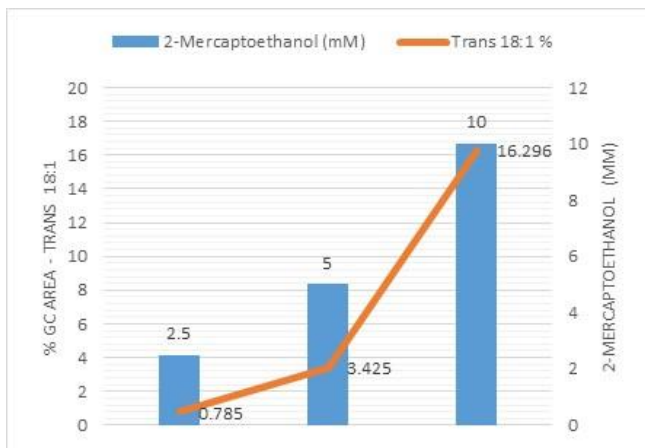


**Figure 15.** trans 18:1 isomer formation in POPC vesicles treated with 0.15 mM Cu-TPMA-Phen and different concentrations of 2-ME under *aerobic conditions*.

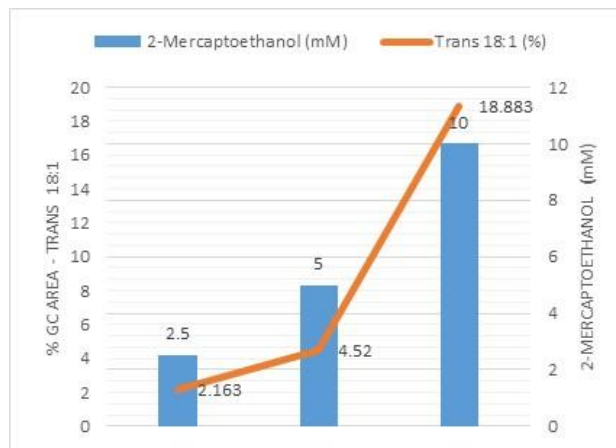


**Figure 16.** trans 18:1 isomer formation in POPC vesicles treated with 0.15 mM Cu-TPMA-Phen and different concentrations of 2-ME under *anaerobic conditions*.

**Table 3.** The concentration effect of Cu-TPMA-Phen on the % formation of trans 18:1 isomer in POPC liposomes after incubation for 240 min at 37 °C.

Cu-TPMA-Phen (mM)	2-Mercaptoethanol (10 mM)	
	<i>Aerobic Conditions</i>	<i>Anaerobic Conditions</i>
0.15	16.296	18.883
0.5	4.837	6.534
1.0	4.336	4.375

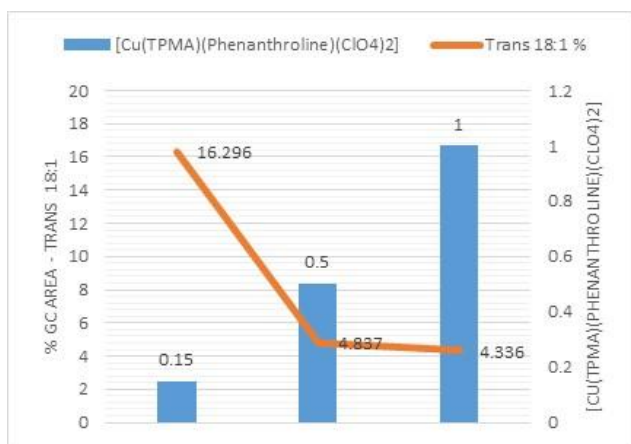


**Figure 17.** trans 18:1 isomer formation in POPC vesicles treated with 2-ME (10 mM) and different concentrations of Cu-TPMA-Phen under *aerobic conditions*.

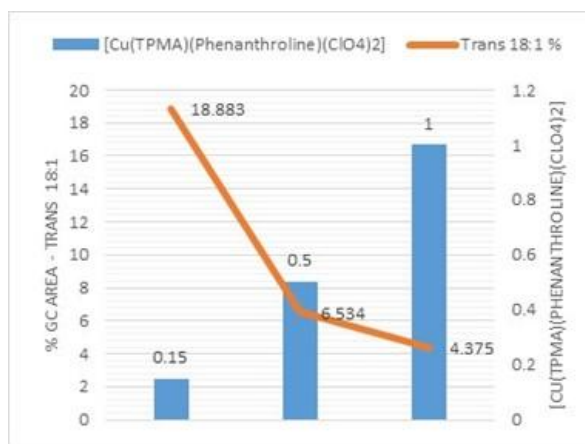


**Figure 18.** trans 18:1 isomer formation in POPC vesicles treated with 2-ME (10 mM) and different concentrations of Cu-TPMA-Phen under *anaerobic conditions*.

In the heterogeneous environment of the vesicles, thiols can be incorporated into the bilayer or be dissolved in the aqueous phase. Two other thiol compounds, which are hydrophilic, cysteine and glutathione, were added in POPC liposomes and their efficiency to interact with the copper complex and generate the thiyl radical able to lead in isomerization was tested, as reported in **Table 4** and in **Figures 19,20**. In contrast with 2-mercaptoethanol that is able to be diffused freely in the liposomes suspension due to its amphiphilic character, the other two thiol compounds that were used cannot enter in the hydrophobic region of the membrane and as a result the formation yield of the trans 18:1 isomer is significantly lower. Comparison of the three different thiols suggests that the isomerization rate follows the lipophilicity order of the three compounds (i.e., 2-mercaptoethanol > GSH > CySH) and indicates that the CyS• radical is unable to migrate into the lipid compartment.

**Table 4.** Time course of cis-trans isomerization of 18:1 residues in POPC liposomes, in the presence of 0.15 mM Cu-TPMA-Phen using different thiol compounds, under aerobic and anaerobic conditions and incubation at 37 °C.

Time (min)	2- Mercaptoethanol (10 mM)		l-cysteine (10 mM)		Reduced Glutathione (10 mM)	
	Aerobic Conditions	Anaerobic Conditions	Aerobic Conditions	Anaerobic Conditions	Aerobic Conditions	Anaerobic Conditions
10	6.191	7.882	0.627	0.428	2.122	1.124
20	7.202	9.444	0.743	0.866	2.380	1.997
30	8.322	9.746	0.745	0.893	2.623	3.111
60	9.381	11.642	0.782	1.171	2.631	3.388
120	13.604	18.883	0.827	1.322	2.755	5.046
240	16.296	20.175	1.005	2.963	2.953	7.266

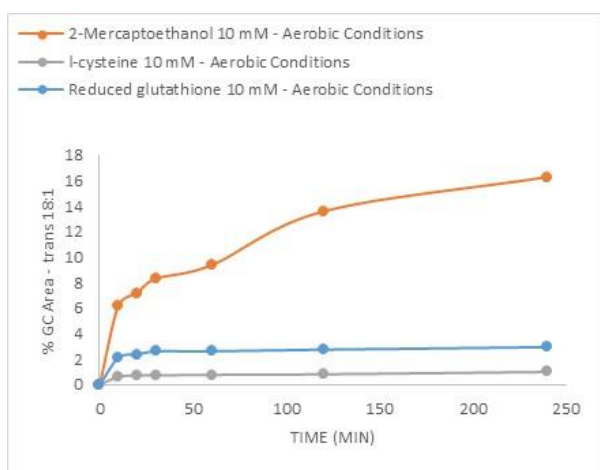


**Figure 19.** trans 18:1 isomer formation in POPC vesicles treated with 10 mM concentration of different thiols, 0.15 mM Cu-TPMA-Phen and incubation at 37 °C under aerobic conditions.

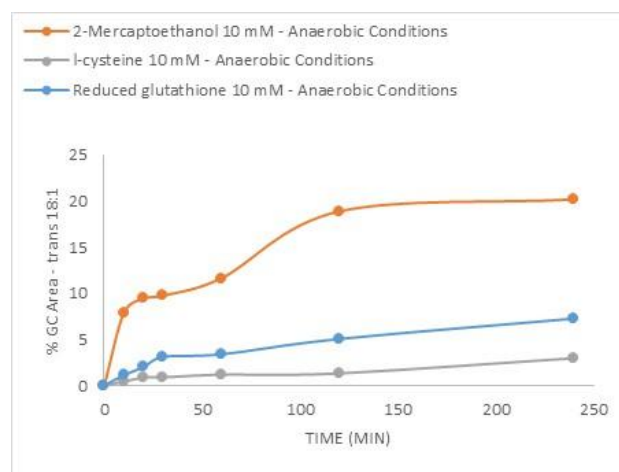


**Figure 20.** trans 18:1 isomer formation in POPC vesicles treated with 10 mM concentration of different thiols, 0.15 mM Cu-TPMA-Phen and incubation at 37 °C under anaerobic conditions.

Our experimental data pointed out that after 120 min, the cis-trans isomerization is slower probably because the thiyl radical is not present anymore. In fact, as it is previously described, two molecules of thiol can react and form the corresponding disulfide. In this case, the thiyl radical is

quenched and no longer able to be added in the double bond leading in formation of the trans isomer. However, the percentage of trans is increased (**Table 5**) as reported in **Figures 21,22** with a new drop wise addition of another amount of thiol after the first 120 min of incubation, proving also that Cu(II) is regenerated and can react with a new added thiol to form the Cu(II)-thiol complex.

**Table 5.** Time course of cis-trans isomerization of 18:1 residues in POPC liposomes, in the presence of 0.15 mM Cu-TPMA-Phen with and without addition of new amount of 2-ME, under aerobic/anaerobic conditions and incubation at 37 °C.

Time (min)	<i>Aerobic Conditions</i>		<i>Anaerobic Conditions</i>	
	<i>Without new addition of 2-ME</i>	<i>Addition of another 10 mM 2-ME after 120 min</i>	<i>Without new addition of 2-ME</i>	<i>Addition of another 10 mM 2-ME after 120 min</i>
10	6.191	6.191	7.882	10.767
30	8.322	8.322	9.746	12.228
60	9.381	9.381	11.642	14.386
120	13.604	13.604	18.883	18.883
125		17.552		21.898
130		24.257		23.789
150		25.481		29.658
240	16.296	26.675	20.175	58.504

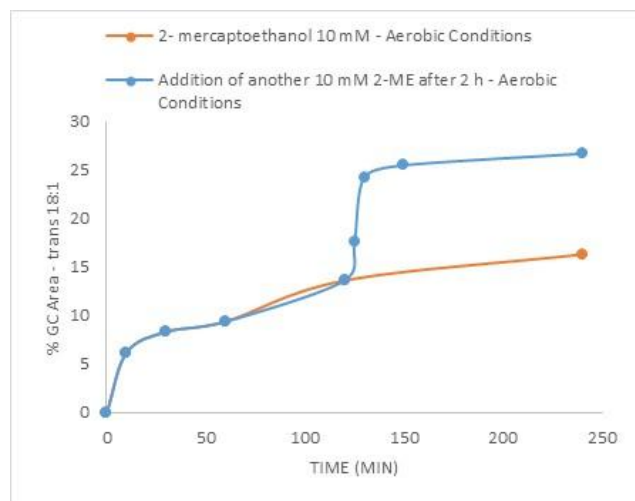


**Figure 21.** Time course of trans 18:1 isomer formation in POPC vesicles treated with 0.15 mM Cu-TPMA-Phen in the presence of oxygen and  
 I. 10 mM of 2-ME  
 II. 10 mM of 2-ME and addition of another 10 mM of 2-ME after 120 min.

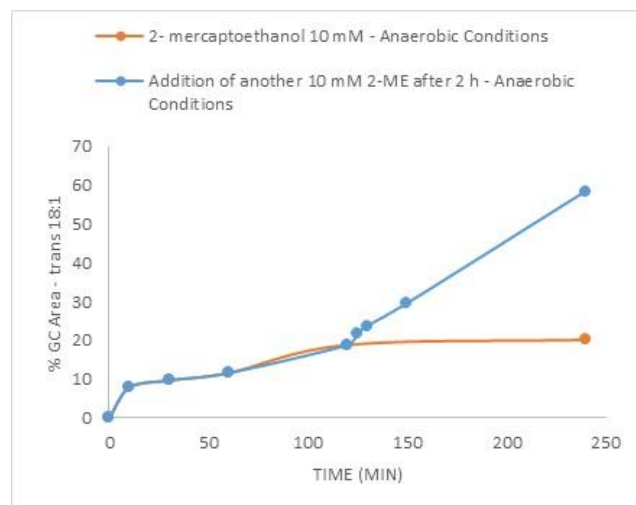


**Figure 22.** Time course of trans 18:1 isomer formation in POPC vesicles treated with 0.15 mM Cu-TPMA-Phen in the absence of oxygen and  
 I. 10 mM of 2-ME  
 II. 10 mM of 2-ME and addition of another 10 mM of 2-ME after 120 min.

Another experiment was the addition of 2-mercaptoethanol (10 mM) every 60 min, starting from 10 mM and gradually after 240 min the final concentration of thiol reached 40 mM, as shown in the **Table 6** and **Figure 23**.

**Table 6.** Time course of cis-trans isomerization of 18:1 residues in POPC liposomes, in the presence of 0.15 mM Cu-TPMA-Phen with and without addition of new amount of 2-ME every 60 min, under aerobic conditions and incubation at 37 °C.

<i>2-Mercaptoethanol (10 mM)</i>			
<b>Time (min)</b>	<i>Without new addition of 2-ME</i>	<i>Addition of 10 mM 2-ME every 60 min</i>	
10	6.191	6.191	(2-ME total = 10 mM)
30	8.322	8.322	(2-ME total = 10 mM)
60	9.381	9.381	(2-ME total = 10 mM)
120	13.604	17.694	(2-ME total = 20 mM)
180	14.944	23.470	(2-ME total = 30 mM)
240	16.296	37.417	(2-ME total = 40 mM)

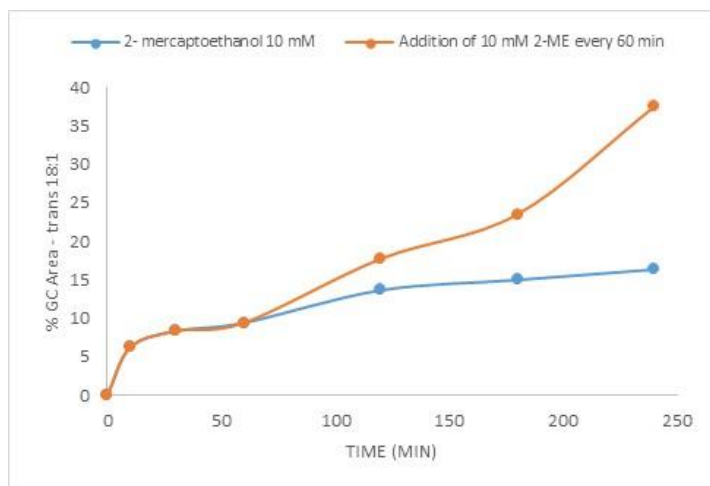


**Figure 23.** Time course of trans 18:1 isomer formation in POPC vesicles treated with 0.15 mM Cu-TPMA-Phen in the presence of oxygen and

- i. 10 mM of 2-ME and
- ii. addition of 10 mM of 2-ME every 60 min and incubation at 37 °C.

Moreover, under aerobic conditions the same experimental procedure was followed, with the difference that this time the drop wise addition of 2-mercaptoethanol, using a syringe pump lasted 60 min. Samples were analyzed in different times during the addition, in order to gain an insight of the reaction. The work-up was made directly, without incubation at 37 °C and the results are reported in **Table 7** and **Figure 24**.

**Table 7.** Time course of 18:1 trans isomer formation in POPC liposomes, the presence of 0.15 mM Cu-TPMA-Phen and drop wise addition of 2-ME with duration 60 min, under aerobic conditions.

2-Mercaptoethanol (10 mM)	
Time (min)	Aerobic Conditions
10	0.121
30	0.542
45	4.772
60	8.117

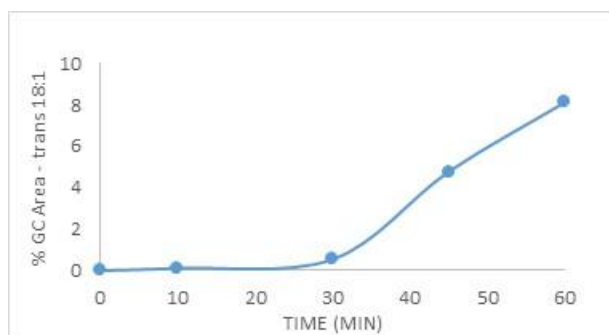


**Figure 24.** Time course of trans 18:1 isomer formation in POPC vesicles treated with 0.15 mM Cu-TPMA-Phen and drop wise addition of 10 mM 2-ME during 60 min, under aerobic conditions.

Another interesting experiment in order to understand the chemical behavior of the copper complex was the treatment with antioxidant. More specifically, in the reaction vessel, which contained the POPC liposomes and the copper complex, 60  $\mu\text{M}$  of l-ascorbic acid were added and then 10 mM of 2-mercaptoethanol were transferred dropwisely, under aerobic conditions. Our hypothesis was that due to its lipophilic ligands, the complex would not be located in the suspension, but it should be incorporated into the phospholipid bilayer, as shown in the **Figure 25** below. In this case, after the interaction between the complex and the thiol, the formation of the thiyl radical would lead to the cis-trans isomerization as described previously.

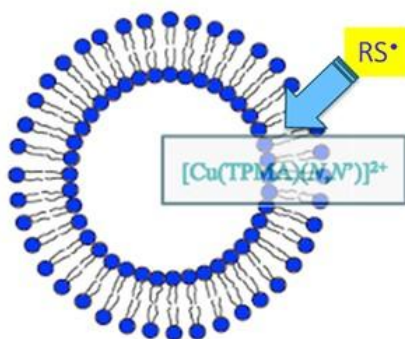


**Figure 25.** A large unilamellar vesicle (LUV) and insertion of the Cu-TPMA-Phen in the bilayer, followed by interaction with the amphiphilic thiol, which leads in generation of thiyl radicals.

On the other hand, if the copper complex was located on the suspension, once the thiyl radical is formed, it should be quenched by l-ascorbic acid and the cis-trans isomerization would not occur. Our experiments have shown that indeed the cis-trans isomerization takes place in the presence of l-ascorbic acid and the results are reported below.

**Table 8.** Cis- trans isomerization of 18:1 residues in POPC liposomes, in the presence of 0.15 mM Cu-TPMA-Phen addition of 60  $\mu$ M l-ascorbic acid and drop wise addition of 10 mM of 2-ME, under aerobic conditions and incubation at 37  $^{\circ}$ C.

2-Mercaptoethanol (10 mM)		
Time (min)	l-Ascorbic Acid ( $\mu$ M)	Aerobic Conditions
120	No	10.740
120	60	10.591
240	60	12.219

We were also interested to compare the isomerization yields of the copper complex Cu-TPMA-Phen with the parent compound  $[\text{Cu}(1,10\text{-Phen})_2]^{2+}$  in the presence of 2-mercaptoethanol, under aerobic conditions and incubation at 37  $^{\circ}$ C. These experiments prove that the different ligands, which are coordinated in the copper, are possible to affect the yield of isomerization due to stereo chemical and electronic reasons. The results regarding this set of experiments are reported in **Table 9** and **Figure 26**.

**Table 9.** Time course of cis-trans isomerization of 18:1 residues in POPC liposomes in the presence of 0.15 mM Cu-TPMA-Phen or the parent compound  $[\text{Cu}(1,10\text{-Phen})_2]^{2+}$ , with 10 mM of 2-ME under aerobic - anaerobic conditions and incubation at 37  $^{\circ}$ C.

Time (min)	Aerobic Conditions		Anaerobic Conditions	
	Cu-TPMA-Phen	$[\text{Cu}(1,10\text{-Phen})_2]^{2+}$	Cu-TPMA-Phen	$[\text{Cu}(1,10\text{-Phen})_2]^{2+}$
10	6.191	10.936	7.882	3.670
30	8.322	13.331	9.746	5.135
60	9.381	15.173	11.642	6.482
120	13.604	15.558	18.883	11.613
240	16.296	15.814	20.175	12.417

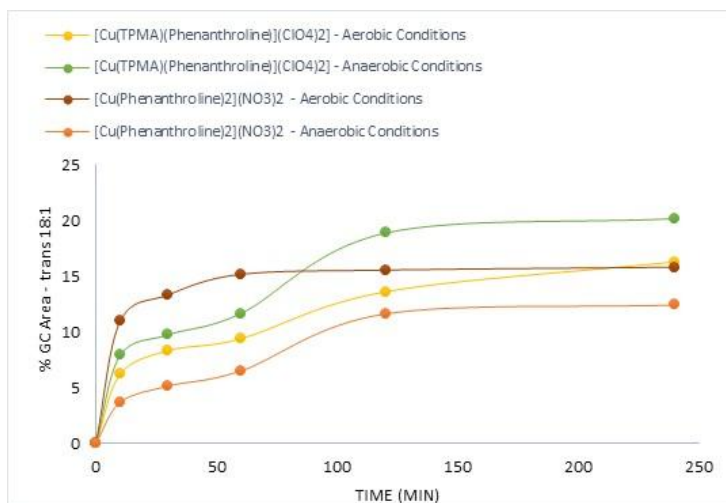


**Figure 26.** Time course of trans 18:1 isomer formation in POPC vesicles treated with 0.15 mM Cu-TPMA-Phen and the parent compound  $[\text{Cu}(1,10\text{-Phen})_2]^{2+}$  in the presence of 10 mM 2-ME, under aerobic and anaerobic conditions and incubation at 37 °C.

### 2.2.3. MUFA- and PUFA-containing Vesicles

In our studies liposomes consisted of high purity soybean lecithin containing different percentages of saturated, mono- and poly- unsaturated fatty acids were also tested, as presented in **Figure 27**.

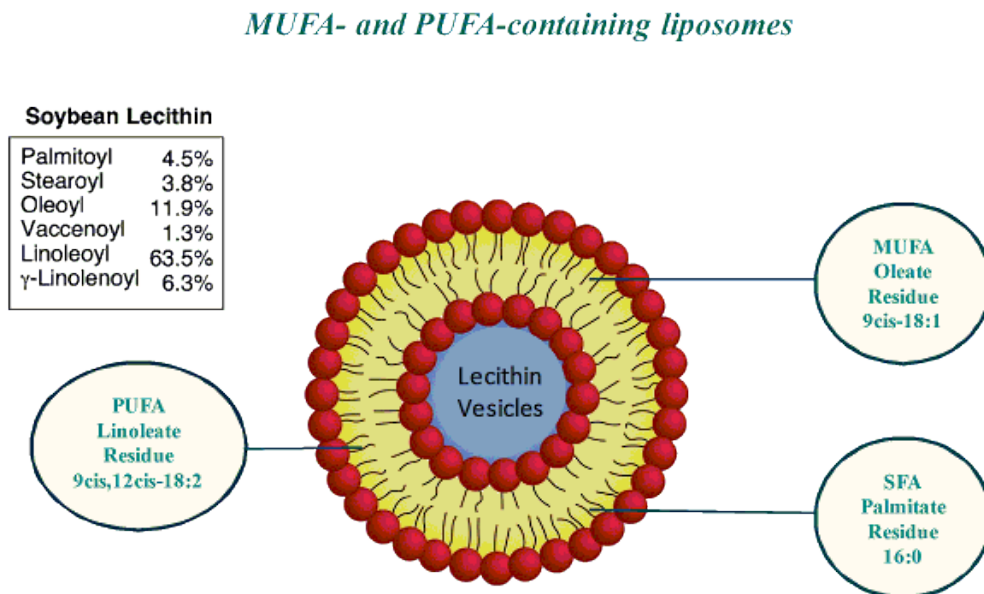


**Figure 27.** Different percentages of SFA, MUFA and PUFA fatty acid residues in liposomes composed by soybean lecithin.

This type of biomimetic model provides the advantage to investigate both the cis-trans isomerization of MUFA (oleic acid can be transformed into elaidic acid) as described previously and at the same time to evaluate the pathways of oxidation – isomerization, in which the PUFA residues can be partitioned (see **Figure S2** in Appendix). The experiments were carried out in the presence of 0.15 mM Cu-TPMA-Phen, 10 mM of 2-mercaptoethanol and incubation at 37 °C. Under these conditions thiyl radicals ( $\text{HOCH}_2\text{CH}_2\text{S}^\bullet$ ) are generated and these species are able to attack the double bonds of the linoleic acid residue. Taking into account the formation yields of mono- and di-trans in linoleic acid residue, it is evident that the thiyl radical attack the double

bonds in a step-by-step cis-trans isomerization.<sup>140</sup> Moreover, as presented in **Figure 28** the mono-trans isomers can be considered as precursors of the di-trans isomers.

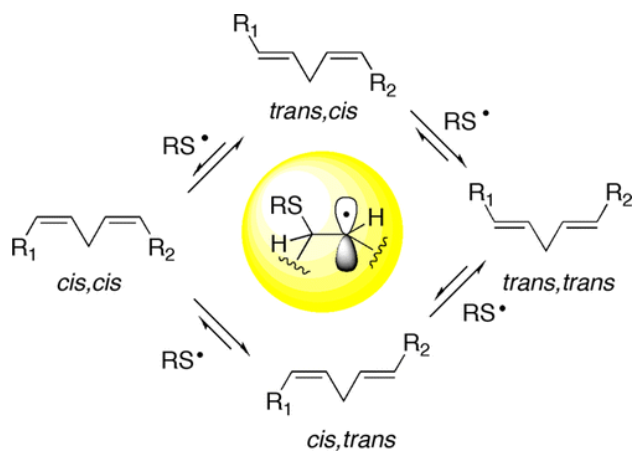


**Figure 28.** Cis-trans isomerization of PUFA catalyzed by thiyl radicals.<sup>140</sup>

In our experiments not only the mono-trans isomers were detected, but also the di-trans isomers of linoleic acid residue were identified. In the **Figures 29, 30** and **31**, a detailed study on the oleic and linoleic transformations to their corresponding geometrical isomers is reported.

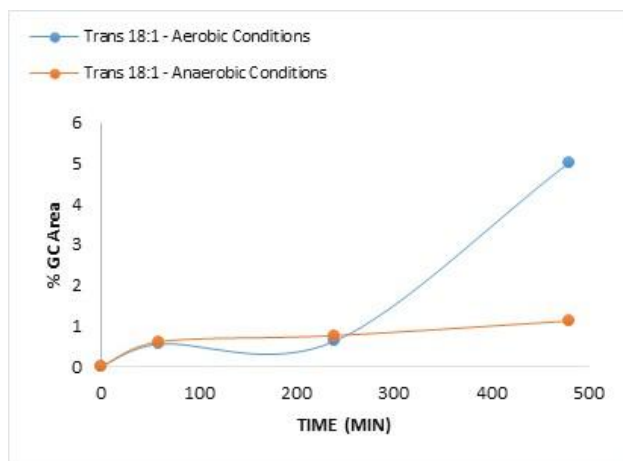


**Figure 29.** Time course of trans 18:1 isomer formation in lecithin vesicles treated with 0.15 mM Cu-TPMA-Phen drop wise addition of 10 mM 2-ME and incubation at 37 °C.

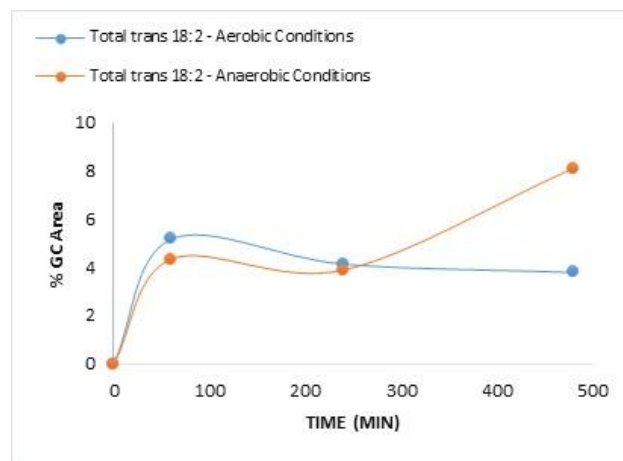


**Figure 30.** Time course of total trans 18:2 isomer formation in lecithin vesicles treated with 0.15 mM Cu-TPMA-Phen, drop wise addition of 10 mM 2-ME and incubation at 37 °C.

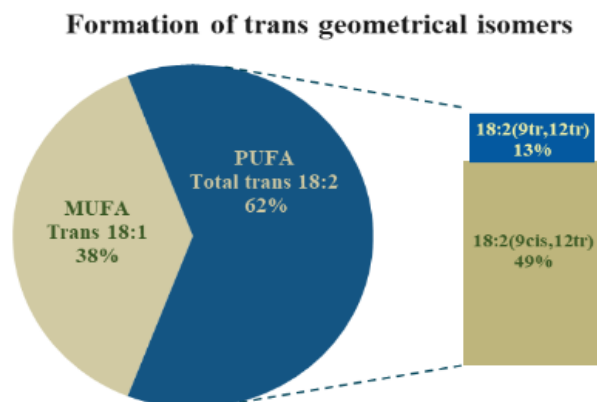
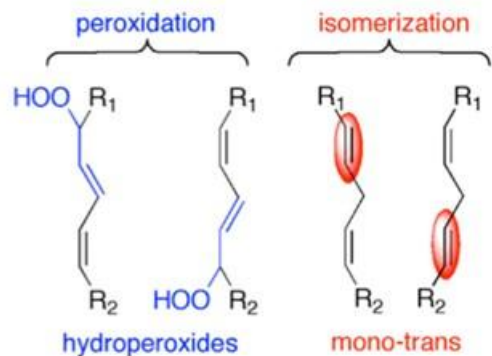


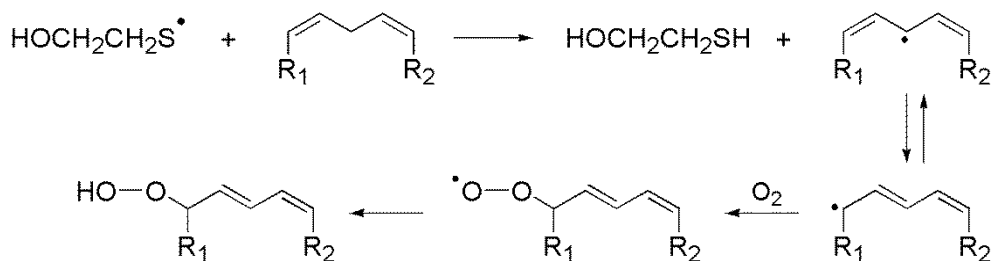
**Figure 31.** Estimation of isomerization in MUFA and PUFA residues in lecithin liposomes in the presence of 0.15 mM Cu-TPMA-Phen, 10 mM 2-ME and incubation at 37 °C under anaerobic conditions.

Apart from the cis-trans isomerization, the moiety of PUFA is prone to further transformations by other free radical routes depending on the conditions applied, aerobic or anaerobic.



**Scheme 3.** The parallel involvement of PUFA residues in peroxidation and isomerization processes.<sup>140</sup>

Our experiments provided strong evidence that in the presence of 0.15 mM Cu-TPMA-Phen, 10 mM 2-ME and incubation at 37 °C both pathways were clearly operative. An important aspect on PUFAs reactivity is the methylene-interrupted double bonds and the presence of bisallylic positions from which the hydrogen abstraction is possible to occur. In the conditions applied the thiyl radical  $\text{HOCH}_2\text{CH}_2\text{S}^\bullet$  that is generated can abstract the bisallylic hydrogen, giving rise in the formation of carbon-centered radicals.



**Scheme 4.** Mechanism of peroxidation reaction that leads in a decreased PUFA content.

Under aerobic conditions, these carbon-centered radicals react with  $\text{O}_2$  to give peroxy radicals that propagate the lipid peroxidation, which eventually lead to a decreased PUFA content. Under anaerobic conditions, the disappearance of PUFA occurring by peroxidation process was not found to be important, while the geometrical isomerization of linoleic fatty acid residue in lipid

vesicles appears to be the main process. Our results regarding PUFA peroxidation are reported in **Figure 32** below.

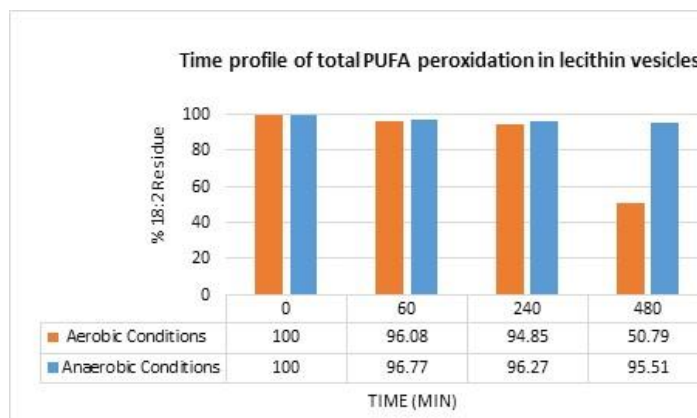


**Figure 32.** Time profile of total peroxidation in liposomes composed by high purity lecithin, after addition of 0.15 mM Cu-TPMA-Phen, 10 mM 2-ME and incubation at 37 °C. The estimation of consumption is based on the ratio SAT/PUFA, which found as peaks of the GC analysis of their corresponding FAME.

[Lecithin is consisted by linoleic (9cis,12cis-18:2), which is in abundance, and a-linolenic (9cis,12cis,15cis-18:3) fatty acid residue].

### **2.3. Conclusions**

The use of copper complexes for redox and oxidative-based mechanisms in therapeutic strategies is an important field of multidisciplinary research. Herein, a novel Cu(II) complex's reactivity towards the fatty acid moieties of phospholipids was studied, using the liposome model to work in a biomimetic environment. The liposome behaviour confirmed that MUFA and PUFA fatty acid moieties, as representation of cellular membranes, are affected by oxidative and isomerisation reactions. In parallel, is reported the study of the different reactivity of thiyl radicals generated from amphiphilic and hydrophilic thiols in the presence of Cu-TPMA-Phen. These experiments give preliminary, but important elements of copper(II) complex reactivity in cell membrane models, pointing mainly to the cell membranes that are subjects of strong interest for chemotherapeutic activities. The reactivity of copper complexes with fatty acids is very important for a metallomic-integrated approach and our results offer several new insights for understanding the interactions of the metallome with lipidomics. The trans fatty acid formation catalysed by thiyl radicals, generated from the metal-based response, can be developed for the investigation of multi-targeted drug design in anticancer therapies, including the relevance of the thiol and copper-complex partitions between aqueous and lipid phases, as evaluated by the biomimetic model of liposomes.

### **Chapter 3: Trans Lipid Library; Synthesis of Docosahexaenoic Acid (DHA) Monotrans Isomers - Regioisomer Identification & Model Studies in DHA-Containing Liposomes**

Continuing our studies on the artificial chemical nuclease's reactivity towards the unsaturated fatty acid residues, I thought it would be interesting to investigate vesicles composed by the most electron-rich polyunsaturated fatty acid, due to an increased probability of lipid damage; the docosahexaenoic acid (DHA) which contains six cis double bonds.

However, in the literature there were not enough data regarding the characterization of the six monotrans DHA regioisomers and they were an open issue to address for analytical, biological, and nutraceutical applications. Therefore, my research aimed in building-up a library of the monotrans DHA isomers. The studies included the preparation, separation, and first identification of each isomer by a dual approach consisting of the following:

1. the direct thiyl radical-catalyzed isomerization of cis-DHA methyl ester and
2. the two-step synthesis from cis-DHA methyl ester via monoepoxides as intermediates, which are separated and identified by nuclear magnetic resonance spectroscopy, followed by elimination for the unequivocal assignment of the double bond position.

The results were published in *Chemical Research in Toxicology*<sup>141</sup> Menounou G., Giacometti G., Scanferlato R., Dambruoso P., Sansone A., Tueros I., Amézaga J., Chatgililoglu C. and Ferreri C.; **2018** 31 (3), 191-200, Trans Lipid Library: Synthesis of Docosahexaenoic Acid (DHA) Monotrans Isomers and Regioisomer Identification in DHA-Containing Supplements. (DOI: 10.1021/acs.chemrestox.8b00021)

As discussed in **Chapter 1**, cis polyunsaturated fatty acids (PUFA) are essential components of human fats, particularly important for biological functions, such as for example to form membrane phospholipids and signaling molecules. In vivo, the omega-3 fatty acid docosa-4Z,7Z,10Z,13Z,16Z,19Z-hexaenoic acid (cis-DHA)(**Figure 33**) is produced through several steps of elongation and desaturation from alpha-linolenic acid (octa-9Z,12Z,15Zdecatrienoic acid), the essential precursor taken exclusively from the diet.<sup>142</sup>

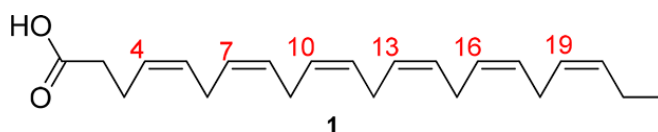
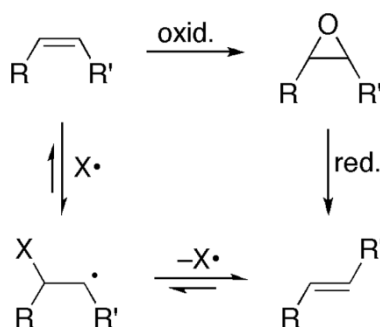


**Figure 33.** Structure of DHA (4Z,7Z,10Z,13Z,16Z,19Z-docosahexaenoic acid).

This nine-step biosynthesis is variably efficient in humans; therefore, the semiessential nature of DHA is now worldwide recognized by Health Agencies.<sup>143</sup> Because of its importance for correct human growth, adequate daily intakes of 100–200 mg have been established by the main international food safety and health agencies from dietary sources, such as algae or fish, especially in children and pregnant women.<sup>144</sup> This led to an increased marketing of DHA-rich formulas, either as functional foods and supplements. On the other hand, the multiple roles of DHA for molecular pathways and signaling have attracted interest in the past decade, all biological activities being strictly dependent from the structural requisite of the cis geometry.<sup>145</sup> When high temperatures and low pressures are used in deodorization processes,<sup>146</sup> to eliminate the unpleasant fishy smell of oils, the natural cis structure of the polyunsaturated fatty acids is affected and the formation of geometrical trans isomers was demonstrated.<sup>147,148</sup> The health consequences of trans PUFA are matters of several studies that evidenced harmful roles in cardiovascular health and pregnancy,<sup>149,150</sup> whereas it is worth noting that omega-3 supplementation in persons with cardiovascular diseases<sup>151,152</sup> and pregnant women<sup>153,154</sup> is highly recommended. In the frame of our research on the free radical modifications of biomolecules, we studied geometrical trans fatty acids (TFA) obtained from an isomerization process catalyzed by sulfur-centered radicals, which occurs via an addition–elimination mechanism without involving the shift of the double bond, with interesting insights for polyunsaturated fatty acids.<sup>155,156</sup> The number of geometrical isomers for the unsaturated fatty

acid is calculated as to  $2^n$ , where  $n$  is the number of double bonds; therefore, in the case of long-chain PUFA, such as DHA, a high number of isomers can be calculated ( $2^6 = 128$ ).

However, because of the step-by-step mechanism of this reaction, monotrans isomers are the first and major products, and they are also the most relevant products of radical stress in biological systems, where the low radical concentration produced *in vivo* is able to involve one double bond, as examined by using the biomimetic model of membranes in the form of unilamellar liposomes. Indeed, monotrans isomers of arachidonic acid in the 5 and 8 positions were found to be the most relevant products created during oxidative metabolism with production of thiyl radicals, distinguishable from TFA obtained from the dietary intake and metabolic transformation of chemically manipulated oils containing trans isomers of linoleic acid.<sup>71,157,158,159</sup> Some attention has been given to the biological effects of specific monotrans isomers, showing differences from the natural cis analogues.<sup>160,161,162,163</sup> However, extension of such studies is limited by the availability of TFA molecular library and by the few commercially available TFAs. Synthetic routes to PUFA monotrans isomers are useful to build up the trans lipid library and address analytical protocols and biological studies. In the past, our group first characterized the monotrans isomers of arachidonic acid (4 isomers)<sup>140</sup> and eicosapentaenoic acid (EPA, 5 isomers)<sup>164</sup> using gas chromatography (GC) and carbon-13 nuclear magnetic resonance (<sup>13</sup>CNMR) in combination for the assignment of each isomer structure. In the case of EPA, the efficiency of a dual synthetic approach was tested in order to obtain the five monotrans isomers in comparison with the isomers coming from the free radical-catalyzed isomerization, as shown in **Scheme 5**.



**Scheme 5.** Dual Synthetic approach to obtain the geometrical trans isomer: From cis-alkene via epoxide formation and ring opening, or via radical-based isomerization.

The strategy of separation and assignment of the monoepoxide structures, prior to the elimination, successfully worked for the first unambiguous determination of the trans alkene position, integrating previous data in the literature.<sup>165,166,167</sup> We considered the dual approach shown in **Scheme 5** to be useful also for the synthesis of the monotrans DHA isomers. Only the 4E regioisomer is commercially available as methyl ester and can be used as GC reference, whereas in literature monotrans DHA isomers were analyzed by several authors after deodorization/isomerization reactions of DHA-rich oils, assaying various conditions of GC analysis but lacking a specific regioisomer assignment.<sup>147,148,162,166,167</sup> As far as the synthesis of the DHA monoepoxides is concerned, the classical epoxidation reaction can lead to these compounds,<sup>168</sup> which are named epoxydocosapentaenoic acid (EDP). 4,5-EDP and 19,20-EDP were known<sup>165,169,170,171</sup> also due to their biological relevance as metabolites of cytochrome P450.<sup>172,173</sup>

The strategy of the separation of the intermediate monoepoxide regioisomers was successful to unambiguously individuate the epoxidation of the double bond position, using mono- and bidimensional nuclear magnetic resonance (NMR) experiments. Consequently, after ring opening, dibromide formation and elimination from each monoepoxide regioisomer double bond was unequivocally established, thus allowing for the assignment of the corresponding peaks in the GC analysis. This double approach clarified that the direct isomerization by free radical-catalyzed reaction gives the six isomers as exclusive products within a few minutes. The usefulness of such identification was then assayed for analysis of fish oil and its isomerization products, also in view of applying the analytical route to the purity of fish oil preparations, which is a hot topic of food research.<sup>148,174,175</sup> Trans-containing triglycerides were studied and it was highlighted that NMR represents a powerful analytical methodology to apply directly on the oil without transformation to fatty acid methyl esters.<sup>176</sup>

Moreover, DHA due to its unique effect of altering membrane composition, is often regarded as the major omega-3 fatty acid involved in anticancer activity.<sup>177</sup> Although use of DHA as an anticancer drug to prevent or treat human cancer in clinical settings has not yet been well established, recent studies suggest that DHA can be very effective as an adjuvant with other anticancer agents.<sup>178</sup> There are studies reporting that oxidized DHA leads to DNA adduct formation, therefore this induced oxidative DNA damage triggers cell cycle arrest and apoptosis in cancer cells.<sup>179,180</sup> Several *in vitro* and animal studies suggest combining DHA with other anticancer agents often improves efficacy of anticancer drugs as well as reduces therapy-associated side effects.<sup>181</sup> Docosahexaenoic acid (DHA), *in vitro* and *in vivo*, used along with anticancer drugs, has improved cancer treatment outcome. In fact, there are clinical studies in the

literature reporting positive results with omega-3 supplements in oncologic patients.<sup>182</sup> There are beneficial effects of omega-3 fatty acids supplements in patients undergoing chemotherapy and/or radiotherapy on different outcomes, being the preservation of body composition the most evident.<sup>183</sup> Incorporation of DHA in cellular membranes improves drug uptake, whereas increased lipid peroxidation is another mechanism for DHA-mediated enhanced efficacy of anticancer drugs.<sup>184,185</sup> In 1998, Hawkins et al. reported that apoptotic death of human Mia-PaCa-2 pancreatic cancer cells induced by PUFAs varies with double bond number and involves an oxidative mechanism.<sup>186</sup> They found correlations between the number of fatty acid double bonds and the proportion of apoptotic cells. This information trigger our experimental design towards DHA-containing liposomes as biomimetic model of cell membranes, since DHA represents the most electron rich and crucial PUFA.

The monotrans DHA library and GC characterizations were firstly applied to the analysis of omega-3 containing supplements in capsules commercially available in Italy and Spain, evidencing trans isomer contamination in the oil ingredients. Secondly, the cis-trans isomerization process was examined in DHA-containing liposomes in the presence of Cu-TPMA-Phen and 2-mercaptoethanol as reducing agent to evaluate the altered configuration of DHA.

### 3.1. Materials and Methods

Chloroform, methanol, n-hexane, 2-propanol, and acetonitrile were purchased from Merck (HPLC purity). Absolute ethanol was purchased from BDH Prolabo VWR (AnalaR NORMAPUR) and 2-mercaptoethanol was purchased from Aldrich. Silver nitrate, 30% aq NHOH and anhydrous sodium sulfate ( $\text{Na}_2\text{SO}_4$ ) were purchased from Carlo Erba. All fatty acid methyl esters (FAME) used as reference standard for GC analyses were purchased from Aldrich, Fluka, or Sigma and used without further purification. 4E,7Z,10Z,13Z,16Z,19Z DHA-methylester was purchase from Lipidox (Lidingo, Sweden). Deuterated benzene and deuterated  $\text{CDCl}_3$  were purchased from Eurisotop (France). Silica-gel thin-layer chromatography (analytical and preparative) was performed on Merck silica gel 60 plates (0.25 and 2 mm thickness, respectively).

Regarding the experimenrs with liposomes, vesicles composed by 20% 18:0-22:6 PC/POPC in 1 mM concentration were prepared. Samples were degassed under argon for 15 min. In addition, the stock solution of 2-mercaptoethanol was prepared (the water was degassed for 15 min and then 2-ME was added under argon stream). The anaerobic conditions were maintained during the incubation period by creating pressure of argon inside the reaction vial.

**GC Analyses.** Fatty acid methyl esters were analyzed by gas chromatograph (Agilent 6850, Milan) equipped with a 60 m X 0.25 mm X 0.25  $\mu\text{m}$  (50%-cyanopropyl)-methylpolysiloxane column (DB23, Agilent, U.S.A.). The instrument has a flame ionization detector (FID) that requires air (450 mL/min) and hydrogen (40 mL/min) and is maintained at a temperature of 250  $^\circ\text{C}$ . Two identical equipment conditions were used for the analyses, applying the same injection temperature (230  $^\circ\text{C}$ ) but different oven conditions and carrier gas.

Method A: from an initial temperature of 165  $^\circ\text{C}$  held for 3 min, followed by an increase of 1  $^\circ\text{C}/\text{min}$  up to 195  $^\circ\text{C}$ , held for 40 min. A final ramp, with a temperature increase of 10  $^\circ\text{C}/\text{min}$  up to a maximum temperature of 240  $^\circ\text{C}$ , was maintained for 10 min for column purge. A constant pressure mode (29 psi) was chosen with helium as carrier gas. Methyl esters were identified by comparison with the retention times of commercially available standards or trans fatty acid references, obtained as described elsewhere.

Method B: temperature started from 195  $^\circ\text{C}$ , held for 26 min, followed by an increase of 10  $^\circ\text{C}/\text{min}$  up to 205  $^\circ\text{C}$ , held for 13 min, followed by a second increase of 30  $^\circ\text{C}/\text{min}$  up to 240  $^\circ\text{C}$ ,

held for 10 min. A constant pressure mode (29 psi) was chosen with hydrogen as carrier gas. GC/MS spectra were recorded on a Clarus 500 GC apparatus equipped with a Clarus 560S mass spectrometer (GC/MS transfer line temperature 230 °C) and a 60 m X 0.25 mm X 0.25 µm (50%cyanopropylphenyl)-dimethylpolysiloxane column (DB225 ms, Agilent, U.S.A.), using an injector temperature of 230 °C, a split ratio of 50:1, and helium as carrier gas at a constant flow of 1.2 mL/min, with the following oven conditions: temperature started from 195 °C, held for 52 min, followed by an increase of 3 °C/min up to 205 °C, held for 10 min, followed by a second increase of 3 °C/min up to 225 °C, held for 15 min and a final increase of 5 °C/min up to 230 °C, held for 10 min.

**Photolysis.** Photolysis was carried out in a quartz photochemical reactor (Sigma-Aldrich) equipped with a 5.5 W low-pressure mercury lamp. The temperature was maintained at (22 ± 2)°C by means of a thermostat bath. Nuclear Magnetic Resonance (NMR). All NMR spectra were collected with a fully automated Agilent NMR system, consisting of a 54 mm bore, 500 MHz (11.7 T) Premium Shielded superconducting magnet, a DD2 Performa IV NMR console, and the Agilent OneNMR probe. All samples were dissolved in C<sub>6</sub>D<sub>6</sub> and transferred in 3 mm thin wall NMR tubes (Wilmad 335-PP-8). After having calibrated each sample of pw90, the following seven NMR experiments were collected

on each sample (2D experiments were collected with 50% NUS and F2 sw (<sup>1</sup>H): 10 ppm, from -0.5 to 9.5 ppm):

- <sup>1</sup>H NMR spectra: pw90 was calibrated for each sample, sw: -0.5 to 9.5 ppm
- one gHSQC: F1 sw (<sup>13</sup>C) 135 ppm, from 5.0 to 140 ppm; nt = 32; ni = 512; res: 33 Hz (0.26 ppm.) F2 sw (<sup>1</sup>H): 10 ppm, from -0,5 to 9,5 ppm, NUS: 50%.
- two bsgHSQCAD: first F1 sw (<sup>13</sup>C): 60 ppm, from 5.0 to 65 ppm; nt = 32; ni = 512; res: 15 Hz (0.12 ppm). F2 sw (<sup>1</sup>H): 10 ppm, from -0.5 to 9.5 ppm, NUS: 50%. second: F1 sw (<sup>13</sup>C): 20 ppm, from 120.0 to 140 ppm; nt = 32; ni = 512; res: 5 Hz (0.04 ppm). F2 sw (<sup>1</sup>H): 10 ppm, from -0.5 to 9.5 ppm, NUS: 50%.
- one gHMBCAD: F1 sw (<sup>13</sup>C): 175 ppm, from 5.0 to 180 ppm; nt = 64; ni = 512; res: 43 Hz (0.34 ppm). F2 sw (from -0.5 to 9.5 ppm, NUS: 50%.
- two bsgHMBC: first F1 sw (<sup>13</sup>C): 60 ppm, from 5.0 to 65 ppm; nt = 64; ni = 512; res: 15 Hz (0.12 ppm). F2 sw (<sup>1</sup>H): 10 ppm, from -0.5 to 9.5 ppm, NUS: 50%. second: F1sw(<sup>13</sup>C): 60 ppm, from 120.0 to 180 ppm; nt = 64; ni = 512; res: 15 Hz (0.12 ppm). F2 sw (<sup>1</sup>H): 10 ppm, from -0.5 to 9.5 ppm, NUS: 50%.

## 3.2. Epoxidation of Methyl All-(Z)-4,7,10,13,16,19-docosaheptaenoate

### 3.2.1. Synthesis of Epoxydocosapentaenoic Acid Methyl Ester (EDP-Me)

#### *Regioisomers*

A 5.84 mM solution of meta-chloroperoxybenzoic acid in dichloromethane (2.5 mL corresponding to 0.0146 mmol; 2.51 mg) was added dropwise to a solution of DHA methyl ester **1** (50 mg; 0.146 mmol) in dichloromethane (2.5 mL). After the addition was completed, the mixture was stirred for 10 min at room temperature under argon atmosphere, following the formation of monoepoxides with traces of diepoxides by TLC. Eluent: 7/3 n-hexane/diethyl ether; DHA-Me  $R_f = 0.9$ , first mixture (**5**, **6** and traces of **4**)  $R = 0.7$ , second mixture (**3** and **7**)  $R_f = 0.6$ , pure isomer (**2**)  $R_f = 0.5$ : bisepoxides  $R_f \leq 0.4$ ). Work-up was carried out by addition of 5 mL of ice-cold  $\text{NaHCO}_3$  (25% w/v) stirred for 2 min. Then, the reaction mixture was transferred in a separating funnel, the aqueous layer was discarded and the organic layer was washed two times with  $\text{NaHCO}_3$ , deionized  $\text{H}_2\text{O}$  and dried over  $\text{Na}_2\text{SO}_4$ . The crude was purified with flash chromatography (eluent: 9/1 n-hexane/diethyl ether) to give a first fraction containing an inseparable mixture (colorless oil; 8 mg; 0.0223 mmol; 15.3% yield) containing 13,14-EDP-Me (**5**), 16,17EDP-Me (**6**) with traces of 10,11-EDP **4** and of residual starting material (**1**). Structures **5** and **6** in **Figure 34**, were found in a 29:71 ratio, respectively, as calculated by the integration of protons of C-22 on  $^1\text{H}$  NMR spectrum (trace II in **Figure 37**). EDP-Me regioisomers **5** and **6** were further purified by preparative TLC using 100 mL toluene/500  $\mu\text{L}$  isopropanol as the eluent: ( $R_f = 0.5$ , pure isomer **6**, and  $R_f = 0.4$ , pure isomer **5**) to give pure **6** (3 mg; 0.0084 mmol; 37.5% yield) with only traces of **4**.

The second fraction contained an inseparable mixture of 7,8-EDPMe (**3**) and 19,20-EDP-Me (**7**) (colorless oil; 7 mg; 0.0195 mmol; 13.4% yield) found in a 43:57 ratio, respectively, as calculated by the integration of protons of C-22 on  $^1\text{H}$  NMR spectrum (trace III in **Figure 37**). The subsequent fraction contained pure 4,5EDP-Me (**2**) regioisomer (colorless oil; 5 mg; 0.0134 mmol; 9.2% yield) identified as shown in **Figure 37** (trace IV) for the C22 triplet at  $^1\text{H}$  NMR. The starting material DHA-Me (**1**) recovered was 30 mg (0.0877 mmol; 60% recovered yield).

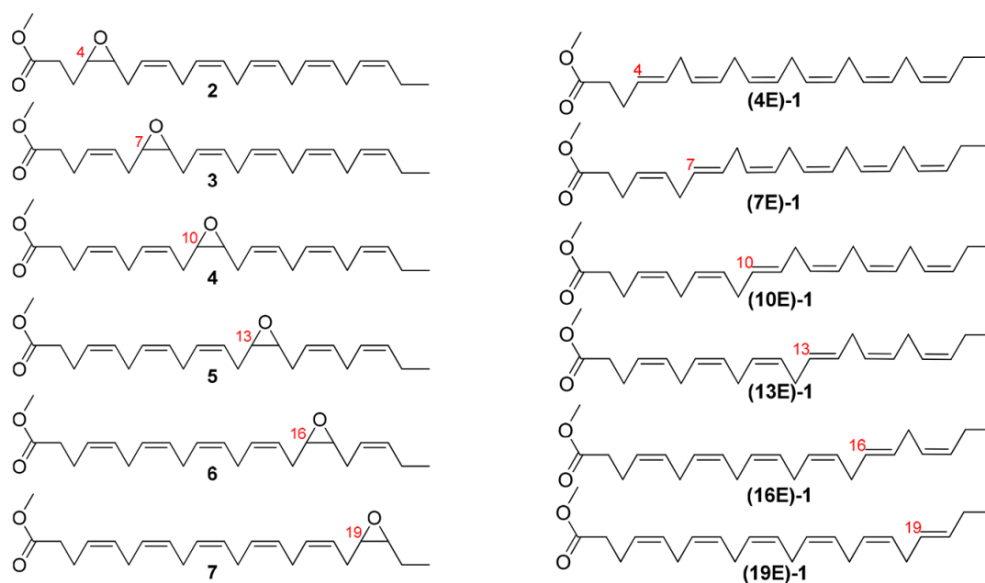


**Figure 34.** Structures of the six EDP regioisomers (left) and the corresponding monotrans DHA methyl ester isomers (right).

The structural assignment of each regioisomer in the fractions was performed by dissolving the fractions in  $C_6D_6$  as NMR solvent in which they are stable and carrying out mono- and bidimensional experiments. **Table S1** and **Figure S5** in Appendix report the detailed  $^1H$  and  $^{13}C$  NMR resonances attributed to the regioisomers, as well as to cis-DHA methyl ester. For the  $^1H$  NMR of the monoepoxides, see **Figures S7, S10** and **S11** in the Appendix. 4,5-EDP (**2**) and 19,20-EDP (**7**) were previously reported in  $CDCl_3$  (cf. **Table S1**). The 2D NMR experiments for the assignment of the C and H resonances in the EDP regioisomers are also shown (**Figures S8** and **S9**). Here below, a summary of the main NMR spectroscopy for the EDP regioisomers assignment is provided.

*Methyl (Z)-13,14-Epoxy-all-(Z)-4,7,10,16,19-docosahexaenoate (5).*  $^1H$  NMR ( $C_6D_6$ , 500 MHz):  $\delta_H$  5.25 - 5.55 (m, 10H), 3.31 (s, 3H), 2.72 - 2.83 (m, 8H), 2.25 - 2.41 (m, 4H), 2.12 (s, 4H), 1.93 - 2.00 (m, 2H), 0.88 (t,  $J = 7.30$  Hz, 3H).  $^{13}C$  NMR ( $C_6D_6$ , 126 MHz):  $\delta_C$  172.35 (C1), 131.90 (C20), 130.53 (C17), 130.19 (C10), 129.02 (C5), 128.32 (C8), 128.11 (C4), 127.87 (C7), 126.82 (C19), 124.76 (C11), 124.55 (C16), 55.66 (C14), 55.65 (C13), 50.65 (C1'), 33.63 (C2), 26.35 (C15), 26.34 (C12), 25.78 (C9), 25.68 (C18), 25.57 (C6), 22.75 (C3), 20.53 (C21), 14.03 (C22).

*Methyl (Z)-16,17-Epoxy-all-(Z)-4,7,10,13,19-docosahexaenoate (6).*  $^1H$  NMR ( $C_6D_6$ , 500 MHz):  $\delta_H$  5.25 - 5.55 (m, 10H), 3.31 (s, 3H), 2.72 - 2.83 (m, 8H), 2.25 - 2.41 (m, 4H), 2.12 (s, 4H), 1.87 - 1.94 (m, 2H), 0.86 (t,  $J = 7.30$  Hz, 3H).  $^{13}C$  NMR ( $C_6D_6$ , 126 MHz):  $\delta_C$  172.35 (C1), 133.81

(C20), 130.19 (C13), 129.02 (C5), 128.40 (C10), 128.32 (C8), 128.11 (C4), 127.87 (C7), 127.70 (C11), 124.76 (C14), 123.66 (C19), 55.79 (C17), 55.65 (C16), 50.65 (C1'), 33.63 (C2), 26.34 (C15), 26.22 (C18), 25.78 (C12), 25.66 (C9), 25.57 (C6), 22.75 (C3), 20.53 (C21), 14.00 (C22).

*Methyl (Z)-7,8-Epoxy-all-(Z)-4,10,13,16,19-docosaheptaenoate (3)*. <sup>1</sup>H NMR (C<sub>6</sub>D<sub>6</sub>, 500 MHz): δ<sub>H</sub> 5.35 - 5.51 (m, 10H), 3.30 (s, 3H), 2.69 - 2.85 (m, 8H), 2.19 - 2.32 (m, 4H), 2.08 - 2.14 (m, J = 7.30 Hz, 4H), 1.93 - 2.04 (m, 2H), 0.89 (t, J = 7.50 Hz, 3H). <sup>13</sup>C NMR (C<sub>6</sub>D<sub>6</sub>, 126 MHz): δ<sub>C</sub> 172.30 (C1), 131.82 (C20), 130.17 (C11), 130.08 (C4), 128.35 - 127.80 (C13, C14, C16 and C17), 127.06 (C19), 125.77 (C5), 124.78 (C10), 55.65 (C8), 55.63 (C7), 50.66 (C1'), 33.51 (C2), 26.35 (C9), 26.23 (C6), 25.78 (C12), 25.75 - 25.60 (C15), 25.58 (C18), 22.83 (C3), 20.55 (C21), 14.07 (C22).

*Methyl (Z)-19,20-Epoxy-all-(Z)-4,7,10,13,16-docosaheptaenoate (7)*. <sup>1</sup>H NMR (C<sub>6</sub>D<sub>6</sub>, 500 MHz): δ<sub>H</sub> 5.25 - 5.52 (m, 10H), 3.31 (s, 3H), 2.73 - 2.86 (m, 9H), 2.60 (dt, J = 4.20, 6.40 Hz, 1H), 2.25 - 2.37 (m, 3H), 2.04 - 2.16 (m, J = 7.30 Hz, 3H), 1.40 (ddq, J = 7.30, 7.30, 14.10 Hz, 1H), 1.28 (ddq, J = 6.10, 7.30, 13.50 Hz, 1H), 0.84 (t, J = 7.70 Hz, 3H). <sup>13</sup>C NMR (C<sub>6</sub>D<sub>6</sub>, 126 MHz): δ<sub>C</sub> 172.32 (C1), 130.03 (C16), 129.06 (C5), 128.35 - 127.80 (C7, C8, C10, C11, C13 and C14), 128.08 (C4), 124.96 (C17), 57.38 (C20), 55.75 (C19), 50.65 (C1'), 33.64 (C2), 26.31 (C18), 25.79 (C15), 25.75 - 25.60 (C9 and C12), 25.58 (C6), 22.76 (C3), 21.10 (C21), 10.45 (C22).

*Methyl (Z)-4,5-Epoxy-all-(Z)-7,10,13,16,19-docosaheptaenoate (2)*. <sup>1</sup>H NMR (C<sub>6</sub>D<sub>6</sub>, 500 MHz): δ<sub>H</sub> 5.23 - 5.55 (m, 10H), 3.29 (s, 3H), 2.65 - 2.88 (m, 10H), 2.13 - 2.27 (m, 3H), 1.95 - 2.09 (m, 3H), 1.68 - 1.76 (m, 1H), 1.58 - 1.68 (m, 1H), 0.89 (t, J = 7.63 Hz, 3H). <sup>13</sup>C NMR (C<sub>6</sub>D<sub>6</sub>, 126 MHz): δ<sub>C</sub> 172.35 (C1), 131.89 (C20), 130.27 (C8), 128.63/128.38/128.11/128.96 (C13, C14, C16 and C17), 128.42 (C11), 127.95 (C10), 127.19 (C19), 124.78 (C7), 56.07 (C5), 55.32 (C4), 50.85 (C1'), 30.76 (C2), 26.38 (C6), 25.86 (C9), 25.75 (C12 and C15), 25.66 (C18), 23.42 (C3), 20.66 (C21), 14.17 (C22).

*Methyl All-(Z)-4,7,10,13,16,19-Docosaheptaenoate (1)*. <sup>1</sup>H NMR (C<sub>6</sub>D<sub>6</sub>, 500 MHz): δ<sub>H</sub> 5.24 - 5.47 (m, 12H), 3.31 (s, 3H), 2.73 - 2.88 (m, 10H), 2.29 (dddd, J = 0.80, 1.40, 7.34, 14.70 Hz, 1H), 2.29 (dddd, J = 0.80, 1.40, 7.30, 14.70 Hz, 1H), 2.11 (t, J = 7.40 Hz, 2H), 1.95 - 2.03 (m, 2H), 0.89 (t, J = 7.61 Hz, 3H). <sup>13</sup>C NMR (C<sub>6</sub>D<sub>6</sub>, 126 MHz): δ<sub>C</sub> 174.32 (C1), 131.78 (C20), 129.08 (5), 128.50 (C17), 128.22 (C14), 128.15 (C8, C10 and C11), 128.11 (C7, C13 and C19), 128.06 (C4), 127.91 (C16), 50.65 (C1'), 33.65 (C2), 25.67 (C15), 25.66 (C9), 25.65 (C18), 25.57 (C6), 25.56 (C12), 22.75 (C3), 20.54 (C21), 14.08 (C22).

### 3.2.2. Transformation of EDP-Me Regioisomers to Monotrans DHA-Me Isomers

The reaction is described for 16,17-EDP-Me and 13,14-EDP-Me (first fraction of the EDP chromatographic separation) and the same steps were followed for the other isolated EDP-Me fractions.

#### Step 1. (Bromination of Epoxide)

To a freshly prepared solution of triphenylphosphine dibromide (7 mg; 0.0167 mmol) in dry dichloromethane (50  $\mu$ L) a solution containing a mixture of EDP regioisomers, **6** and **5**, (3 mg; 0.0084 mmol containing traces of 10,11-EDP **4**) in dry dichloromethane (100  $\mu$ L) and pyridine (1  $\mu$ L) was added, stirring at 0  $^{\circ}$ C under argon atmosphere. The mixture was left stirring overnight at 5  $^{\circ}$ C, and then was quenched with a 1 M aqueous solution of hydrochloric acid (0.5 mL) and extracted three times with chloroform/ethanol (4/1). The reaction was monitored by TLC for the ring opening as dibromide (7/3 n-hexane/diethyl ether, starting material  $R_f$  = 0.7 and dibromide product  $R$  = 0.4). The organic layers were collected, dried over  $\text{Na}_2\text{SO}_4$  and evaporated under vacuum. The crude containing methyl 16,17-dibromo-(4Z,7Z,10Z,13Z,19Z)-docosapentaenoate and 13,14-dibromo-(4Z,7Z,10Z,16Z,19Z)-docosapentaenoate (with traces of the 10,11-dibromoderivative) was used for the next step. The same reaction was also performed for the inseparable mixture of the EDP-Me regioisomers **3** and **7** and for the EDP-ME regioisomer **4**. In all cases, the reaction crude was used for the next step.

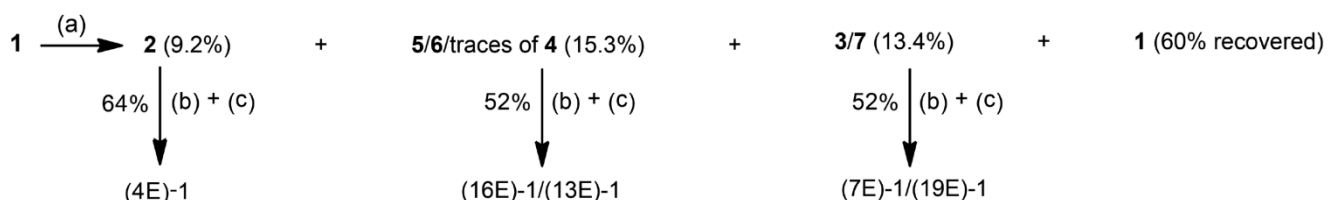
#### Step 2. (Elimination)

To an ice-cooled slurry of activated zinc (4.7 mg; 0.072 mmol), acetic acid (2  $\mu$ L), and N,N-dimethylformamide (150  $\mu$ L), a solution of methyl 16,17-dibromo(4Z,7Z,10Z,13Z,19Z)-docosapentaenoate and traces of 13,14-dibromo-(4Z,7Z,10Z,16Z,19Z)-docosapentaenoate (3 mg; 0.0060 mmol) in N,N-dimethylformamide (100  $\mu$ L) was added, and the mixture was stirred at 0  $^{\circ}$ C for 14 h. The reaction was monitored by TLC (eluent: 7/3 n-hexane/diethyl ether) evidencing the formation of alkenes ( $R$  = 0.9) in the presence of traces of starting material ( $R_f$  = 0.4). At this point, the reaction was stopped by addition of a 1 M aqueous hydrochloric acid solution (1 mL), and the precipitate was filtered off. The filtrate was extracted three times with a mixture of chloroform/ methanol (3/1). The organic layers were collected and dried over  $\text{Na}_2\text{SO}_4$ . The solvent was removed under vacuum to afford a colorless oil (1.5 mg; 0.0044 mmol; 73% yield).

The reaction crude was analyzed by Ag-TLC (eluent: 1/9 n-hexane/diethyl ether with 0.4% MeOH) evidencing the presence of two spots, referred to monotrans DHA-Me and cis DHA-Me (see **Figure S12b** in Appendix). The other two crude reaction mixtures of dibromides were treated for elimination as described above. The debromination reaction occurred also in the second fraction transformed into the dibromide intermediates affording methyl (4Z,7Z,10Z,13Z,16Z,19E)docosahexaenoate and methyl (4Z,7E,10Z,13Z,16Z,19Z)-docosahexaenoate (colorless oil; 3.5 mg; 0.0010 mmol; 86% yield), as well as, for the last EDP fraction affording methyl (4E,7Z,10Z,13Z,16Z,19Z)docosahexaenoate (colorless oil).

The elimination products were then analyzed by GC taking advantage of the parallel NMR assignments of regioisomers, thus allowing for the attribution of the trans double bond position. **Figures S15–S17** in Appendix are the GC traces of the elimination of the three EDP fractions, in comparison with the trans isomer mixture obtained by photolysis and with literature data.<sup>147,148,162,166,167</sup> The assignment of the monotrans isomer peaks in the GC analysis was obtained on the basis of the starting monoepoxide assignment (**Figure 36**).

The **Scheme 6** below summarizes the formation of monoepoxides and the chromatographic separation of fractions that underwent the bromination-elimination step affording the separation of the monotrans regioisomers.



**Scheme 6.** Two-Step Transformation of All-Cis DHA-Me into Monotrans Isomers.<sup>a</sup>

<sup>a</sup>Yields of the products are in parentheses: (a) *m*-CPBA, DCM, RT, 10 min; (b) dry DCM, pyridine, Ph<sub>3</sub>PBr<sub>2</sub>, 5°C, overnight followed by (c) DMF, activated Zn, AcOH, 0°C, 10 h.

### 3.3. Synthesis of Monotrans DHA-Me Isomers by Photolysis

A 15 mM solution of DHA-Me ester (20 mg, 0.058 mmol) in 2-propanol (3.87 mL) was transferred into a quartz photochemical reactor (Sigma-Aldrich) equipped with a 5.5 W low-pressure mercury lamp. The reaction mixture was degassed with argon for 20 min, then an aliquot of a previously degassed stock solution of 2-mercaptoethanol in 2-propanol was added (0.03 mmol) and the UV lamp was turned on for 5 min at the temperature of  $22 \pm 2$  °C, kept by means of a thermostat bath. The reaction was monitored by Ag-TLC, spraying the plate with cerium ammonium sulfate/ammonium molybdate reagent (CAM), to evidence the formation of the monotrans fraction together with ditrans, tritran products, in order to stop the reaction when monotrans isomers were prevalently formed in the presence of remaining cis-DHA (see **Figure S12a** in Appendix). The solvent was removed under vacuum, and addition of chloroform with further evaporation under vacuum helped the removal of 2-mercaptoethanol. The crude of the reaction was subsequently dissolved in 1 mL of *n*-hexane and loaded onto a preparative Ag-TLC plate. A rapid and efficient separation was obtained using 1:9 *n*-hexane/diethyl ether with 0.4% MeOH as mobile phase. After elution, the plate portion corresponding to the monotrans isomer fraction ( $R_f = 0.58$ ), detected by spraying a small portion of the plate with CAM, was scraped off. Silica was washed with chloroform (3 X 5 mL). The solvent was evaporated to give a solid material, which is the Ag-fatty acid complex insoluble in *n*-hexane. This material was dissolved in a 5% aqueous solution of  $\text{NH}_4\text{OH}$ , vigorously stirred (600 rpm) for 10 min and extracted with aliquots of *n*-hexane (3 X 5 mL). Finally, the organic phase was dried over  $\text{Na}_2\text{SO}_4$ , filtered and evaporated. The unreacted all-cis DHA-Me was recovered and subjected to a second isomerization cycle. This procedure led to the collection of a colorless oil that corresponded to the monotrans DHA methyl ester isomer mixture (5.2 mg, 0.0152 mmol, and overall yield from two isomerization cycles 26%). GC analysis was carried out under the conditions described in Materials and Methods (see trace II, **Figure 36** or trace II in **Figure 38**).  $^{13}\text{C}$  NMR (**Figures S13 and S14** in Appendix) of the mixture of monotrans DHA-Me isomers obtained from the isomerization and from the purification were also performed.

$^{13}\text{C}$  NMR ( $\text{C}_6\text{D}_6$ )  $\delta$  10.94, 13.72, 14.12, 20.44, 20.56, 22.76, 25.26, 25.57, 25.66, 27.12, 28.01, 28.17, 28.57, 29.24, 30.39, 33.67, 33.71, 35.64, 45.29, 50.64, 50.73, 61.17, 126.93, 127.12, 127.48, 127.67, 127.86, 128.14, 128.48, 128.78, 128.81, 129.28, 129.37, 131.66, 131.68, 131.71, 131.75, 131.97, 131.99, 132.00, 132.23, 132.27, 132.49, 132.52, 132.55, 172.35, 172.37.

After purification the  $^{13}\text{C}$  NMR of the pure monotrans fraction was carried out (see **Figure S14** in Appendix):  $^{13}\text{C}$  NMR ( $\text{C}_6\text{D}_6$ )  $\delta$  14.10, 20.55, 22.75, 30.40, 33.65, 50.65, 127.47, 127.67, 127.86, 131.68, 131.72, 131.77, 132.02, 132.28, 172.33.

### 3.4. Isomerization of Fish Oil by Photolysis

A sample of commercially available fish oil, used as omega-3 containing ingredient for food and nutraceutical preparation, was isomerized following the procedure above described for the DHA-Me isomerization. After 30 min, 30% of total trans content was obtained as determined after transesterification to the corresponding FAME and GC analysis. In Appendix, the  $^{13}\text{C}$  NMR of the oil prior and after isomerization are reported (**Figures S25 and S26**). By GC analysis of the FAME obtained from the triglyceride transesterification the cis and trans fatty acid contents were also determined. In **Figure 38** of the main text the GC separation of the DHA isomers is shown, in comparison with the monotrans DHA methyl ester isomer library. In **Figures S27–S30** in Appendix, two different GC methods were used with hydrogen or helium as carrier gas in order to evidence the best fatty acid separation.

### 3.5. Analysis of Monotrans DHA Isomers from Commercially Available Supplements

Available Supplements: Nineteen DHA-containing supplements in soft-gel capsules were examined for their cis and trans fatty acid contents, being six products commercially available in Italy and 13 in Spain. The oily content was taken from the capsules, and the lipids were extracted according to the Folch method.<sup>187</sup> Briefly, approximately 3 mg of each sample was dissolved in 2:1 chloroform/methanol (3 mL) and partitioned with brine (1 mL); the extracted organic phases

(3 X 3 mL) containing lipids were joined and dried with anhydrous Na<sub>2</sub>SO<sub>4</sub>. After filtration, the solvent was eliminated using a rotary evaporator and the oily residue was left under vacuum for 10 min to remove any possible trace of water. The lipid extract was checked by TLC (mobile phase: n-hexane/diethyl ether 7:3) and then treated with freshly prepared 0.5 M KOH/MeOH solution for 30 min at room temperature under stirring. Reaction was quenched using brine and fatty acid methyl esters (FAME) were extracted using n-hexane (3x 3 mL); the organic phase was collected and dried with anhydrous Na<sub>2</sub>SO<sub>4</sub>. After filtration and solvent evaporation, the FAME mixture was dissolved in 10 µL n-hexane and 1 µL was injected for GC analysis. **Tables S2** and **S3** in Appendix report the FAME content: products 1–6 are omega-3 supplements present in the Italian market and products 7–19 are present in the Spanish market.

### 3.6. LUVET Preparation

A mixture of 20 % 1-stearoyl-2-docosahexaenoyl-sn-glycero-3-phosphocholine/1-palmitoyl-2-oleoylphosphatidylcholine in chloroform solution (111 µL of 18:0-22:6 PC with 11.1 mg of 16:0-18:1 PC dissolved in 1 mL chloroform) was evaporated to a thin film in a test tube under a stream of argon and then kept under high-vacuum for 30 min at room temperature.

In order to obtain a final concentration of 70 mM phospholipid content, 250 µL tridistilled water were added and by vortexing for 7 min under an argon atmosphere multilamellar vesicles were formed. Large unilamellar vesicles (LUV) with a mean diameter of 156-158 nm were prepared by extrusion technique using LiposoFast and a 200 nm polycarbonate membrane filter as described previously.<sup>133</sup> The size of the liposomes was measured using dynamic light scattering (DLS) methodology. The LUVET stock suspensions were transferred into a vial and stored at 4 °C for a maximum of two days.

#### 3.6.1. Isomerisation vs Peroxidation of PC in LUVET

The total volume for every reaction was 1 mL of LUVET stock (phospholipid concentration of 1 mM). More specifically an aliquot of 14.5 µL fatty acid content from the stock solution was added in tridistilled water in the reaction vessel. To the liposome suspension, the copper complex was transferred (0.15 mM) and the reaction remained under stirring for 2 min. From stock solutions in

tridistilled water and final concentration in the reaction 10 mM, the thiol, 2-mercaptoethanol was added to the reaction drop wise (0.5 mM/min) using a syringe pump. Each reaction vessel was incubated at 37 °C and, in order to follow the formation of trans fatty acid residues, samples were analysed at different times. The work-up of the vesicles was made with 2:1 chloroform/methanol, extracting and collecting the organic phases dried over anhydrous sodium sulphate and evaporating the solvent under vacuum at room temperature. The phospholipid extracts were treated with 0.5 M KOH/MeOH, in a transesterification type of reaction for 10 min at ambient temperature. The reaction was quenched with addition of tridistilled water and an extraction with *n*-hexane followed. The organic layer containing the corresponding fatty acid methyl esters (FAME) was analysed by GC for the determination of the content.

## 3.7. Results and Discussion

### 3.7.1. Dual Synthetic Approach for DHA Transformation and Monotrans DHA Isomer Identification

According to **Scheme 5** we approached the dual synthetic strategy first by carrying out the direct radical-catalyzed isomerization of DHA methyl ester, as described previously by our group for EPA,<sup>163</sup> thus obtaining a mixture of the six monotrans DHA isomers (**Figure 34**). Ag-TLC was used to purify the monotrans DHA isomers from the starting material (**Figure 35**, lane C).

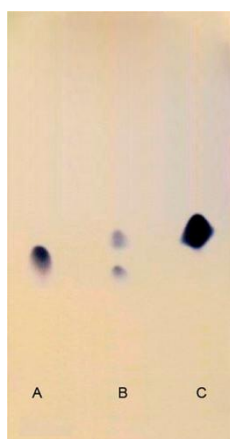


**Figure 35.** Ag-TLC (eluent: 1/9 n-hexane/diethyl ether with 0.4% MeOH) of the transformation of one monoepoxide fraction (second fraction) via bromination and elimination reactions. A: standard all-cis DHA-Me. B: elimination reaction showing the presence of all-cisDHA-Me and monotrans isomers (19E and 7E) of DHA-Me. C: mixture of monotrans DHA-Me obtained by thiyl-radical catalyzed isomerization after purification as reported in *Experimental Section*.

The recognition of each monotrans isomer was not realizable at this stage, however satisfactory separation of these isomers could be obtained by gas chromatography, the GC trace showing five out of six separable peaks, meaning that only two isomers are superimposed. It is also worth noting that one monotrans DHA isomer elutes similarly to cis-DHA (**Figure 36**, GC trace II). GC analysis, under the conditions described in *Materials and Methods* (trace II, **Figure 36**) gave a pattern of peaks similar to those described in literature.<sup>147,148,166,168</sup> At this point the assignment of each monotrans isomer could not be performed. Only by elution of the commercially available 4E-DHA-Me, the third eluting peak could be assigned to this isomer (**Figure 36**, trace V). By the

second synthetic route DHA methyl ester was transformed in two-steps to give the corresponding monotrans alkenes (**Scheme 5**), via monoepoxide formation, ring-opening of the epoxide, using the stereoselective formation of the dibromide derivatives, followed by elimination reaction, that provide the trans geometry of each starting double bond. In this strategy, the key step is the separation and characterization of the monoepoxide products, in order to assign the double bond position for the subsequent elimination step. *Meta*-chloroperoxybenzoic acid (*m*-CPBA) epoxidation followed by purification by flash chromatography (with 9/1 n-hexane/diethyl ether as the eluent; see TLC separation with 7/3 n-hexane/diethyl ether in **Figure S4** in Appendix, provided three fractions of monoepoxide regioisomers. The structures of the six regioisomers are shown in **Figure 34**. Under our experimental conditions, described in the *Materials and Methods*, the 4-monoepoxide (compound **2**) was isolated in pure form as a third fraction of the chromatography. The other regioisomers were obtained in the first and second chromatographic fractions, each fraction as a mixture of two compounds.

EDPs are biologically relevant compounds obtained from DHA by cytochrome P450 enzyme, exhibiting a variety of biological effects in inflammation, pain, angiogenesis and cancer.<sup>172</sup> Actually cytochrome P450 is able to provide the stereoselective epoxidation of DHA, preferably at the last double bond obtaining 19,20-EDP.<sup>170</sup> However, also 16,17-EDP, 13,14-EDP, 10,11-EDP, and 7,8-EDP have been detected and separated by HPLC analysis, whereas 4,5-EDP was reported to be unstable.<sup>173</sup> We were interested to carry out mono- and bidimensional NMR experiments in order to assign the epoxide position in each compound of the reaction mixture. It is worth noting that the use of deuterated benzene (C<sub>6</sub>D<sub>6</sub>) as NMR solvent is required, in order to avoid decomposition during the experiment in the slightly acidic environment of deuterated chloroform. We performed also the spectrum of DHA-Me in deuterated benzene for examining the epoxidation results using the same experimental conditions (see **Figure S5** in Appendix). **Table S1** in Appendix collects the <sup>13</sup>C NMR data of the EDP isomers and the 10,11-EDP regioisomer is not presented because it was formed only in traces. The reasons for the scarce formation of this stereoisomer in the epoxidation reaction were not investigated. In Appendix, **Figure S5** shows the structures of the five EDP isomers with their proton and carbon atom resonances as assigned in this study using deuterated benzene as solvent. The NMR spectra of all the five EDP isomers are reported in the *Materials and Methods*. In order to assign the monoepoxide resonances, we examined <sup>1</sup>H and <sup>13</sup>C NMR resonances comparing with DHA-Me for each fraction separated by column chromatography. The subsequent transformation of monoepoxides, forming *in situ* the corresponding dibromides followed by elimination to the corresponding alkenes, was performed in one step for each fraction. The latter reaction sequence

was adapted for DHA methyl ester from a procedure described for arachidonic acid methyl ester<sup>71,160</sup> and successfully applied to eicosapentanoic acid methyl ester (EPA).<sup>164</sup> During the *in situ* transformation of epoxides to dibromide derivatives and the subsequent elimination to trans alkenes, the concerted elimination is not the only occurring mechanism for which the double bond can be formed. Therefore, the presence of cis-DHA was detected in all the resulting elimination crude mixtures. Having recognized in each starting fraction the monoepoxide structures as major and minor isomers, as described in the NMR section and summarized in **Scheme 6**, the assignment of the corresponding monotrans DHA isomers could be satisfactorily carried out examining the peaks present in the GC traces of the DHA-Me isomers after the two-steps synthesis, as shown in **Figure 36** (traces II, IV, V).

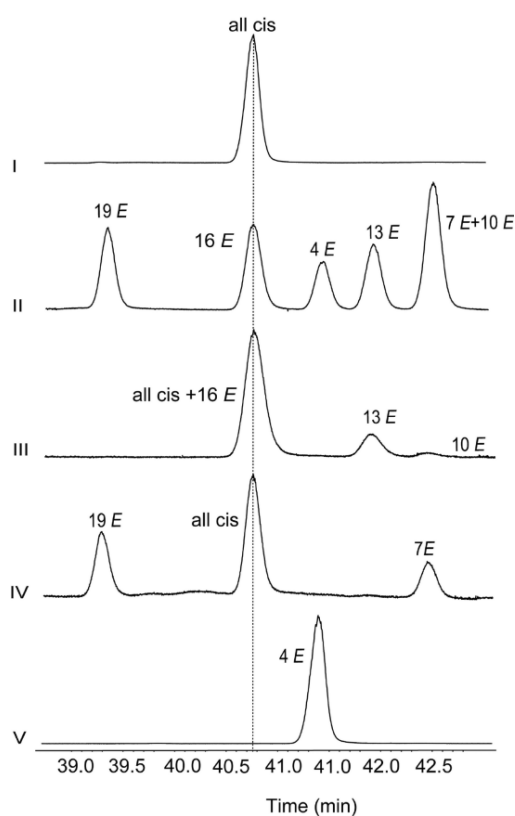
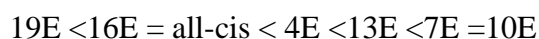


**Figure 36.** GC chromatograms of the 39.0–42.5 min region referred to (I) all cis-DHA methyl ester; (II) mixture of monotrans DHA methyl ester isomers obtained by photolysis in the presence of thiyl radicals; (III) 16*E*-isomer superimposed with all cis-DHA methyl ester, 13*E* and traces of 10*E*; (IV) 19*E*, all cis-DHA methyl ester and 7*E*; and (V) 4*E* (commercially available product).

The isomer overlapping with DHA-Me is the 16*E* monotrans DHA-Me, and the 7*E* and 10*E* monotrans DHA-Me are also superimposed (lanes (III) and (IV) corresponding to the conversion of these two monoepoxide fractions according to **Scheme 6**). It is worth recalling that the 10*E* isomer was obtained from the traces of the 10,11-EDP, formed with the lowest yield among all EDP isomers, as ascertained by the study of the NMR spectra reported in the following section. Finally, the following GC order of elution could be assigned:



This is the first time the assignment of monotrans geometrical isomers of the omega-3 fatty acid DHA is made, by a combination of Ag-TLC, NMR spectroscopy, gas chromatography, and this result contributes to the library of noncommercially available trans isomers developed by us for the long-chain polyunsaturated fatty acids (LC-PUFA) omega-6 and omega-3.

### 3.7.2. NMR Study of the EDP Isomers and the Monotrans DHA Isomers

As previously mentioned, the  $^1\text{H}$  and  $^{13}\text{C}$  NMR spectra of the EDP and monotrans DHA-Me isomers obtained in this work (**Figure 37**) were carried out in  $\text{C}_6\text{D}_6$ , primarily used to avoid decomposition of the monoepoxide compounds. The  $^1\text{H}$  NMR spectra of the EDP regioisomers was very diagnostic for the terminal methyl group (C-22), that appears as triplet in the 0.80–0.91 ppm region and is influenced by the relative position of the epoxide functionality. As shown in **Figure 37**, in the starting material, DHA-Me the triplet is centered at 0.885 ppm (trace I), whereas the pure 4,5-EDP isomer (isolated by chromatography) shows the triplet centered at 0.888 ppm (trace IV).

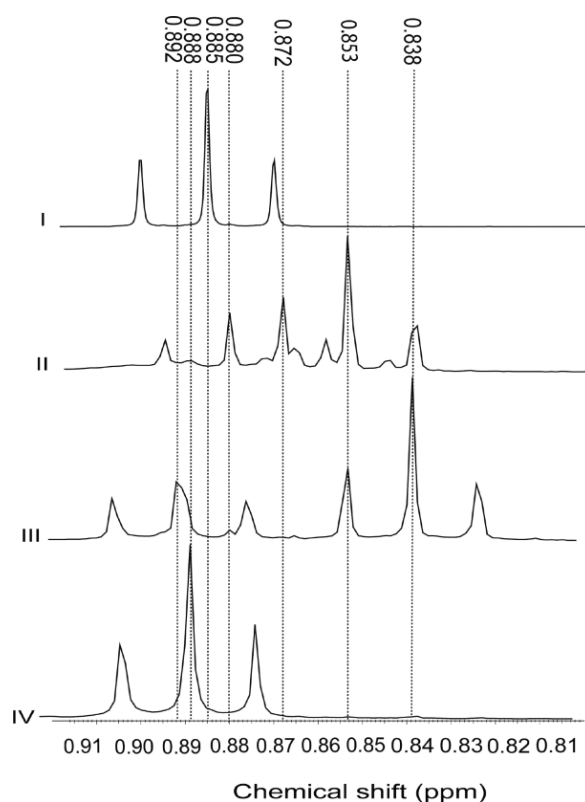


**Figure 37.**  $^1\text{H}$  NMR region (0.81–0.91 ppm) related to the terminal methyl group (C-22) of EDP regioisomers (spectra run in  $\text{C}_6\text{D}_6$ ). The triplet is centered at different ppm in relationship with the position of the epoxide along the fatty acid chain; (I) DHA-Me all-cis; (II) mixture of 13,14-EDP **5**, 16,17-EDP **6** (traces of 10,11-EDP **4**); (III) mixture of 7,8-EDP **3** and 19,20-EDP **7**; (IV) 4,5-EDP **2**.

Two other fractions obtained from the chromatographic separation contained four other isomers (see **Scheme 6**): (i) a mixture with the 16,17-EDP isomer with the triplet centered at 0.853 ppm and the 13,14-EDP isomer with the triplet centered at 0.880 ppm, with traces of the 10,11-EDP isomer (**Figure 37**, trace II); (ii) a mixture with the 19,20-EDP isomer with the triplet at 0.838 ppm (major isomer) and the 7,8-EDP isomer with the triplet at 0.892 ppm. The assignment of the triplet was made by correlation experiments, crossing the  $^1\text{H}$  and  $^{13}\text{C}$  resonances of the methyl group and epoxide carbon atoms, respectively (see **Figure S9** in Appendix). Examining the  $^{13}\text{C}$  NMR spectrum of the EDP regioisomers and using the assigned resonances of starting DHA-Me, the carbon atom resonances of the epoxide function were determined. In fact, for the 16,17-monoepoxide, two peaks at 55.79 and 55.65 ppm can be assigned to the carbon atoms of the epoxide function, because at the same time in the spectrum are absent the chemical shifts of the ethylenic carbon atoms assigned at the C16–C17 double bond of DHA-Me (128.50 and 127.91 ppm, respectively). The 13,14-EDP has two peaks at 55.66 and 55.65 ppm assigned to the epoxide function, because the C13–C14 double bond resonances of DHA-Me at 128.22 and 128.11 ppm are not present. The 19,20-EDP has the epoxide carbon atoms at 57.38 and 55.75 ppm, and correspondently the chemical shifts at 131.78 and 127.11 ppm (C19–C20 of DHA-Me) are absent. In the 19,20-EDP regioisomer, the chemical shift of the C-22 is noticeably moved at 10.45 ppm (instead of the range 14.08–14.00 ppm for all the other EDP regioisomers), indicating an upfield shift due to a different electronic distribution influencing the end of the carbon atom chain (i.e., the  $\omega$  position). The 7,8-EDP showed the chemical shifts of the epoxy carbon atoms at 55.65 and 55.63 ppm, corresponding to the absence of the resonances at 128.15 and 128.11 ppm (C7–C8 in the DHA-Me). Finally, for the EDP in the position 4,5, the epoxy function was individuated by the chemical shifts at 56.07 and 55.32 ppm corresponding to the absence of the peaks at 129.08 and 128.06 ppm (C4–C5 of DHA-Me). Bidimensional experiments can also be performed to acquire more data on these assignments. A representative description of the assignment of resonances to 7,8- and 19,20-EDP isomers obtained by HSQC/HMBC experiments is shown in Appendix (**Figure S9**). By this additional information, we could increase data on the epoxide assignments; however, the above-described  $^1\text{H}$  and  $^{13}\text{C}$  NMR characteristics satisfactorily individuated the EDP regioisomers. As far as the DHA monotrans isomers are concerned, they were obtained from the EDP two-step transformation as shown in **Scheme 5**, as well as mixture of the six isomers by radical catalyzed isomerization of the all-cis DHA-Me. This latter mixture was examined by NMR and **Figure 38** shows a trace of the enlargement of the  $^{13}\text{C}$  NMR region corresponding to the C-20 resonance (traces I and II, panel b), which was found to be diagnostic for the geometrical isomers.

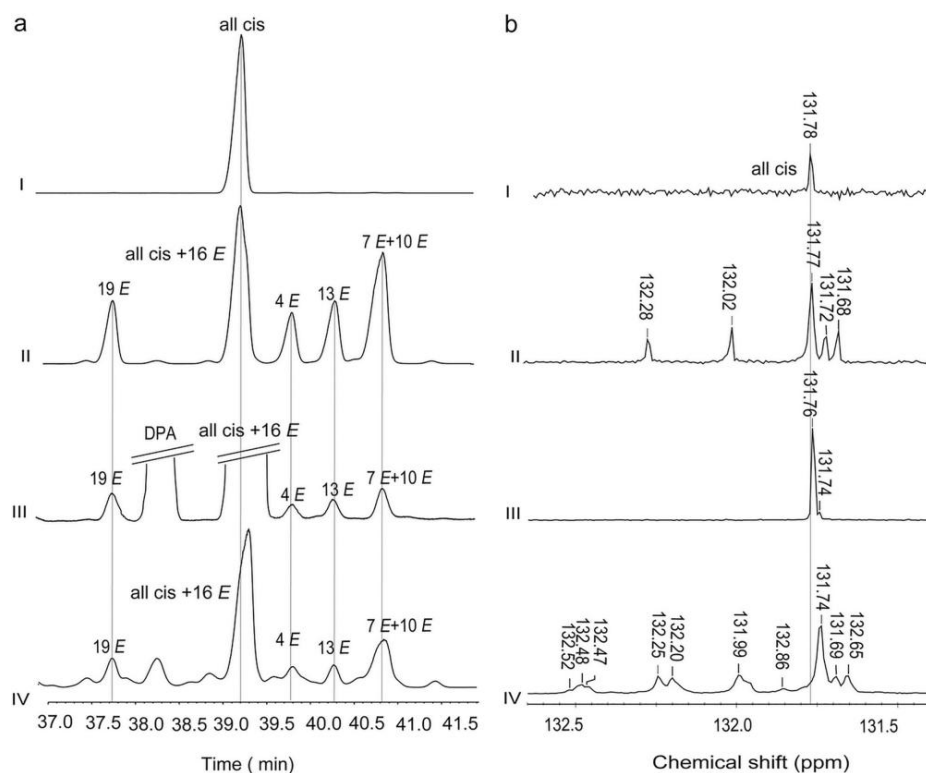


**Figure 38.** (Panel a) Partial GC traces of: (I) all-cis DHA-Me; (II) the six DHA-Me monotrans isomers and all-cis DHA-Me; (III) FAME obtained from the transesterification of DHA-containing fish oil. The presence of monotrans DHA isomers as contaminants is visible when the trace is expanded (X 10); (IV) DHA-Me isomers obtained after isomerization and transesterification of fish oil (this mixture contains mono-, di-, and tri-trans isomers). (Panel b) Enlargement of the  $^{13}\text{C}$  NMR region (131.5–132.5 ppm) corresponding to the C-20 ethylenic carbon atom of: (I) all-cis DHA-Me; (II) the six DHA-Me monotrans isomers and all-cis DHA-Me; (III) DHA-containing triglycerides from fish oil; (IV) DHA-containing triglycerides from fish oil after isomerization (this mixture contains mono-, di-, and tri-trans isomers).

The C-20 atom is the most deshielded among the olefinic peaks, and its distance from the position of the trans double bond in the fatty acid chain influences its chemical shift. Five different chemical shifts for this carbon atom could be individuated in the monotrans isomer mixture isolated from the isomerization (trace II in **Figure 38**, panel b), one of them representing two overlapped resonances, and they are clearly different from the C-20 of DHA-Me appearing at 131.78 ppm (cf. trace I in **Figure 38**, panel b). The importance of the last vinylic carbon atom of the PUFA fatty acid chain was previously described for arachidonic and eicosapentaenoic acids.<sup>157,164</sup> The present data support the use of NMR spectroscopy for the analysis of natural and marine oils, as already shown by other groups<sup>188,189,190</sup> and recently reviewed.<sup>191</sup> The herein described chemical synthesis of monotrans DHA isomers, as well as our previously published

work on trans lipid library,<sup>71,140,156,157</sup> certainly increase availability of reference compounds and will help to gather more information by the powerful NMR methodology.

### *3.7.3. Isomerization of DHA-Containing Fish Oil and Determination of the Monotrans DHA Isomer Content in Commercially Available Supplements*

Natural oils are important sources of cis PUFA, and trans isomers of EPA and DHA are contaminants after deodorization or distillation procedures that are used in order to eliminate the fishy odor. PUFA isomerization in oils has been described by heating procedures<sup>147,167</sup> or p-toluene sulfinic acid treatment,<sup>174</sup> whereas we reported the isomerization of some oils by thiyl radical catalyzed process,<sup>176</sup> but not of fish oils. The isomerization of a sample of DHA-containing fish oil commercially available as raw material for food or supplements was performed. The reaction was carried out as described in the *Materials and Methods*, and GC analysis was performed after transesterification of the triglycerides into the corresponding FAMES. **Figure 38** (panel a) shows the GC regions corresponding to FAMES from fish oil in the starting material (trace III), and it is worth noting that in this sample monotrans DHA isomers are already present as contaminants, as it can be seen by comparison with the FAME of the oil after free radical-catalyzed isomerization (trace IV), and related cis and monotrans DHA-Me isomers (traces I and II). In the same **Figure 38** (panel b), the enlarged region of the <sup>13</sup>C NMR spectra corresponding to the C-20 (ethylenic carbon atom) resonance is shown for the DHA-containing triglycerides of fish oil (trace III) in comparison with the all-cis DHA-Me (trace I). It is gratifying to see that the C-20 chemical shift is similar for FAME and triglycerides that contains the DHA moieties. Moreover, after fish oil isomerization, trans-DHA-containing triglycerides show strong similarity of the C20 resonances for the monotrans DHA-Me isomers that were previously described. In Appendix, the full <sup>13</sup>C NMR spectra of the fish oil triglycerides before and after the isomerization are shown (**Figures S25** and **S26**). It is worth mentioning that the GC resolution of monotrans isomers achieved under our analytical conditions, using a specific oven program with a 60 m X 0.25 mm X 0.25 μm (50%-cyanopropyl)-methylpolysiloxane column, were obtained after testing several gas chromatographic conditions, in particular concerning the carrier gas. Using natural sources of fatty acids as marine oils, it was envisaged that other long-chain fatty acids can elute in the region of the DHA-Me and its monotrans isomers. This was the

case of C22-PUFAs, such as 22:5  $\omega$ -3 (DPA) and 22:6  $\omega$ -6, as well as long chain saturated and monounsaturated fatty acids, such as C24:0 and C24:1. In Appendix, **Figures S27–30** show the peak resolution connected with the two GC experimental conditions that are described in *Materials and Methods*. We were aware that a very careful study was carried out with a 200 m SLB IL111 ionic liquid column verifying the accuracy of the proposed method using Standard Reference Material (SRM) 3275 “Omega-3 and Omega-6 Fatty Acids in Fish Oil” from the National Institute of Standards and Technology (NIST).<sup>175</sup> We could compare the reported results with our method using hydrogen as carrier gas (**Figure S29** in Appendix), and it was gratifying to see that interferences with other fatty acids can be avoided also under our conditions. As already shown for EPA isomers,<sup>164</sup> the use of hydrogen as carrier gas together with specific oven temperature program is satisfactory, in terms of no interferences by C22-PUFAs and long chain saturated and monounsaturated fatty acids.

The combination of GC and <sup>13</sup>C NMR analyses, the latter using the resonance of the C-20, can be of diagnostic value for individuating monotrans DHA isomers, with the advantage that <sup>13</sup>C NMR can be performed directly on the triglycerides without any transformation. In this case, it is also worth noting that by studying the region between 130.40 and 132.60 ppm, also in different NMR solvents, the overview of omega-6 and omega-3 monotrans isomer content can be obtained. This overall picture can be relevant for further developments in metabolomics research. The analysis of the triglyceride fractions contained in DHA-containing supplements available on the markets in Italy and Spain was performed. As matter of fact, analytical protocol to run quality control of supplements are increasingly addressed for the safety of producers and consumers, and researchers raised problems of oxidized or trans contaminants by evaluating commercial products of different countries.<sup>174,175</sup> **Table 10** shows our results in terms of fatty acids, such as omega-3 DPA, DHA, the DHA monotrans isomers and the monounsaturated 24:1, detected in some representative supplements available in Italian and Spanish markets, presenting low and high-content of monotrans DHA isomers.

**Table 10.** Representative Fatty Acid Contents in Terms of DPA, DHA, 24:1, and Monotrans DHA Isomers Eluting in the GC Time Window of 37–41.5 min (See Figure 23 and Figures S23–26) Obtained from Natural Oils of Commercially Available Supplements in Italy and Spain<sup>a</sup>.

	1	2	4	5	8	13	14	15	19
22:6 $\omega$ 3 trans- $\Delta$ 19	0.12 $\pm$ 0.01	0.06 $\pm$ 0.00	0.13 $\pm$ 0.08	0.12 $\pm$ 0.04	0.09 $\pm$ 0.01	0.27 $\pm$ 0.03	0.34 $\pm$ 0.03	0.31 $\pm$ 0.02	0.66 $\pm$ 0.24
22:5 $\omega$ 3 (DPA)	3.67 $\pm$ 0.07	4.31 $\pm$ 0.02	3.91 $\pm$ 0.18	0.15 $\pm$ 0.02	2.10 $\pm$ 0.03	9.94 $\pm$ 0.32	1.17 $\pm$ 0.02	13.32 $\pm$ 0.04	2.09 $\pm$ 0.33
22:6 $\omega$ 3 (DHA)	18.51 $\pm$ 0.10	20.64 $\pm$ 0.37	20.98 $\pm$ 0.07	57.35 $\pm$ 0.15	14.60 $\pm$ 0.15	83.68 $\pm$ 0.17	86.19 $\pm$ 0.11	78.78 $\pm$ 0.11	76.75 $\pm$ 0.41
22:6 $\omega$ 3 trans- $\Delta$ 4	0.08 $\pm$ 0.00	0.01 $\pm$ 0.00	0.07 $\pm$ 0.00	0.17 $\pm$ 0.00	0.08 $\pm$ 0.00	0.09 $\pm$ 0.03	0.16 $\pm$ 0.02	0.18 $\pm$ 0.03	0.30 $\pm$ 0.01
22:6 $\omega$ 3 trans- $\Delta$ 13	0.19 $\pm$ 0.02	0.02 $\pm$ 0.00	0.14 $\pm$ 0.03	0.33 $\pm$ 0.01	0.09 $\pm$ 0.01	0.10 $\pm$ 0.04	0.46 $\pm$ 0.03	0.35 $\pm$ 0.02	0.74 $\pm$ 0.02
24:1	0.34 $\pm$ 0.03	0.10 $\pm$ 0.00	0.66 $\pm$ 0.01	nd	0.24 $\pm$ 0.01	0.14 $\pm$ 0.03	nd	nd	0.34 $\pm$ 0.14
22:6 $\omega$ 3 trans- $\Delta$ 7+ $\Delta$ 10	0.26 $\pm$ 0.04	0.02 $\pm$ 0.00	0.29 $\pm$ 0.02	0.50 $\pm$ 0.02	0.07 $\pm$ 0.00	0.20 $\pm$ 0.03	0.68 $\pm$ 0.01	0.49 $\pm$ 0.03	1.00 $\pm$ 0.14
total monotrans DHA	0.75 $\pm$ 0.04	0.11 $\pm$ 0.00	0.63 $\pm$ 0.08	1.12 $\pm$ 0.04	0.33 $\pm$ 0.01	0.66 $\pm$ 0.04	1.64 $\pm$ 0.03	1.33 $\pm$ 0.03	2.70 $\pm$ 0.25

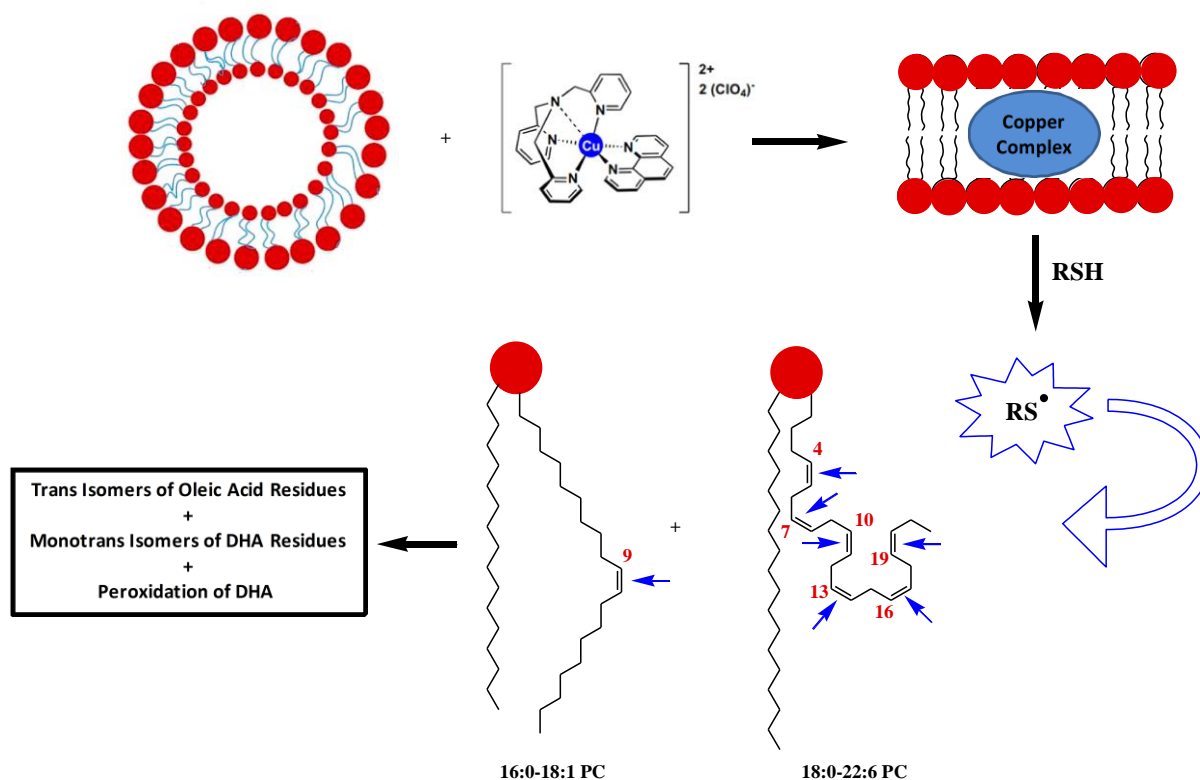
<sup>a</sup>The values are expressed as percentages relative to 100% of the fatty acid peak areas identified in the GC analysis. In **Tables S2** and **S3** (Supporting Information), the complete analysis for 19 products is reported.

The values of these fatty acids are shown as relative percentages (% rel) in the whole fatty acid composition determined on the natural oil ingredient of the capsules. The full fatty acid analysis referred to 19 products of Italian and Spanish markets are available in Appendix (**Tables S2 and S3** and **Figures S27–30** of representative GC chromatograms).

In **Table 10** is shown that the percentage of monotrans DHA isomers was found between 0.11% and 2.70%, with the highest trans contents contained in the DHA-richest formulas (cf. product 19 and product 2 in **Table 10**). This would suggest that the procedures in order to enrich DHA content in the oil be responsible of raising the isomer presence in the resulting material. Our studies on the trans lipid library support previously reported analyses of PUFA-containing oils and supplements, discovering contaminations either as oxidation and isomerization products,<sup>147,148,166,167,174,175</sup> addressing the important issue of the precise monotrans isomer identification in case of EPA and DHA. This is strongly needed especially because health benefits are highly discussed for omega-3 supplements, whereas contaminants can certainly annihilate positive effects in a dose-proportional manner, as shown by us in a murine model.<sup>161</sup>

### 3.7.4. Model Studies in DHA-Containing Liposomes and Cu-TPMA-Phen-Induced Lipid Damage

In 20 % 18:0-22:6 PC/16:0-18:1 PC liposome composition the chemical reactivity of the MUFA residue of oleic *versus* the PUFA residue of DHA was compared. In the **Scheme 7** is presented the general approach.



**Scheme 7.** Cartoon presenting the incorporation of the Cu-TPMA-Phen in the liposome bilayer, the generation of the thiyl radical and subsequent attack to the MUFA and PUFA residues.

In the absence of oxygen the cis-trans isomerization was the main process depicted and different time points were evaluated during the reaction. In fact, after 8 hr of incubation at 37 °C in the presence of 0.15 mM Cu-TPMA-Phen and 10 mM 2-mercaptoethanol the monotrans isomers of DHA represented the 3.099 %, whilst the trans isomer of oleic the 7.305 % of the total fatty acid

composition. These values are reported as relative percentages (% rel) of the total fatty acid peak areas detected in the GC analysis.

We were interested in evaluating the changes in stereochemistry induced by the conversion of the double bond from cis to trans geometry under the reaction applied. In **Figure 39** is reported the cis-trans isomerization yields of MUFA and PUFA residues. The numbers shown were obtained by the relative % of the GC area and the conversion of cis fatty acid residue to each trans isomer was calculated separately.

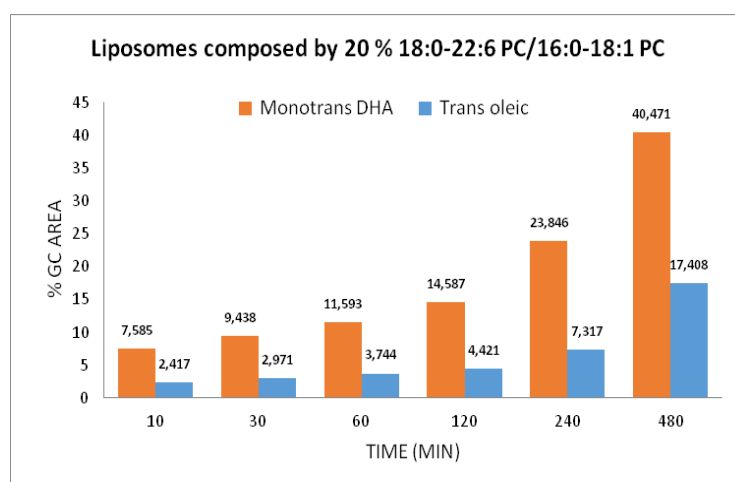


**Figure 39.** Reactivity of oleic versus DHA acid residues. The results obtained after incubation of liposomes composed by 20% 18:0-22:6 PC/16:0-18:1 PC at 37 °C under anaerobic conditions, in the presence of 0.15 mM Cu-TPMA-Phen and 10 mM 2-mercaptoethanol at different time points.

The mixture of the monotrans DHA methyl ester isomers, obtained previously by photolysis, was employed as reference for the recognition of the positional monotrans DHA isomers (see **Figure S30** in Appendix). Based on the fully characterized analytical GC library, the DHA isomers formed in the phospholipid bilayer after treatment with Cu-TPMA-Phen and 2-ME, appeared to be products of a regioselective thiyl radical attack.<sup>192</sup> The DHA's supramolecular organization of vesicles has a profound effect on the isomerization outcome, involving the differentiation of the double-bond reactivity depending on its location. The amphiphilic thiyl radical HOCH<sub>2</sub>CH<sub>2</sub>S<sup>•</sup>, diffusing from the aqueous phase to the hydrophobic region of the membrane bilayer, starts to

isomerize the double bonds nearest to the glycerol backbone,<sup>193</sup> that is nearest to the aqueous phase.

As reported in **Figure 40**, in this studied model the preferential positional order of conversion of stereochemistry and formation of monotrans double bonds in DHA's residues is the following

$$4E > 19E > 13E.$$

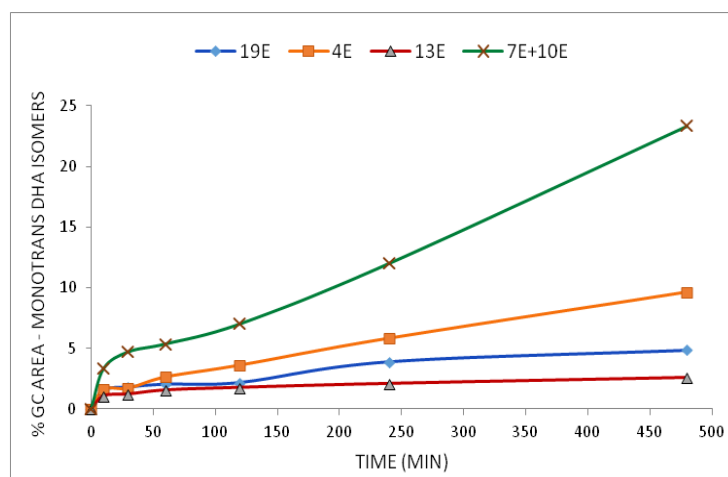


**Figure 40.** The influence of the phospholipid organization in 20 % 18:0-22:6 PC/16:0-18:1 PC liposome membranes leads in a regioselective formation of monotrans DHA isomers.

The double bonds in positions 13 and 19 are located in the terminal part of the hydrophobic fatty acid chain and it could be expected their position in the deeper part of the bilayer. But if the location is in the “membrane core”, then it would be expected 19E to be formed in a low percentage during the isomerization process given by the diffusing thiyl radical. There are a few studies of the DHA conformational changes as free fatty acid in model vesicles, where the different positions of the six double bonds of this PUFA are considered.<sup>194,195,196</sup> The rotational dynamics of omega-3 fatty acids are modulated by surrounding phospholipids and it has been demonstrated that DHA is able to change conformations quickly (nanosecond time scale) in a membrane environment.<sup>194</sup> In our case the DHA is one of the four residues of the membrane phospholipids and the location of the double bonds are not known. In the literature are reported studies on model membrane structure and electron density that have shown the DHA increased electron

density in the phospholipid head group region presumably due to DHA-surface interactions associated with a coincident electron density reduction in the membrane hydrocarbon core.<sup>195</sup> In **Figure 41** is presented the time-averaged conformation of DHA in which the double bond in position 19 is located in closer proximity to the bilayer borders explaining the reason of the preferential isomerization and formation of monotrans 19*E*.

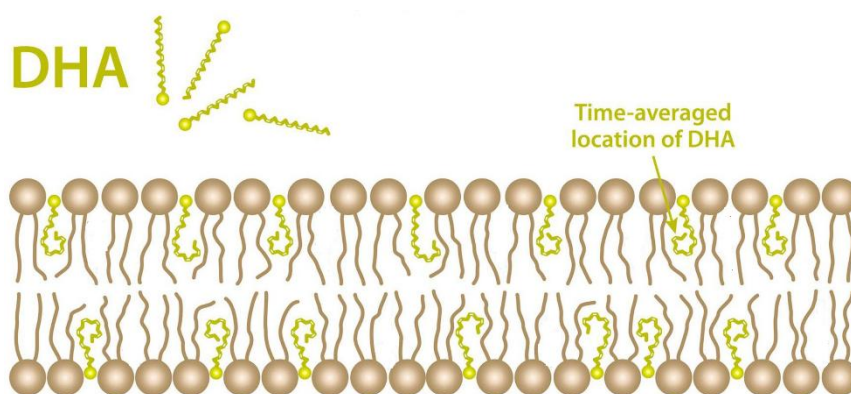


**Figure 41.** Schematic illustration of the proposed conformation of DHA on membrane structure. DHA interact with distinct regions in the headgroup region of the membrane lipid bilayer, due to rapid conformational changes associated with its chemical structure.<sup>195</sup>

As far as concerns the consumption via peroxidation pathway, the presence or absence of oxygen appeared to be critical for the reaction's outcome and the results are reported in **Figure 42**.

In particular, under anaerobic conditions in the presence of 0.15 mM Cu-TPMA-Phen and 10 mM 2-mercaptoethanol, PUFA were decreased by 15 % after 8 hr of incubation at 37 °C. The main process depicted was the cis-trans isomerization of both MUFA and PUFA with the yields discussed above.

However, under aerobic conditions, the consumption of the PUFA content was much more evident. In fact, the loss of PUFA was estimated 18 % after 2 hr of incubation and the content was strongly diminished up to 59 % after 8 hr of incubation at 37 °C.

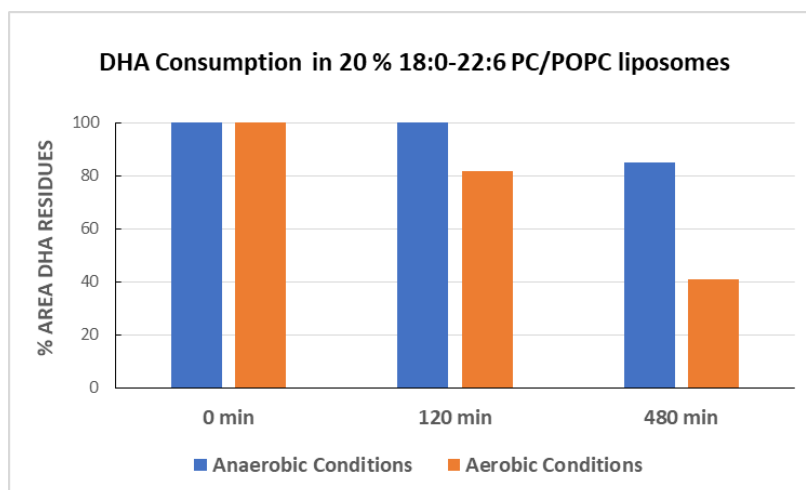


**Figure 42.** Peroxidation pathway in liposomes composed by 20 % 18:0-22:6 PC/16:0-18:1 PC, after addition of 0.15 mM Cu-TPMA-Phen, 10 mM 2-ME and incubation at 37°C at two different time points, where also the presence or absence of oxygen is evaluated. The estimation of consumption is based on the ratio 16:0/22:6, which found as peaks of the GC analysis of their corresponding FAME.

These results concerning the oxidative and cis-trans lipid isomerisation processes, obtained in the biomimetic model of 20 % DHA-containing vesicles, are informative of the molecular reactivity of the complex. Thereby explaining at least in part, the absence of trans isomers in the presence of oxygen.

Our results can contribute to the understanding of the behaviour of metal complexes as antitumoral drugs and their association with the lipid damage effect, in particular indicating the interactions of metallome with membrane lipids as indicated by these novel biomimetic studies.

### 3.8. Conclusions

In conclusion, here we showed the extension of the trans lipid library to include an important long chain PUFA such as DHA, with the individuation of its structural changes due to chemical treatment as well as free radical reactivity, converting the cis geometry into trans. It is expected that this new knowledge will successfully integrate other analytical methodologies for the quality control of trans fats in health care and food products needed by regulatory bodies all over the world. The valuable spectra obtained and fully characterized were in benefit of our research towards the investigation of the artificial chemical nuclease's Cu-TPMA-Phen interaction with DHA fatty acid residues in model studies. The monotrans mixture obtained from the free radical catalyzed isomerization of DHA methyl ester was used as reference for recognition of the positional isomers that were formed in the presence of a thiol and the artificial chemical nuclease.

The above described results represent preliminary observations of the regioselective cis-trans isomerization of DHA in biomimetic models of cellular membranes and furnish an aspect of the mechanistic scenario of DHA's important role in antitumoral treatments. Our studies provide an insight of the novel metallodrug Cu-TPMA-Phen molecular mechanism via free radical production in the presence of DHA composed liposomes. Using a 20 % 18:0-22:6 PC/16:0-18:1 PC liposome composition, the ability of MUFA and PUFA residues to partition between isomerisation and consumption processes was investigated and it was evidenced that the supramolecular organization of phospholipids in the membrane is related to the geometrical isomerism.

As a chemical biology model for antitumoral strategies, liposomes highlight the role of cell membranes, with synergic roles for chemotherapeutic effects. Fatty acid recruitment and membrane formation are attracting a lot of interest in cancer, and in this context the loss of the natural cis geometry and the oxidation-induced lipid remodelling are worthy of deeper studies in anticancer strategies. Finally, our results indicate the dual drug's effect towards not only the DNA but also the membrane lipids.

## Chapter 4: Novel Artificial Chemical Nucleases Induce DNA Cleavage

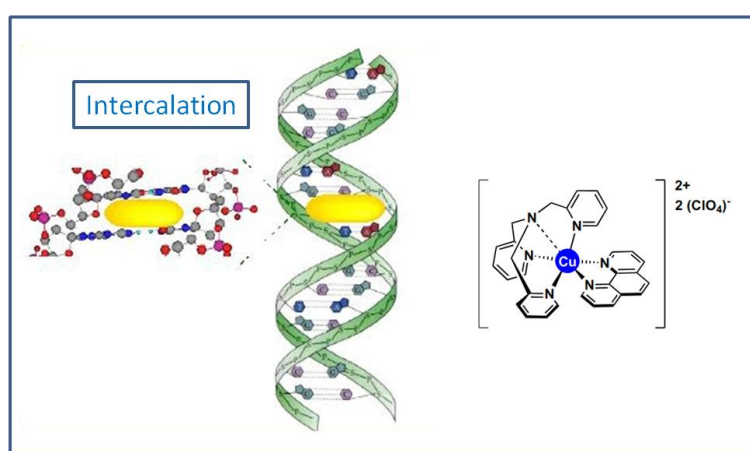
The project described in this chapter was carried out in the frames of my secondment at Dublin City University, in the National Institute for Cellular Biotechnology under the supervision of Professor Andrew Kellett. The synthesis, purification and full spectroscopic characterization of the complexes used was achieved by ESR Nicolo Fantoni. The results obtained by my work were focused on the AMN's series  $[\text{Cu}(\text{TPMA})(\text{N},\text{N}')_2]^2$  reactivity and the induced DNA damage. I examined the ability of these materials for precise cleavage of DNA along with the oxidation properties. Finally, DNA damage fragments were produced in DCU laboratories after treatment with AMN. The isolation, purification and enzymatic digestion to single nucleosides was achieved in CNR, Bologna along with the studies of lesions by stable isotope dilution LC-MS / MS analysis.

The majority of the results presented in this Chapter were published in Chem. Eur. J.; Zuin Fantoni, N. , Molphy, Z. , Slator, C. , Menounou, G. , Toniolo, G. , Mitrikas, G. , McKee, V. , Chatgialloglu, C. and Kellett, A. (2018), Polypyridyl-based Copper Phenanthrene Complexes: A New Type of Stabilized Artificial Chemical Nuclease. (doi:10.1002/chem.201804084).

### 4.1. Introduction

A very promising strategy against diseases such a cancer, is the insertion of molecules between the planar bases of DNA with ultimate goal to inhibit DNA replication in rapidly growing cancer cells.<sup>19</sup> This process is well known as intercalation and the outcome is correlated with structural distortions towards the DNA helix. Small molecules that cleave DNA play important roles in gene editing and cancer chemotherapy such as the metallo-intercalators, which are complexes of a metal cation with polycyclic aromatic ligands.<sup>196</sup> The mechanism of intercalation was proposed for the first time by Leonard Lerman in 1961, as it follows.<sup>197</sup> In aqueous isotonic solution, the cationic intercalator is attracted electrostatically to the surface of the polyanionic DNA. The negative charges of oxygen atoms in the phosphate groups across the DNA's structure are balanced by sodium and/or magnesium cations, which play the role of a "condensation cloud". In the case of metallo-intercalators, the metal center displaces these cations that surround DNA and as a result, a weak

electrostatic association is formed between the metallo-intercalator and the outer surface of DNA.<sup>198</sup> From this position, the planar ligand diffuses along the surface of the DNA and may slide into the hydrophobic environment found between two base pairs that may transiently "open" to form an intercalation site. This process allows the intercalator to move away from the hydrophilic environment surrounding the DNA into the intercalation site.<sup>199</sup> The base pairs transiently form such openings due to energy absorbed during collisions with solvent molecules. In **Scheme 8** is presented the dynamically open space between the DNA base pairs by unwinding, in order for the potential metallointercalator to fit in.



**Scheme 8.** Novel metallodrug's Cu-TPMA-Phen reactivity as intercallator.

This unwinding initiate a cascade of local structural changes to the DNA strand, such as lengthening or twisting of the base pairs. Once the structural modifications occur, functional changes of DNA are inevitable.<sup>200</sup> These changes are mediated by reactive oxygen species often leading in inhibition of transcription and replication, as well as other DNA repair processes, which makes intercalators high potential anticancer therapeutics.<sup>201</sup> Moreover, since ROS are generated in the vicinity of nucleic acids, are able to react with the sugar part of the nucleosides by an electron abstraction, leading to long range electron transfer (ET) reactions across the double helix. The intercalators might either donate electrons to, or accept electrons from, the double helix, thus actively participating in ET reactions.<sup>202</sup> During this process among the ROS formed, superoxide ion can abstract an electron to form a DNA base radical cation, commonly termed a "hole". These holes can migrate by electron transfer (ET)

over quite long distances along the DNA double helix, generally ending at guaninerich regions because of their lower oxidation potential.<sup>203</sup> As presented in **Figure 43** below, the resulting guanine radical cations ( $G^\bullet$ ) can be removed by a variety of reactions, for instance by further oxidation to 8-oxoguanine and subsequent repair. There is evidence that G-C rich areas of the DNA can act as electron sinks to remove “holes” from important coding regions.<sup>204</sup>

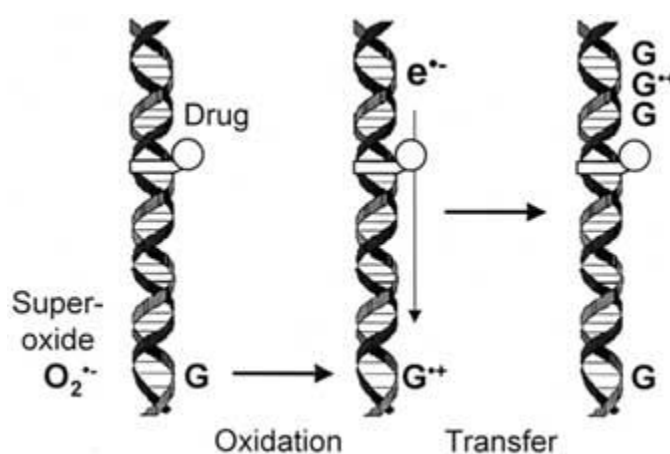


**Figure 43.** Cartoon showing how ROS such as superoxide ion interact with DNA to form a radical cation (“hole”) that can subsequently migrate by ET along the double helix. Migration generally terminates at a G-C rich region where the radical cation is removed by other oxidation reactions. However, it may also interact with and influence the action of DNA binding proteins. The presence of an intercalated DNA binding drug, acting as either electron donors or electron acceptors, can potentially modulate ET reactions.<sup>202</sup>

Alternatively, a more potent ROS such as a hydroxy radical might abstract hydrogen from the sugar moiety of DNA, initiating a sequence that results in DNA cleavage.

## 4.2. Copper Complexes as Intercalators with Endonuclease Reactivity

In general, metallo-intercalators mimic the cleavage portion of natural endonuclease machinery by cutting DNA molecules at or near specific base sequences.<sup>205</sup> As they are versatile and amenable to engineering, coordination compounds with artificial metallo-nuclease (AMN) activity are an attractive alternative to natural nucleases where, despite their sequence specificity, limited selectivity impedes precise cleavage of longer DNA fragments.<sup>143,206,207</sup> The advantage of metallo-nucleases is the fact that induce cleavage in DNA by targeting the cancer cells and impeding faithful cell replication by an oxidation pathway, mediated by formation of ROS.<sup>21,208,209</sup> Once the DNA damage occurs is generally irreversible and relies on binding of the activated AMN to its requisite target site *via* groove binding, insertion or intercalation interactions.<sup>210</sup> Copper compounds are attractive choices for AMNs given their biologically-accessible redox properties and wide structural variability.<sup>65</sup> Another factor is the bioavailability and essentiality of copper to the human body where a daily uptake of between 1.0 – 3.0 mg is required.<sup>211</sup> Copper ion homeostasis may, therefore, facilitate both tolerance and the active transport of exogenous copper based AMNs.<sup>212</sup> A wide range of copper(II) AMNs are known,<sup>213,214,215</sup> but one of best studied examples is Sigman's reagent  $[\text{Cu}(\text{1,10-phenanthroline})_2]^{2+}$  (Cu-Phen), which oxidises DNA in the presence of a reductant and/or oxidant. The mechanism of Cu-Phen, in its reduced Cu(I) form, includes intercalation in A-T rich sites in the minor groove before abstracting a hydrogen atom from the C1' position of deoxyribose to mediate strand excision.<sup>216,217,218,219,220</sup>

Inspired by Cu-Phen, heteroleptic systems were designed with phenazine intercalators (*e.g.* dipyridoquinoxaline (DPQ), dipyridophenazine (DPPZ), and benzo[*i*]dipyridophenazine (DPPN))<sup>221,222</sup> together with TPMA due to the stabilisation and coordination flexibility of this ligand, as presented in **Figure 44**.

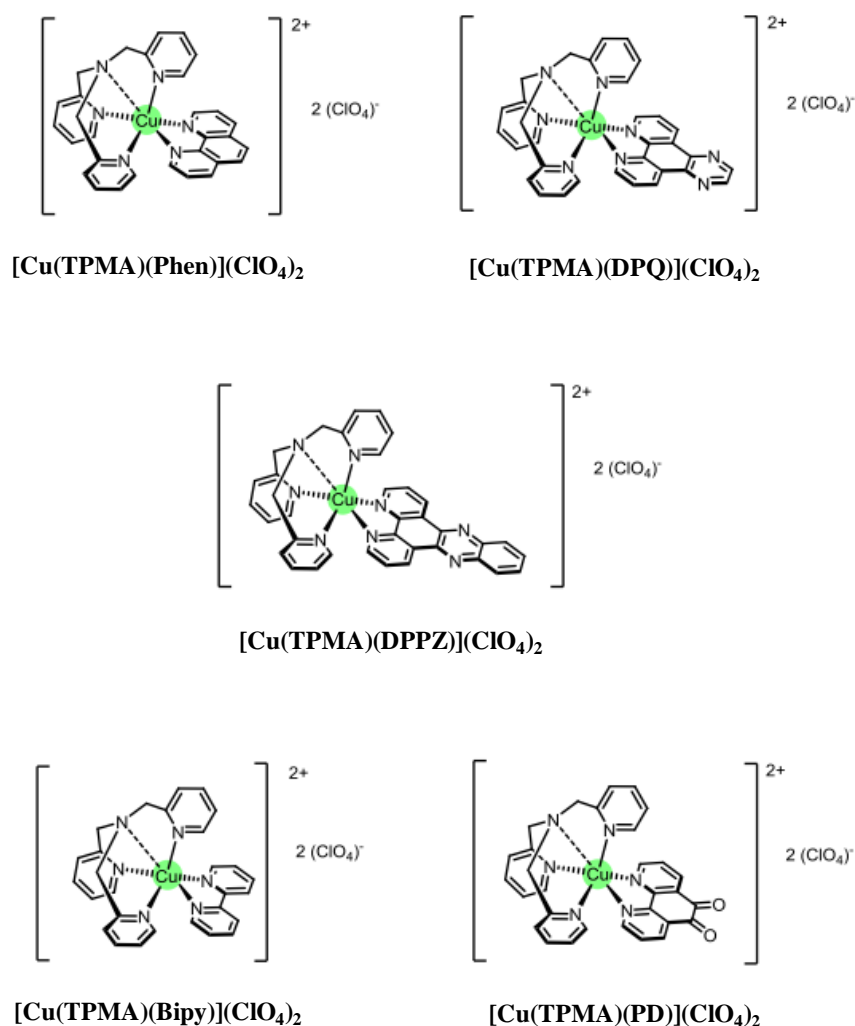
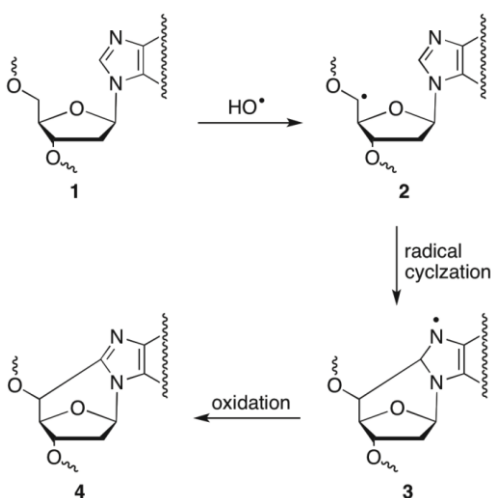


**Figure 44.** Structures of the five  $[\text{Cu}(\text{TPMA})(N,N')]^{2+}$  complexes.

The complexes are effective AMNs when reduced to Cu(I) and the damage profiles show enhanced activity compared to classical Sigman and Fenton reagents. In our studies, we investigated the DNA oxidation properties of the  $[\text{Cu}(\text{TPMA})(N,N')]^{2+}$  complex series. More specifically, using supercoiled pUC19 DNA the efficiency of single-strand breaks (SSBs) and double-strand breaks (DSBs) in a concentration range for each complex, presence / absence of reductant and different incubation time points was determined with the use of gel electrophoresis. An interesting scenario regarding the mechanism of action of these novel intercalators was furnished in the presence of major groove recognition elements, spin-trapping scavengers of reactive oxygen species (ROS) and DNA repair enzymes with glycosylase and/or endonuclease activity.

### 4.3. AMN's Reactivity and Formation of Lesions

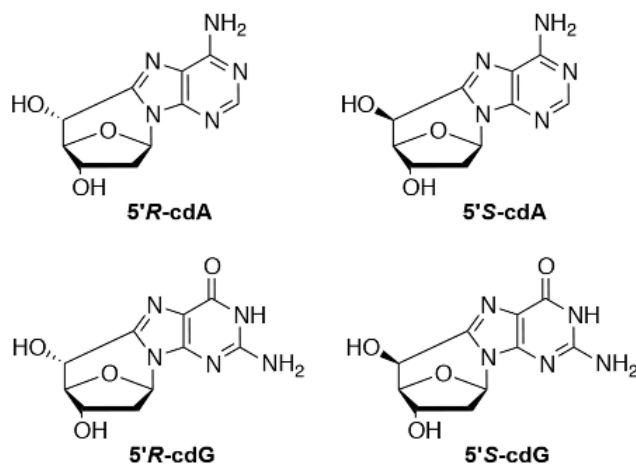
As discussed previously, the artificial chemical nucleases interact with DNA in a targeted manner and is expected a site-specific modification *via* oxidative/free radical chemistry. We thought to investigate the DNA damage mechanism and the formation of specific oxidative lesions of nucleic acids,<sup>223</sup> such as 8-oxo nucleotide formation, as well as a characteristic modification of purine nucleosides, the 5',8-cyclo-2'-deoxyadenosine (cdA) and 5',8-cyclo-2'-deoxyguanosine (cdG), which are considered biomarkers of radical stress.<sup>224,225</sup> 5,8-cyclopurines, both adenosine and guanosine are identified as lesions in human cellular DNA and they are proven to be highly mutagenic. These lesions are known to accumulate with aging in a tissue specific manner<sup>226</sup> and are recognized by the human nucleotide excision repair system.<sup>227,228</sup> cPu are formed by the action of hydroxyl radicals ( $\bullet\text{OH}$ ) and they are considered as tandem lesions due to the fact that the damage occurs at two sites, both the sugar part of the molecule and also at the purine base.<sup>229</sup> The mechanism that these lesions are formed, is described in the following scheme.



**Scheme 9.** Purine 2'-deoxynucleoside (**1**) reacts with hydroxyl radical (HO) yielding the purine 5',8-cyclo-2'-deoxynucleoside (cPu, **4**) via cyclisation of C5' radical (2→3).

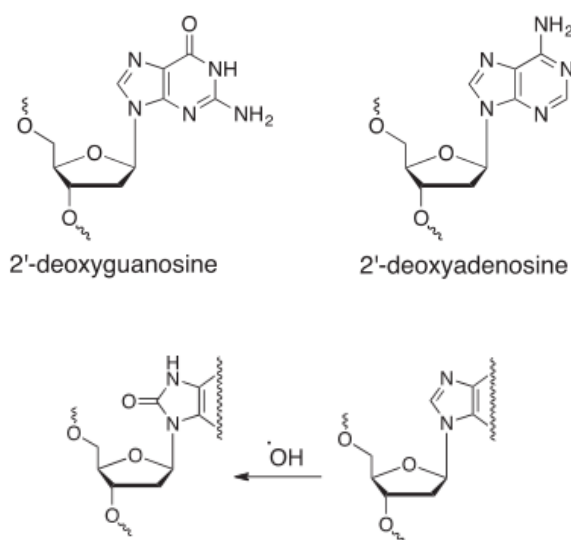
It is known that the initial step towards their formation is the abstraction of the H5' hydrogen atom of the 2'-deoxyribose moiety by hydroxyl radical, followed by intramolecular cyclization between C5' and C8 and subsequent oxidation of the N7 radical.<sup>230,231</sup> When this intramolecular cyclization takes place it is possible to achieve the formation of the two

diastereoisomers  $5'R$  and  $5'S$  of the 5',8-cyclo-2'-deoxyadenosine (cdA) and 5',8-cyclo-2'-deoxyguanosine (cdG), these structures are presented in **Scheme 10**.



**Scheme 10.** Structures of 5',8-cyclo-2'-deoxyadenosine (cdA) and 5',8-cyclo-2'-deoxyguanosine (cdG) in their  $5'S$  and  $5'R$  diastereomeric forms.

In contrast to sugar H-atom abstraction, both hydroxyl radical and superoxide radical anion attack on purine base moieties is widely known to generate lesions of 8-oxo-dG and 8-oxo-dA (**Scheme 11**), that impact on genome structural integrity, mutagenicity, excision repair, and polymerase fidelity.<sup>232,233</sup>



**Scheme 11.** Purine 2'-deoxynucleosides react with hydroxyl radicals yielding in 8-oxo-dG and 8-oxo-dA lesions.

We thought to treat supercoiled plasmid DNA with two different AMN's Cu-TPMA-Phen or Cu-Oda in the presence of reductant and incubation at 37 °C for 1 hr. Regarding Cu-Oda, this agent's ability to catalyze intracellular superoxide ( $O_2^{\cdot-}$ ) and singlet oxygen ( $^1O_2$ ) formation, as radical species mediating the oxidative DNA damage, was recently demonstrated.<sup>234</sup> The radical specie mediating the scission mechanism of Cu-TPMA-Phen is superoxide ( $O_2^{\cdot-}$ ) as discussed previously. We were interested to examine if the formation of the lesions described above occurs after treatment with these two metallodrugs.

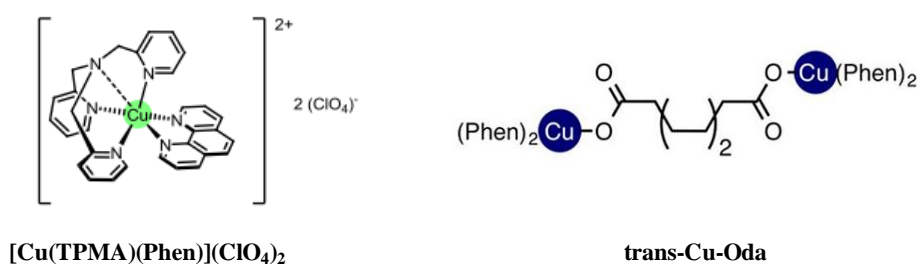


**Figure 45.** Molecular structures of Cu-TPMA-Phen and *di*-nuclear copper complex Cu-Oda.

The DNA damage fragments were extracted, isolated, and purified for oxidative lesion quantification analysis. These fragments were enzymatically hydrolyzed to single nucleosides and analyzed by stable isotope liquid chromatography with tandem mass spectrometry for the determination of the oxidatively-induced purine lesions (8-oxo-dA, 8-oxo-dG, 5'*R*-cdA, 5'*S*-cdA, 5'*R*-cdG and 5'*S*-cdG) in accordance to the protocol established by our group.<sup>235,236</sup> The quantification of the lesions (in lesions/ $10^6$  normal nucleosides units) in the digested samples (spiked with the isotopic labelled internal standards of 8-oxo-dA, 8-oxo-dG, 5'*R*-cdA, 5'*S*-cdA, 5'*R*-cdG and 5'*S*-cdG prior to digestion) was based on the parallel quantification of the unmodified nucleosides after HPLC clean-up and sample enrichment and the quantification of the single lesions by stable isotope dilution LC-MS/MS analysis.

## 4.4. Materials and Methods

### 4.4.1. DNA Binding Studies

#### Topoisomerase I Inhibition Assay

400 ng of pUC19 plasmid DNA (NEB, N3041) were exposed to varying concentrations of each copper complex (0.1 - 400  $\mu$ M) for 30 min at room temperature ( $\sim$ 20  $^{\circ}$ C) in a final volume of 20  $\mu$ L containing 80 mM HEPES buffer (pH 7.2), 10X CutSmart<sup>®</sup> buffer (NEB, B7204), and 100X BSA (NEB, B9000). 1 unit of topoisomerase I (*E. coli*) (NEB, M0301) was added to the reaction mixture and incubated for 20 min at 37  $^{\circ}$ C to ensure relaxation of supercoiled plasmid DNA. The reaction was stopped through the addition of 0.25% SDS and 250  $\mu$ g/mL protein kinase (Sigma Aldrich). To remove protein from the DNA, samples were then incubated for 30 min at 50  $^{\circ}$ C. DNA supercoiling was assessed by agarose gel electrophoresis in the absence of EtBr. 6X loading dye was added and topoisomers of DNA were separated by electrophoresis in 1X TBE buffer at room temperature for 240 min at 40 V and 180 minutes at 50 V. The agarose gel was post-stained using an EtBr bath and photographed using a UV transilluminator.<sup>237</sup>

### 4.4.2. DNA Damage Studies

#### DNA Cleavage in the Presence of Added Reductant

Stock solutions of the complexes were initially prepared in DMF and further dilutions prepared in 80 mM HEPES buffer (pH 7.2). 400 ng superhelical pUC19 plasmid DNA was exposed to increasing concentrations of each test complex in the presence of 25 mM NaCl and 1 mM Na-*L*-ascorbate. Reaction mixtures were vortexed and incubated at 37  $^{\circ}$ C for 30 min. 6X loading buffer (Fermentas) containing 10 mM Tris-HCl, 0.03% bromophenol blue, 0.03% xylene cyanole FF, 60% glycerol, 60 mM EDTA was added to each sample before loading onto a 1.2 % agarose gel containing 4  $\mu$ L EtBr. Electrophoresis was carried out at 70 V for 90 minutes in 1X TAE buffer and photographed using a UV transilluminator.<sup>221</sup>

### DNA Cleavage in the Presence of Non-Covalent DNA Binding Agents

400 ng pUC19 was pre-incubated with 25 mM NaCl, 1 mM Na-*L*-ascorbate and 8  $\mu$ M of methyl green in 80 mM HEPES for 45 min at 37 °C. Samples were vortexed and varying concentrations of test complexes were then introduced (Cu-TPMA: 10, 15, 20, 25  $\mu$ M and Cu-TPMA-Phen / CuTPMA-DPQ / Cu-TPMA-DPPZ: 1, 2.5, 5, 7.5  $\mu$ M). The reaction mixture was further incubated at 37 °C for 30 min and subjected to gel electrophoresis (prepared and stained as previously described).<sup>238</sup>

### DNA Cleavage in the Presence of ROS Scavengers

The assay was conducted according to the method recently reported by Slator *et al.*<sup>234</sup> Briefly, to a final volume of 20  $\mu$ L, 80 mM HEPES, 25 mM NaCl, 1 mM Na-*L*-ascorbate, and 400 ng of pUC19 DNA were treated with varying drug concentrations (Cu-TPMA: 5, 10, 15, 20, 25  $\mu$ M and Cu-TPMAPhen / Cu-TPMA-DPQ / Cu-TPMA-DPPZ: 1, 2, 3, 4, 5  $\mu$ M) in the presence ROS scavengers; 4,5dihydroxy-1,3-benzenedisulfonic acid (Tiron) (10 mM), D-Mannitol (10 mM), *N*'-dimethylthiourea (10 mM), L-Methionine (10 mM), KI (10 mM), DMSO (10 %) and EDTA (100  $\mu$ M).<sup>239</sup> Reactions were vortexed and incubated at 37 °C for 30 min and electrophoresis carried out as previously stated.

### DNA Cleavage in the Presence of Repair Enzymes

Supercoiled pUC19 DNA (400 ng) in 8 mM HEPES, 25 mM NaCl, 1 mM Na-*L*-ascorbate in a final volume of 20  $\mu$ L, was pre-incubated with test series for 30 min at 37 °C at various concentrations. The following reactions were supplemented with associated buffers as per manufacturer recommendations; those with Fpg contained 1 mg/mL BSA and 1X NEB Buffer 1, Endo III with 1X NEB Buffer 1, Endo IV with 1X NEB Buffer 3, Endo V with 1X NEB Buffer 4 and hAAG with 1X ThermoPol. Subsequently, 2U of repair enzymes FpG (NEB, M0240S), endonuclease (Endo) III (NEB, M0268S), Endo IV (NEB, M0304S), Endo V (NEB, M0305S) and hAAG (NEB, M0313S) were added to the reaction mixture and incubated for 30 min, 37 °C. Samples were denatured with 0.25 % SDS, 250  $\mu$ g/mL proteinase K and heated to 50 °C for 20 min. Reactions solutions were loaded onto a 1.2%

agarose gel (4  $\mu$ L EtBr) with 6X loading buffer and subjected to electrophoresis at 70 V for 70 min and imaged using UV transilluminator.

#### 4.4.3. Identification and Quantification of 8-oxo-Pus and cdPus Lesions In The Presence of AMNs

Nuclease P1 from *Penicillium Citrinum*, phosphodiesterase I and II, alkaline phosphatase from bovine intestinal mucosa, DNase I and DNase II, benzonase 99%, BHT, deferoxamine mesylate and pentostatin were purchased from Sigma-Aldrich, RNase T1 was from Thermo Fisher Scientific and RNase A from Roche Diagnostic GmbH, (Mannheim, Germany). The 3 kDa cut-off filters were obtained from Millipore (Bedford, USA). Solvents (HPLC-grade) were purchased from Fisher Scientific.

#### pUC19 Plasmid DNA Treated with Cu-TPMA-Phen or Cu-Oda to Induce Cleavage

Stock solutions of the complexes were initially prepared in DMF and further dilutions prepared in 80 mM HEPES buffer (pH 7.2). 400 ng superhelical pUC19 plasmid DNA was exposed to 2.5  $\mu$ M concentration of Cu-TPMA-Phen or Cu-Oda in the presence of 25 mM NaCl and 1 mM Na-L-ascorbate. Reaction mixtures were vortexed and incubated at 37 °C for 60 min. Reactions were repeated to generate sufficient stocks of nicked and linear pUC19 for subsequent experiments. Nicked and linearized dsDNA were then purified from the enzymatic reaction using QIAquick purification (QIAGEN, Baltimore, MD), eluted in pure water, and quantified using the NanoDrop (ND-1000) spectrophotometer.<sup>240</sup>

#### Enzymatic Digestion of the dsDNA Samples (SC, OC, L) to Nucleosides

About 20  $\mu$ g isolated DNA were dissolved in 100  $\mu$ L of Ar flushed 10 mM Tris-HCl (pH 7.9), containing 10 mM MgCl<sub>2</sub>, 50 mM NaCl, 0.2 mM pentostatin, 5  $\mu$ M BHT and 3 mM deferoxamine and the internal standards were added ([<sup>15</sup>N<sub>5</sub>]-5'S-cdA, [<sup>15</sup>N<sub>5</sub>]-5'R-cdA, [<sup>15</sup>N<sub>5</sub>]-5'S-cdG, [<sup>15</sup>N<sub>5</sub>]-5'R-cdG and [<sup>15</sup>N<sub>5</sub>]-8-oxo-dA). Three units of benzonase (in 20 mM Tris-HCl pH 8.0, 2 mM MgCl<sub>2</sub> and 20 mM NaCl), 4 mU phosphodiesterase I, 3 U DNase I, 2 mU of phosphodiesterase II and 2 U of alkaline phosphatase were added and the mixture was

incubated at 37 °C. After 21 h, 35 µL of Ar flushed buffer containing 0.3 M AcONa (pH 5.6) and 10 mM ZnCl<sub>2</sub> were added along with 0.5 U of Nuclease P1 (in 30 mM AcONa pH 5.3, 5 mM ZnCl<sub>2</sub> and 50 mM NaCl), 4 mU PDE II and 125 mU of DNase II and the mixture was further incubated at 37 °C for extra 21 h. A step-quenching with 1% formic acid solution (final pH 7) was followed, the digestion mixture was placed in a microspin filter (3 kDa) and the enzymes were filtered off by centrifugation at 14.000 g. (4 °C) for 20 min. Subsequently, the filtrate was freeze-dried before HPLC analysis, clean-up and enrichment.<sup>241</sup>

#### Analysis by High-Performance Liquid Chromatography, Clean-up and Enrichment

HPLC-UV clean-up and enrichment of the enzyme free samples were performed on a 4.6 mm x 150 mm Atlantis® dC18, 100 Å column (5 µm particle size, Waters) loaded with a 4.6 mm x 20 mm Guard Column 2pK (Atlantis® dC18 5µm, Waters) on a Waters Alliance® HPLC System (Waters e2695 Separations Module) including a Waters 2998 Photodiode Array (PDA) detector. The Empower 3 software was used for the chromatographic instrument control and data processing. The gradient program used an eluent composed by 2 mM ammonium formate (solvent A), acetonitrile (solvent B) and methanol (solvent C) and the flow rate was set at 1 mL/min. Briefly, the gradient program initiated with 99% solvent A, increasing solvent B from 1% to 30% within 35 min, then immediately solvent C from 0% to 40% for 5 min, closing with initial conditions for 5 min re-equilibration. The fractions containing the lesions were collected (the time windows were identified by injection of a pure standard of a lesions mixture). The collected fractions were freeze-dried, pooled, freeze-dried again, and redissolved in Milli-Q water before been injected for LC-MS/MS analysis. The quantification of the unmodified nucleosides was based on their absorbance at 260 nm.<sup>233b</sup>

#### Measurement of Modified Nucleosides by LC-ESI-MS/MS

An LC-MS/MS system Finnigan TSQ Quantum Discovery Max triple-stage quadrupole mass spectrometer (Thermo, USA), equipped with electrospray ionization (ESI) source in positive mode was employed for the detection and quantification of the lesions in the enzymatically digested DNA samples. Separation of target analytes was achieved with a Finnigan Surveyor LC system, equipped with a Finnigan Surveyor AS autosampler (Thermo, USA). The Xcalibur software 2.1 SP 1160 was used to control the mass spectrometric parameters and for

data acquisition. The collected fractions after HPLC analysis were subsequently injected to the LC-MS/MS system loaded with a 2.1 mm × 150 mm Atlantis dC18, 100 A column (3 μm particle size, Waters) guarded by a 2.1 mm × 10 mm Guard Column 2pK (Atlantis<sup>®</sup> dC18 3 μm, Waters). The gradient elution program used for the chromatographic separation of the DNA lesions initiated with 99% of 2 mM ammonium formate (solvent A) and 1% acetonitrile (solvent B) (held for 1 min), increasing solvent B from 1% to 9.8% within 20 min and then immediately to 15% solvent B (held for 5 min), closing with initial conditions for 10 min re-equilibration. The flow rate remained constant at 0.2 mL/min, the injection volume was 30 μL and column temperature was set at 30 °C. Detection was performed in multiple reaction monitoring mode (MRM) using the two most intense and characteristic precursor/product ion transitions for each DNA lesion.<sup>233b</sup>

#### Statistical Analysis

A two-tailed  $p$ -value  $< 0.05$  was considered to indicate a statistically significant difference. Statistical analysis was performed using  $t$ -test by comparing the means of DNA sample treated with one of the two artificial chemical nucleases (Two-Sample Assuming Unequal Variances) and error bars represent standard deviation of the mean, calculated from three independent samples. \*denotes a statistically significant difference ( $p \leq 0.05$ ), \*\*denotes a statistically significant difference  $p \leq 0.001$  and \*\*\*denotes a statistically significant difference  $p \leq 0.0001$  between the groups.

## 4.5. Results and Discussion

### 4.5.1. DNA Binding Studies - Topoisomerase I-Mediated Relaxation

The five  $[\text{Cu}(\text{TPMA})(N,N')]^{2+}$  complexes have broadly similar structures and in the **Figure 46** below the structural characteristics of each artificial chemical nuclease is presented. All organic ligands were characterized by  $^1\text{H}$  and  $^{13}\text{C}$  nuclear magnetic resonance and also by Fourier transform infrared (FTIR) spectroscopies. Each Cu(II) complex was isolated in order to moderate to high yields and characterized by elemental analysis, ESI-MS, UV-Vis and cw-EPR was employed to analyze the copper complex solution structures.

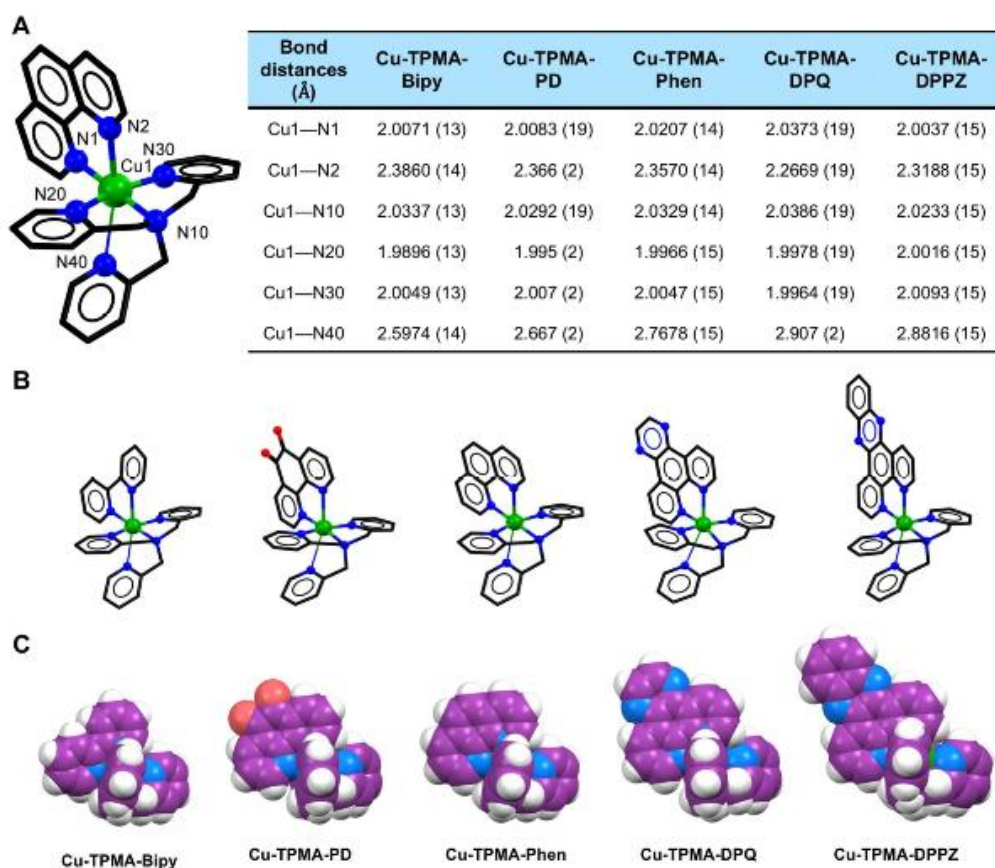
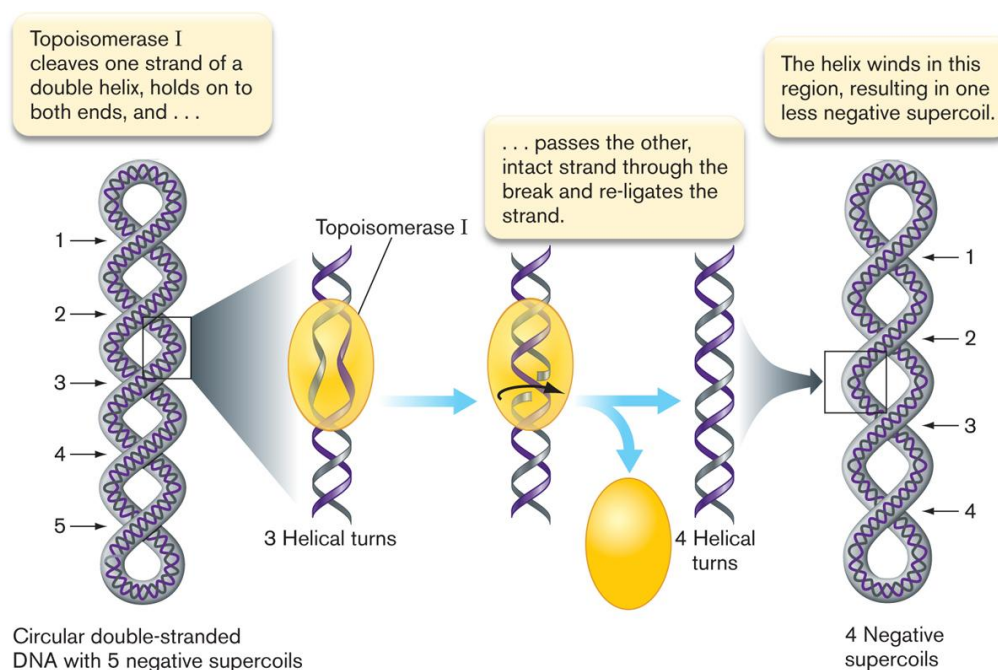


**Figure 46.** (A) Perspective view of Cu-TPMA-Phen cation highlighting the numbering scheme of non-carbon atoms and table outlining the six Cu—N distances found in Cu-TPMA-Bipy, Cu-TPMA-PD, Cu-TPMA-Phen, Cu-TPMA-DPQ and Cu-TPMA-DPPZ complexes respectively; (B) perspective views of the complexes (anions and hydrogen atoms omitted for clarity and the long Cu1—N40 bond is shown as a thin line. Colour scheme: copper, green; nitrogen, blue; carbon, black; oxygen, red); and (C) space filled view of the complex series (Colour scheme: copper, green; nitrogen, blue; carbon, plum; and oxygen, red).

Among the experiments performed towards the investigation of these novel metallodrugs' mechanism, are the ones regarding the DNA binding. Although several biochemical and biophysical methods are available to study the intercalation of a small molecule between two consecutive base pairs of DNA, the topoisomerase I-mediated DNA relaxation assay was chosen.<sup>242</sup> This assay is highly efficient and in the test supercoiled plasmid (pUC19) DNA is used to mimic the topological constraints of genomic DNA. Topoisomerase I is fundamental in biological systems as DNA supercoiled is generated during cellular processes including gene transcription, DNA replication, recombination and repair; this enzyme acts by forming a transient break in the DNA phosphodiester backbone permitting topological relaxation to occur prior to strand resealing. Topoisomerase I is capable of manipulating DNA structures via formation of a protein / DNA complex (referred to as the “cleavable complex”) in a 1:1 stoichiometry able to cut one strand of the double DNA helix.<sup>243</sup> Subsequently, a reversible nicking reaction occurs from a nucleophilic attack between the free 5'-OH group of the opened strand and the 3'-phosphotyrosyl bond, to give back a native and relaxed DNA helix and a functional free topoisomerase I enzyme, ready to initiate a new enzymatic cycle. Topoisomerase is described like a hand as it surrounds with its fingers tightly clamped around the DNA helix,<sup>244</sup> and the enzymatic reaction cycle is presented in **Scheme 12** below.



**Scheme 12.** Cartoon representation of topoisomerase I enzymatic reactivity.<sup>245</sup>

The unwinding assay using topo I relies on the ability of the enzyme to efficiently relax the plasmid with its bound intercalator followed by the resupercoiling of the plasmid upon removal of the intercalator.<sup>246</sup> Circular DNA can assume different degrees of supercoiling ranging from the fully relaxed form to the fully supercoiled form. The degree of supercoiling defines distinct forms of the plasmid referred to as topoisomers. Topoisomers can be separated as more or less discrete bands using gel electrophoresis since resistance to migration through such gels decreases with degree of supercoiling. The degree of supercoiling present after treatment reflects the degree of intercalation.<sup>247</sup>

In our studies unwinding by copper(II) complexes was examined between 0.1 – 400  $\mu\text{M}$  and the results pointed out that although Cu-TPMA-Phen could not unwind pUC19 below 50  $\mu\text{M}$ , Cu-TPMA-DPQ and Cu-TPMA-DPPZ complexes fully relaxed (0) the plasmid at 1.0  $\mu\text{M}$  with higher concentrations generating a positively (+) supercoiled DNA indicating a strong propensity to intercalate as presented in **Figure 47**.

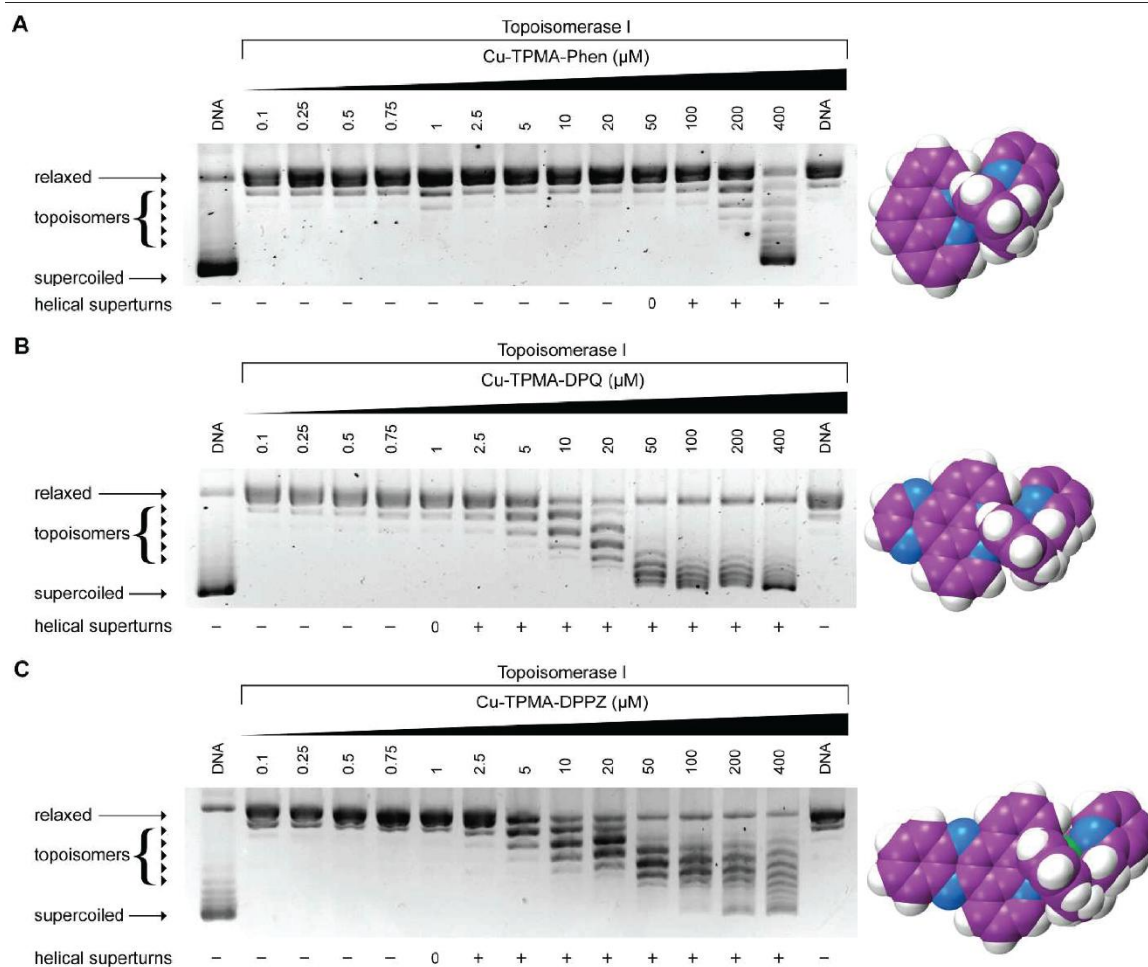


**Figure 47.** Release of topological tension from supercoiled plasmid DNA using the topoisomerase I-mediated relaxation assay in the presence of increasing concentrations of A Cu-TPMA-Phen; B Cu-TPMA-DPQ and C Cu-TPMA-DPPZ along with space-filling view of respective complex. Color scheme: copper, green; nitrogen, blue; carbon, plum; and oxygen, red).

This type of assay proves the ability of compounds to unwind negatively supercoiled DNA plasmid upon intercalative binding.

#### 4.5.2. Artificial Chemical Nuclease Activity

In the next steps, the studies regarding the DNA cleavage occurred. As discussed previously, in the absence of exogenous reductant no reaction took place, even over an extended concentration range as evidenced by electrophoresis (see Appendix **Figure S31**). The *in situ* generation of copper(I)<sup>248</sup> is crucial in order the artificial chemical nuclease to initiate the mechanism of cleavage and it has been demonstrated that the mixing of ascorbate and Cu(II) generates very active oxygen species, which have DNA scission reactivity.<sup>249,250</sup> Once copper(I) is formed, it can be linked with an oxygen atom of the phosphate group in the nucleobase structure and spontaneously the aromatic ligand of the complex intercalates *via*  $\pi$  stacking interactions with the desoxyribose.<sup>251</sup>

The most suitable conditions to compare the copper complexes involved the addition of exogenous reductant (ascorbate) to the complex, followed by 30 min incubation with pUC19. Under these conditions Cu-TPMA (10 – 25  $\mu$ M) was found to nick DNA and fully convert supercoiled (SC) to open circular (OC) DNA (**Figure 48**, lanes 1 – 5), while Cu-TPMA-Bipy and Cu-TPMA-PD were incapable of mediating appreciable oxidative DNA damage (Appendix **Figure S-32**). Cu-TPMA-Phen, Cu-TPMA-DPQ and Cu-TPMA-DPPZ complexes however, all produced OC DNA at lower concentrations (1.0 – 7.5  $\mu$ M) with linear conformations (L) arising with Cu-TPMA-Phen and Cu-TPMA-DPQ complexes (**Figure 48**, lanes 6-20).

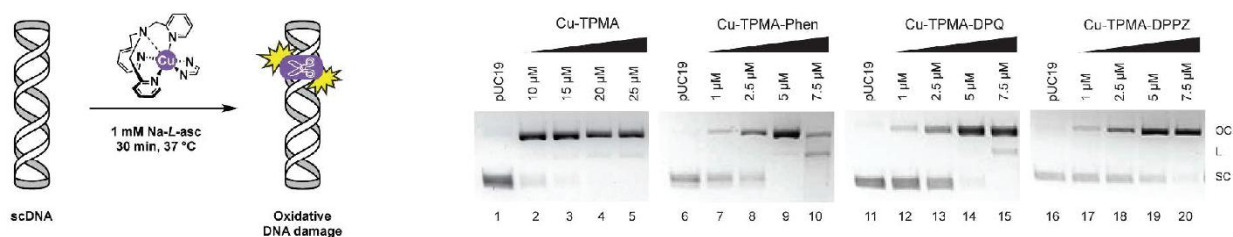


**Figure 48.** Cartoon representation of nuclease experiment where 400 ng pUC19 supercoiled DNA was treated with increasing concentrations of Cu-TPMA (lanes 2-5), Cu-TPMA-Phen (lanes 7-10), Cu-TPMA-DPQ (lanes 12-15) and Cu-TPMA-DPPZ (lanes 17-20) in the presence of 1 mM Na-L-ascorbate.

The overall trend in chemical nuclease activity is



that indicates the ancillary *N,N'* phenanthrene group is critical to ROS catalysis at the DNA interface.

### 4.5.3. Oxidative DNA Cleavage in the Presence of Non-Covalent DNA Binding Agents

In an attempt to determine DNA cleavage site specificity, the major groove (methyl green, MG) binder was pre-incubated with pUC19 DNA prior to the addition of test complex in the presence of reductant. MG significantly enhanced the oxidative chemical nuclease activity of Cu-TPMA-Phen (**Figure 49** lanes 7-10) and Cu-TPMA-DPQ (**Figure 49** lanes 12-15) when compared with MG-free experiments (**Figure 48** lanes 10 and 15). Here, plasmid DNA was completely degraded by 7.5  $\mu\text{M}$  of Cu-TPMA-Phen with extensive shearing evident in the Cu-TPMA-DPQ treated sample (**Figure 49** lanes 9-10 and 14-15). MG-directed enhancement of Cu-TPMA and Cu-TPMA-DPPZ complexes also occurred where the emergence of linear (L) DNA with 25  $\mu\text{M}$  treatment of Cu-TPMA (**Figure 49** lane 5), and full conversion of SC to OC by 5.0  $\mu\text{M}$  of Cu-TPMA-DPPZ (**Figure 49** lane 20) was observed. These results indicate the minor groove as the main site of oxidative DNA damage; by limiting access to the major groove with MG, the minor groove becomes 'primed' for DNA-metal complex interactions and, for this series significant additional damage was observed.

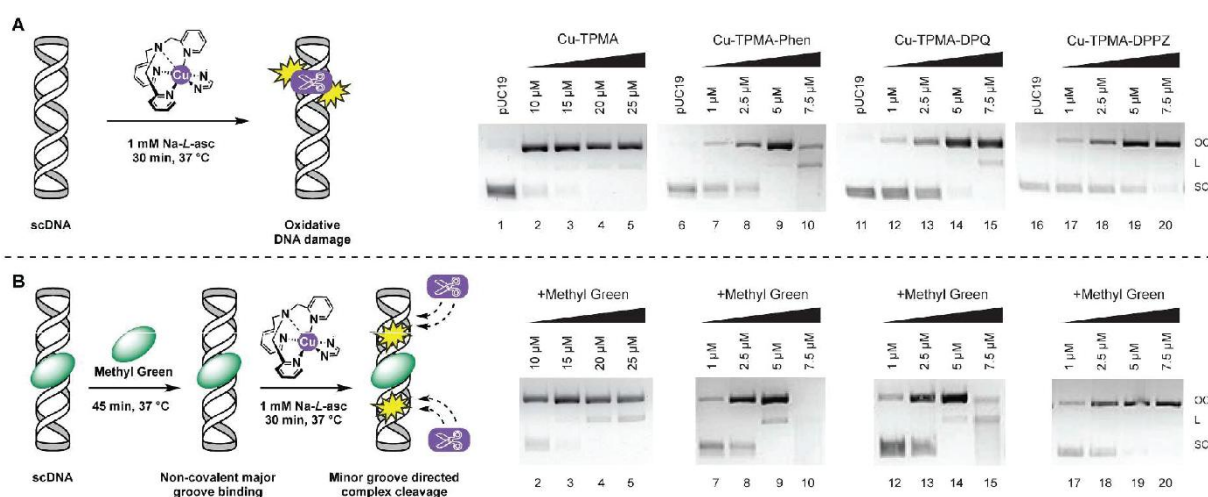


**Figure 49.** A) Cartoon representation of nuclease experiment where 400 ng pUC19 supercoiled DNA was treated with increasing concentrations of Cu-TPMA (lanes 2-5), Cu-TPMA-Phen (lanes 7-10), Cu-TPMA-DPQ (lanes 12-15) and Cu-TPMA-DPPZ (lanes 17-20) in the presence of 1 mM Na-L-ascorbate. B) Cartoon representation of DNA cleavage in the presence of non-covalent agent methyl green when 400 ng pUC19 supercoiled plasmid was pre-treated with the major groove binding agent methyl green prior to the introduction of Cu-TPMA (lanes 2-5), Cu-TPMA-Phen (lanes 7-10), Cu-TPMA-DPQ (lanes 12-15) and Cu-TPMA-DPPZ (lanes 17-20) in the presence of 1 mM Na-L-ascorbate.

#### 4.5.4. DNA Damage Mechanism

The one-electron difference between Cu(II) and Cu(I) allows copper to promote radical reactions, giving rise in the formation of ROS in the DNA interface. A variety of experiments was carried out including pre-incubation with ROS specific scavengers such as 4,5-dihydroxy-1,3-benzenedisulfonic acid (tiron), D-mannitol, L-methionine, and *N,N'*-dimethylthiourea (DMTU). These compounds were employed to probe the role of superoxide ( $O_2^{\cdot-}$ ), the hydroxyl radical ( $\cdot OH$ ), hydrogen peroxide ( $H_2O_2$ ), hypochlorous acid (HOCl) or a combination. The objective of this investigation was to gain an insight of the generated species that represent an important aspect of the mechanism. The results shown in **Figure 50**, point out that  $O_2^{\cdot-}$  is the most prevalent radical specie involved in the cleavage mechanism as in all cases, pre-incubation with tiron significantly impeded AMN activity. In these experiments, delayed onset of OC-DNA formation, inhibition of L-DNA, and protection of SC-DNA were evident.  $H_2O_2$  is also generated as part of the mechanism as DMTU somewhat impeded chemical nuclease activity.

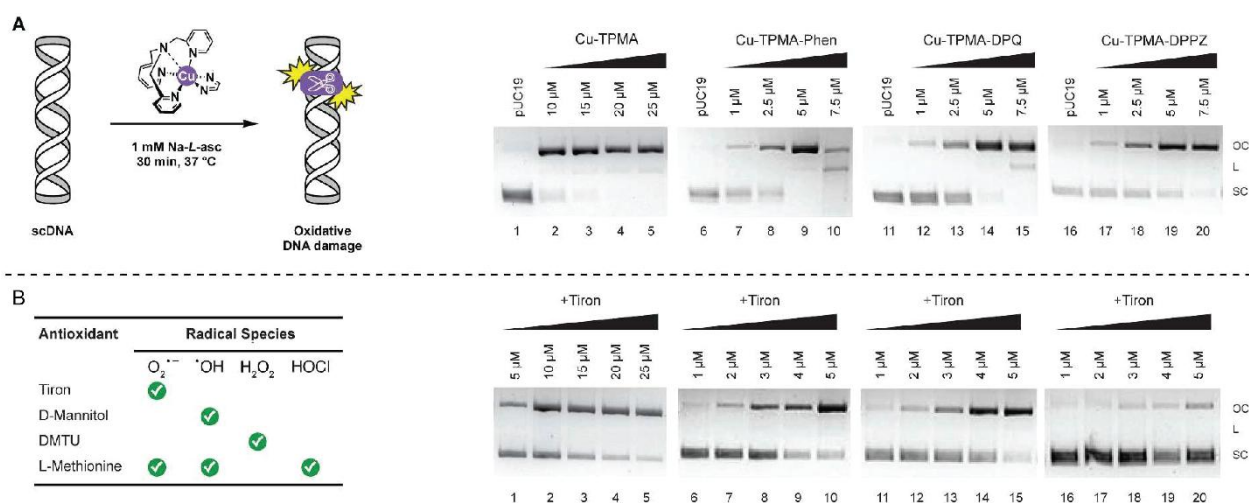


**Figure 50.** A) Cartoon representation of nuclease experiment where 400 ng pUC19 supercoiled DNA was treated with increasing concentrations of Cu-TPMA (lanes 2-5), Cu-TPMA-Phen (lanes 7-10), Cu-TPMA-DPQ (lanes 12-15) and Cu-TPMA-DPPZ (lanes 17-20) in the presence of 1 mM Na-L-ascorbate. B) Table showing ROS scavenging species employed in this study where 400 ng pUC19 supercoiled DNA was treated with increasing concentrations of Cu-TPMA (lanes 1-5), Cu-TPMA-Phen (lanes 6-10), Cu-TPMA-DPQ (lanes 11-15) and Cu-TPMA-DPPZ (lanes 16-20) in the presence of 1 mM Na-L-ascorbate and 10 mM scavenging species 4,5-Dihydroxy-1,3-benzenedisulfonic acid (Tiron).

Interestingly, as evidenced in **Figure 51** scavenging the OH radical had no influence on DNA cleavage and these results were validated in two independent experiments using D-mannitol and DMSO.

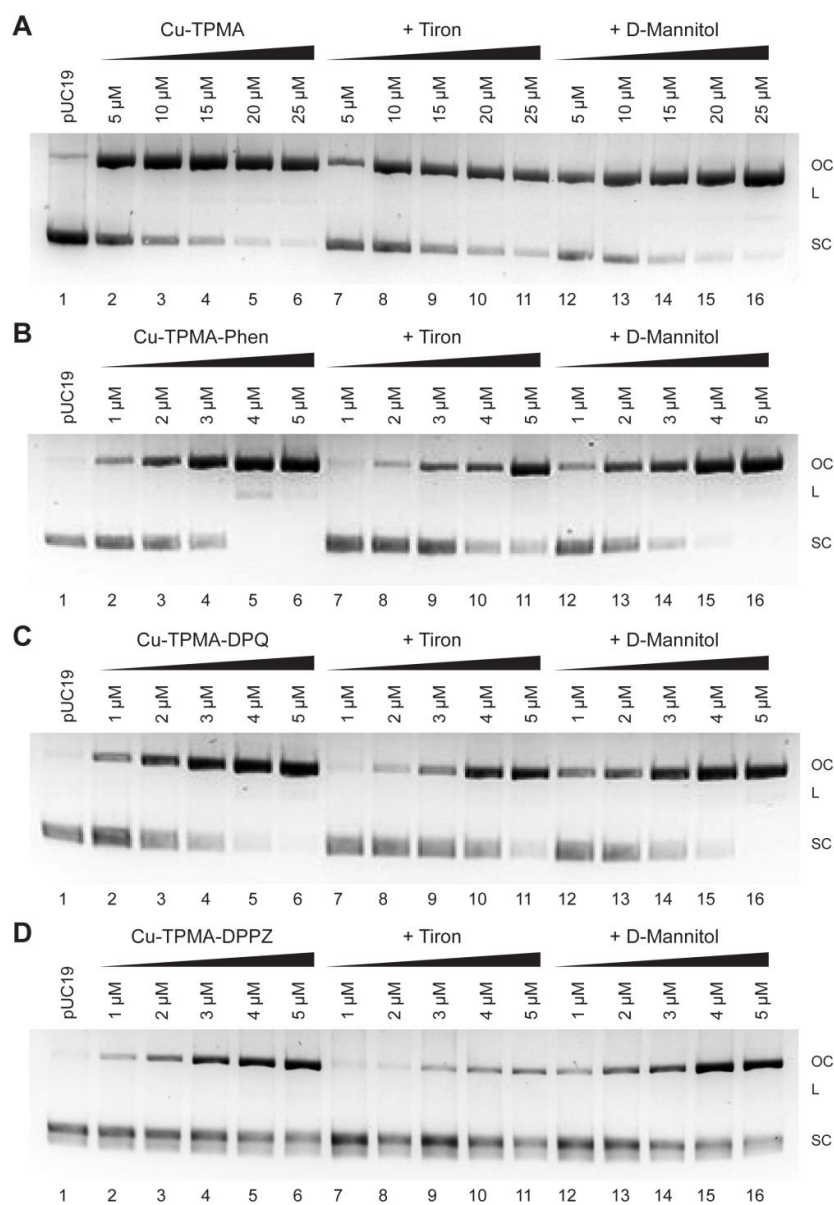


**Figure 51.** 400 ng pUC19 supercoiled DNA was treated with increasing concentrations of A) Cu-TPMA, B) Cu-TPMA-Phen, C) Cu-TPMA-DPQ and D) Cu-TPMA-DPPZ (lanes 1-6) in the presence of 1 mM Na-Lascorbate and 10 mM scavenging species 4,5-Dihydroxy-1,3-benzenedisulfonic acid (Tiron) (lanes 7-11) and D- Mannitol (lanes 12-16).

It is suggested that since the  $\cdot\text{OH}$  radical is not significant, the AMN activity of this class departs from classical Fenton-type or Haber-Weiss pathways.

#### 4.5.5. DNA Repair Enzyme Recognition

In another interesting series of experiments, DNA repair enzymes with glycosylase/endonuclease activity were used in order to demonstrate the distinctive DNA oxidation chemistry. In excision repair (BER) mechanism, repair enzymes are intrinsic check-points able to restore spontaneous DNA decomposition and mis-incorporation of mismatch sites, oxidized lesions and/or alkylated bases during the cell cycle.<sup>252</sup> A range of enzymes isolated from both prokaryotic and eukaryotic sources are able to recognize specific nucleoside modifications and excise the damage site to prime for subsequent repair processes. Cleavage experiments to identify the mechanism of oxidative damage utilizing a selected range of repair enzymes. Repair proteins with sole or combined lesion recognition, known as glycoylases, can incise DNA by removing the base and generating abasic sites (AB). Glycoylases and several repair endonucleases also recognise AP (apurine / apyrimidine) sites and mediate strand nicking adjacent to the base-free lesion (**Figure 52**) which can be identified by increased nicked, linear, and sheared forms of plasmid DNA. The enzymes used with endonuclease activity are reported below, as well as the nucleotide sequence recognized for cleavage for each restriction site.

- **Fpg** (formamidopyrimidine [fapy]-DNA glycosylase) (also known as 8-oxoguanine DNA glycosylase) acts both as a N-glycosylase and an AP-lyase. The N-glycosylase activity releases damaged purines from double stranded DNA, generating an apurinic (AP site). The AP-lyase activity cleaves both 3' and 5' to the AP site thereby removing the AP site and leaving a 1 base gap. Some of the damaged bases recognized and removed by Fpg include 7, 8-dihydro-8-oxoguanine (8-oxoguanine), 8-oxoadenine, fapy-guanine, methy-fapy-guanine, fapy-adenine, aflatoxin B<sub>1</sub>-fapy-guanine, 5-hydroxy-cytosine and 5-hydroxy-uracil.<sup>253,245</sup>
- **Endo III** Endonuclease III (Nth) protein from *E. coli* acts as both N-glycosylase and a AP-lyase. The N-glycosylase activity releases damaged pyrimidines from double-stranded DNA, generating a basic (AP site). The AP-lyase activity of the enzyme cleaves 3' to the AP site leaving a 5' phosphate and a 3' ring opened sugar. Some of the damaged bases recognized and removed by Endonuclease III include urea, 5, 6 dihydroxythymine, thymine glycol, 5-hydroxy-5 methylhydanton, uracil glycol, 6-hydroxy-5, 6-dihydrothimine and methyltartronylurea.<sup>245,254</sup>
- **Endo IV** Endonuclease IV can act on a variety of oxidative damage in DNA. The enzyme is apurinic/apyrimidinic (AP) endonuclease that will hydrolyse intact AP sites in DNA. AP

sites are cleaved at the first phosphodiester bond that is 5' to the lesion leaving a hydroxyl group at the 3' terminus and a deoxyribose 5'-phosphate at the 5' terminus. The enzyme also has a 3'-diesterase activity and can release phosphoglycolaldehyde, intact deoxyribose 5-phosphate and phosphate from the 3' end of DNA.<sup>255,256</sup>

- **Endo V** Endonuclease V is a repair enzyme found in *E. coli* that recognizes deoxyinosine, a deamination product of deoxyadenosine in DNA. Endonuclease V, often called deoxyinosine 3' endonuclease, recognizes DNA containing deoxyinosines (paired or not) on double-stranded DNA, single-stranded DNA with deoxyinosines and to a lesser degree, DNA containing abasic sites or urea, base mismatches, insertion/deletion mismatches, hairpin or unpaired loops, flaps and pseudo-Y structures. It is believed that Endonuclease V needs another protein to repair the DNA, as it does not remove the deoxyinosine or the damaged bases. Endonuclease V cleaves the second phosphodiester bonds 3' to the mismatch of deoxyinosine (2), leaving a nick with 3'-hydroxyl and 5'-phosphate.<sup>257,258,259,260</sup>
- **hAAG** Human Alkyladenine DNA Glycosylase (hAAG) excises alkylated and oxidative DNA damaged sites, including 3-methyladenine, 7-methylguanine, 1,N-ethenoadenine and hypoxanthine. hAAG catalyzes the hydrolysis of the N-glycosidic bond to release the damaged base. hAAG is also known as methylpurine DNA glycosylase (MPG) or 3-methyladenine-DNA glycosylase (ANPG).<sup>254,261</sup>

Reaction conditions for Cu-TPMA-Phen, Cu-TPMA-DPQ, Cu-TPMA-DPPZ (0.5 – 2.5  $\mu\text{M}$ ) complexes were optimized to initiate cleavage of pUC19 SC-DNA to OC and L forms (**Figure 53**) prior to repair enzyme addition (**Figure 52A**). These reactions were compared to 1 h exposure of pUC19 to each complex in the absence of repair enzymes (lanes 1-4, **Figure 52C** and D). Overall, enhanced cleavage activities in the order



were identified with limited change or inhibition occurring in the presence of Endo IV (**Figure 52D**). Control experiments involving Cu-Phen (0.5 – 2.5  $\mu\text{M}$ ), Cu-TPMA (1.0 – 20.0  $\mu\text{M}$ ) and the hydroxyl radical ( $\bullet\text{OH}$ ) generated from a  $\text{Cu}^{+2+}/\text{H}_2\text{O}_2$  / Fenton system were examined for comparative purposes (**Figure 52C** and **Figure S 33**). Here, enhanced activity by Cu-Phen in the presence of Endo III (APyrimidine) but not FpG (APurine) indicates preferential oxidative

damage of thymine residues. pUC19 in the presence of Fenton's reagent underwent additional cleavage by FpG, Endo III, and Endo IV which supports formation of oxidized purine and pyrimidine bases together with abasic sites by the  $\bullet\text{OH}$  radical. Interestingly, DNA damage by phenanthroline-containing complexes (Cu-TPMA-Phen and Cu-Phen) was attenuated upon addition of Endo IV and we propose this inhibition arises from covalent stabilization of the DNA adduct Endo IV complex. Additionally, since Endo IV had limited effects with Cu-TPMA, CuTPMA-DPQ, and Cu-TPMA-DPPZ this interaction seems phenanthroline ligand-specific.<sup>219,262</sup> These results are in good agreement with that work since trapping  $\text{O}_2^{\bullet-}$  with tiron and stabilizing Endo IV with Phen complexes reduces oxidative DNA damage. hAAG enhanced the cleavage activity of  $[\text{Cu}(\text{TPMA})(N,N')]^{2+}$  complexes but not  $[\text{Cu}(\text{TPMA})]^{2+}$  and, when combined with observations of additional DNA damage with Endo V, it seems reasonable to suggest deoxyinosine (dI) or free-base hypoxanthine is generated by these ternary compounds. dI is a naturally occurring noncanonical base that arises from deamination of adenine,<sup>263</sup> however it can be formed from radical generation of Ade-N6-yl.<sup>264</sup> The Ade-N6-yl radical may also be generated by  $\text{Cu}^{2+}/\text{H}_2\text{O}_2$  with elegantly designed immuno-spin trapping experiments establishing its formation *via* a 5,5'-dimethyl-1-pyrroline N-oxide (DMPO) nucleoside adduct.<sup>265</sup> The extent of hAAG-mediated DNA damage observed here is dependent on the ancillary ligand choice with bulkier intercalators giving rise to more extensive shearing (DPPZ > DPQ > Phen) suggesting a possible alternative deoxyinosine oxidation pathway.

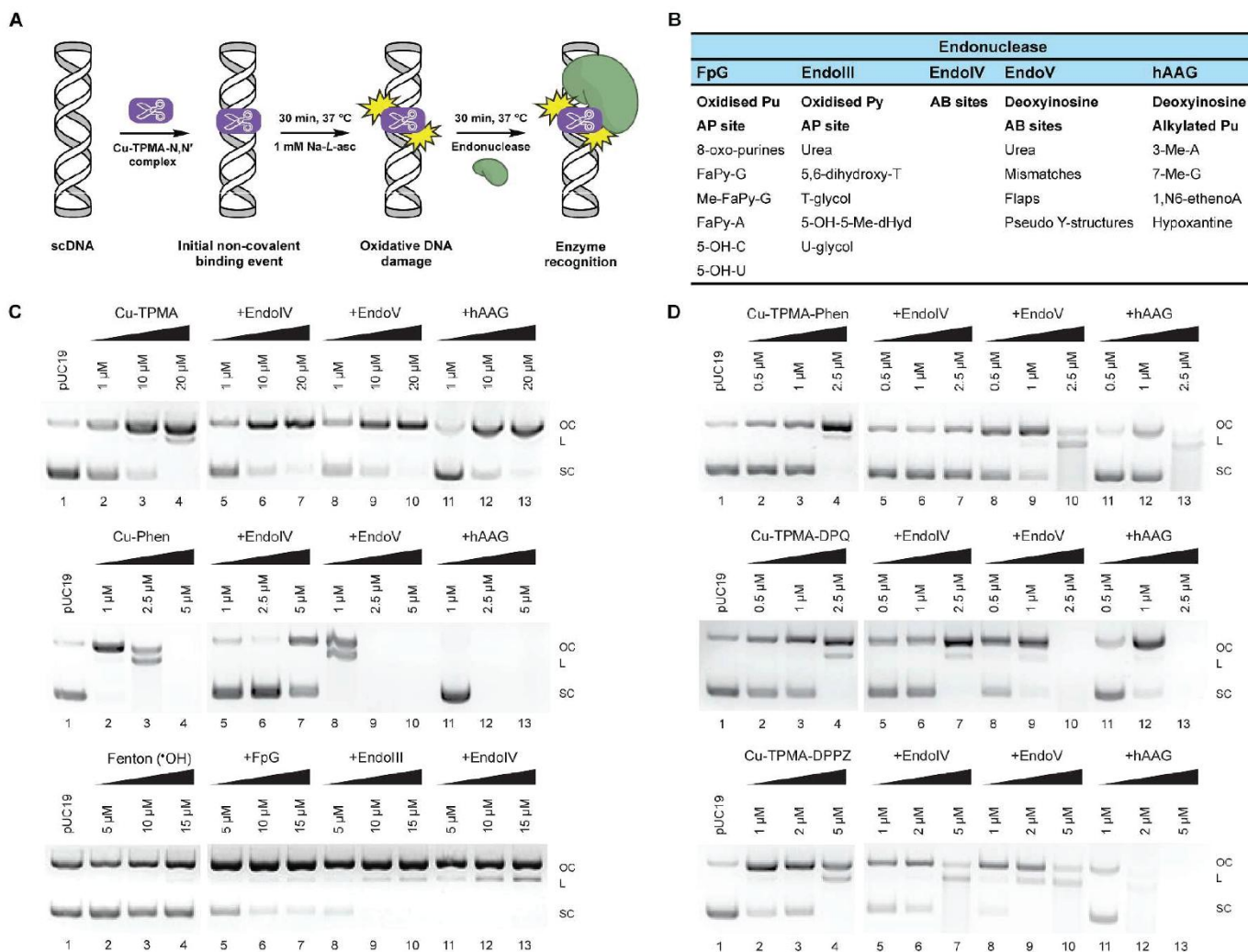


**Figure 52.** A) Cartoon representation of repair enzyme experiments. B) Table highlighting base lesion recognized or excised by respective repair enzymes. Abbreviations are as follows: A = adenine, G = guanine, T = thymine, C = cytosine, U = uracil, Pu = purines (A and G), Py = pyrimidines (C, T and U), Me = methyl, OH = hydroxy, H = hydro, dH = dihydro, FaPy = formamidopyrimidine, dHyd = deoxyhydantone, Me-Tar-U = methyltartronylurea, dI = deoxyinosine, dU = deoxyuracil. C) 400 ng pUC19 supercoiled DNA treated with increasing concentrations of Cu-TPMA and Cu-Phen (lanes 2-4) in the presence of 1 mM Na-L-ascorbate and 2U repair enzymes Endo IV (lanes 5-7), Endo V (lanes 8-10) and hAAG (lanes 11-13). Hydroxyl radical generated from  $\text{Cu}^{2+} / \text{H}_2\text{O}_2$  Fenton-system (lanes 2-4) in the presence of 1 mM Na-L-ascorbate and 2U repair enzymes Fpg (lanes 5-7), Endo III (lanes 8-10) and Endo IV (lanes 11-13). D) Cu-TPMA-Phen, Cu-TPMA-DPQ and Cu-TPMA-DPPZ (lanes 2-4) in the presence of 1 mM Na-L-ascorbate (lanes 2-4) in the presence of 1 mM Na-L-ascorbate and 2U repair enzymes Endo IV (lanes 5-7), Endo V (lanes 8-10) and hAAG (lanes 11-13).

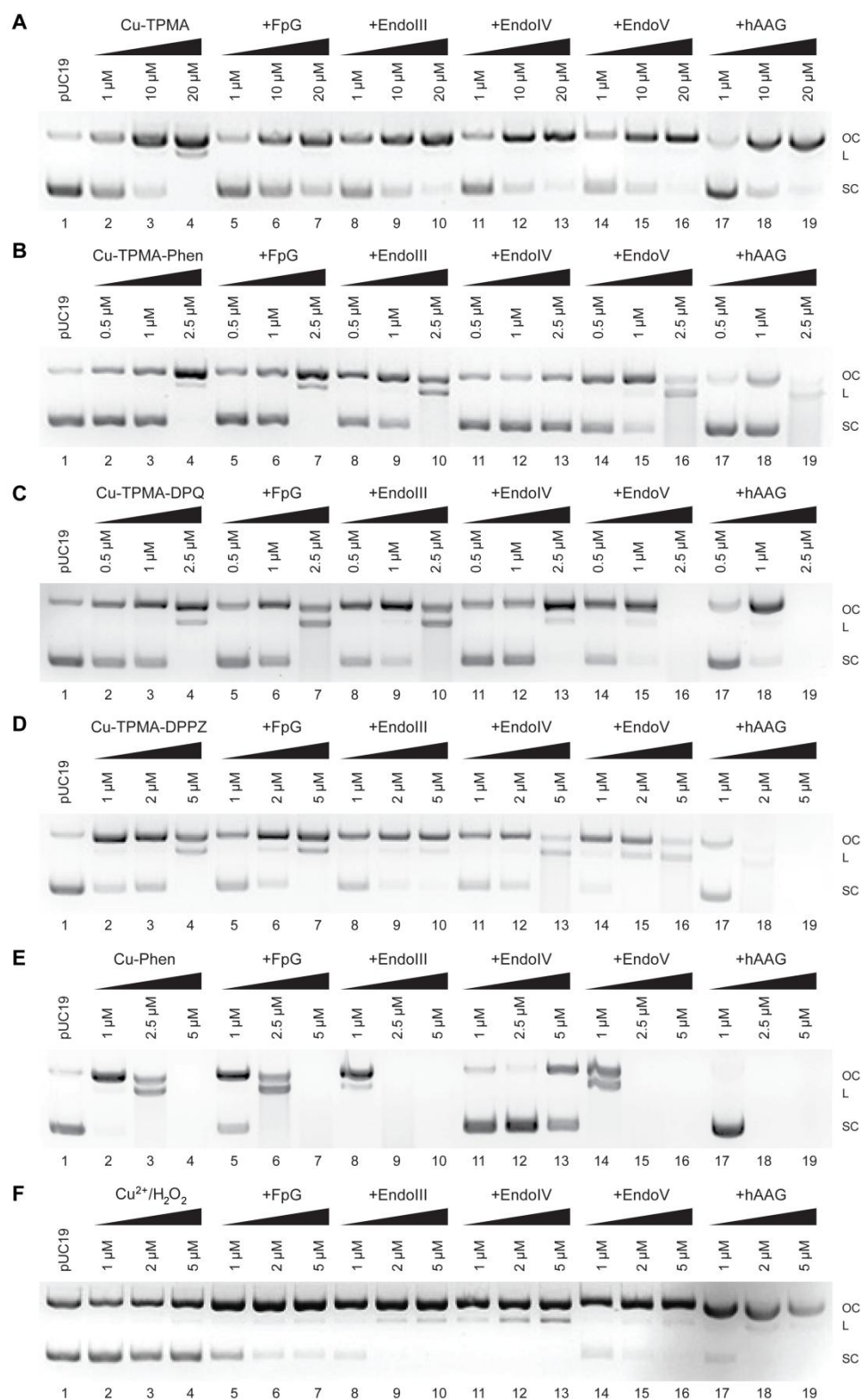


**Figure 53.** 400 ng pUC19 supercoiled DNA was treated with increasing concentrations of A) Cu-TPMA; B) Cu-TPMA-Phen; C) Cu-TPMA-DPQ; D) Cu-TPMA-DPPZ; E) CuPhen and F)  $\bullet\text{OH}$  - generated from  $\text{Cu}^{2+}/\text{H}_2\text{O}_2$ /Fenton-system (lanes 2-4) in the presence of 1 mM Na-L-ascorbate and in the presence of 2U of either FpG (lanes 5-7), Endo III (lanes 8-10), Endo IV (lanes 11-13), Endo V (lanes 14-16) or hAAG (lanes 17-19).

#### 4.5.6. AMNs-induced Oxidative Cleavage in Supercoiled Plasmid DNA

Plasmid pUC19 DNA was pre-incubated with Cu-TPMA-Phen or Cu-Oda at 37 °C for 1 h and to achieve the optimum annealing conditions a concentration range of the chemical nuclease in the presence of Na-*L*-ascorbate, as reducing agent (**Figure 54**) was tested by gel electrophoresis. The concentration pattern for the two complexes were identical and here as an example is presented the concentration range of gel electrophoresis regarding the Cu-TPMA-Phen.

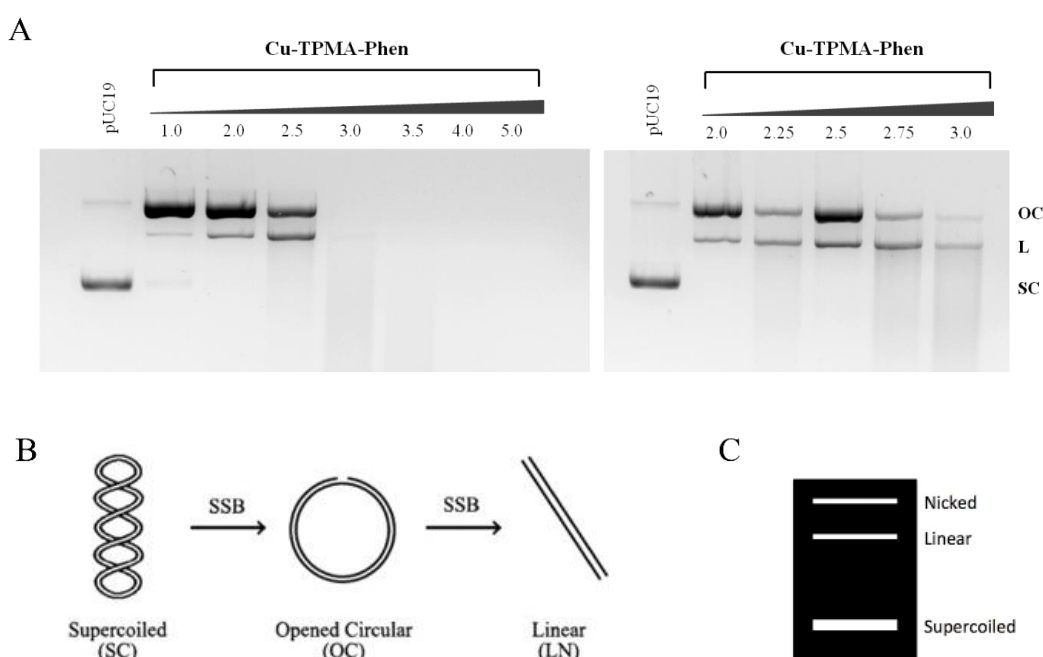


**Figure 54.** A) 400 ng pUC19 supercoiled DNA was treated with increasing concentrations of Cu-TPMA-Phen in the presence of 1 mM Na-*L*-ascorbate (Supercoiled (SC), relaxed (OC), and linear (L) pUC19 tertiary dsDNA structures). B) Conformation changes of the circular plasmid DNA. C) Identification of Supercoils and Nicks with gel electrophoresis.

The nuclease activity at 2.5 μM resulted in a satisfactory profile of DNA cleavage for both compounds. The reactions were repeated in order to generate sufficient stock of superhelical, nicked, and linear pUC19 for deoxynucleoside lesion experiments. At the end of each reaction, the nicked and linearized dsDNA obtained, was extracted and further purified using QIAquick

purification (QIAGEN, Baltimore, MD), eluted in pure water and quantified in triplicate using the NanoDrop (ND-1000) spectrophotometer.

#### Quantification of Purine Lesions in dsDNA Conformers

The double stranded DNA samples were analysed for both detection and quantification of the oxidative lesions 5',8-cyclo-2'-deoxyadenosine (cdA) and 5',8-cyclo-2'-deoxyguanosine (cdG), 7,8-dihydro-8-oxo-2'-deoxyguanosine (8-oxo-dG) and 7,8-dihydro-8-oxo-2'-deoxyadenosine (8-oxo-dA). Many efforts have been devoted during the last two decades to the identification and measurement of cdA and cdG lesions in DNA samples. As discussed previously, the initial step for the formation of these lesions is H5' abstraction by HO• followed by an intramolecular attack of C5' radical to the purine moiety. We were interested in evaluating these cyclopurine lesions along with 8-oxo-dG and 8-oxo-dA, due to the fact that they are “pure” hydroxyl radical-derived products and cannot derive from accidental oxidation of the material or other mechanistic pathways. The absence or presence of these modified nucleosides would provide strong evidence regarding the artificial chemical nucleases mechanism and the ability of these materials to lead in formation of hydroxyl radical. In the experiments plasmid pUC19 supercoiled DNA was treated with 2.5  $\mu$ M of Cu-TPMA-Phen or Cu-Oda in the presence of 1 mM Na-*L*-ascorbate and the DNA samples were incubated at 37 °C for 1 hr. As reported in the **Table 11** and **12** regarding the cdPus lesions there were no differences among the control and the treated with copper complexes samples.

**Table 11.** The levels (lesions/10<sup>6</sup> nucleosides) of 5'S-cdA, 5'R-cdA, 5'S-cdG, 5'R-cdG, 8-oxo-dG and 8-oxo-dA in plasmid pUC19 supercoiled DNA. The samples were treated with 2.75 μM of Cu-TPMA-Phen or Cu-Oda in the presence of 1 mM Na-L-ascorbate and were incubated at 37 °C for 1 hr. The numbers in the boxes represent the values of cdPus and 8-oxo-Pus levels from the measurement of the DNA samples treated with the corresponding artificial chemical nuclease.

	5'R-cdG	5'R-cdA	5'S-cdG	8-oxo-dG	5'S-cdA	8-oxo-dA
<b>Control_1</b>	1,136845	0,781867	0,544125	51,04514	0,726369	2,469849
<b>Control_2</b>	1,076143	0,798517	0,559943	51,86645	0,692755	2,518789
<b>Control_3</b>	1,002763	0,739285	0,545907	49,7245	0,66878	2,334653
<b>Cu-Oda_1</b>	1,099999	0,74943	0,557849	65,48203	0,696774	2,84609
<b>Cu-Oda_2</b>	1,020544	0,81555	0,528505	65,80299	0,717631	2,886687
<b>Cu-Oda_3</b>	1,087859	0,749696	0,553309	67,78948	0,723262	2,82568
<b>Cu-TPMA-Phen_1</b>	0,948632	0,822891	0,566882	52,42743	0,678022	2,52534
<b>Cu-TPMA-Phen_2</b>	1,0793	0,795448	0,533879	51,63888	0,6807	2,528848
<b>Cu-TPMA-Phen_3</b>	1,004791	0,734759	0,531472	51,69227	0,675909	2,434307

**Table 12.** The levels (lesions/10<sup>6</sup> nucleosides) of 5'S-cdA, 5'R-cdA, 5'S-cdG, 5'R-cdG, 8-oxo-dG and 8-oxo-dA in plasmid pUC19 supercoiled DNA treated with Cu-TPMA-Phen or Cu-Oda. The numbers in the boxes represent the mean value (± standard deviation) of cdPus and 8-oxo-Pus levels from the measurement of three DNA samples.

	5'R-cdG	5'R-cdA	5'S-cdG	8-oxo-dG	5'S-cdA	8-oxo-dA
<b>Control</b>	1,072 ± 0,067	0,773 ± 0,031	0,550 ± 0,009	50,879 ± 1,081	0,696 ± 0,029	2,441 ± 0,095
<b>Cu-Oda</b>	1,069 ± 0,043	0,772 ± 0,038	0,547 ± 0,016	66,358 ± 1,250	0,713 ± 0,014	2,853 ± 0,031
<b>Cu-TPMA-Phen</b>	1,011 ± 0,066	0,784 ± 0,045	0,544 ± 0,020	51,920 ± 0,441	0,678 ± 0,002	2,496 ± 0,054

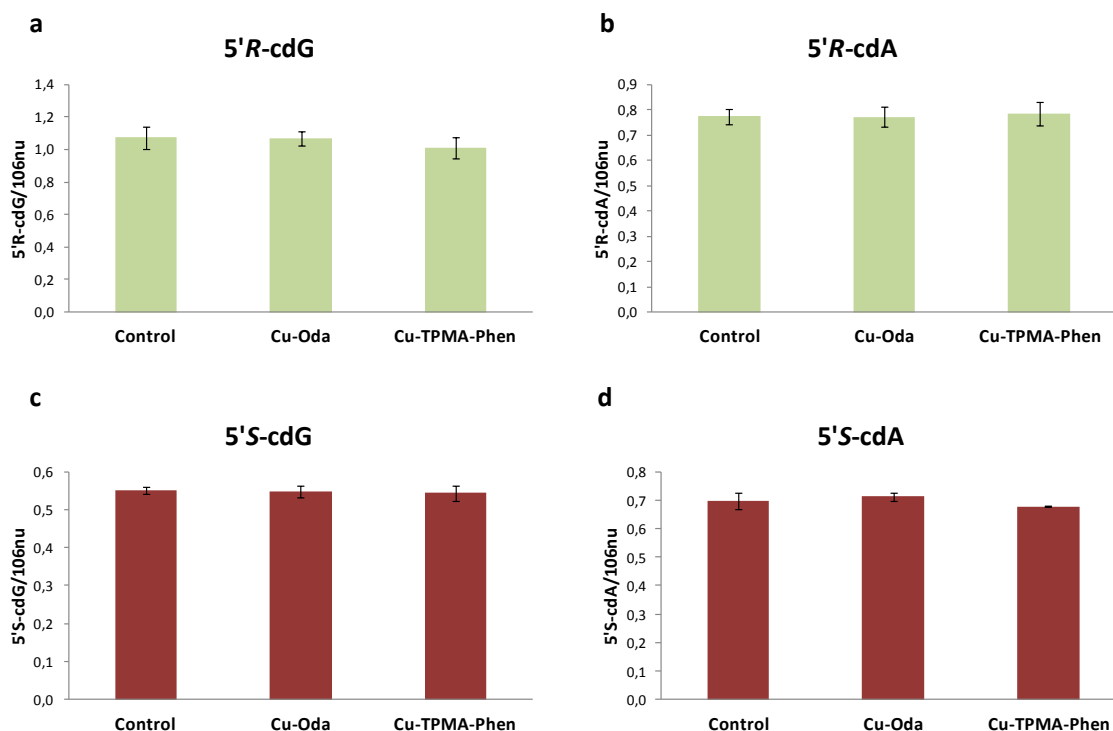


**Figure 55.** Levels of four cPu measured by LC-MS/MS in plasmid pUC19 supercoiled DNA treated with Cu-TPMA-Phen or Cu-Oda. Error bars represent standard deviation of the mean, calculated from three independent samples.

The results presented in **Figure 55** regarding Cu-TPMA-Phen are in good agreement with the results obtained from the gel electrophoresis, in which using D-mannitol or DMSO as OH radical scavengers had no influence on DNA cleavage. Three independent experiments evidence that •OH radical is not significant and the AMN activity does not follow the classical Fenton-type mechanism.

The reaction to obtain the DNA damage fragments was not carried out under anaerobic conditions. Therefore, in the presence of molecular oxygen and due to the redox potential of the copper complex the superoxide anion is generated, as suggested by the inhibition of damage in DNA when scavenging with tiron. Superoxide anion is the precursor of hydrogen peroxide<sup>266</sup> giving rise in the formation of 8-oxo-dA and 8-oxo-dG lesions. In the literature it is known that oxidative damage, such as 8-oxodeoxyguanosine (8-oxodG) lesions in DNA, is generated by endogenous by-products of cellular metabolism, such as hydrogen peroxide (H<sub>2</sub>O<sub>2</sub>).<sup>267</sup>

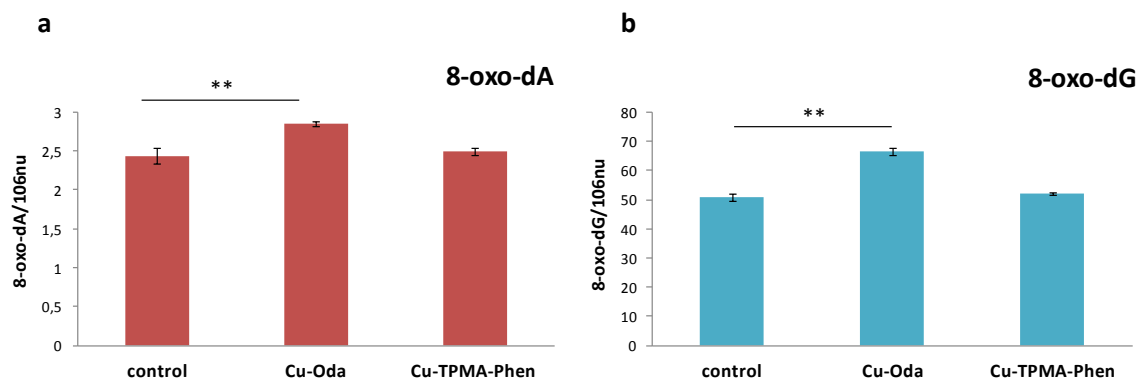


**Figure 56.** Levels of 8-oxo-dA and 8-oxo-dG measured by LC-MS/MS in plasmid pUC19 supercoiled DNA treated with Cu-TPMA-Phen or Cu-Oda. Statistical analysis was performed using *t*-test by comparing the means of DNA sample treated with one of the two artificial chemical nucleases (Two-Sample Assuming Unequal Variances) and error bars represent standard deviation of the mean, calculated from three independent samples. \*denotes a statistically significant difference ( $p \leq 0.05$ ), \*\*denotes a statistically significant difference  $p \leq 0.001$  and \*\*\*denotes a statistically significant difference  $p \leq 0.0001$  between the groups.

The overall 8-oxo lesion formation, regardless of topology, followed 8-oxo-dG  $\gg$  8-oxo-dA (**Figure 56**) after treatment with both AMNs. However, statistically significant difference was observed only in the presence of the di-nuclear copper complex Cu-Oda. These results point out that the ligand groups on the metallodrug play an important role. Although scavenger experiments showed that both AMNs are able to generate superoxide radical anion, the bulky ligand of TPMA can interfere and act as a block; ROS formation might not be in the vicinity of nucleic acids therefore the oxidative DNA damage does not occur.

## 4.6. Conclusions

The experiments presented proved that copper(II) artificial chemical nucleases are very promising materials as therapeutic agents especially when combined with specific scaffolds, essential for controlling stability and reactivity. DNA binding was identified and topoisomerase I-mediated relaxation revealed the importance of *N,N'* ligand choice to intercalation as Cu-TPMA-DPQ and Cu-TPMA-DPPZ complexes unwound supercoiled pUC19 DNA with greater efficiency. Further analysis showed the minor groove as the preferred site for AMN activity as pre-exposure to a major groove binder (methyl green) enhanced overall oxidative damage sensitivity to supercoiled pUC19 DNA. In terms of the oxidative mechanism, trapping experiments show that the complexes do not follow classical Fenton-type or Haber-Weiss processes but instead generate superoxide- and, to a somewhat lower extent, hydrogen peroxide during the catalytic ROS process. To delineate this activity from that of classical copper-bis-1,10-phenanthroline (Cu-Phen), Fenton-type systems, and the  $[\text{Cu}(\text{TPMA})]^{2+}$  cation, DNA repair enzyme recognition experiments were conducted. DNA damage lesions formed by Cu-TPMA-Phen, -DPQ, and -DPPZ complexes were not recognized by FpG or Endo III, which suggests—in contrast with Cu-Phen and Fenton's reagent—an oxidation pathway independent of oxidized purine and pyrimidine bases, respectively. The activity of Endo IV, which recognizes both apurine and apyrimidine sites, was inhibited by Cu-Phen and Cu-TPMA-Phen and it appears likely, therefore, that a covalent DNA-complex-enzyme adduct is realized. The role of deoxyinosine (dI) in the DNA damage process was established since hAAG and Endo V both enhanced cleavage activity of  $[\text{Cu}(\text{TPMA})(N,N')]^{2+}$  complexes; the ancillary ligand choice is important here with bulkier intercalators giving rise to more extensive hAAG-mediated shearing in the order DPPZ > DPQ > Phen.

In addition, cyclopurine lesions and 8-oxo-purines were identified and quantified on dsDNA mixtures of supercoiled (SC), open circular (OC), and linear (L) conformation, after treatment with Cu-TPMA-Phen or Cu-Oda in the presence of reductant. In the enzymatically digested nucleosides an HPLC clean-up protocol was applied and the fractions of interest containing the lesions, were collected and analyzed by LC-MS/MS. We focused on the four cPu lesions that are correlated directly with  $\text{HO}^\bullet$ -induced DNA damage due to the fact that they are strong candidate biomarkers in cancer diagnostics, particularly for their stability during the analytical procedures. However, the levels of these lesions were identical with the control proving that the hydroxyl radicals are not generated in the presence of these chemical nucleases. Finally,

the 8-oxopurine lesions appeared to have statistically significant differences in respect with the control; an interesting outcome that can be explained if we take into account the stereochemical factor of the bulky TPMA ligand in respect with the linear Cu-Oda. These results pointed towards the generation of hydrogen peroxide during the catalytic ROS process and the oxidation pathway induced by AMNs.

## Appendix

### Part I – Studies on Lipid Damage

#### 5.1. UV-VIS Spectra

##### *Reduction of Cu(II) to Cu(I) in Cu-TPMA-Phen and Formation of Thiyl Radical*

As shown in **Figure S1** regarding the d-d metal absorptions of Cu(II) complex a maximal absorbance at 626 nm was recorded, which falls after adding the thiol and at the same time a new absorbance at 412 nm rises. An intermediate complex of Cu(II)-thiol is generated, since the thiol is coordinated temporarily on the metal. In the following step via a redox-based mechanism Cu(I) is generated from Cu(II) and thiyl radical is formed. Probably small structural adjustments are necessary so that the copper(II) will be able to bind with the thiol. However, due to the multidentate ligand ability of this synthetic material any side effect on the overall stability of the complex was not noticed.

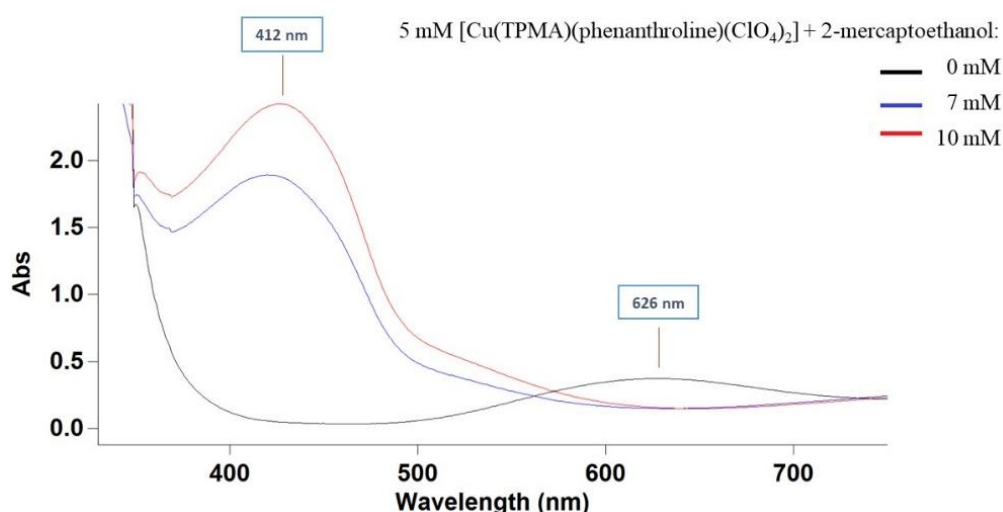


**Figure S1.** Selected spectra are shown after mixing the copper(II) complex with 2-ME at room temperature. As the reaction proceeds and the copper is reduced more and more by the addition of thiol, the fluorescence intensity is also increased.

## 5.2. Gas Chromatography

The phospholipids from 1-palmitoyl-2-oleoylphosphatidylcholine or soybean lecithin were examined by GC after transesterification to fatty acid methyl esters (FAME). The calibration of the gas chromatographic peak areas was effected by using the peak area of palmitic acid as the internal standard to quantify the corresponding presence of the unsaturated fatty acids and establish their reaction yields after the experiments.

After the reaction under the conditions described in **Chapter 2** was performed, GC was used to separate cis and trans isomers. In particular, in the figure below is reported the result of the experiment regarding the MUFA containing liposomes, under aerobic conditions prior and after treatment with Cu-TPMA-Phen and thiol (2-mercaptoethanol) and incubation at 37 °C for 60 min. In this figure it is evidenced the isomerization of oleic acid residue into its trans isomer, which is elaidic acid.

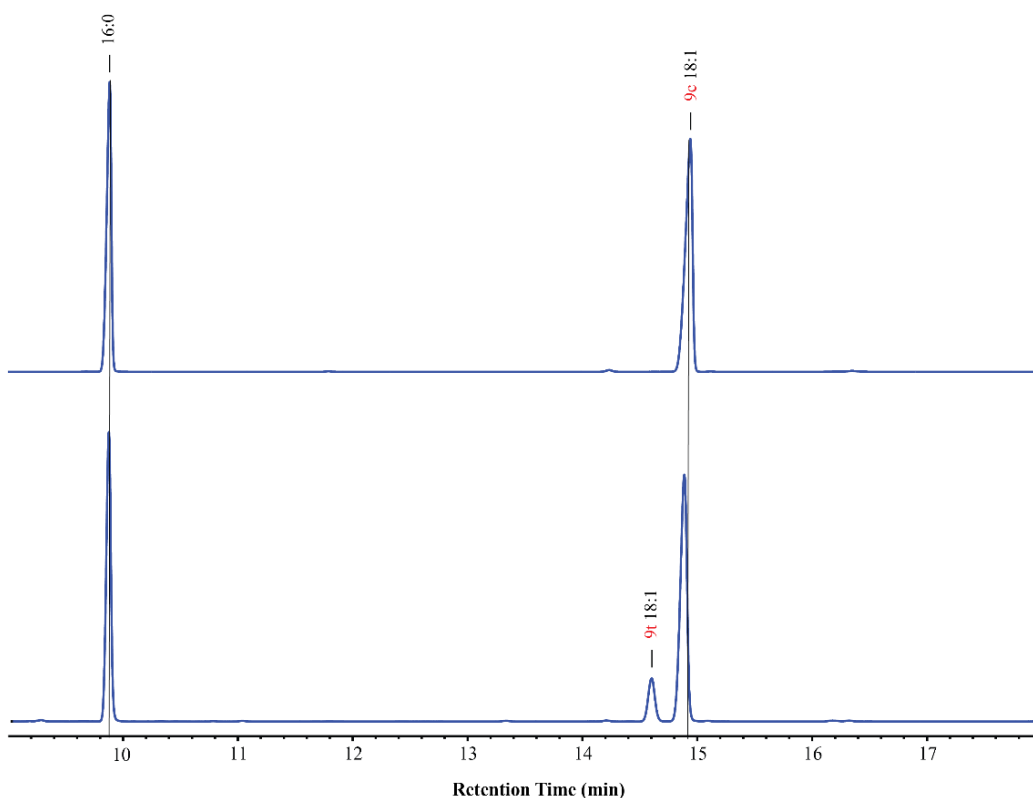


**Figure S2.** GC chromatogram of FAMEs obtained before and after incubation of POPC liposomes at 37 °C for 60 min, under aerobic conditions in the presence of 0.15 mM Cu-TPMA-Phen and 10 mM 2-ME.

In the experiments with the MUFA composed liposomes, no peroxidation was observed neither in aerobic nor in anaerobic conditions, due to the fact that the MUFA moiety of oleic acid (9cis-18:1) is not so prone to oxidation as PUFAs are. Therefore, this fatty acid residue can be targetted by thiyl radical only in a catalysed isomerization pathway.

On the other hand, in lecithin liposomes the PUFA can be partitioned both in isomerization or peroxidation pathways. We decided to monitor the 18:1 and 18:2 fatty acids under different liposome incubation conditions, since these two fatty acids are the most representative unsaturated moieties of the mixture. In **Figure S3**, is shown the GC chromatogram of lecithin FAMES without any treatment (starting material) trace I, also traces II and III, report the two different profiles depending on the presence or absence of oxygen after treatment with Cu-TPMA-Phen and thiol (2-mercaptoethanol) and incubation at 37 °C for 480 min.

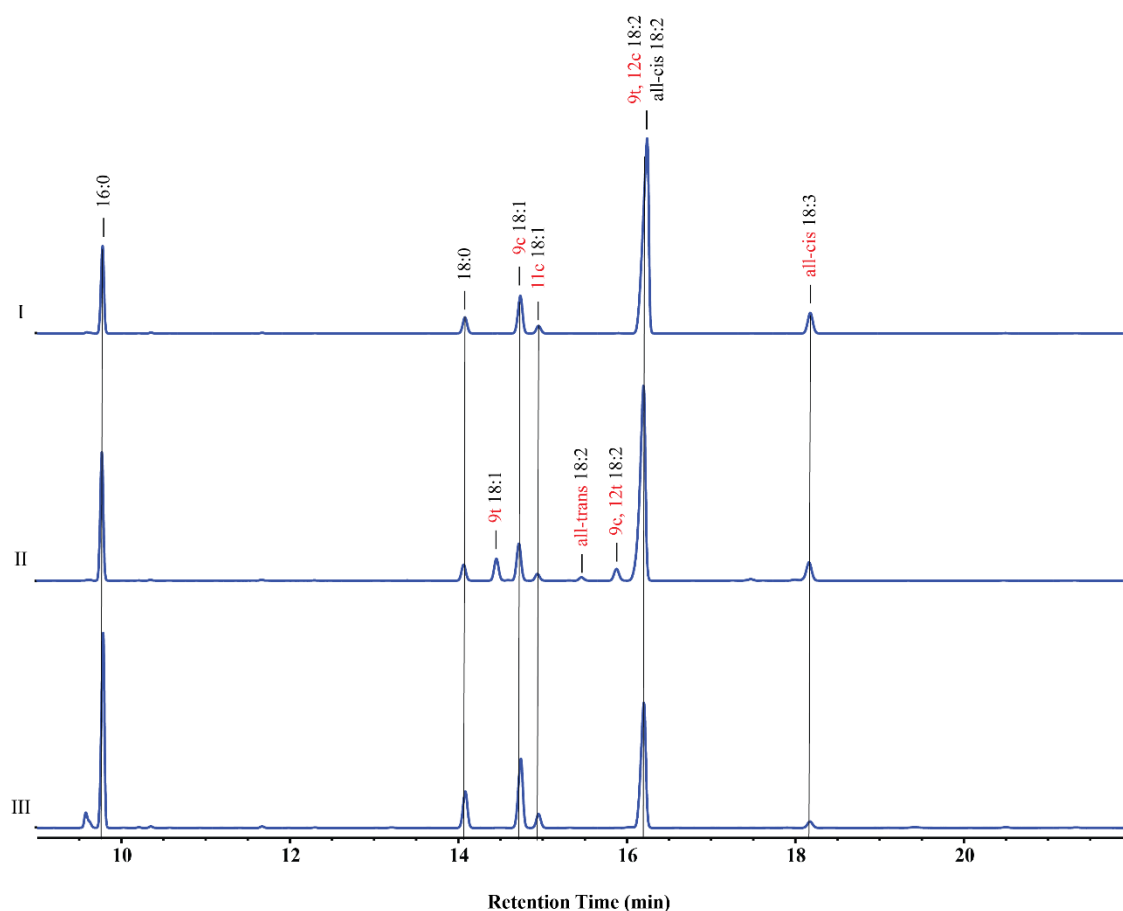


**Figure S3.** GC chromatogram of FAMES obtained before any treatment (trace I); after incubation of lecithin liposomes at 37 °C for 480 min in the presence of 0.15 mM Cu-TPMA-Phen and 10 mM 2-mercaptoethanol under anaerobic conditions (trace II); same reaction conditions but under aerobic conditions (trace III).

### 5.3. Thin Layer Chromatography (T.L.C.)

#### *Formation of Epoxydocosapentaenoic (EDP) Acid Methyl Esters and Separation of Regioisomers*

The formation of the DHA mono-epoxide regioisomers as described in **Chapter 3** was monitored by TLC using 7/3 *n*-hexane/Et<sub>2</sub>O as mobile phase. The fractions were separated by column chromatography and used for the analytical characterization.

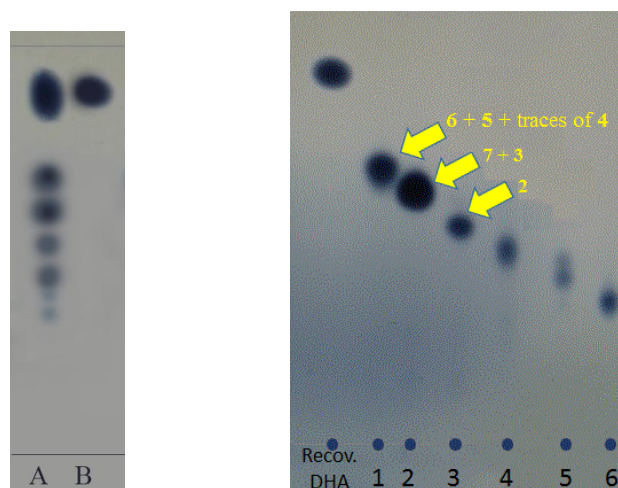


**Figure S4.** TLC after DHA-Me epoxidation and column separation. LEFT TLC: (A) Reaction mixture, (B) all-cis DHA-Me. RIGHT TLC: DHA-Me and epoxide fractions: 1-2-3 mono-epoxide fractions and assignment, as described in the main text separated using 7/3 *n*-hexane/ diethyl ether as mobile phase.

## 5.4. NMR Assignments of EDP Isomers Methyl Esters

The NMR spectra were carried out in C<sub>6</sub>D<sub>6</sub> for stability reasons. The C resonances were attributed by comparison with the DHA assignment individuating five EDP regioisomers for the resonances for the carbon atoms of the epoxy functionality. The <sup>13</sup>C NMR in CDCl<sub>3</sub> of two epoxy-isomers 4,5-EDP and 19,20-EDP were described in the literature and they are reported in the table below.

**Table S1.** <sup>13</sup>C NMR Resonances of EDP isomers methyl esters.

Literature Data (in CDCl<sub>3</sub>)

This work (in C<sub>6</sub>D<sub>6</sub>)

19,20	4,5	Carbon Atom	DHA-Me	16,17	13,14	19,20	7,8	4,5
173.5	173.33	C1	172.33	172.35	172.35	172.32	172.30	172.35
130.4	132.18	C2	33.65	33.63	33.63	33.64	33.51	30.76
129.3	130.82	C3	22.75	22.75	22.75	22.76	22.83	23.42
128.4	128.74	C4	128.06	128.11	128.11	128.08	130.08	55.32
128.2	128.64	C5	129.08	129.02	129.02	129.06	125.77	56.07
128.2	128.50	C6	25.57	25.57	25.57	25.58	26.23	26.38
128.1	128.09	C7	128.11	127.87	127.87		55.63	124.78
128.1	127.96	C8	128.15	128.32	128.32	128.35 – 127.80	55.65	130.27
127.9	127.85	C9	25.66	25.66	25.78	25.75 – 25.60	26.35	25.86
127.9	127.13	C10	128.15	128.40	130.19		124.78	127.95
124.5	124.33	C11	128.15	127.70	124.76	128.35 – 127.80	130.17	128.42
58.3	56.77	C12	25.56	25.78	26.34	25.75 – 25.60	25.78	25.75
56.5	56.10	C13	128.11	130.19	55.65			128.63/128.38/
51.6	51.88	C14	128.22	124.76	55.66	128.35 – 127.80	128.35 – 127.80	128.11/128.96
34.0	31.14	C15	25.67	26.34	26.35	25.79	25.75 – 25.60	25.75
26.2	26.35	C16	127.91	55.65	124.55	130.03		128.63/128.38/
25.8	25.96	C17	128.50	55.79	130.53	124.96	128.35 – 127.80	128.11/128.96
25.7	25.79	C18	25.65	26.22	25.68	26.31	25.58	25.66
25.7	25.77	C19	128.11	123.66	126.82	55.75	127.06	127.19
25.6	25.69	C20	131.78	133.81	131.90	57.38	131.82	131.89
22.8	23.49	C21	20.54	20.53	20.53	21.10	20.55	20.66
21.1	20.70	C22	14.08	14.00	14.03	10.45	14.07	14.17
10.7	14.41	C1'	50.65	50.65	50.65	50.65	50.66	50.85

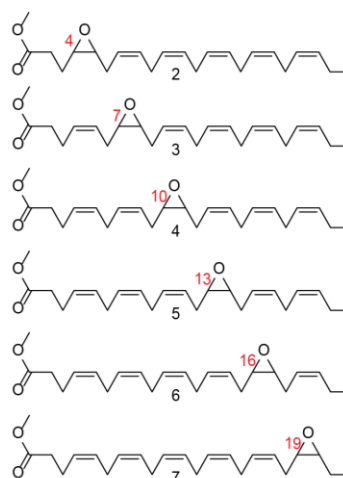
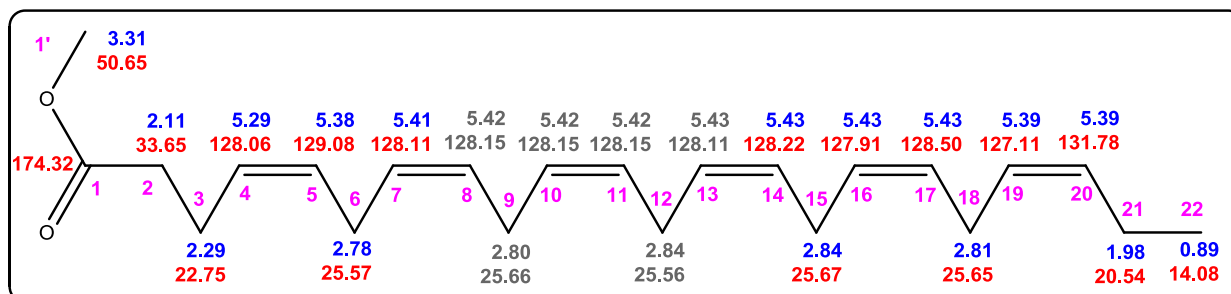
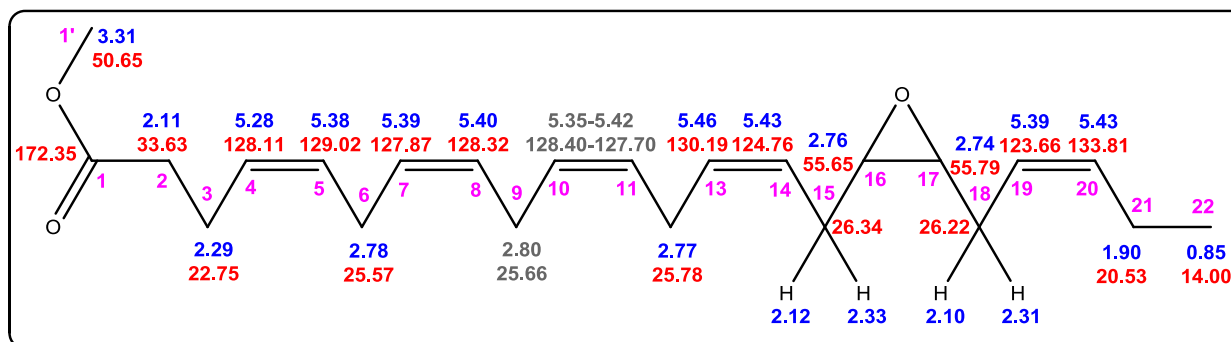


**Figure S5.** Summary of the  $^1\text{H}$  and  $^{13}\text{C}$  resonances assignments for the all-cis DHA-Me and EDP regioisomers.

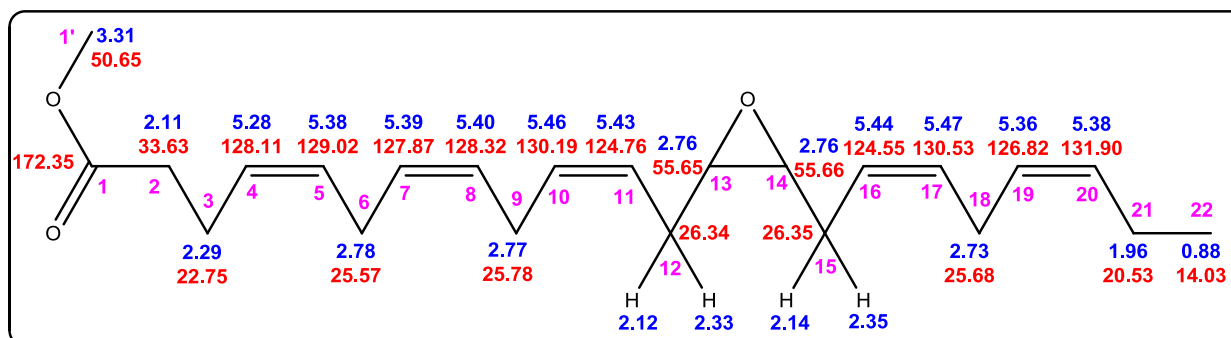
*All-(Z)-4,7,10,13,16,19-DHA-Me (1).*



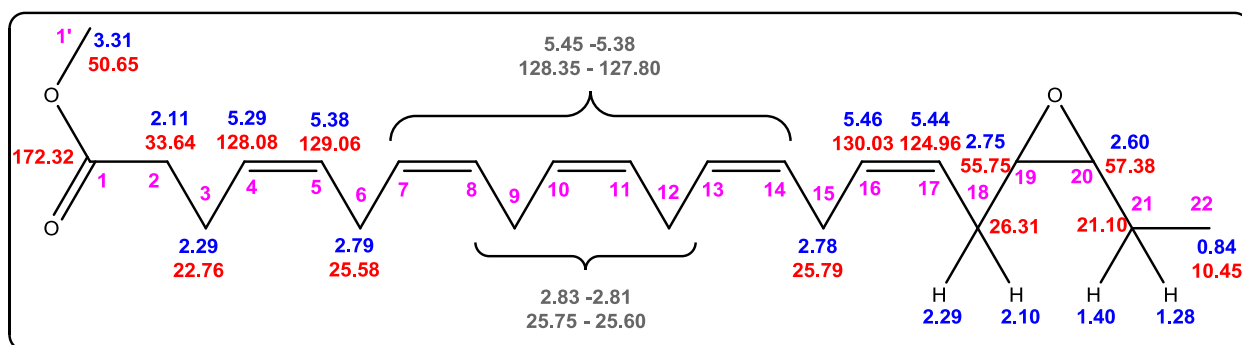
*16,17-EDP-Me (6).*



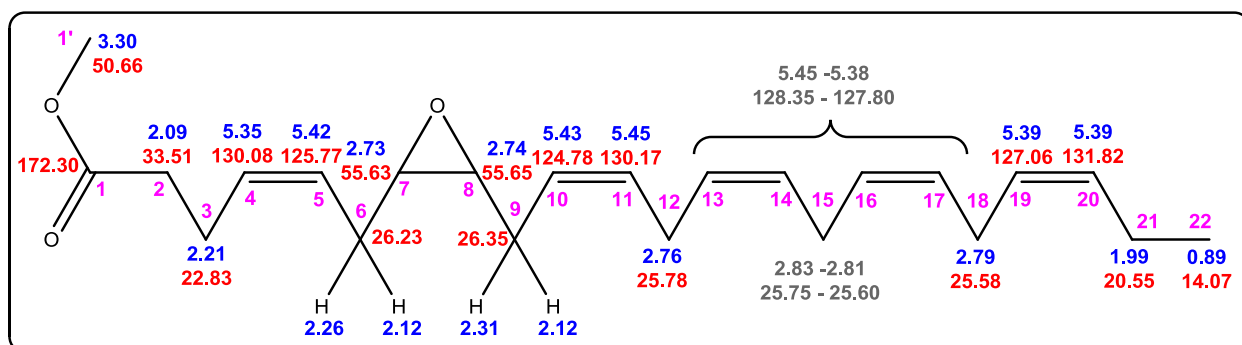
*13,14-EDP-Me (5).*



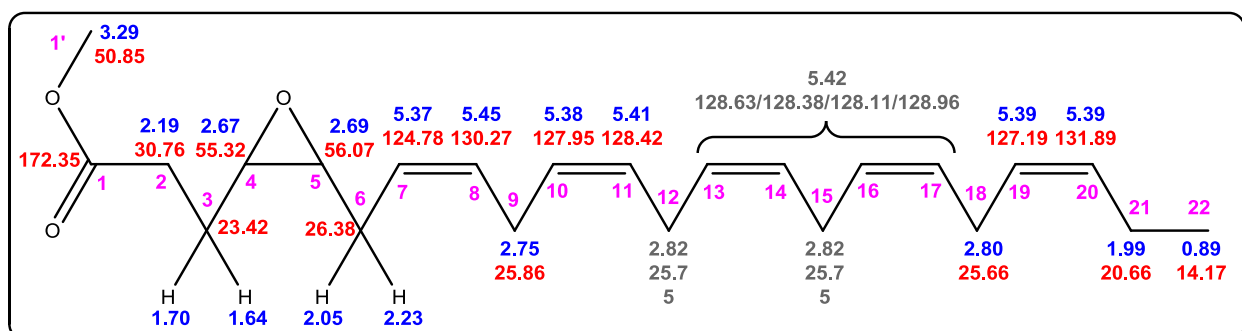
19,20-EDP-Me (7).

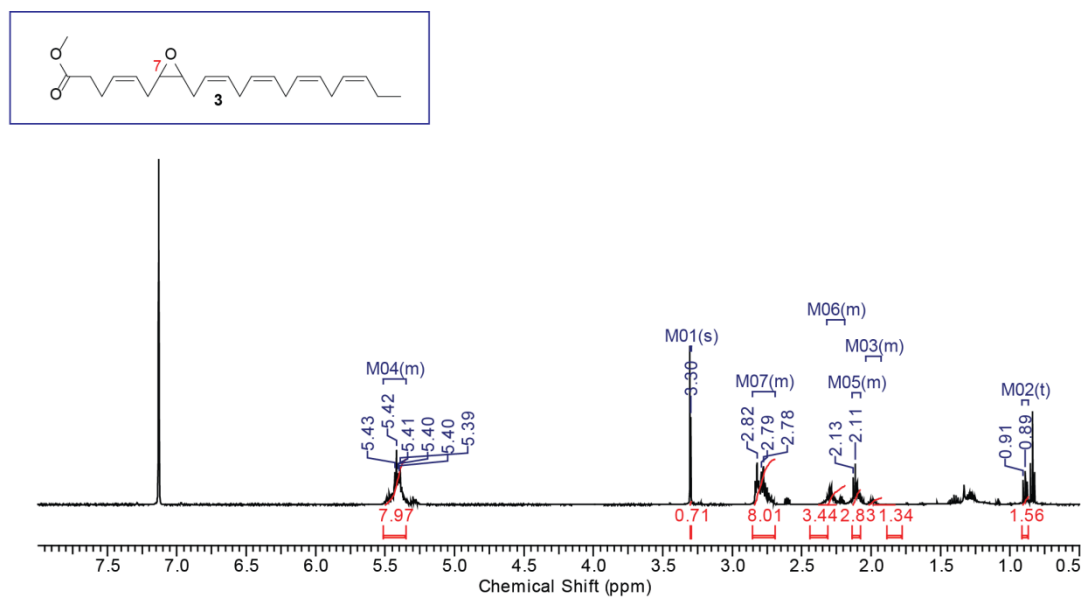
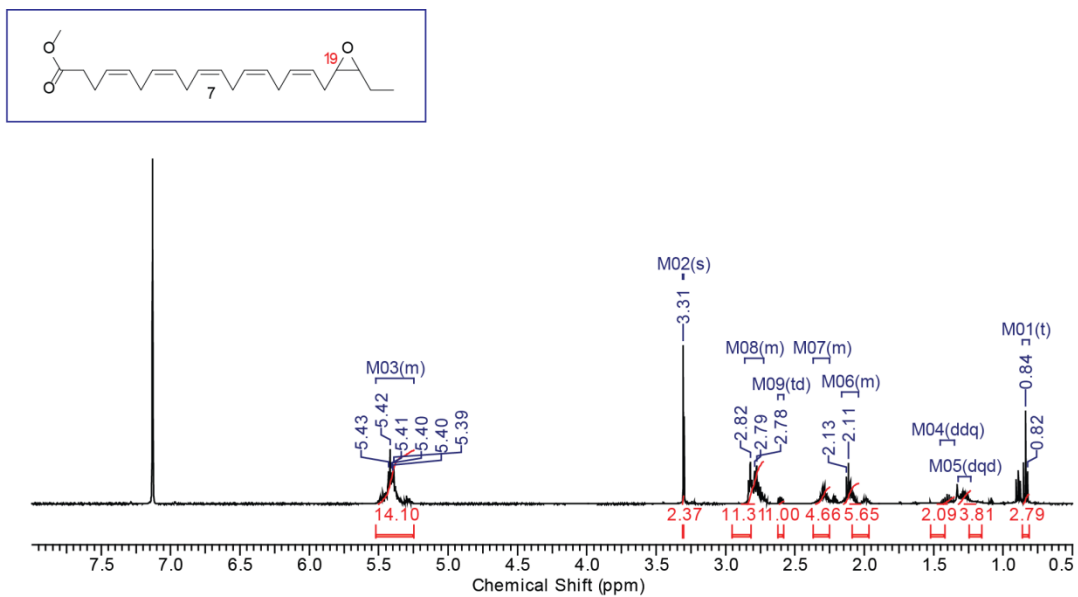


7,8-EDP-Me (3).



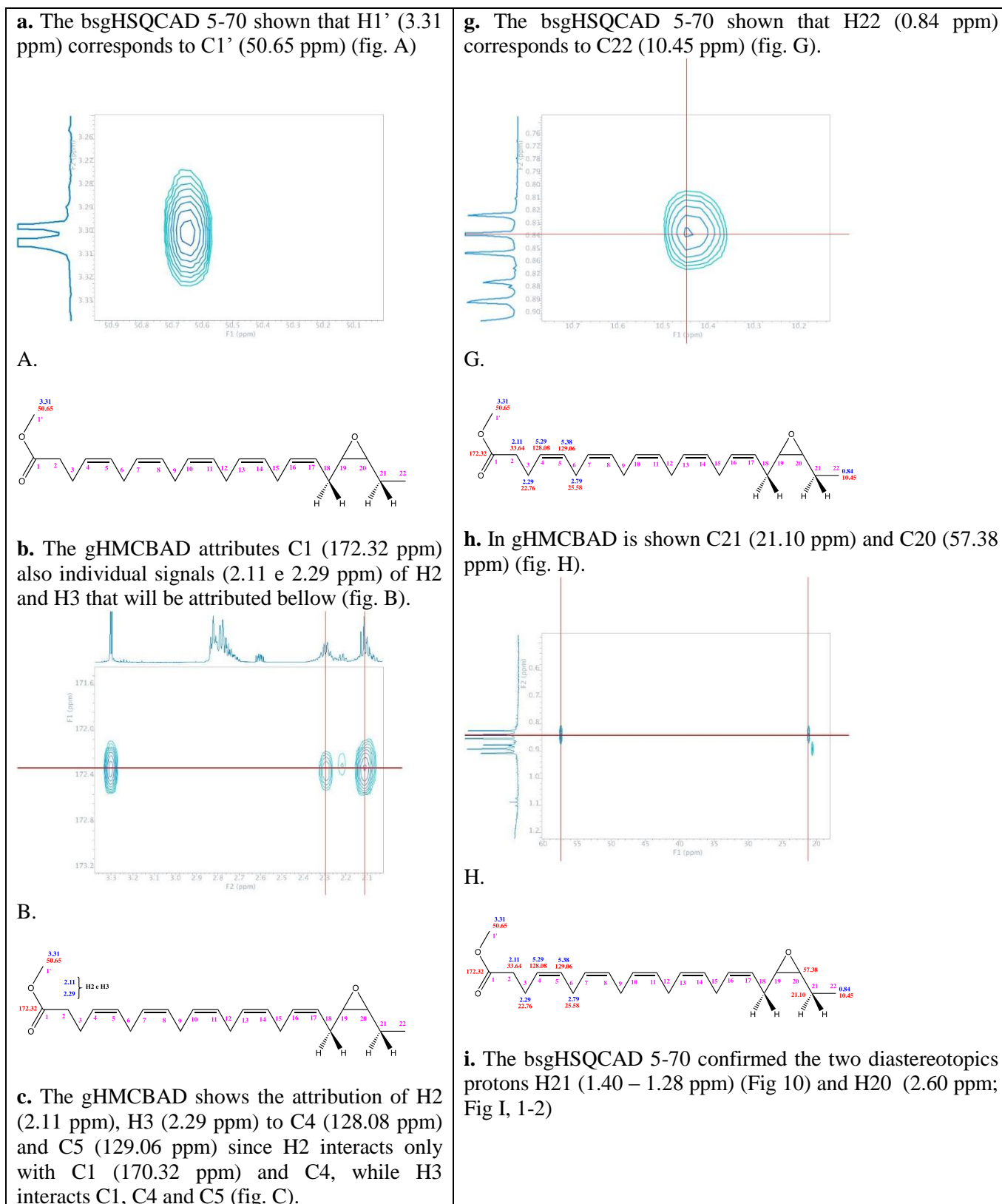
4,5-EDP-Me (2).

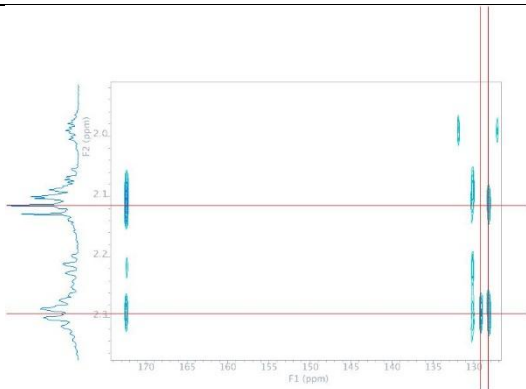




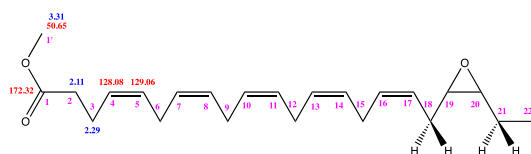
**Figure S6.**  $^1\text{H}$  NMR spectrum ( $\text{C}_6\text{D}_6$ ) of the second fraction after epoxidation reaction (mixture of the monoepoxides **7**, major, and **3**, minor; major/minor ratio: 57:43).

**Figure S7.** 2D NMR experiment (HSCQ / HMBC) in C<sub>6</sub>D<sub>6</sub> on the EDP second fraction for the assignment of the 7,8-EDP regioisomer (connections follow the left lane a-n, then the right lane o-s).

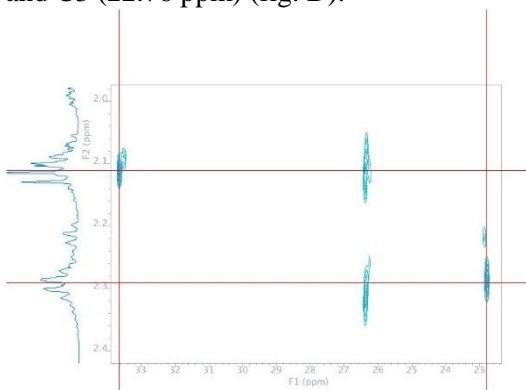




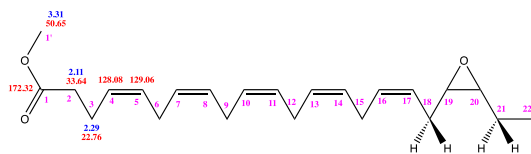
C.



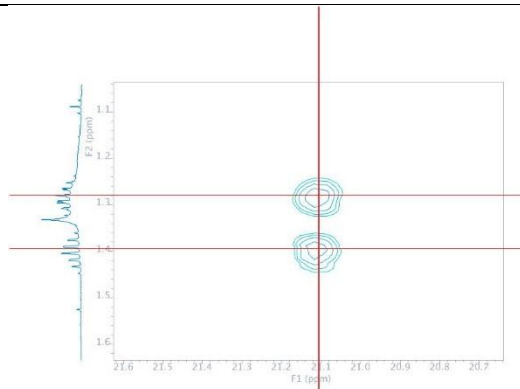
d. The bsgHSQCAD 5-70 shows C2 (33.64 ppm) and C3 (22.76 ppm) (fig. D).



D.



e. In bsgHSQCAD 110-140 the protons H4 (5.29 ppm) and H5 (5.38 ppm) are shown (fig. E).



I1.

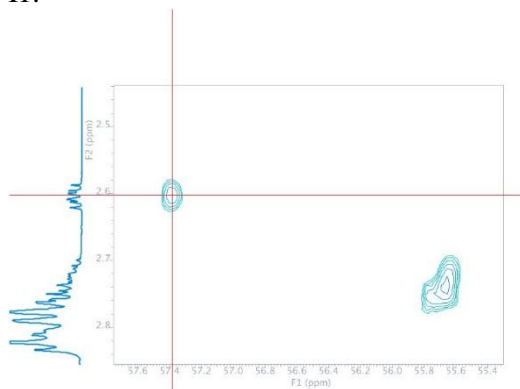
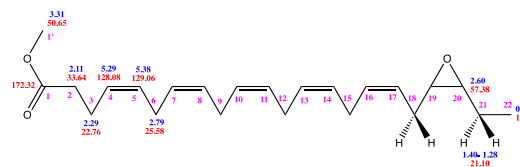
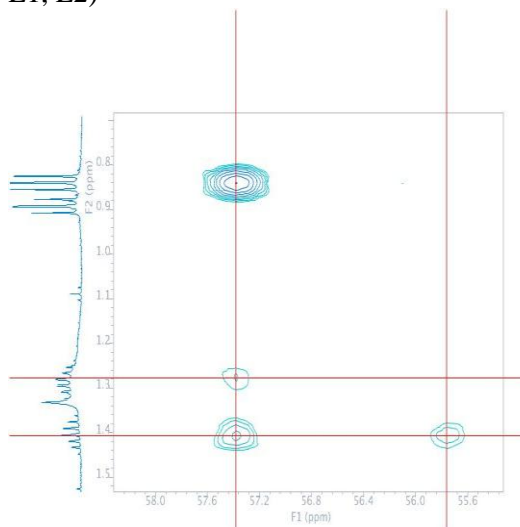


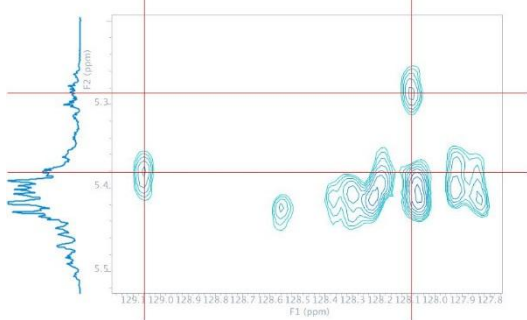
Fig 12.



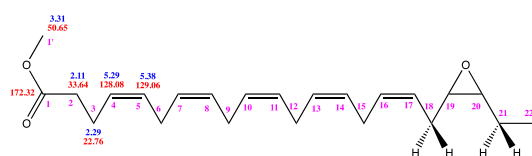
I. The gHMCBAD shows C19 (55.75 ppm; Fig 12) and the bsgHSQCAD 5-70 confirms H19 (2.75 ppm; Fig 13) (figs. L1, L2)



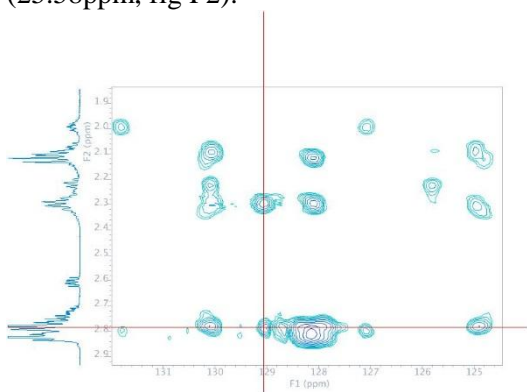
L1.



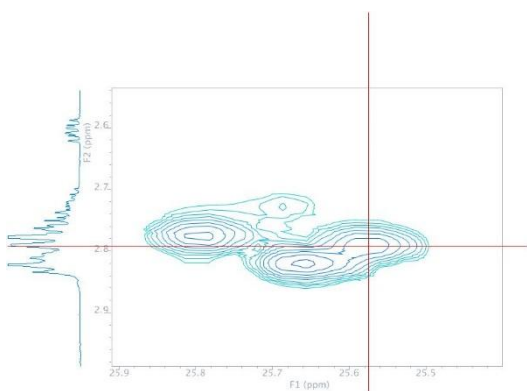
E.



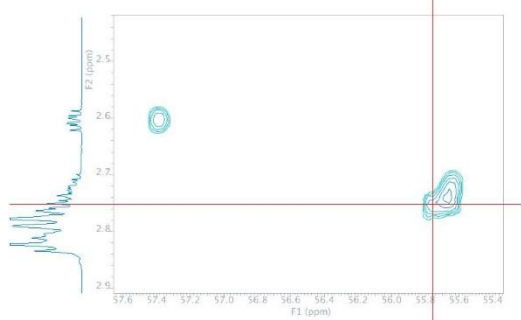
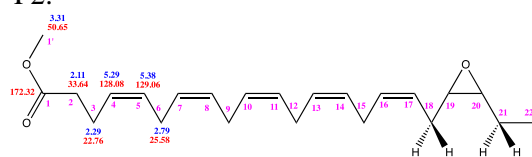
**f.** From gHMBCAD is confirmed that H6 (2.79 ppm) interacts with C4 (129.06 ppm; fig F1) and also from bsgHSQCAD 5-70 is shown C6 (25.58ppm, fig F2).



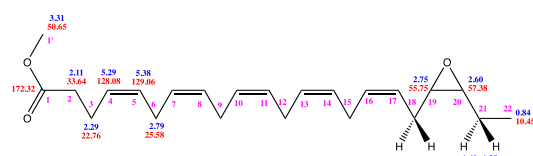
F1.



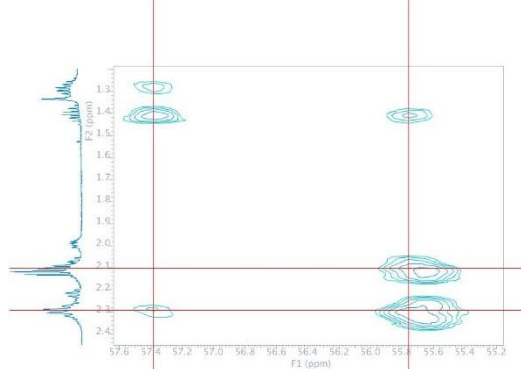
F2.



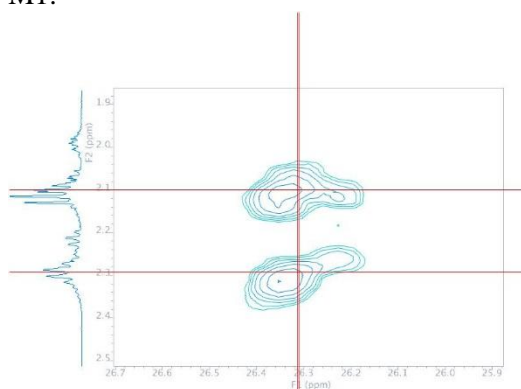
L2.



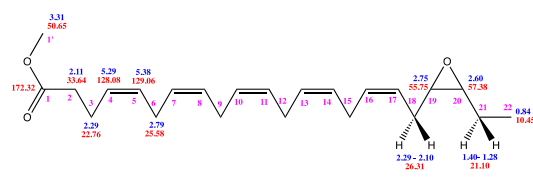
**m.** From gHMBCAD the two diastereotopic protons H18 are confirmed (2.29 – 2.10 ppm; Fig M1) and bsgHSQCAD 5-70 shows C18 (26.31 ppm; Fig M2)



M1.



M2.



**n.** From gHMBCAD C17 and C16 were identified (130.03

At this point, the overlapping of the signals made the attributions difficult, and for this reason we proceed with the attribution starting from the C22.

and 124.96 ppm, fig N1), while bsgHSQCAD 110-140 attributes the corresponding protons (130.03/5.46 ppm; 124.96/5.44 ppm, fig N2). Finally, gHMCBAD shows that H17 is attached (5.44 ppm) to C19 (fig N3).

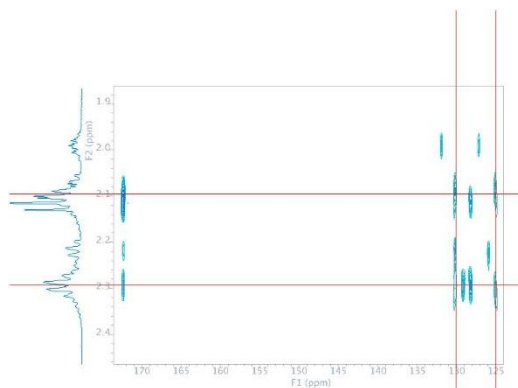


Fig N1.

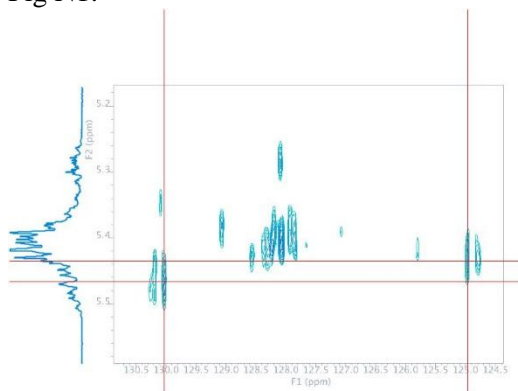


Fig N2.

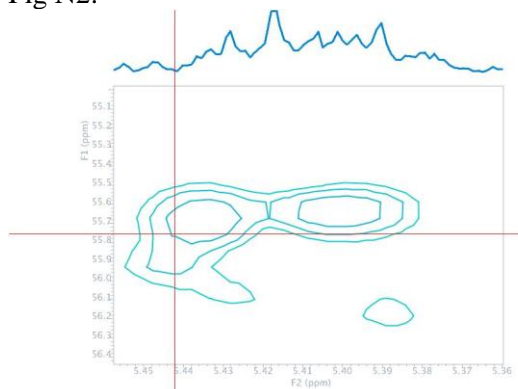
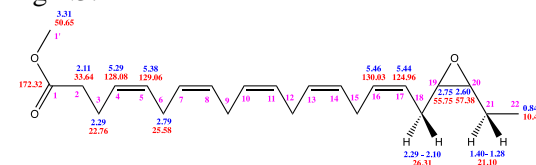


Fig N3.



o. From gHMCBAD proton H15 was identified (2.78 ppm, fig O1) and bsgHSQCAD 5-70 provides strong evidence that H15 is attached to C15 (130.03/5.46 ppm; fig O2).

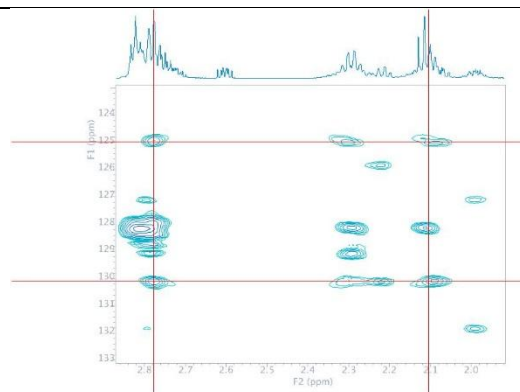


Fig. O1

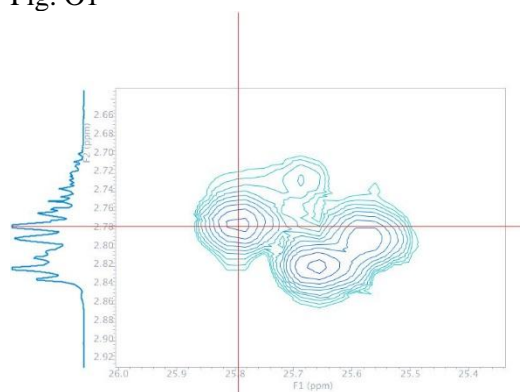
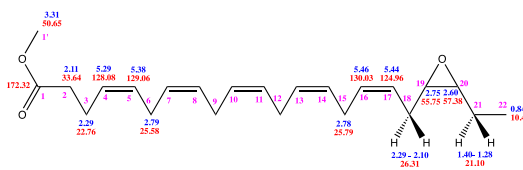


Fig. O2



**Figure S8.** Relevant correlations in the 2D NMR experiment (HSCQ / HMBC) in  $C_6D_6$  for the assignment of the 19,20-EDP regioisomer (connections follow the left lane a-f, then the right lane g-o).

**a.** The bsgHSQCAD 5-70 shown that the proton H1' (3.30 ppm) corresponds to C1' (50.66 ppm) (Fig. A)

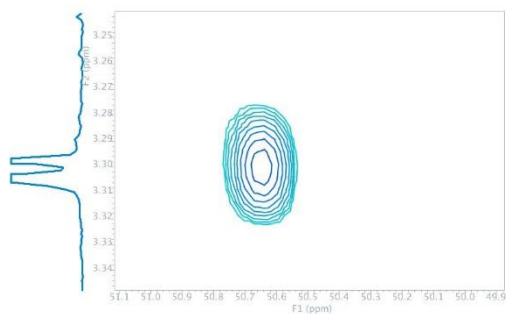
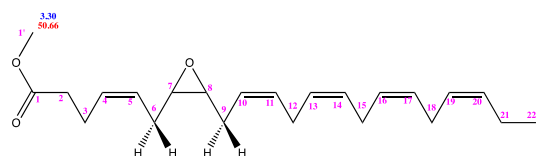


Fig A.



**b.** The gHMBCAD shows the attribution of C1 (172.30 ppm) and also the individual signals (2.09 e 2.21 ppm) correspond to the protons H2 and H3.

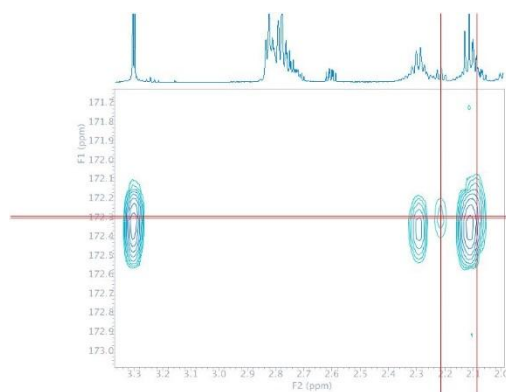
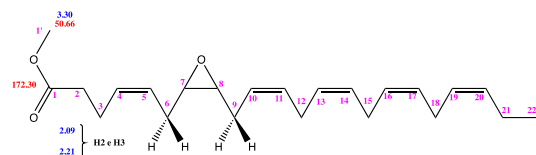


Fig B.



**c.** The gHMBCAD shows the attribution of H2 (2.09 ppm), H3 (2.21 ppm), C4 (130.08 ppm) and C5 (125.77 ppm). In addition, H2 interacts with C1 (170.30 ppm) and C4, while H3 interacts with C1, C4 and C5.

**o.** The bsgHSQCAD 5-70 shows that proton H22 (0.89 ppm) corresponds to C22 (14.07 ppm).

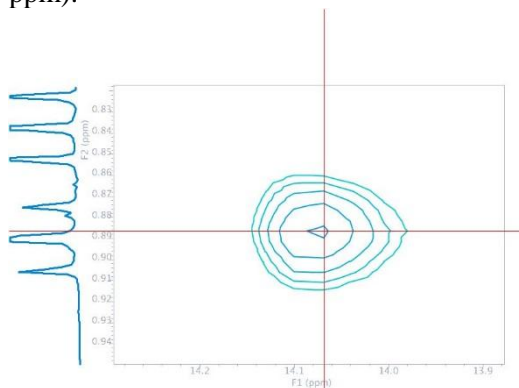
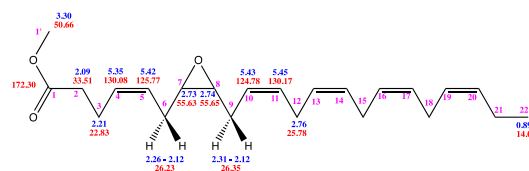


Fig. O1



**p.** The gHMBCAD indicates C21 (131.82 ppm) and C20 (20.55 ppm).

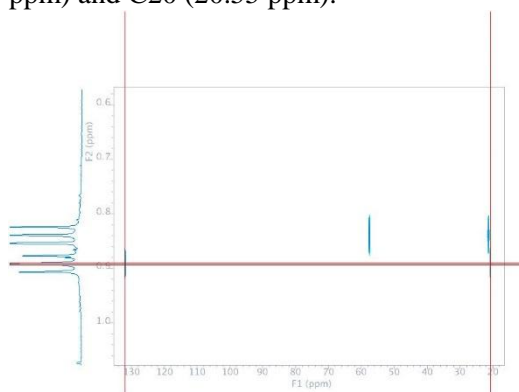
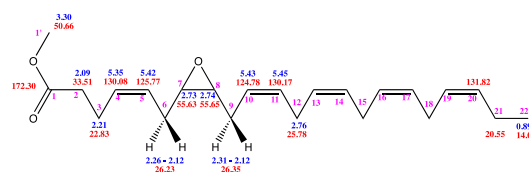


Fig. P1



**Q.** The bsgHSQCAD 5-70 indicates H21 (1.99 ppm) (Fi. Q1) and bsgHSQCAD 110-140 indicates H20 (5.39 ppm; Fi. Q2)

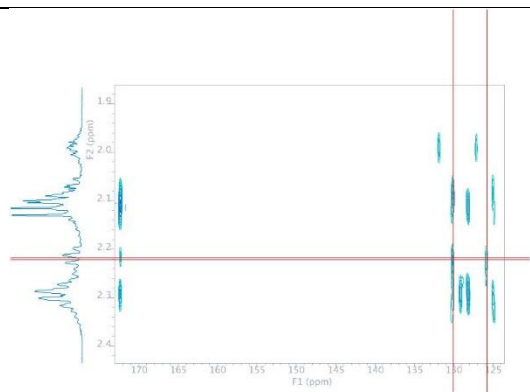
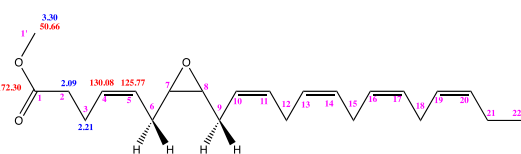


Fig C.



**d.** From bsgHSQCAD 5-70 C2 was identified (33.51 ppm) and also C3 (22.83 ppm).

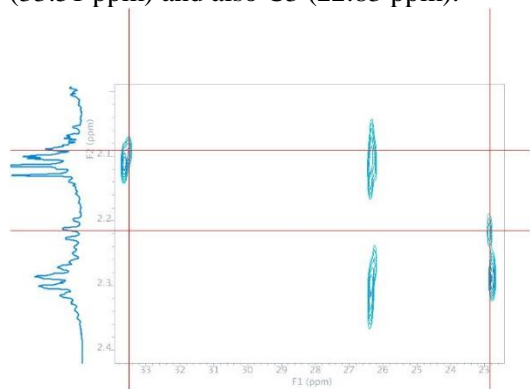
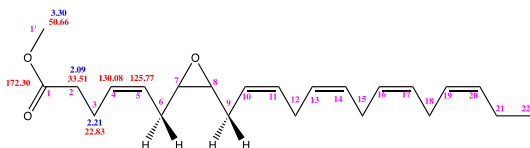


Fig D.



**e.** The bsgHSQCAD 110-140 shows H4 (5.35 ppm) and H5 (5.42 ppm).

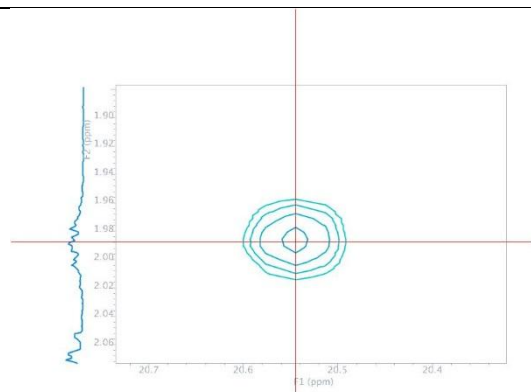
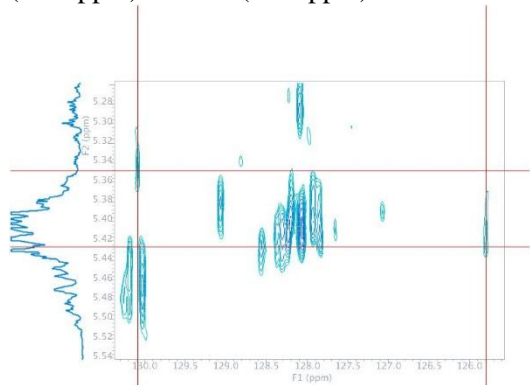


Fig. Q1

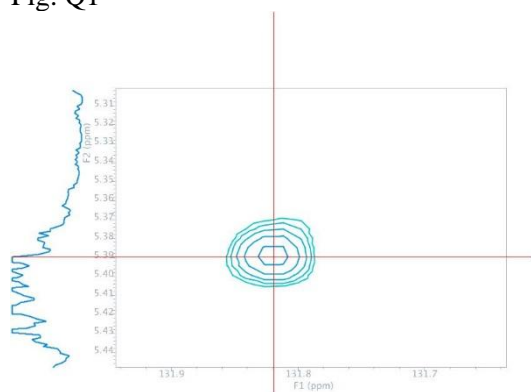
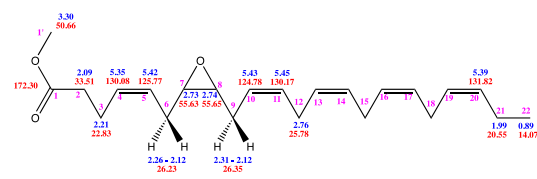


Fig. Q2



**r.** The gHMCBAD indicated C19 (127.06 ppm; Fig. R1) and with bsgHSQCAD 110-140, H19 was identified (5.30 ppm; Fig. R2)

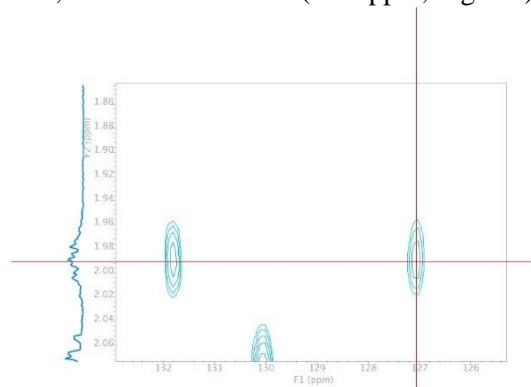
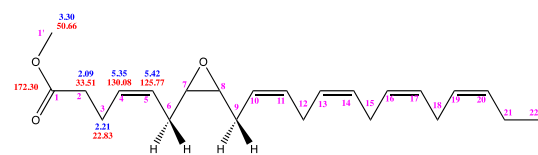


Fig. R1

Fig E.



f. With gHMBCAD the proton H6 was identified (2.26 ppm) which interacts with C4 (130.08 ppm) and C5 (125.77 ppm).

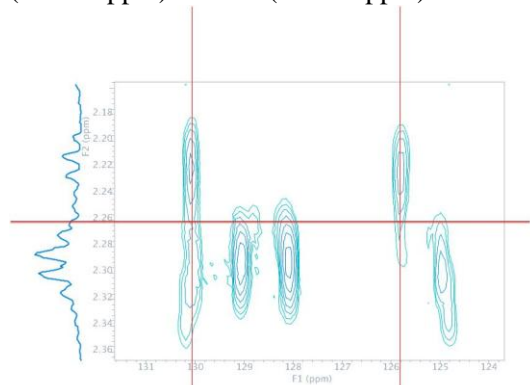
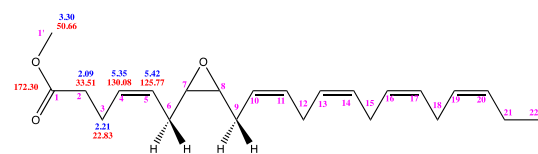


Fig. F



g. From bsgHSQCAD 5-70 it was confirmed C6 (26.23 ppm) and the other individual H6 (2.12 ppm) which is diastereotopic.

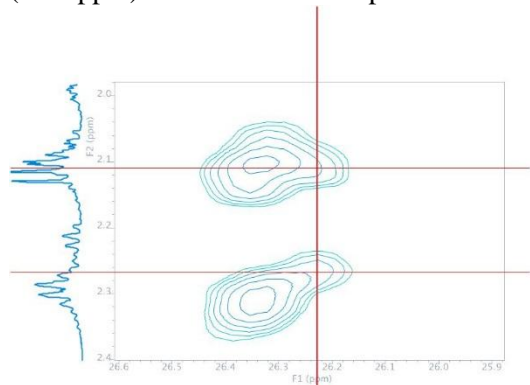
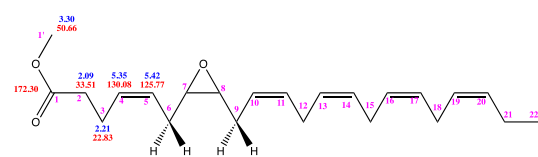


Fig. G



h. The gHMBCAD concerns C7 (55.63 ppm).

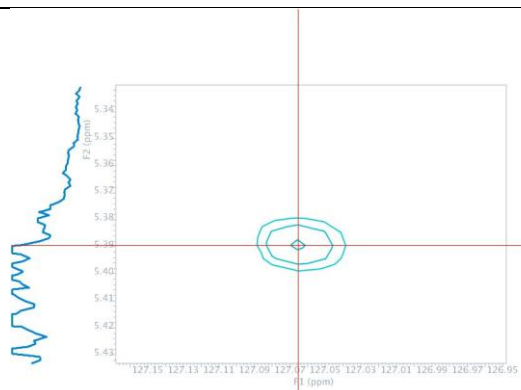
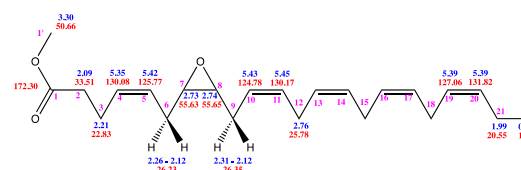


Fig. R2



s. The gHMBCAD shows C18 (25.58 ppm; Fig. S1) and with bsgHSQCAD 5-70 we manage to identify H18 (2.79 ppm; Fig. S2)

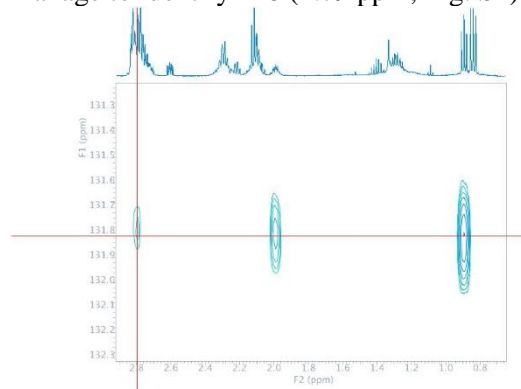
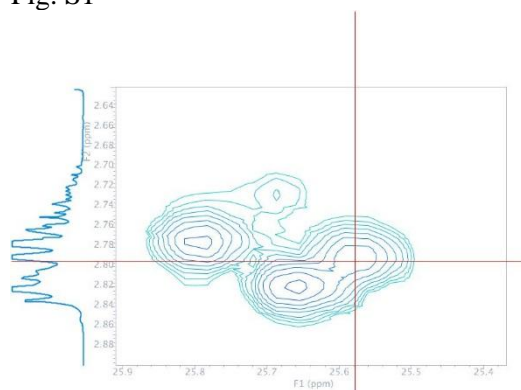
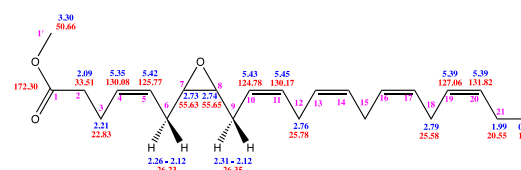


Fig. S1



FigS2



At this point, the exact attribution of the

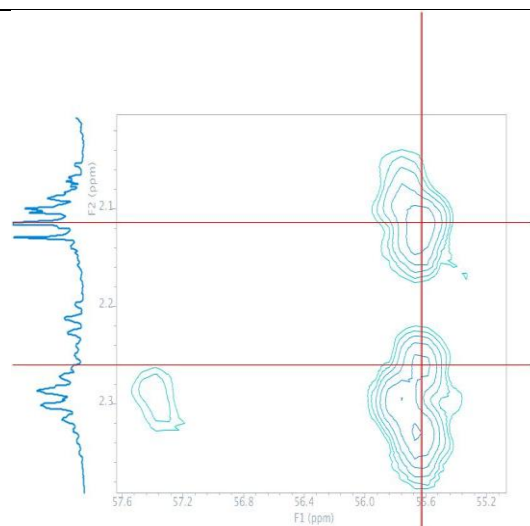
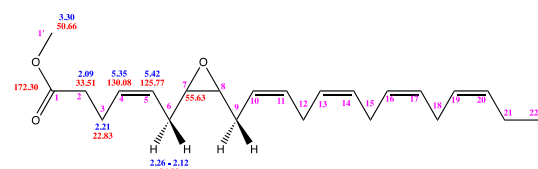


Fig. H



i. With bsgHSQCAD 5-70 the proton H7 was characterized (2.73 ppm).

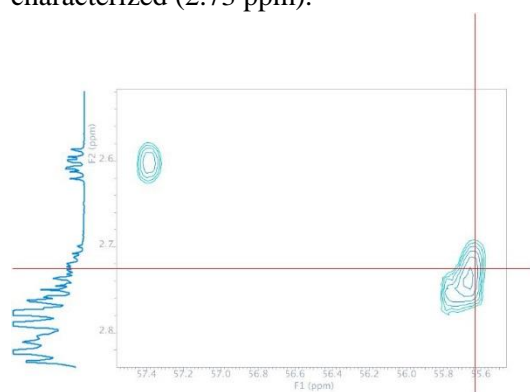
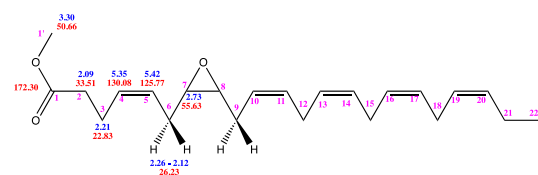


Fig. I



i. At gHMCBAD C7 interacts with H9 (2.31 and 2.12 ppm) which are diastereotopic, and also with C8 (55.65 ppm) (fig. L1). The correlations proton – carbon are assigned with bsgHSQCAD 5-70 (figs. L2-L3).

remaining resonances could not be done due to the overlapping of the signals.

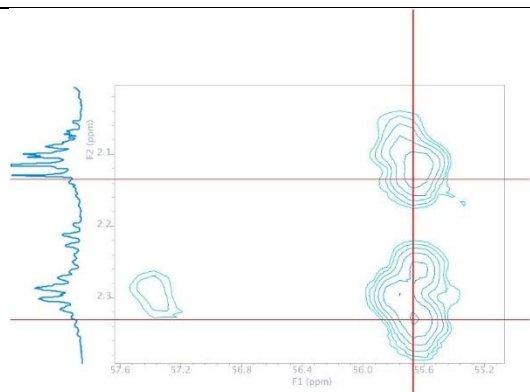


Fig. L1

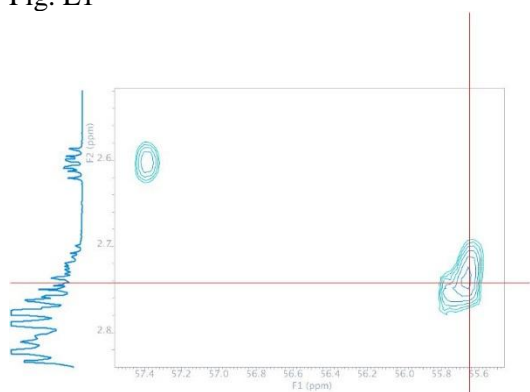


Fig. L2

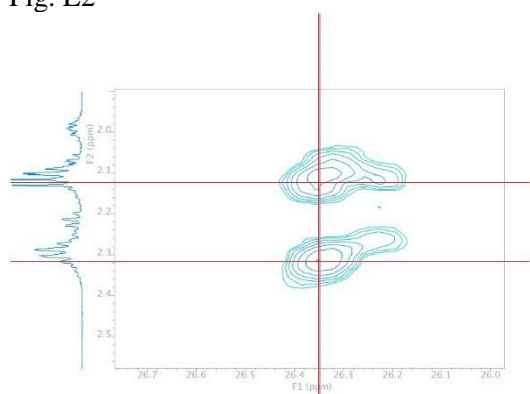
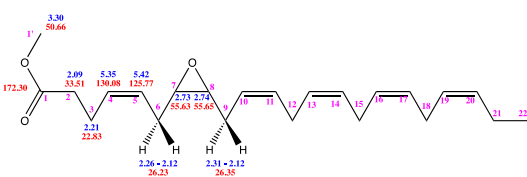


Fig. L3



**M.** In gHMCBAD the two protons H9 interact only with the two vinyl carbons C10 (124.78 ppm) and C11 (130.17 ppm) (Fi. M1), which relative protons are attributed with bsgHSQCAD 110-140 (Fig. M2), and their position is attributed through HMCBAD (Fig. M3)

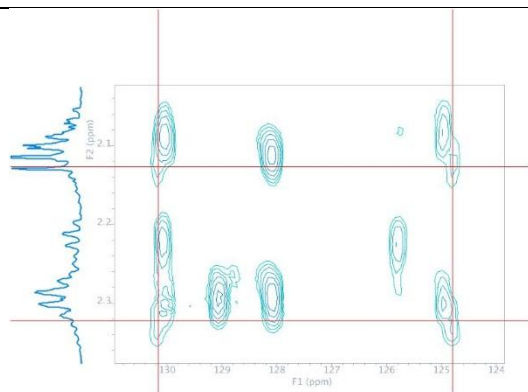


Fig. M1

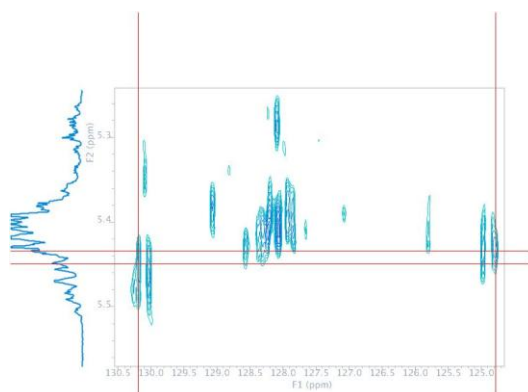


Fig. M2

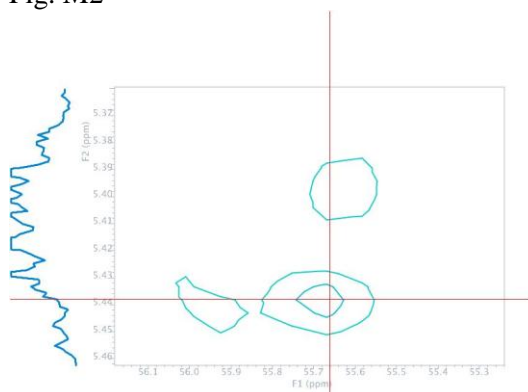
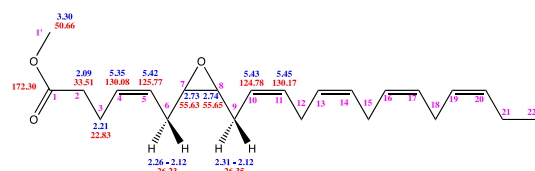


Fig. M3



**n.** In gHMCBAD both C10 and C11 interact with H12 (2.76 ppm; Fig. N1) whose carbon (25.78 ppm) is attributed by bsgHSQCAD 5-70 (Fig.N2).

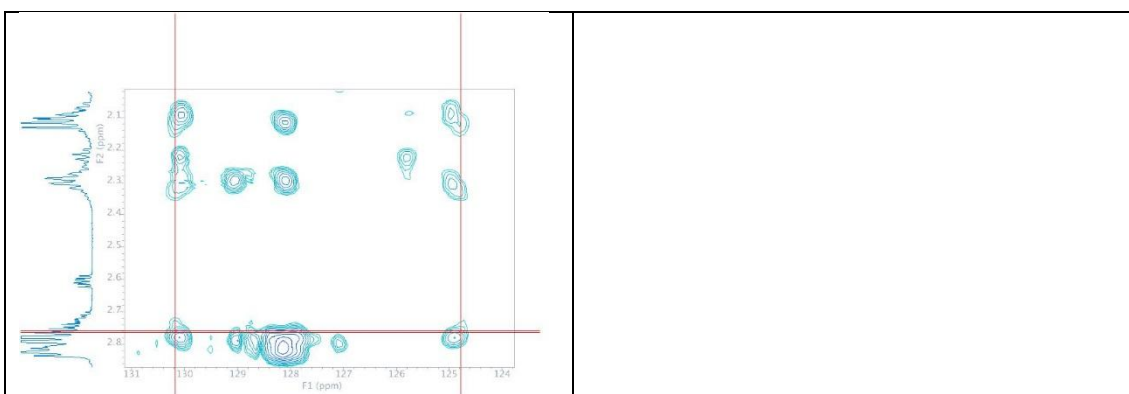


Fig. N1

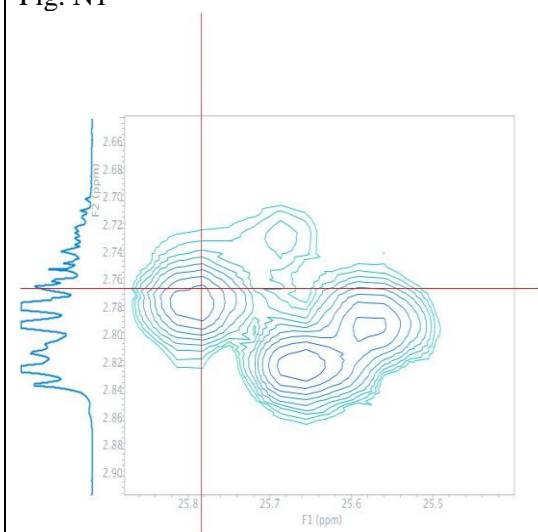
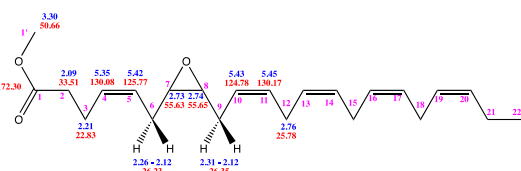
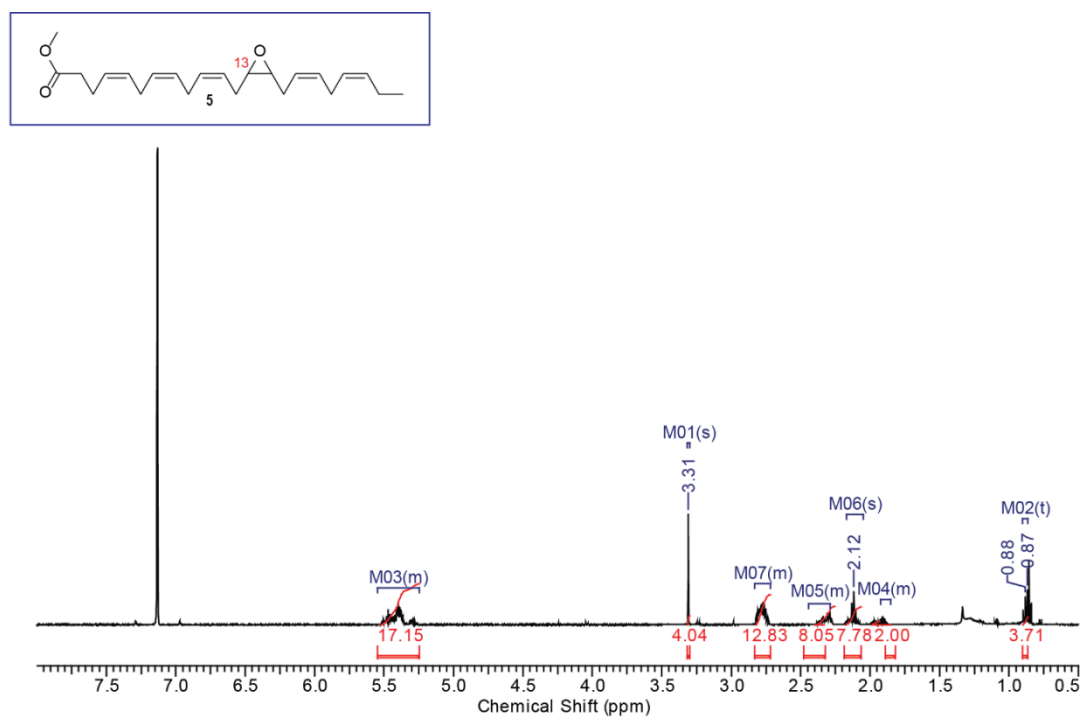
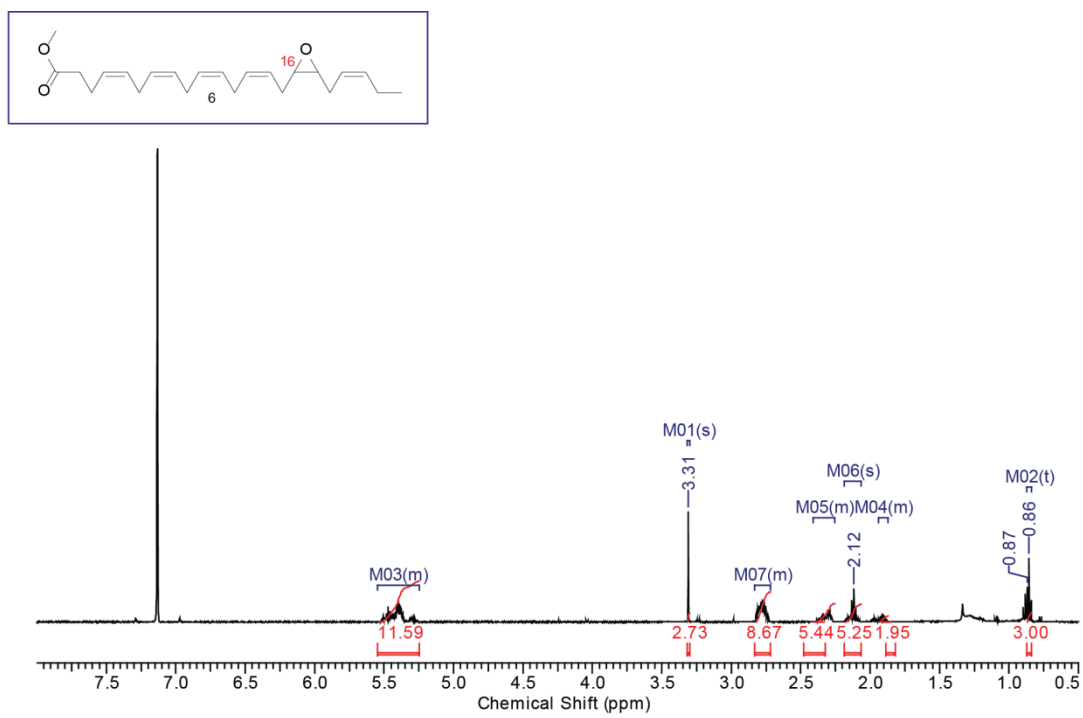


Fig. N2



The same 2D NMR experiments were also performed for the first and the third fraction collected from the column in order to assign the peaks and characterize the epoxides. In the next figures the protons NMR are presented.



**Figure S9.**  $^1\text{H}$  NMR spectrum of the first fraction in  $\text{C}_6\text{D}_6$  as a mixture of 4 different compounds: 16,17-EDP (**6**) and 13,14-EDP (**5**) were the principal components of the mixture and were fully NMR characterized, evaluating also the (**6**)/(**5**) ratio of 71:29. In the first fraction, traces of residual DHA and of 10,11-EDP were identified.

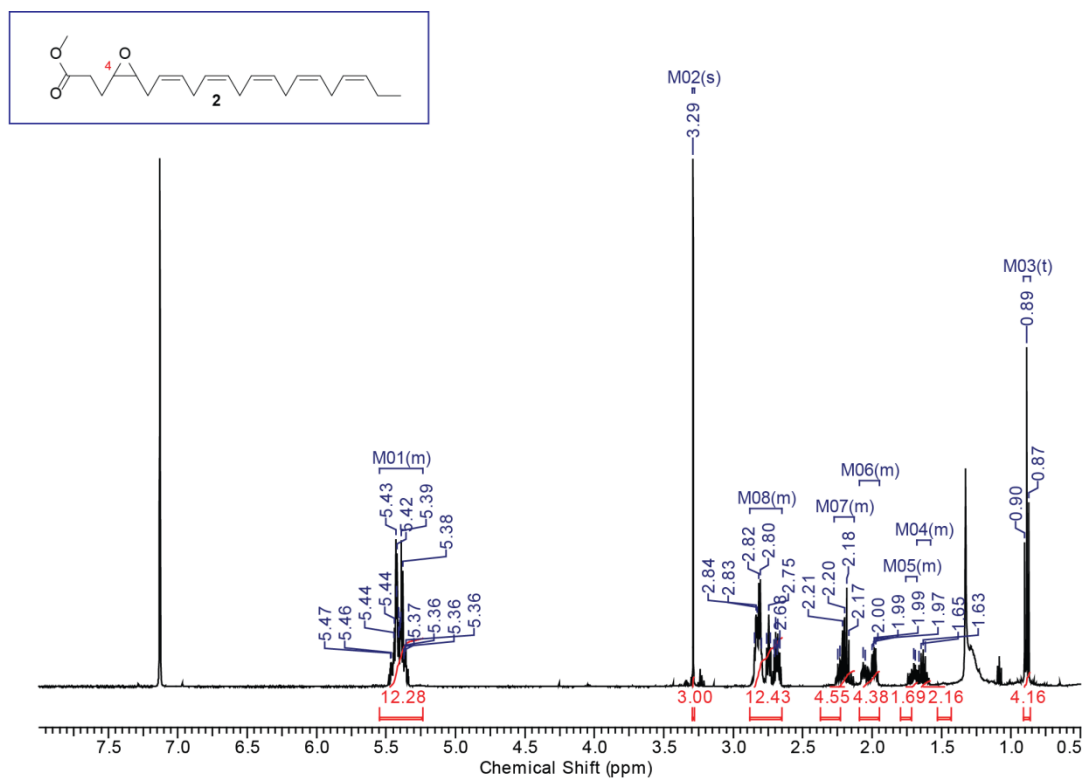


**Figure S10.**  $^1\text{H}$  NMR spectrum of the third fraction in  $\text{C}_6\text{D}_6$  after epoxidation reaction (pure 4,5-EDP, **2**).

## 5.5. Ag-Thin Layer Chromatography

### *TLC Comparison of the Mono-Trans DHA Isomers from the Dibromide Elimination and from the DHA Isomerization*

As described in the main text, the trans-alkenes obtained from the steps of mono-epoxidation-dibromination - elimination were examined by Ag-TLC. Also the monotrans alkene isomer mixture obtained by the radical catalyzed isomerization was examined under the same condition (**Figure S11, a**). **Figure S11 b** shows a representative separation on Ag-TLC of the elimination products obtained from the second fraction of the monoepoxidation reaction (**Figure S4**) in comparison with the mono-trans isomer mixture obtained by isomerization (right lane) and the starting DHA methyl ester (left lane).

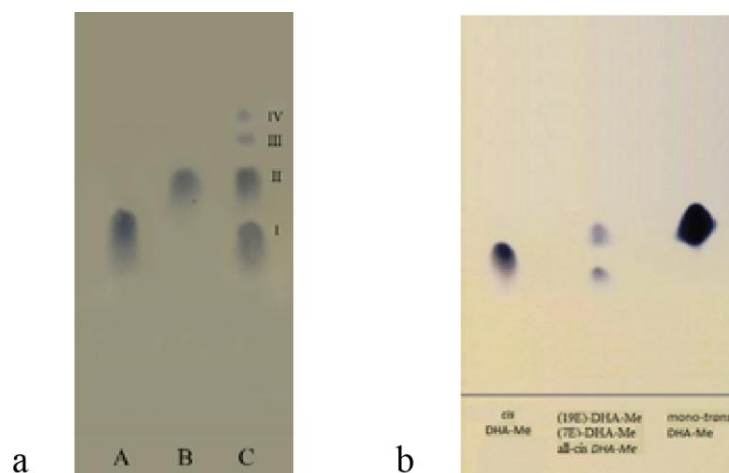


**Figure S11.** (a) Ag-TLC (eluent: 1/9 *n*-hexane/diethyl ether with 0.4% MeOH) showing the formation of monotrans (II) in the presence of traces of di-trans (III) and tri-trans (IV) isomers of DHA-Me (panel a, lane C), in comparison with the isolated monotrans DHA-Me fraction (lane B) and the starting DHA-Me.

(b) Ag-TLC showing the mixture obtained from the bromination/elimination reaction of the monoepoxide fraction II corresponding to 19E and 7E monotrans DHA-Me (central lane) in comparison with all-cis DHA-Me and the isolated monotrans DHA-Me isomers.

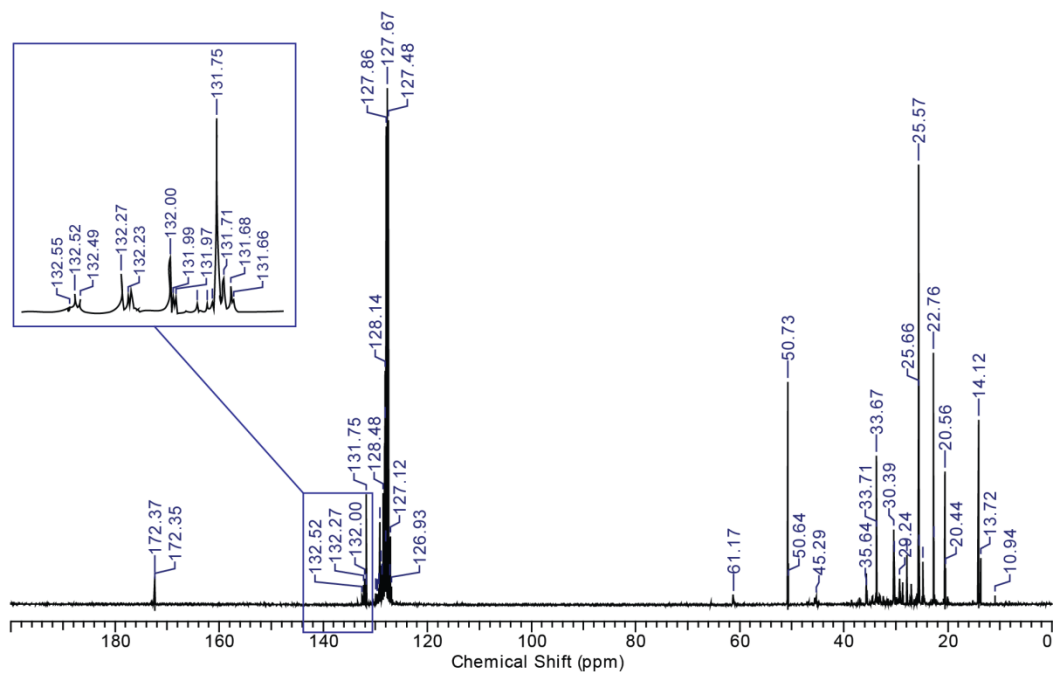


**Figure S12.**  $^{13}\text{C}$  NMR spectrum (in  $\text{C}_6\text{D}_6$ ) of the trans DHA-Me isomer mixture after isomerization.

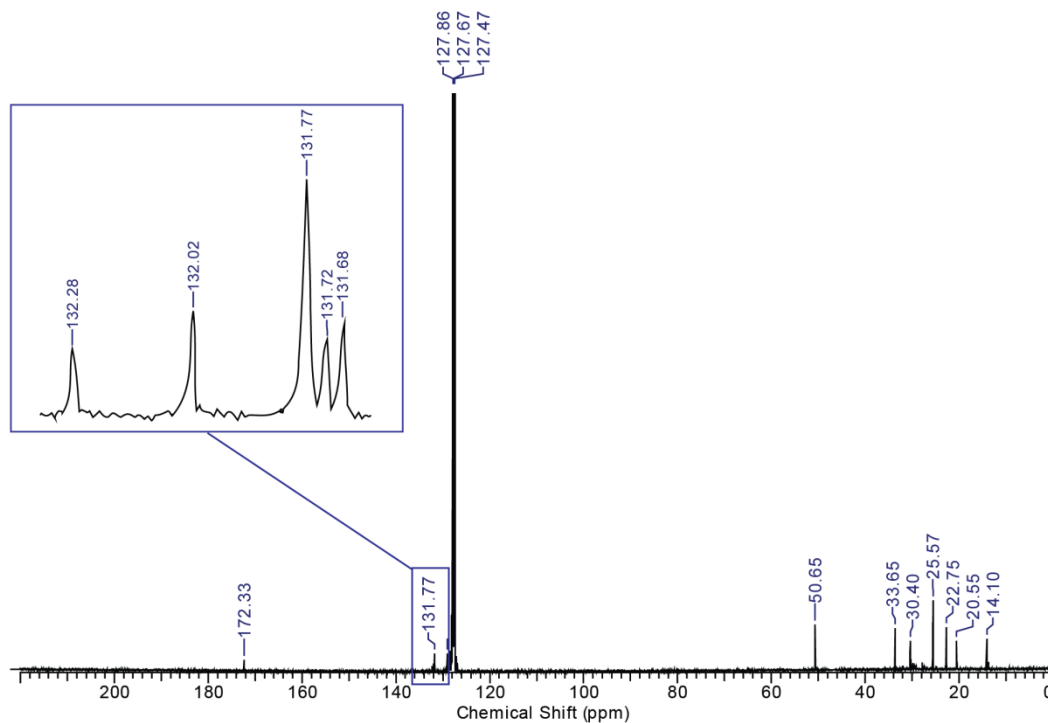


**Figure S13.**  $^{13}\text{C}$  NMR spectrum (in  $\text{C}_6\text{D}_6$ ) of the monotrans DHA-Me isomer mixture after purification.

## 5.6. Gas Chromatographic Analysis of DHA Isomers

### *GC Chromatograms of Mono-Trans DHA-Me Isomers Obtained from the EDP-Me Elimination*

The three fractions of EDP-Me regioisomers isolated from the epoxidation were separately transformed and the alkene mixture was analysed by GC (see **Figure 36** in the main text).

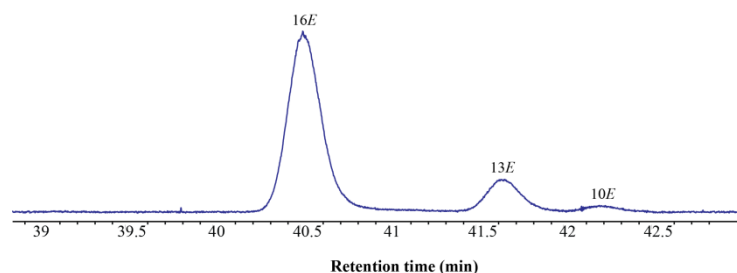


**Figure S14.** GC chromatographic region corresponding to monotrans DHA isomer obtained from the dibromination-elimination reaction on EDP-Me regioisomers isolated in the first fraction. The regioisomer assignment of this monoepoxide fraction was made on the basis of the NMR experiments (see above), therefore the resulting alkene can be assigned to as 16*E*-DHA, whereas the minor alkene product can be assigned to as 13*E*-DHA, with traces of the alkene 10*E*-DHA.

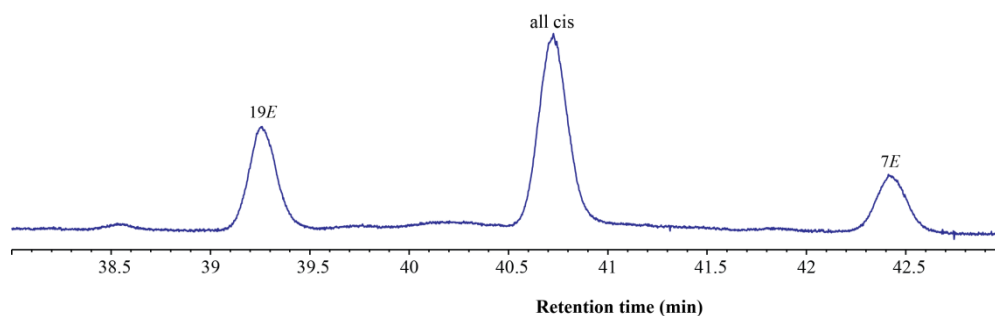


**Figure S15.** GC chromatographic region corresponding to monotrans DHA isomers obtained from the dibromination-elimination reaction on EDP-Me regioisomers isolated in the second fraction. The regioisomer assignment of this monoepoxide fraction was made on the basis of the NMR experiments (see above), therefore the two resulting alkenes can be assigned to as 19*E*-DHA and 7*E*-DHA (obtained in the crude reaction with a 71:29 ratio).

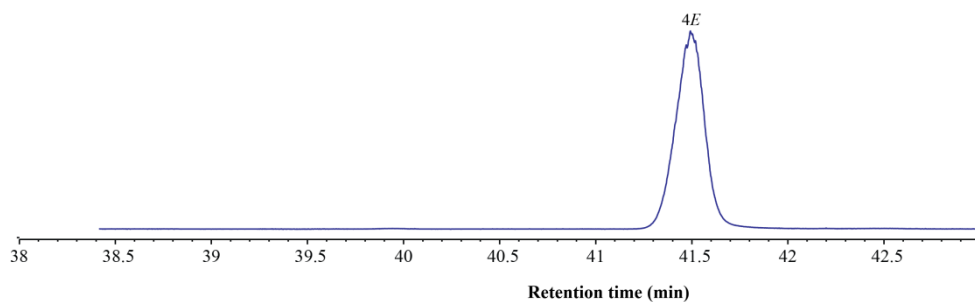


**Figure S16.** GC chromatographic region corresponding to montrans DHA isomer obtained from the dibromination-elimination reaction on EDP-Me regioisomer isolated in the third fraction. The regioisomer assignment of this monoepoxide fraction was made on the basis of the NMR experiments (see above), therefore the resulting alkene can be assigned to *4E*-DHA, with analytical characteristics identical with the commercially available compound.

## 5.7. Gas Chromatography Mass Spectrometry (GC-MS)

### *Analyses of Mono-Trans DHA Regioisomers*

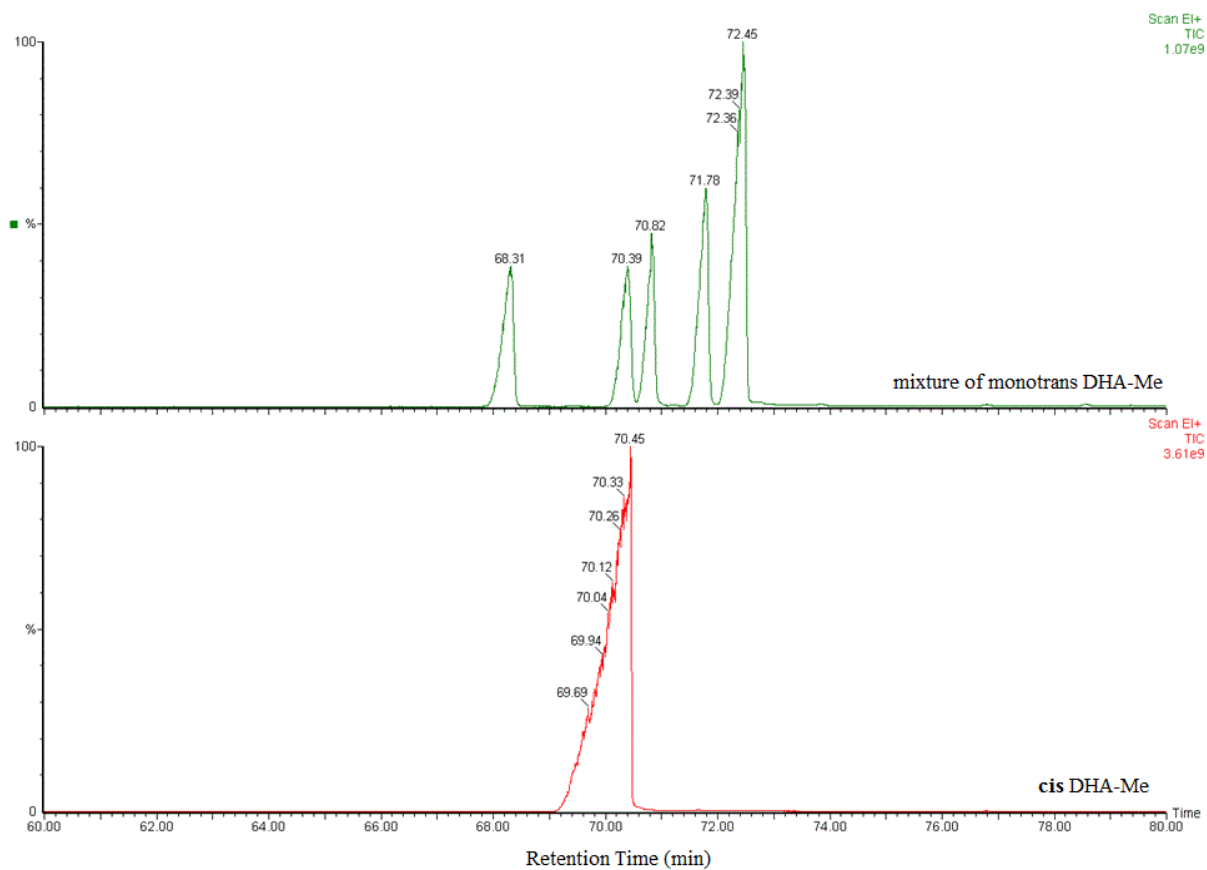


**Figure S17.** GC-MS separation.

DHATRANS 12758 (68.313) Cm (12686:12780)

Scan EI+  
2.02e7

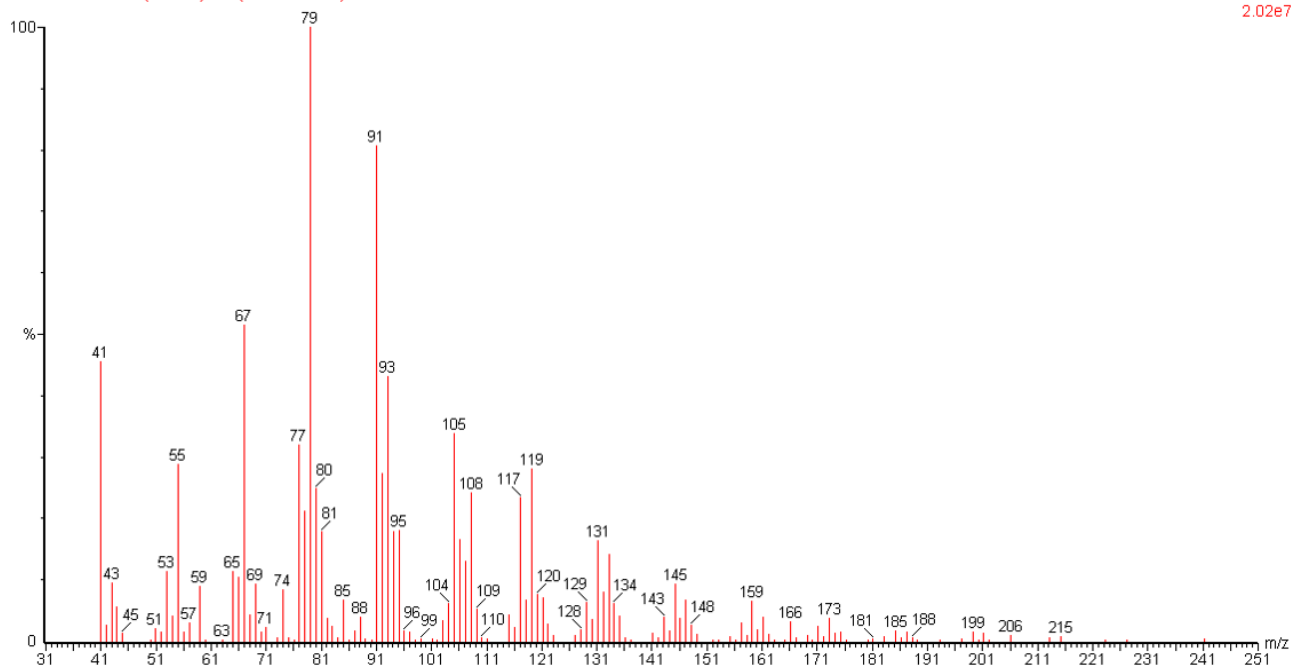


Figure S18. Mass fragmentation at 68.31 min (19E DHA-OMe).

DHATRANS 13174 (70.394) Cm (13121:13192)

Scan EI+  
2.08e7

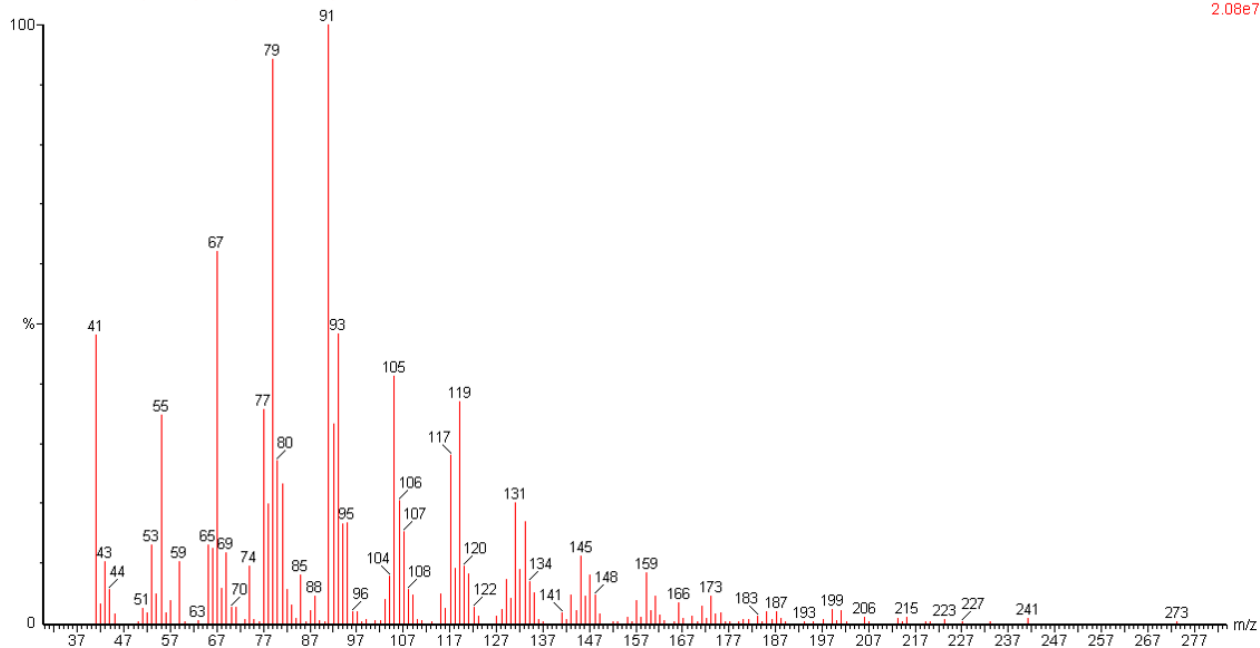
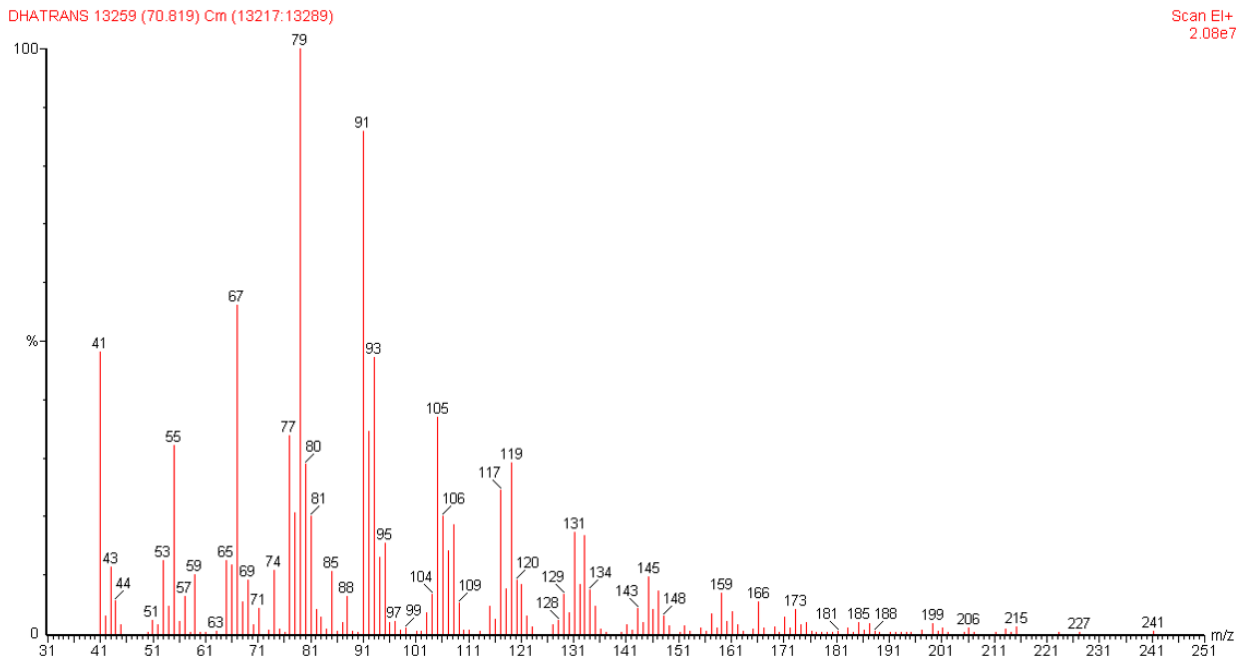
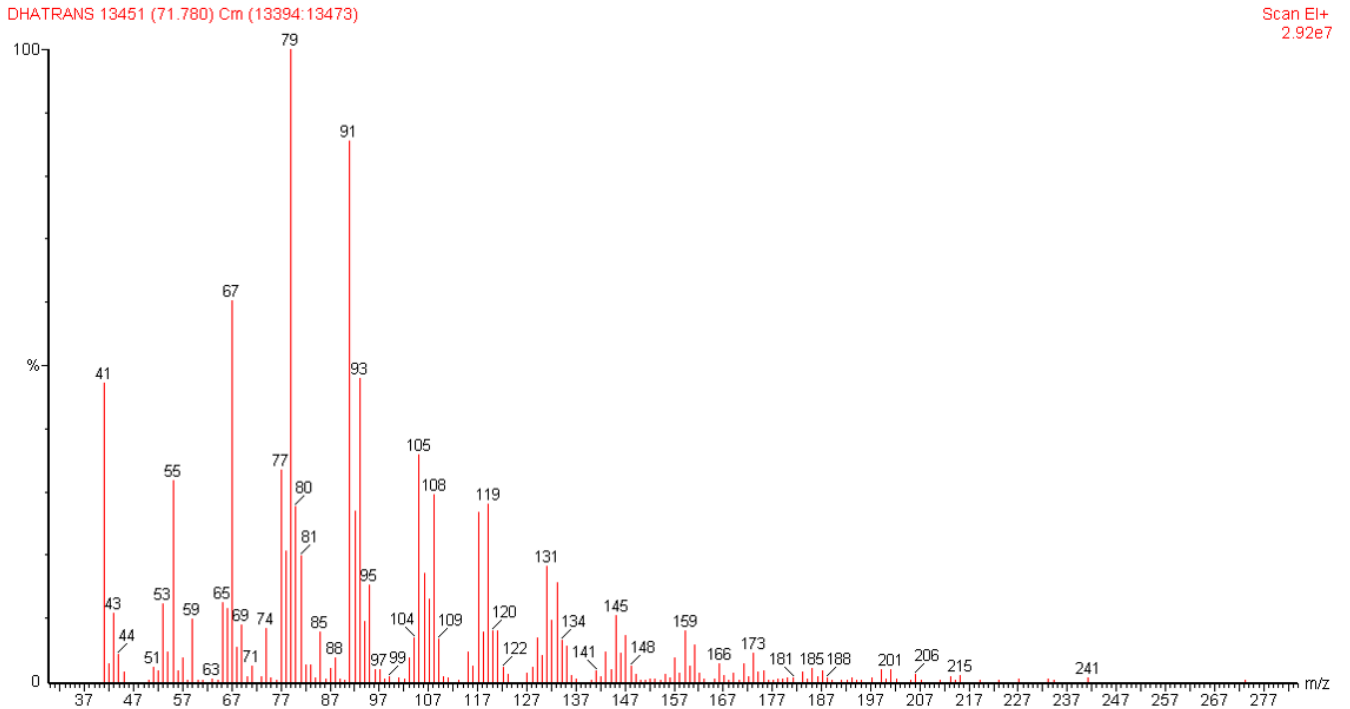


Figure S19. Mass fragmentation at 70.39 min (16E DHA-OMe).



**Figure S 20.** Mass fragmentation at 70.82 min (4*E* DHA-OMe).



**Figure S21.** Mass fragmentation at 71.78 min (13*E* DHA-OMe).

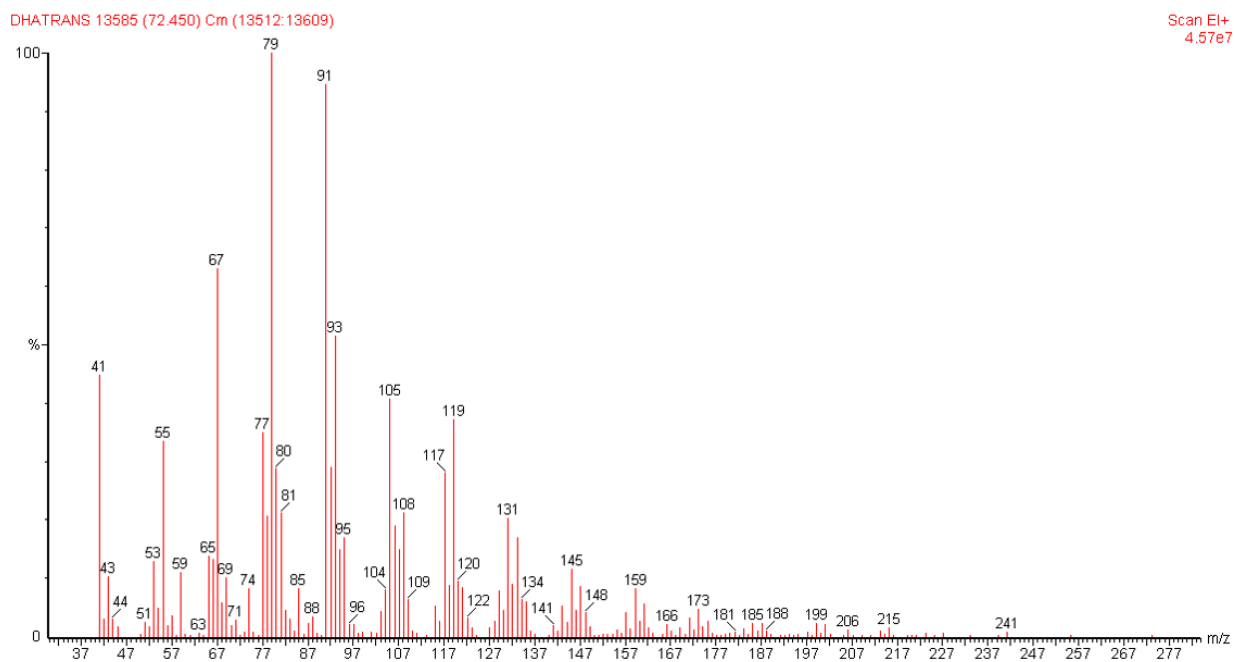


**Figure S22.** Mass fragmentation at 72.45 min (7E + 10E DHA-OMe).

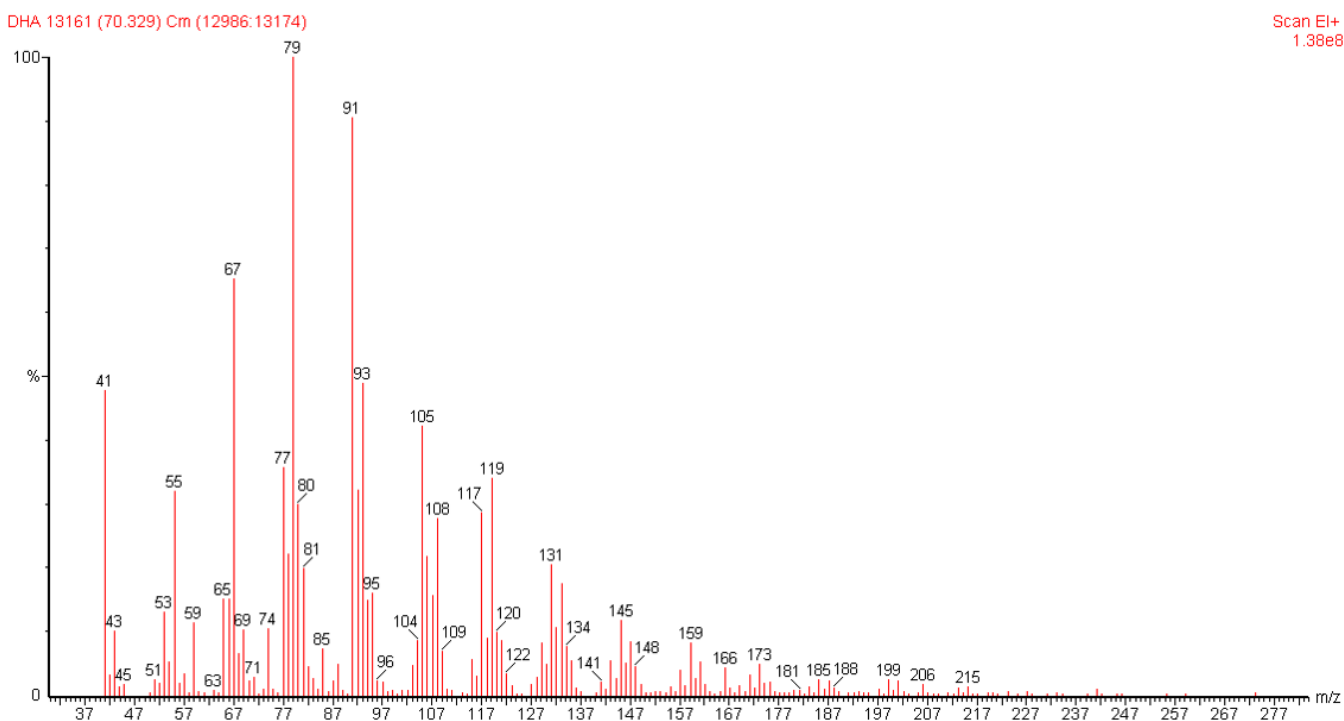


**Figure S23.** Mass fragmentation at 70.33 min (all cis DHA-OMe).

## 5.8. $^{13}\text{C}$ – NMR Spectra

### *Fish Oil Isomerization and Trans-Containing Triglyceride Analysis*

A DHA-rich fish oil used as material for functional foods and supplements was used as a triglyceride source in order to carry out the thiyl radical catalyzed isomerization and analyze the monotrans DHA-containing triglycerides in comparison with the monotrans isomers of DHA methyl ester.

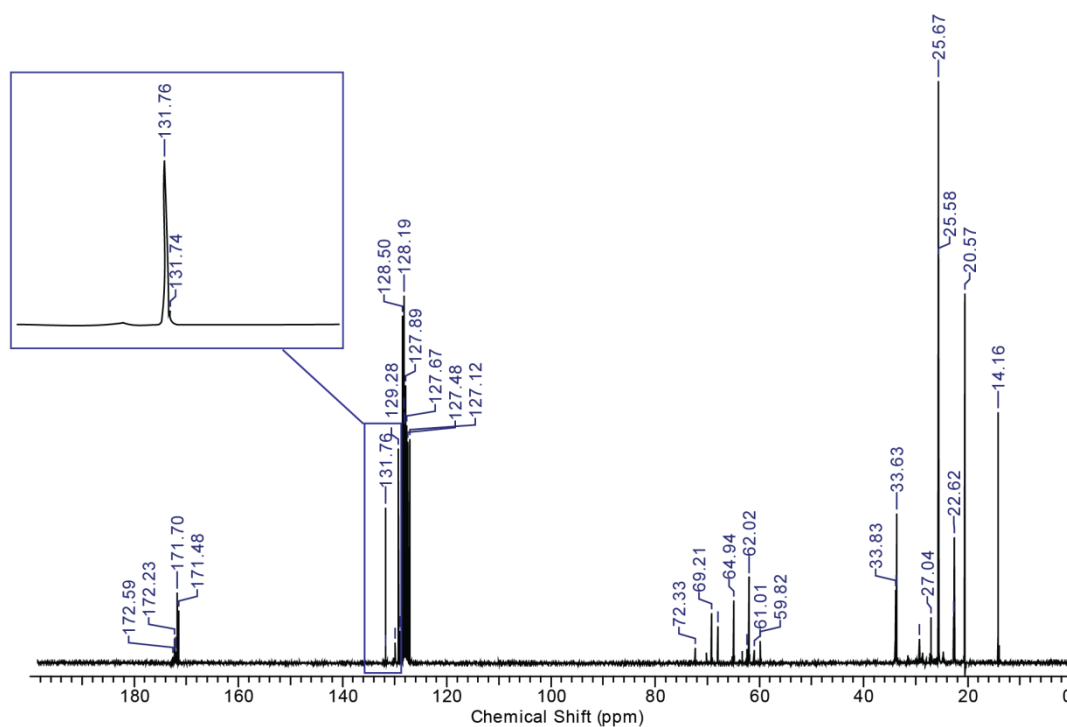


**Figure S24.**  $^{13}\text{C}$  NMR spectrum of DHA-containing triglycerides.

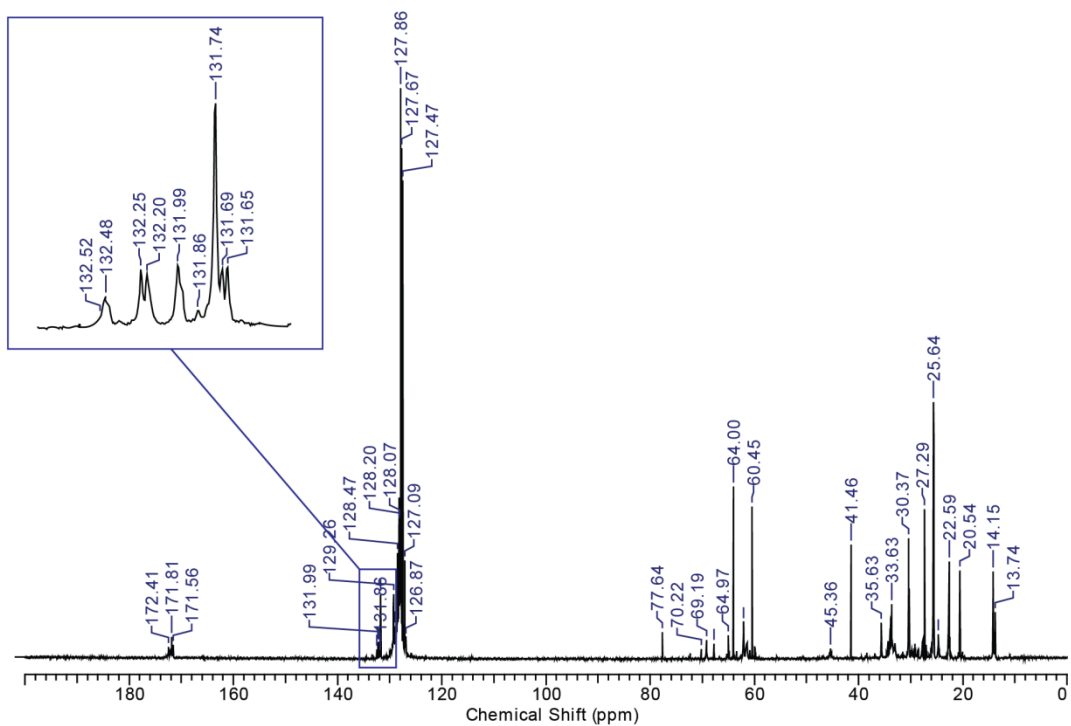


**Figure S25.**  $^{13}\text{C}$  NMR spectrum of DHA-containing triglycerides after isomerization.

## 5.9. Analysis of Omega-3 Containing Supplements

The mono-trans DHA library was used to identify the trans geometrical isomer content in DHA-containing nutraceutical formulas. Commercially available products sold as omega-3 supplement were examined: products 1-6 are present in the Italian market, products 7-19 are present in the Spanish market.

FAME*	1	2	3	4	5	6
14:0	5.75±0.04	0.56±0.01	6.11±0.08	6.01±0.05	0.81±0.03	7.58±0.12
16:0	12.86±0.01	1.45±0.05	22.54±0.15	13.14±0.08	23.48±0.08	19.21±0.14
16:1 trans-Δ <sup>9</sup>	0.34±0.02	0.07±0.01	0.64±0.06	0.46±0.00	nd	0.52±0.02
16:1 cis-Δ6+Δ7	0.16±0.01	0.03±0.00	0.26±0.05	0.15±0.01	nd	0.31±0.01
16:1 cis-Δ9	6.75±0.05	2.31±0.07	9.05±0.03	5.02±0.04	0.44±0.00	9.46±0.06
18:0	3.00±0.05	1.44±0.06	3.17±0.05	3.86±0.01	1.48±0.12	4.07±0.13
18:1 trans-Δ9	0.11±0.03	0.04±0.00	0.11±0.00	0.09±0.00	nd	0.13±0.00
18:1 trans-Δ11	0.06±0.02	0.01±0.00	0.62±0.01	0.02±0.00	nd	0.08±0.00
18:1 cis-Δ9	8.41±0.04	10.09±0.10	26.70±0.10	6.39±0.13	0.02±0.00	10.43±0.05
18:1 cis-Δ11	2.73±0.09	3.59±0.07	5.48±0.03	2.41±0.05	0.56±0.04	3.61±0.11
18:2 trans-Δ12	nd	0.13±0.01	0.07±0.00	nd	0.03±0.00	0.01±0.00
18:2 trans-Δ9	nd	0.05±0.02	0.03±0.00	0.02±0.00	0.08±0.00	0.03±0.00
18:2 ω6	1.36±0.05	2.18±0.09	1.83±0.04	1.08±0.01	0.14±0.00	1.45±0.01
18:3 ω6	0.32±0.08	0.29±0.03	0.03±0.00	0.43±0.00	nd	0.30±0.02
18:3 ω3	0.58±0.06	0.98±0.08	0.69±0.03	0.49±0.01	nd	0.93±0.11
20:0	0.22±0.02	0.13±0.00	0.14±0.00	0.37±0.00	0.31±0.01	0.50±0.05
20:1	0.98±0.08	1.06±0.04	7.75±0.05	1.44±0.12	nd	1.52±0.00
20:3 ω6	0.25±0.09	0.41±0.04	0.07±0.00	0.27±0.00	0.21±0.01	0.23±0.04
20:4 trans-Δ14	0.04±0.00	0.01±0.00	nd	0.03±0.00	nd	0.03±0.03
20:4 ω6	1.95±0.07	2.35±0.07	0.19±0.01	1.82±0.10	0.13±0.00	1.31±0.11
20:4 other mono-trans	0.04±0.00	0.06±0.00	nd	0.05±0.00	nd	0.04±0.02
20:3 ω3	0.12±0.00	0.17±0.00	0.12±0.01	0.10±0.01	nd	0.10±0.02
20:5 ω3 trans-Δ17	0.13±0.00	0.09±0.01	0.01±0.00	0.12±0.03	nd	0.03±0.00
20:4 ω3	1.08±0.04	2.05±0.06	0.64±0.07	1.14±0.01	0.91±0.01	0.95±0.01
20:5 ω3	28.05±0.28	44.34±0.12	3.47±0.05	27.40±0.15	0.66±0.01	20.53±0.26
20:5 ω3 other mono-trans	0.62±0.02	0.07±0.00	0.02±0.00	0.56±0.00	nd	0.06±0.00
22:0	0.09±0.02	0.08±0.00	0.04±0.00	0.13±0.01	0.20±0.01	0.14±0.00
22:1	0.12±0.01	0.08±0.00	2.06±0.05	0.28±0.06	nd	0.28±0.03
22:5 ω6	0.70±0.03	0.69±0.00	nd	0.55±0.00	11.91±0.13	nd
<b>22:6 ω3 trans-Δ19</b>	<b>0.12±0.01</b>	<b>0.06±0.00</b>	<b>0.53±0.03</b>	<b>0.13±0.08</b>	<b>0.12±0.04</b>	<b>0.03±0.00</b>
22:5 ω3	3.67±0.07	4.31±0.02	0.77±0.05	3.91±0.18	0.15±0.02	2.44±0.14
22:6 ω3	18.51±0.10	20.64±0.37	3.69±0.04	20.98±0.07	57.35±0.15	12.98±0.15
<b>22:6 ω3 trans-Δ4</b>	<b>0.08±0.00</b>	<b>0.01±0.00</b>	<b>0.43±0.03</b>	<b>0.07±0.00</b>	<b>0.17±0.00</b>	<b>0.06±0.05</b>
<b>22:6 ω3 trans-Δ13</b>	<b>0.19±0.02</b>	<b>0.02±0.00</b>	<b>0.44±0.02</b>	<b>0.14±0.03</b>	<b>0.33±0.01</b>	<b>0.03±0.02</b>
24:1	0.34±0.03	0.10±0.00	1.30±0.00	0.66±0.01	nd	0.57±0.10
<b>22:6 ω3 trans-Δ7+Δ10</b>	<b>0.26±0.04</b>	<b>0.02±0.00</b>	<b>1.00±0.01</b>	<b>0.29±0.02</b>	<b>0.50±0.02</b>	<b>0.05±0.04</b>
Total SFA	21.92±0.05	3.66±0.10	32.00±0.17	23.52±0.14	26.28±0.21	31.49±0.13
Total MUFA	19.49±0.20	17.27±0.23	52.60±0.14	16.34±0.06	1.03±0.04	26.18±0.03
Total PUFA	55.89±0.25	77.72±0.37	11.51±0.22	57.61±0.05	59.53±0.19	41.22±0.11
PUFA ω6	4.58±0.20	5.93±0.16	2.12±0.05	4.15±0.09	12.39±0.14	3.29±0.10
PUFA ω3	52.01±0.31	72.48±0.51	9.38±0.18	54.01±0.06	59.06±0.18	37.93±0.15
Total TFA	2.00±0.07	0.66±0.04	3.89±0.10	1.98±0.15	1.25±0.02	1.12±0.13
TFA ω3	1.40±0.10	0.27±0.01	2.43±0.09	1.30±0.14	1.13±0.03	0.27±0.08

**Table S2.** Fatty acid content (%rel) determined in omega-3 containing supplements commercially available in Italy. Analyses performed in triplicates (n=3).

\*Fatty acid methyl esters (FAME) expressed as relative percentages of the peak areas detected in the chromatograms (>98% of the total peak areas of the chromatogram recognized by appropriate FAME

references). Monotrans isomers recognized in comparison with the appropriate library as described in the main text; nd= not detectable.

FAME*	7	8	9	10	11	12	13	14	15	16	17	18	19
14:0	0.11±0.00	0.67±0.01	9.39±0.09	8.85±0.04	8.73±0.04	7.28±0.05	0.03±0.00	0.01±0.00	0.01±0.00	10.24±0.19	0.04±0.00	0.18±0.01	0.29±0.00
16:0	0.55±0.01	13.78±0.06	18.15±0.19	19.43±0.13	17.72±0.07	17.68±0.13	0.10±0.00	0.06±0.00	0.06±0.00	42.32±0.69	0.18±0.01	1.02±0.01	1.02±0.18
16:1 trans-Δ <sup>9</sup>	0.01±0.00	0.38±0.03	0.62±0.04	0.59±0.03	0.45±0.03	0.52±0.02	nd	nd	nd	0.63±0.03	0.01±0.00	0.03±0.00	nd
16:1 cis-Δ <sup>6</sup> +Δ <sup>7</sup>	0.01±0.00	0.19±0.02	0.22±0.03	0.28±0.02	0.21±0.01	0.24±0.02	nd	nd	nd	0.07±0.01	0.02±0.00	0.01±0.00	nd
16:1 cis-Δ <sup>9</sup>	0.37±0.00	7.21±0.03	11.14±0.07	10.92±0.04	11.59±0.05	8.88±0.01	0.09±0.00	0.03±0.00	0.01±0.00	3.73±0.32	1.06±0.03	0.53±0.01	0.77±0.03
18:0	6.16±0.03	3.40±0.09	3.41±0.05	3.87±0.01	3.25±0.01	3.91±0.01	0.06±0.00	0.04±0.00	0.03±0.00	1.97±0.17	0.11±0.01	6.51±0.03	2.25±0.14
18:1 trans-Δ <sup>9</sup>	0.13±0.01	0.25±0.09	0.15±0.03	0.17±0.03	0.15±0.03	0.14±0.04	nd	0.01±0.00	nd	0.08±0.02	0.01±0.00	0.15±0.01	nd
18:1 trans-Δ <sup>11</sup>	0.07±0.02	0.22±0.05	0.11±0.04	0.10±0.04	0.03±0.01	0.13±0.02	nd	nd	nd	0.01±0.00	0.01±0.00	0.09±0.00	nd
18:1 cis-Δ <sup>9</sup>	10.25±0.01	17.78±0.06	9.14±0.02	9.09±0.00	8.58±0.01	9.08±0.06	0.24±0.00	0.12±0.00	0.04±0.00	9.04±0.03	7.13±0.06	10.63±0.15	nd
18:1 cis-Δ <sup>11</sup>	4.19±0.06	6.27±0.04	3.55±0.09	3.72±0.03	3.44±0.04	3.15±0.06	0.03±0.00	0.16±0.00	0.01±0.00	5.53±0.02	2.76±0.05	4.61±0.04	nd
18:2 trans-Δ <sup>12</sup>	nd	0.21±0.04	0.08±0.01	0.16±0.02	0.15±0.01	0.17±0.03	nd	nd	nd	0.01±0.00	0.27±0.02	0.12±0.02	nd
18:2 trans-Δ <sup>9</sup>	0.03±0.01	0.60±0.03	0.04±0.00	0.04±0.01	0.04±0.01	0.06±0.01	nd	0.01±0.00	nd	0.03±0.00	0.16±0.01	0.26±0.04	5.61±0.21
18:2 ω <sub>6</sub>	1.54±0.00	3.40±0.05	2.27±0.04	1.79±0.03	1.53±0.02	4.94±0.02	0.05±0.01	0.13±0.00	0.05±0.01	2.07±0.08	1.47±0.02	2.35±0.01	nd
18:3 ω <sub>6</sub>	0.25±0.01	0.56±0.06	0.26±0.03	0.30±0.01	0.35±0.04	2.14±0.07	0.03±0.00	nd	nd	0.14±0.02	0.28±0.03	0.28±0.00	nd
18:3 ω <sub>3</sub>	0.95±0.01	1.53±0.02	0.72±0.04	0.81±0.03	0.81±0.02	0.81±0.02	0.02±0.00	nd	nd	0.85±0.14	0.87±0.03	1.17±0.01	nd
20:0	0.64±0.01	0.24±0.03	0.18±0.02	0.36±0.02	0.31±0.01	0.48±0.03	0.04±0.00	nd	nd	0.08±0.01	0.06±0.00	0.75±0.01	0.30±0.01
20:1	2.79±0.07	0.91±0.03	0.85±0.02	1.14±0.05	0.64±0.04	1.81±0.04	0.08±0.00	0.02±0.00	nd	0.56±0.05	0.47±0.04	2.75±0.03	0.35±0.11
20:3 ω <sub>6</sub>	0.46±0.02	0.21±0.01	0.20±0.03	0.18±0.03	0.23±0.03	0.19±0.04	0.03±0.00	0.01±0.00	nd	0.07±0.02	0.40±0.03	0.48±0.02	0.23±0.00
20:4 trans-Δ <sup>14</sup>	0.06±0.01	0.05±0.04	0.03±0.00	0.02±0.00	0.02±0.00	0.01±0.00	nd	0.03±0.00	nd	0.01±0.00	0.04±0.01	0.09±0.02	nd
20:4 ω <sub>6</sub>	2.27±0.03	1.49±0.03	1.17±0.05	1.19±0.03	1.73±0.01	1.22±0.01	0.12±0.00	0.72±0.00	0.02±0.01	0.28±0.01	2.71±0.04	2.32±0.06	0.48±0.01
20:4 other mono-trans	0.04±0.00	0.05±0.04	0.03±0.00	0.02±0.00	0.02±0.00	0.02±0.00	nd	0.01±0.00	nd	0.02±0.00	0.05±0.02	0.03±0.00	nd
20:3 ω <sub>3</sub>	0.17±0.03	0.13±0.01	0.07±0.01	0.09±0.02	0.07±0.02	0.11±0.01	0.02±0.00	nd	nd	0.09±0.00	0.11±0.03	0.19±0.00	nd
20:5 ω <sub>3</sub> trans-Δ <sup>17</sup>	0.06±0.01	0.11±0.01	0.03±0.00	0.05±0.01	0.06±0.01	0.05±0.01	0.03±0.00	0.01±0.00	0.03±0.01	0.03±0.00	0.08±0.00	0.09±0.02	nd
20:4 ω <sub>3</sub>	1.73±0.02	0.86±0.03	0.74±0.04	0.90±0.02	0.80±0.02	0.92±0.02	0.09±0.00	0.06±0.00	0.09±0.01	0.33±0.01	1.95±0.01	1.65±0.03	nd
20:5 ω <sub>3</sub>	37.56±0.22	21.87±0.19	20.24±0.21	20.00±0.14	21.41±0.11	19.60±0.19	2.29±0.00	3.24±0.01	5.59±0.01	13.48±0.34	48.32±0.17	34.95±0.15	2.35±0.03
20:5 ω <sub>3</sub> other mono-trans	0.07±0.01	0.14±0.02	0.10±0.02	0.06±0.00	0.09±0.01	0.09±0.00	0.04±0.00	0.07±0.01	0.12±0.01	0.14±0.19	0.09±0.00	0.11±0.00	nd
22:0	0.29±0.01	0.08±0.01	0.84±0.07	0.12±0.02	0.11±0.01	0.15±0.01	0.06±0.00	0.02±0.01	nd	0.07±0.01	0.02±0.00	0.28±0.02	0.55±0.08
22:1	0.37±0.02	0.16±0.02	0.14±0.02	0.17±0.02	0.09±0.01	0.44±0.02	0.15±0.00	nd	nd	0.45±0.01	0.03±0.00	0.34±0.03	nd
22:5 ω <sub>6</sub>	nd	nd	nd	nd	nd	nd	1.97±0.00	6.24±0.01	0.52±0.03	nd	0.64±0.03	0.78±0.04	3.92±0.80
22:6 ω <sub>3</sub> trans-Δ <sup>19</sup>	<b>0.06±0.01</b>	<b>0.09±0.01</b>	<b>0.04±0.01</b>	<b>0.04±0.01</b>	<b>0.05±0.00</b>	<b>0.05±0.02</b>	<b>0.27±0.03</b>	<b>0.34±0.03</b>	<b>0.31±0.02</b>	<b>0.02±0.00</b>	<b>0.06±0.01</b>	<b>0.07±0.00</b>	<b>0.66±0.24</b>
22:5 ω <sub>3</sub>	5.20±0.06	2.10±0.03	2.11±0.06	2.13±0.02	2.18±0.01	1.98±0.00	9.94±0.32	1.17±0.02	13.32±0.04	0.38±0.02	3.96±0.02	4.47±0.02	2.09±0.33
22:6 ω <sub>3</sub>	22.60±0.14	14.60±0.15	13.50±0.10	12.90±0.10	14.71±0.05	13.11±0.06	83.68±0.17	86.19±0.11	78.78±0.11	7.16±0.31	26.54±0.09	21.85±0.07	76.75±0.41
22:6 ω <sub>3</sub> trans-Δ <sup>4</sup>	<b>0.02±0.01</b>	<b>0.08±0.00</b>	<b>0.03±0.01</b>	<b>0.03±0.00</b>	<b>0.03±0.01</b>	<b>0.05±0.01</b>	<b>0.09±0.03</b>	<b>0.16±0.02</b>	<b>0.18±0.03</b>	<b>0.02±0.00</b>	<b>0.02±0.00</b>	<b>0.02±0.01</b>	<b>0.30±0.01</b>
22:6 ω <sub>3</sub> trans-Δ <sup>13</sup>	<b>0.02±0.00</b>	<b>0.09±0.01</b>	<b>0.03±0.00</b>	<b>0.02±0.00</b>	<b>0.03±0.02</b>	<b>0.02±0.01</b>	<b>0.10±0.04</b>	<b>0.46±0.03</b>	<b>0.35±0.02</b>	<b>0.02±0.00</b>	<b>0.05±0.00</b>	<b>0.07±0.04</b>	<b>0.74±0.02</b>
24:1	0.97±0.03	0.24±0.01	0.40±0.00	0.47±0.04	0.31±0.02	0.54±0.03	0.14±0.03	nd	nd	0.04±0.00	0.01±0.00	0.75±0.07	0.34±0.14
22:6 ω <sub>3</sub> trans-Δ <sup>7</sup> +Δ <sup>10</sup>	<b>0.03±0.01</b>	<b>0.07±0.00</b>	<b>0.02±0.00</b>	<b>0.02±0.00</b>	<b>0.07±0.02</b>	<b>0.04±0.01</b>	<b>0.20±0.03</b>	<b>0.68±0.01</b>	<b>0.49±0.03</b>	<b>0.01±0.00</b>	<b>0.02±0.00</b>	<b>0.02±0.00</b>	<b>1.00±0.14</b>
Total SFA	7.74±0.03	18.17±0.12	31.96±0.23	32.62±0.14	30.12±0.09	29.50±0.17	0.30±0.00	0.13±0.01	0.10±0.01	54.68±0.71	0.40±0.00	8.73±0.07	4.40±0.22
Total MUFA	18.95±0.16	32.75±0.04	25.45±0.15	25.78±0.10	24.86±0.05	24.12±0.15	0.73±0.03	0.33±0.01	0.06±0.01	19.43±0.29	11.46±0.09	19.62±0.09	1.47±0.19
Total PUFA	72.71±0.20	46.75±0.31	41.29±0.30	40.30±0.10	43.83±0.06	45.02±0.11	96.27±0.14	91.52±0.09	97.85±0.11	24.85±0.66	86.61±0.14	69.72±0.17	81.90±0.61
PUFA ω <sub>6</sub>	4.51±0.07	5.66±0.07	3.90±0.07	3.46±0.09	3.84±0.08	8.49±0.14	2.19±0.01	7.10±0.01	0.59±0.04	2.57±0.12	5.50±0.12	6.21±0.11	4.64±0.81
PUFA ω <sub>3</sub>	68.20±0.26	41.09±0.36	37.39±0.29	36.84±0.19	39.99±0.13	36.53±0.23	96.05±0.14	90.66±0.10	97.78±0.11	22.28±0.78	81.76±0.22	64.29±0.19	81.18±0.61
Total TFA	0.60±0.05	2.33±0.26	1.31±0.09	1.30±0.13	1.19±0.08	1.36±0.14	0.72±0.10	1.78±0.08	1.47±0.09	1.04±0.22	0.88±0.07	1.14±0.08	8.32±0.35
TFA ω <sub>3</sub>	0.26±0.03	0.57±0.04	0.24±0.01	0.22±0.02	0.34±0.06	0.30±0.05	0.72±0.10	1.72±0.08	1.47±0.09	0.24±0.19	0.32±0.01	0.38±0.03	2.71±0.39

**Table S3.** Fatty acid content (%rel) determined in omega-3 containing supplements commercially available in Spain. Analyses performed in triplicates (n=3) of the same sample.

\*Fatty acid methyl esters (FAME) expressed as relative percentages of the peak areas detected in the chromatograms (>98% of the total peak areas of the chromatogram recognized by appropriate FAME references).

§ Mono-trans isomers recognized in comparison with the appropriate library as described in the main text; nd= not detectable.

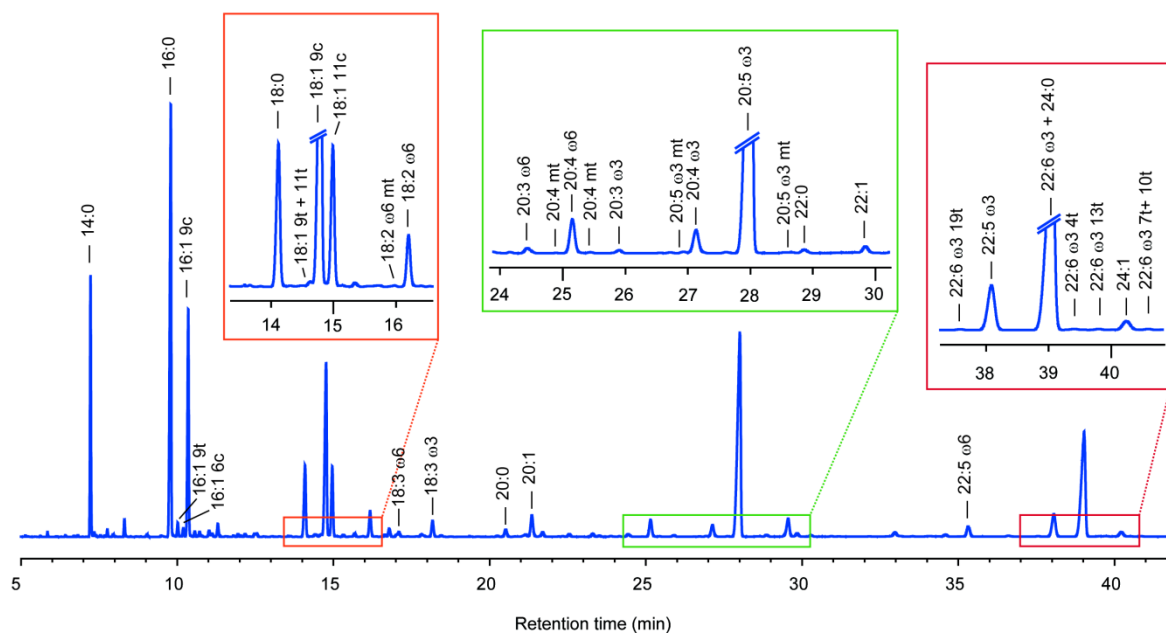


**Figure S26.** Representative GC chromatogram of FAME in fish oil material obtained according to Method A (helium as carrier gas). **Tables S2** and **S3** summarize the results of the analyses.

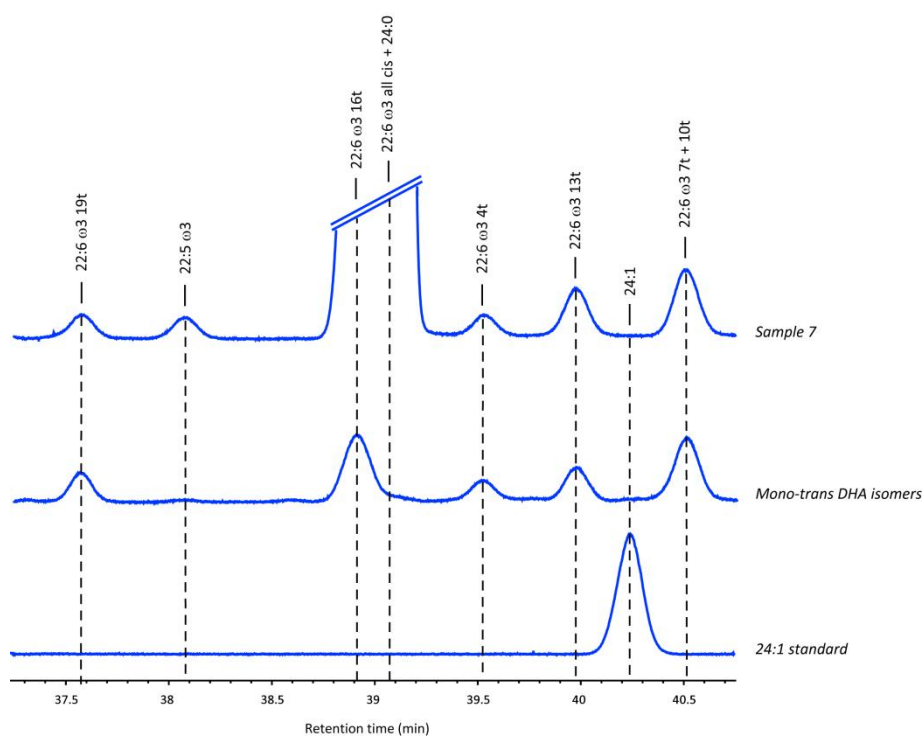


**Figure S27.** Partial GC trace showing the separation of the C22-24 FAME according to Method A (helium as carrier gas). Separation of C24:1 and superimposition of some mono-trans DHA isomers and of C24:0 are shown.

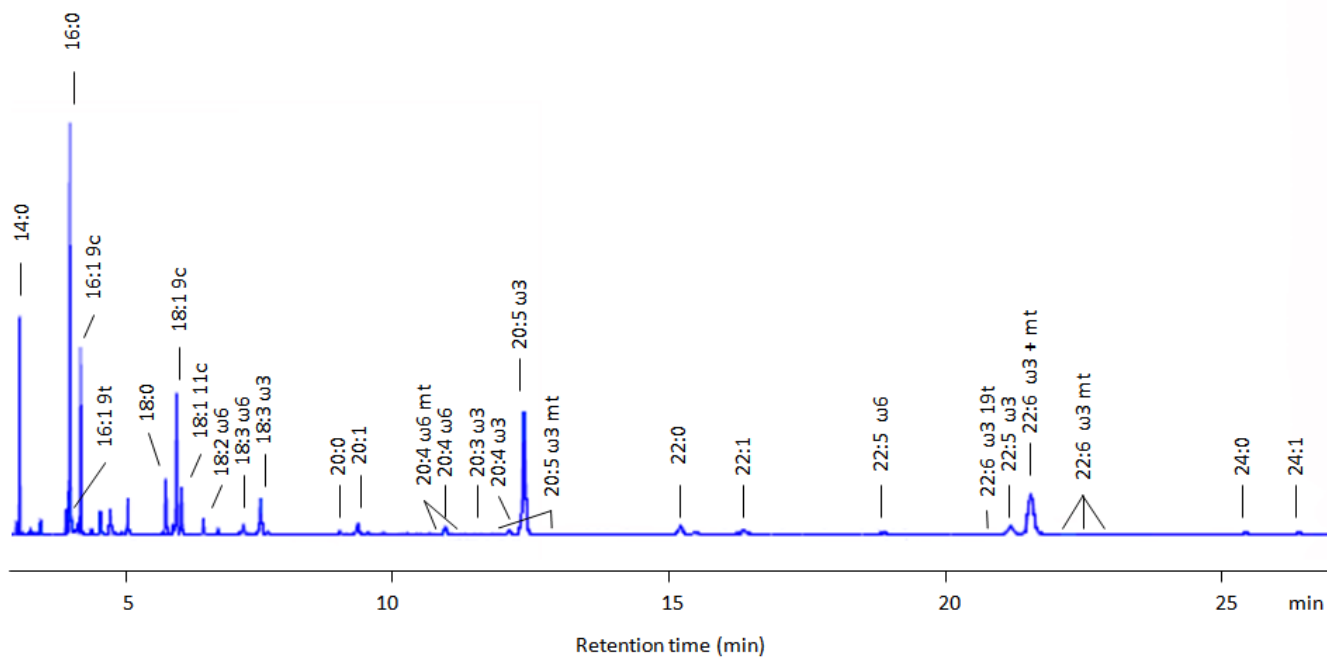


**Figure S28.** Representative GC chromatogram of FAME in fish oil obtained according to Method B (hydrogen as carrier gas). **Tables S2** and **S3** summarize the results of the analyses.

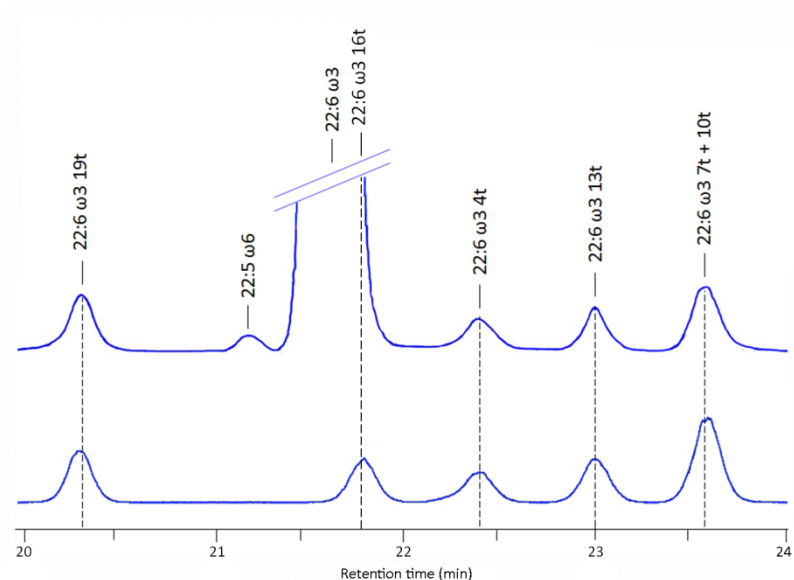


**Figure S29.** Partial GC trace showing the separation of the C22-24 FAME according to Method B (hydrogen as carrier gas). Superimposition of 16 mono-trans DHA isomer with cis-DHA and good separation of the C22:5 ω3 are shown, whereas C22:5 ω-6, C24:0 and C24:1 do not elute in the DHA window.

## 5.10. Gas Chromatographic Identification of FAMES in 20 % 18:0-22:6 PC/16:0-18:1 PC Composition of Vesicles

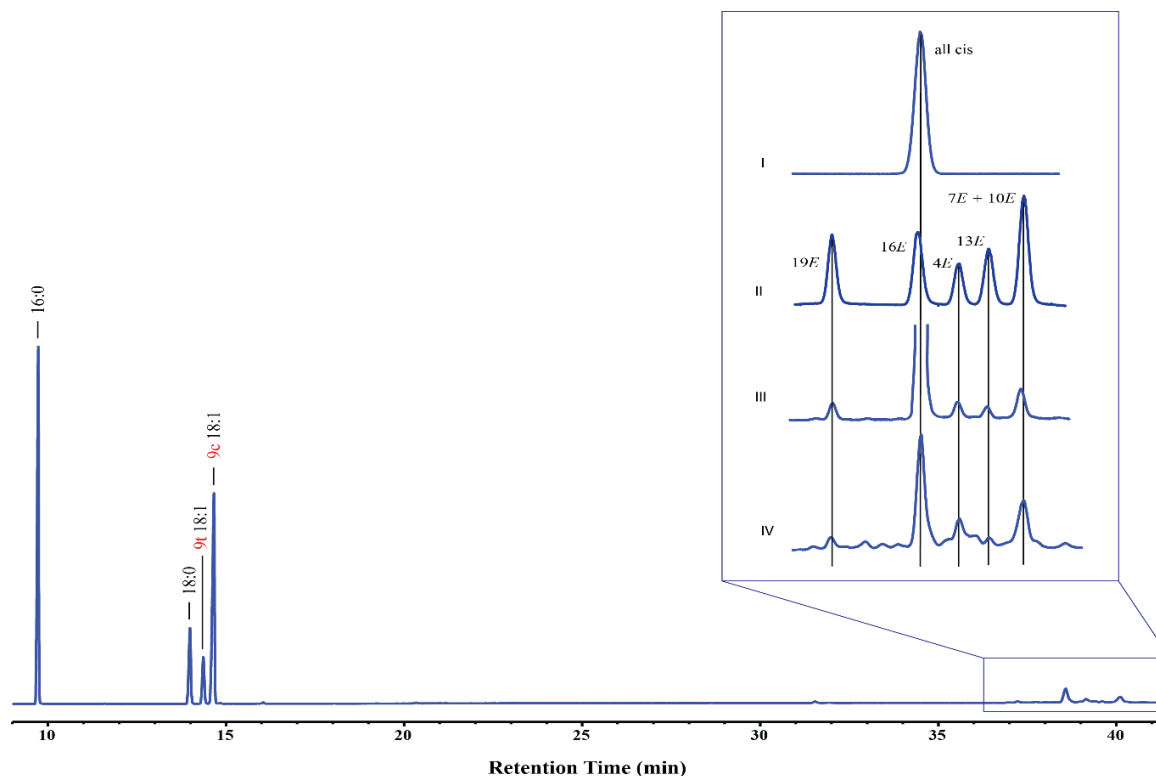


**Figure S30.** GC chromatogram of FAMES obtained after incubation of 20 % 18:0-22:6 PC/16:0-18:1 PC liposomes at 37°C under anaerobic condition in the presence of 0.15 mM Cu-TPMA-Phen and 10 mM 2-mercaptoethanol. In the blue box the GC chromatograms of (I) all cis-DHA in 20 % 18:0-22:6 PC/16:0-18:1 PC liposomes (starting material – no reaction); (II) reference mixture of monotrans DHA methyl ester isomers obtained by photolysis in the presence of thiyl radicals in solution (III) mixture of all cis and monotrans DHA in 20 % 18:0-22:6 PC/16:0-18:1 PC liposomes obtained after 2 hr of reaction (IV) mixture of all cis, monotrans and poly-trans of DHA in 20 % 18:0-22:6 PC/16:0-18:1 PC liposomes obtained after 8 hr of reaction (as presented in the full chromatogram).

## Part II – Studies on DNA Damage

### 5.11. Agarose Gel Electrophoresis

#### *Studies on Cleavage Properties – Absence of Reductant*

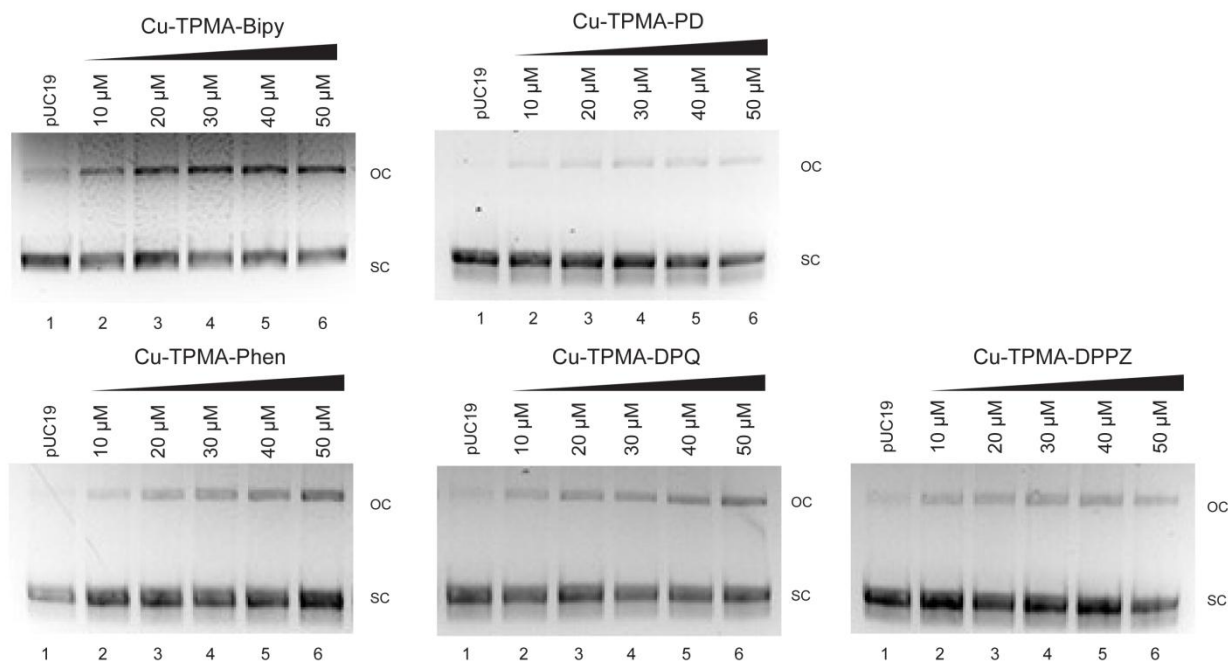


**Figure S31.** 400 ng pUC19 supercoiled DNA was treated with increasing concentrations (10, 20, 30, 40, 50 μM) of Cu-TPMA-Bipy, Cu-TPMA-PD, Cu-TPMA-Phen, Cu-TPMA-DPQ and Cu-TPMA-DPPZ in the absence of 1 mM Na-*L*-ascorbate and incubated at 37 °C for 30 min. Electrophoresis carried out as previously stated.

### *Studies on Cleavage Properties – Presence of Reductant*

Herein, the gel electrophoresis for Cu-TPMA-Bipy and Cu-TPMA-PD in the presence of reductant are presented. These two complexes appear to have the less efficient nuclease reactivity.

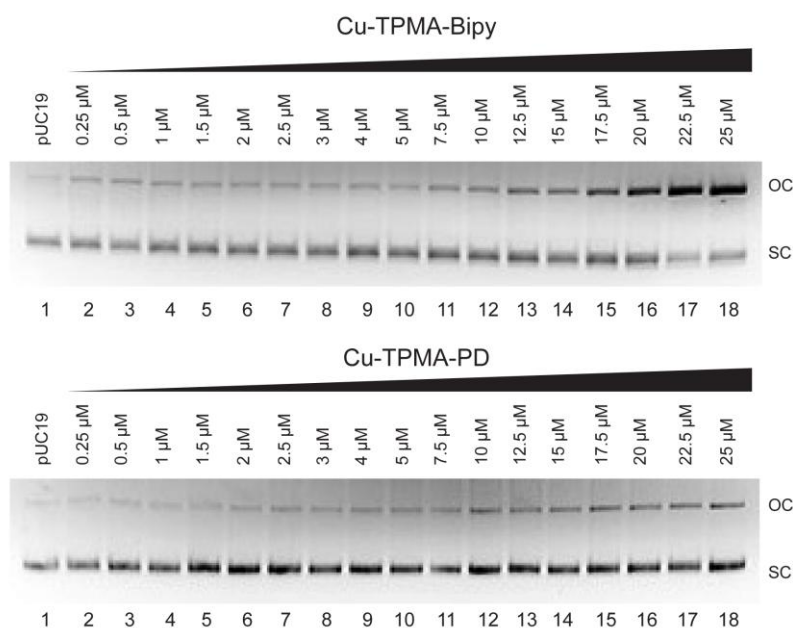


**Figure S32.** 400 ng pUC19 supercoiled DNA was treated with increasing concentrations (0.25 μM –25 μM) of Cu-TPMA-Bipy and Cu-TPMA-PD in the presence of 1 mM Na-*L*-ascorbate and incubated at 37 °C for 30 min. Electrophoresis carried out as previously stated.

### *Enzymatic Controls of Endonucleases Reactivity*

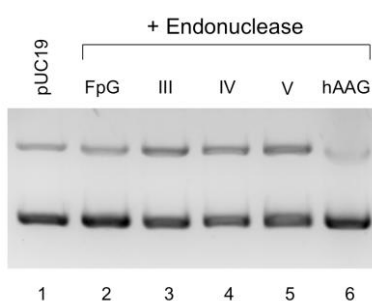


**Figure S33.** 400 ng pUC19 supercoiled DNA (lane 1) in the presence of 1 mM Na-*L*-ascorbate and 2U of either FpG (lane 2), Endo III (lane 3), Endo IV (lane 4), EndoV (lane 5) or hAAG (lane 6). The full experimental conditions are described in **Chapter 4**.

## 5.12. High Pressure Liquid Chromatography (H.P.L.C.)

Supercoiled plasmid pUC19 was knicked by two different artificial chemical nucleases (Cu-TPMA-Phen or Cu-Oda) in the presence of reductant. The damaged dsDNA was enzymatically digested to nucleosides for subsequent detection and quantification of oxidative lesions 8-oxo-Pus and cdPus. The quantification was executed in two independent steps, increasing the overall sensitivity of the method. First, the sample was analysed by an HPLC-UV system coupled with a sample collector. According to this clean-up step, the quantification of the unmodified nucleosides took place, based on their absorbance at 260 nm, whereas the time-windows when the damaged lesions are eluted were collected and pooled.

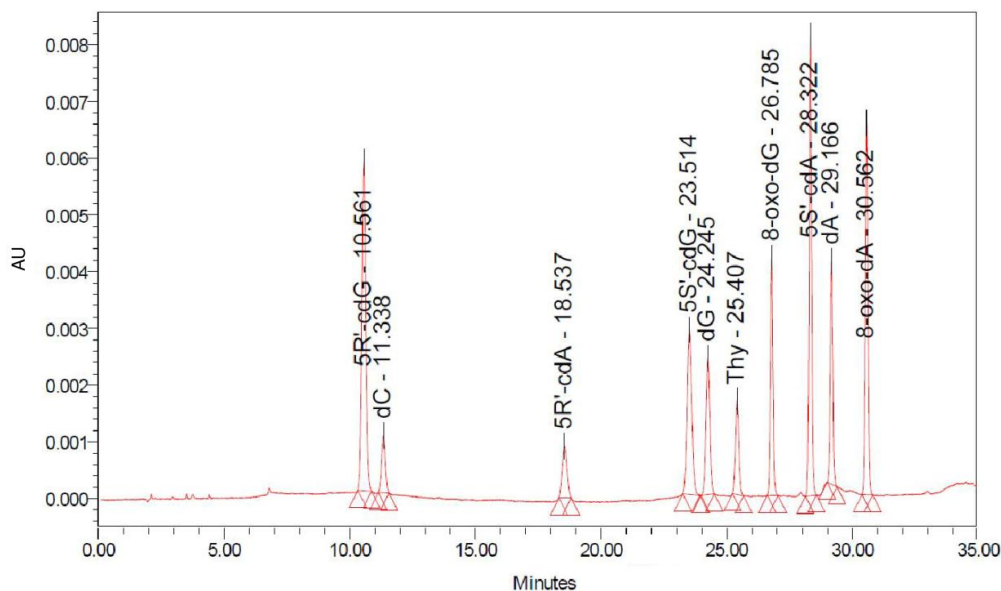


**Figure S34.** A representative optimal HPLC separation (monitored at 260 nm) of the 2'-deoxynucleosides (dA, dC, Thy and dG), purine 5',8-cyclo-2'-deoxynucleosides (5'*R*-cdA, 5'*S*-cdA, 5'*R*-cdG and 5'*S*-cdG) and the purine 8-oxo-2'-deoxynucleosides (8-oxo-dA, 8-oxo-dG). 8-oxo-dG was used as a control against 8-oxo-dA. The analysis was performed on a 4.6 mm x 150 mm Atlantis® dC18, 100 Å column (5 µm particle size, Waters) loaded with a 4.6 mm x 20 mm Guard Column 2pK (Atlantis® dC18 5µm, Waters) on a Waters Alliance ® HPLC System (Waters e2695 Separations Module) including a Waters 2998 Photodiode Array (PDA) detector; mobile phase: 2 mM ammonium formate, acetonitrile and methanol.

### 5.13. Liquid Chromatography Tandem–mass Spectrometry (LC-MS/MS)

The collected fractions were freeze-dried, pooled, freeze-dried again and re-dissolved in Milli-Q water. The concentrated samples containing the modified DNA damage lesion were injected subsequently to LC-MS/MS to be analysed independently. **Figure S35** illustrates the MRM chromatograms of the corresponding mass transitions for 5'*R*-cdG, 5'*S*-cdG, 5'*R*-cdA and 5'*S*-cdA, as well as their isotope-labelled [<sup>15</sup>N<sub>5</sub>]-5'*R*-cdG, [<sup>15</sup>N<sub>5</sub>]-5'*S*-cdG, [<sup>15</sup>N<sub>5</sub>]-5'*R*-cdA, [<sup>15</sup>N<sub>5</sub>]-5'*S*-cdA, which were acquired during LC-MS/MS analysis of the samples.

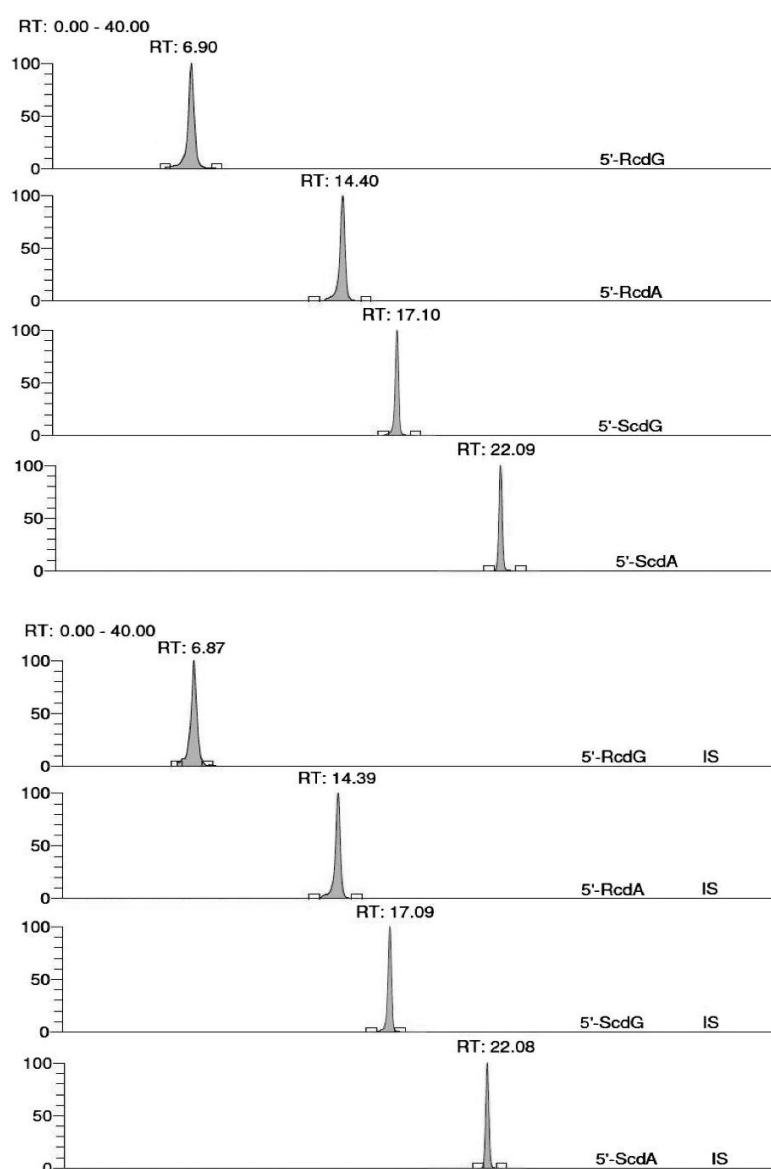


**Figure S35.** MRM chromatograms of quantification ions obtained by LC–MS/MS analysis: Quantification transitions (Upper part)  $m/z$  266  $\rightarrow$   $m/z$  180 (5'*R*-cdG and 5'*S*-cdG),  $m/z$  250  $\rightarrow$   $m/z$  164 (5'*R*-cdA and 5'*S*-cdA); (Lower part)  $m/z$  271  $\rightarrow$   $m/z$  185 ([<sup>15</sup>N<sub>5</sub>]-5'*R*-cdG and [<sup>15</sup>N<sub>5</sub>]-5'*S*-cdG) and  $m/z$  255  $\rightarrow$   $m/z$  169 ([<sup>15</sup>N<sub>5</sub>]-5'*R*-cdA and [<sup>15</sup>N<sub>5</sub>]-5'*S*-cdA).

As shown in **Figure S36**, the fragment ions of  $m/z = 164$  and 180 (together with 169 and 185 for the labelled cdA and cdG, data not shown) are resulting from the cleavage of both the N-glycosidic bond and C4'–C5' bond of the 2-deoxyribose unit.

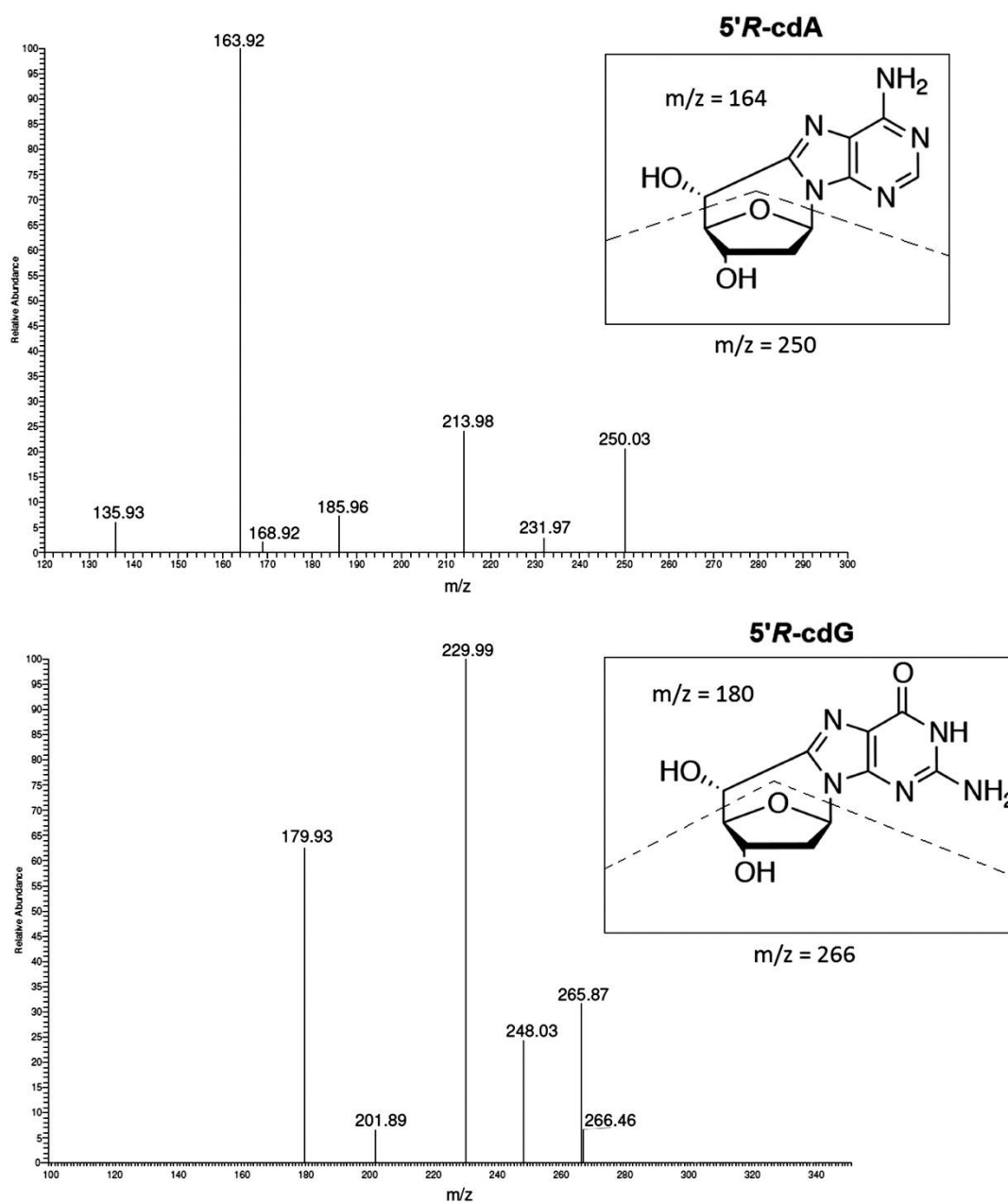


**Figure S36.** MS/MS fragmentation spectra (ESI-MS/MS of the  $[M+H]^+$  ion) of 5'R-cdA ( $m/z$  250→164) and 5'R-cdG ( $m/z$  266→180) lesions (similar fragment ions were observed for 5'S-cdA and 5'S-cdG lesions).

Additionally to cPu lesions, we measured by LC-MS/MS the levels of 8-oxo-dA and 8-oxo-dG, which is a commonly used oxidative DNA damage markers and substrate of base excision repair (BER). As it can be seen in **Figure S37**, the 8-oxo-dA was eluted at 25.2 min and the  $m/z = 267 \rightarrow 151$  transition for this lesion was monitored. The [ $^{15}\text{N}_5$ ]-8-oxo-dA was eluted at the same time, monitored by  $272 \rightarrow 156$  transition (data not shown).

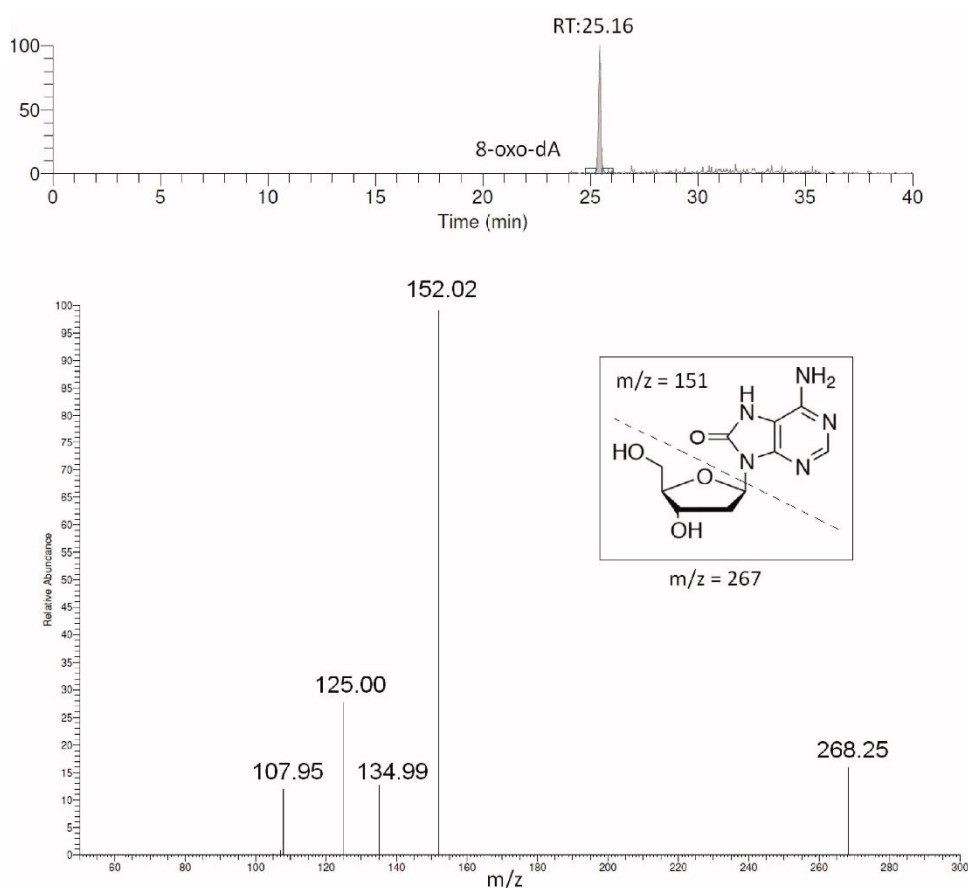


**Figure S37.** MRM chromatogram of the mass transition  $m/z 267 \rightarrow m/z 151$  obtained by LC-MS/MS analysis and MS/MS fragmentation spectrum (ESI-MS/MS of the  $[M + H]^+$  ion) of 8-oxo-dA.

## References

1. GM., C., *The Cell: A Molecular Approach*. 2 ed.; Sinauer Associates: Sunderland (MA), 2000.
2. Cancer Research UK. <https://www.cancerresearchuk.org/>.
3. Health, N. I. o.
4. Lodish H, B. A., Zipursky SL, et al., *Molecular Cell Biology*. 4 ed.; New York 2000.
5. Lunec, J., Free Radicals: Their Involvement in Disease Processes. *Annals of Clinical Biochemistry* **1990**, *27* (3), 173-182.
6. Bandyopadhyay, S.; Mehta, M.; Kuo, D.; Sung, M. K.; Chuang, R.; Jaehnig, E. J.; Bodenmiller, B.; Licon, K.; Copeland, W.; Shales, M.; Fiedler, D.; Dutkowski, J.; Guenole, A.; van Attikum, H.; Shokat, K. M.; Kolodner, R. D.; Huh, W. K.; Aebersold, R.; Keogh, M. C.; Krogan, N. J.; Ideker, T., Rewiring of genetic networks in response to DNA damage. *Science* **2010**, *330* (6009), 1385-9.
7. Pagès, V.; Fuchs, R. P. P., How DNA lesions are turned into mutations within cells? *Oncogene* **2002**, *21*, 8957.
8. Dar, A. C.; Das, T. K.; Shokat, K. M.; Cagan, R. L., Chemical genetic discovery of targets and anti-targets for cancer polypharmacology. *Nature* **2012**, *486*, 80.
9. Baruah, H.; Barry, C. G.; Bierbach, U., Platinum-intercalator conjugates: from DNA-targeted cisplatin derivatives to adenine binding complexes as potential modulators of gene regulation. *Curr Top Med Chem* **2004**, *4* (15), 1537-49.
10. Carvalho, C.; Santos, R. X.; Cardoso, S.; Correia, S.; Oliveira, P. J.; Santos, M. S.; Moreira, P. I., Doxorubicin: the good, the bad and the ugly effect. *Current medicinal chemistry* **2009**, *16* (25), 3267-85.
11. Parker, W. B.; Cheng, Y. C., Metabolism and mechanism of action of 5-fluorouracil. *Pharmacol Ther* **1990**, *48* (3), 381-95.
12. Wozniak, A. J.; Ross, W. E., DNA damage as a basis for 4'-demethylepipodophyllotoxin-9-(4,6-O-ethylidene-beta-D-glucopyranoside) (etoposide) cytotoxicity. *Cancer Res* **1983**, *43* (1), 120-4.
13. Lankadasari, M. B.; Aparna, J. S.; Mohammed, S.; James, S.; Aoki, K.; Binu, V. S.; Nair, S.; Harikumar, K. B., Targeting S1PR1/STAT3 loop abrogates desmoplasia and chemosensitizes pancreatic cancer to gemcitabine. *Theranostics* **2018**, *8* (14), 3824-3840.

14. Pizarro, A. M.; Sadler, P. J., Unusual DNA binding modes for metal anticancer complexes. *Biochimie* **2009**, *91* (10), 1198-1211.
15. Brinkmann, M.; Tallone, E. M.; Wurschmidt, F.; Wulfing, C.; Dieckmann, K. P., [Myocardial infarction in a young patient with seminoma during chemotherapy with cisplatin, etoposide, and bleomycin]. *Aktuelle Urol* **2018**.
16. Siddik, Z. H., Cisplatin: mode of cytotoxic action and molecular basis of resistance. *Oncogene* **2003**, *22* (47), 7265-79.
17. Oun, R.; Moussa, Y. E.; Wheate, N. J., The side effects of platinum-based chemotherapy drugs: a review for chemists. *Dalton Transactions* **2018**, *47* (19), 6645-6653.
18. Interactions of Metallodrugs with DNA. In *NMR of Biomolecules*.
19. Deo, K. M.; Pages, B. J.; Ang, D. L.; Gordon, C. P.; Aldrich-Wright, J. R., Transition Metal Intercalators as Anticancer Agents—Recent Advances. *International Journal of Molecular Sciences* **2016**, *17* (11), 1818.
20. (a) Malina, J.; Novakova, O.; Vojtiskova, M.; Natile, G.; Brabec, V., Conformation of DNA GG Intrastrand Cross-Link of Antitumor Oxaliplatin and Its Enantiomeric Analog. *Biophysical Journal* **2007**, *93* (11), 3950-3962; (b) Bruijninx, P. C.; Sadler, P. J., New trends for metal complexes with anticancer activity. *Current opinion in chemical biology* **2008**, *12* (2), 197-206.
21. Sigman, D. S.; Mazumder, A.; Perrin, D. M., Chemical nucleases. *Chemical Reviews* **1993**, *93* (6), 2295-2316.
22. Fondello, C.; Agnetti, L.; Glikin, G. C.; Finocchiaro, L. M. E., Mechanisms Enhancing the Cytotoxic Effects of Bleomycin plus Suicide or Interferon-beta Gene Lipofection in Metastatic Human Melanoma Cells. *Anticancer Agents Med Chem* **2018**.
23. Bolzan, A. D.; Bianchi, M. S., DNA and chromosome damage induced by bleomycin in mammalian cells: An update. *Mutat Res* **2018**, *775*, 51-62.
24. Ben-Yoseph, O.; Ross, B. D., Oxidation therapy: the use of a reactive oxygen species-generating enzyme system for tumour treatment. *British Journal of Cancer* **1994**, *70* (6), 1131-1135.
25. Tan, L. T.-H.; Chan, K.-G.; Pusparajah, P.; Lee, W.-L.; Chuah, L.-H.; Khan, T. M.; Lee, L.-H.; Goh, B.-H., Targeting Membrane Lipid a Potential Cancer Cure? *Frontiers in Pharmacology* **2017**, *8*, 12.

26. Cort, A.; Ozben, T.; Melchiorre, M.; Chatgililoglu, C.; Ferreri, C.; Sansone, A., Effects of bleomycin and antioxidants on the fatty acid profile of testicular cancer cell membranes. *Biochim Biophys Acta* **2016**, *1858* (2), 434-41.
27. Cort, A.; Ozben, T.; Sansone, A.; Barata-Vallejo, S.; Chatgililoglu, C.; Ferreri, C., Bleomycin-induced trans lipid formation in cell membranes and in liposome models. *Org Biomol Chem* **2015**, *13* (4), 1100-5.
28. Gutteridge, B. H. a. J. M. C., *Free Radicals in Biology and Medicine*. Fifth Edition ed.; Oxford University Press: 2015.
29. Chatgililoglu, C.; Ferreri, C., Trans lipids: the free radical path. *Acc Chem Res* **2005**, *38* (6), 441-8.
30. Chen, C. L.; Tetri, L. H.; Neuschwander-Tetri, B. A.; Huang, S. S.; Huang, J. S., A mechanism by which dietary trans fats cause atherosclerosis. *J Nutr Biochem* **2011**, *22* (7), 649-55.
31. Garcia, S. C.; Grotto, D.; Bulcão, R. P.; Moro, A. M.; Roehrs, M.; Valentini, J.; de Freitas, F. A.; Paniz, C.; Bubols, G. B.; Charão, M. F., Evaluation of lipid damage related to pathological and physiological conditions. *Drug and Chemical Toxicology* **2013**, *36* (3), 306-312.
32. Ferreri, C.; Chatgililoglu, C., Role of fatty acid-based functional lipidomics in the development of molecular diagnostic tools. *Expert Rev Mol Diagn* **2012**, *12* (7), 767-80.
33. Lucio, M.; Ferreira, H.; Lima, J. L.; Reis, S., Use of liposomes as membrane models to evaluate the contribution of drug-membrane interactions to antioxidant properties of etodolac. *Redox Rep* **2008**, *13* (5), 225-36.
34. Thomas, A. H.; Catala, A.; Vignoni, M., Soybean phosphatidylcholine liposomes as model membranes to study lipid peroxidation photoinduced by pterin. *Biochim Biophys Acta* **2016**, *1858* (1), 139-45.
35. Danielli, J. F.; Davson, H., A contribution to the theory of permeability of thin films. *Journal of Cellular and Comparative Physiology* **1935**, *5* (4), 495-508.
36. Singer, S. J.; Nicolson, G. L., The fluid mosaic model of the structure of cell membranes. *Science* **1972**, *175* (4023), 720-31.
37. Biology Wise. <https://biologywise.com/>.
38. Berg JM, T. J., Stryer L, *Biochemistry*. 5th edition ed.; W H Freeman: New York, 2002.
39. Alberts B, J. A., Lewis J, et al., *Molecular Biology of the Cell*. 4th edition ed.; Garland Science: New York, 2002.

40. Cook, H. W., Chapter 5 - Fatty acid desaturation and chain elongation in eukaryotes. In *New Comprehensive Biochemistry*, Vance, D. E.; Vance, J. E., Eds. Elsevier: 1996; Vol. 31, pp 129-152.
41. Dominguez, L. J.; Barbagallo, M., Chapter 3 - Not All Fats Are Unhealthy. In *The Prevention of Cardiovascular Disease Through the Mediterranean Diet*, Sánchez-Villegas, A.; Sánchez-Tainta, A., Eds. Academic Press: 2018; pp 35-58.
42. Kaur, N.; Chugh, V.; Gupta, A. K., Essential fatty acids as functional components of foods- a review. *Journal of Food Science and Technology* **2014**, *51* (10), 2289-2303.
43. Simopoulos, A. P., An Increase in the Omega-6/Omega-3 Fatty Acid Ratio Increases the Risk for Obesity. *Nutrients* **2016**, *8* (3), 128.
44. Laposata, M., Fatty Acids: Biochemistry to Clinical Significance. *American Journal of Clinical Pathology* **1995**, *104* (2), 172-179.
45. Migdal, C.; Serres, M., [Reactive oxygen species and oxidative stress]. *Med Sci (Paris)* **2011**, *27* (4), 405-12.
46. Bergamini, C. M.; Gambetti, S.; Dondi, A.; Cervellati, C., Oxygen, reactive oxygen species and tissue damage. *Current pharmaceutical design* **2004**, *10* (14), 1611-26.
47. Sharma, P.; Jha, A. B.; Dubey, R. S.; Pessarakli, M., Reactive Oxygen Species, Oxidative Damage, and Antioxidative Defense Mechanism in Plants under Stressful Conditions. *Journal of Botany* **2012**, *2012*, 26.
48. Gulati, K.; Rai, N.; Ray, A., Chapter 56 - Effects of Stress on Reproductive and Developmental Biology. In *Reproductive and Developmental Toxicology (Second Edition)*, Gupta, R. C., Ed. Academic Press: 2017; pp 1063-1075.
49. Birben, E.; Sahiner, U. M.; Sackesen, C.; Erzurum, S.; Kalayci, O., Oxidative Stress and Antioxidant Defense. *The World Allergy Organization journal* **2012**, *5* (1), 9-19.
50. Erden-Inal, M.; Sunal, E.; Kanbak, G., Age-related changes in the glutathione redox system. *Cell Biochem Funct* **2002**, *20* (1), 61-6.
51. Vazquez-Medina, J. P., Chapter 3 - Redox Signaling and the Onset of the Inflammatory Cascade. In *Immunity and Inflammation in Health and Disease*, Chatterjee, S.; Jungraithmayr, W.; Bagchi, D., Eds. Academic Press: 2018; pp 37-42.
52. Laurindo, F. R. M., Chapter 10 - Redox Cellular Signaling Pathways in Endothelial Dysfunction and Vascular Disease. In *Endothelium and Cardiovascular*

- Diseases*, Da Luz, P. L.; Libby, P.; Chagas, A. C. P.; Laurindo, F. R. M., Eds. Academic Press: 2018; pp 127-145.
53. Schieber, M.; Chandel, N. S., ROS Function in Redox Signaling and Oxidative Stress. *Current biology : CB* **2014**, *24* (10), R453-R462.
54. Ghosh, N.; Das, A.; Chaffee, S.; Roy, S.; Sen, C. K., Chapter 4 - Reactive Oxygen Species, Oxidative Damage and Cell Death. In *Immunity and Inflammation in Health and Disease*, Chatterjee, S.; Jungraithmayr, W.; Bagchi, D., Eds. Academic Press: 2018; pp 45-55.
55. Mjos, K. D.; Orvig, C., Metallodrugs in Medicinal Inorganic Chemistry. *Chemical Reviews* **2014**, *114* (8), 4540-4563.
56. Leon, I. E.; Cadavid-Vargas, J. F.; Di Virgilio, A. L.; Etcheverry, S. B., Vanadium, Ruthenium and Copper Compounds: A New Class of Nonplatinum Metallodrugs with Anticancer Activity. *Current medicinal chemistry* **2017**, *24* (2), 112-148.
57. Babbs, C. F., Free radicals and the etiology of colon cancer. *Free radical biology & medicine* **1990**, *8* (2), 191-200.
58. Smith, R. C.; Reed, V. D.; Hill, W. E., Oxidation Of Thiols By Copper(II). *Phosphorus, Sulfur, and Silicon and the Related Elements* **1994**, *90* (1-4), 147-154.
59. Choi, J.; Yoon, N. M., Synthesis of Disulfides by Copper-Catalyzed Disproportionation of Thiols. *The Journal of Organic Chemistry* **1995**, *60* (11), 3266-3267.
60. Marzano, C.; Pellei, M.; Tisato, F.; Santini, C., Copper complexes as anticancer agents. *Anticancer Agents Med Chem* **2009**, *9* (2), 185-211.
61. Sigman, D. S.; Kuwabara, M. D.; Chen, C. H.; Bruice, T. W., Nuclease activity of 1,10-phenanthroline-copper in study of protein-DNA interactions. *Methods Enzymol* **1991**, *208*, 414-33.
62. Dasari, S.; Tchounwou, P. B., Cisplatin in cancer therapy: molecular mechanisms of action. *European journal of pharmacology* **2014**, *0*, 364-378.
63. Dorr, R. T., Bleomycin pharmacology: mechanism of action and resistance, and clinical pharmacokinetics. *Semin Oncol* **1992**, *19* (2 Suppl 5), 3-8.
64. Johnstone, T. C.; Park, G. Y.; Lippard, S. J., Understanding and Improving Platinum Anticancer Drugs – Phenanthriplatin. *Anticancer research* **2014**, *34* (1), 471-476.

65. Santini, C.; Pellei, M.; Gandin, V.; Porchia, M.; Tisato, F.; Marzano, C., Advances in copper complexes as anticancer agents. *Chem Rev* **2014**, *114* (1), 815-62.
66. Cook, H. W.; McMaster, C. R., Chapter 7 Fatty acid desaturation and chain elongation in eukaryotes. In *New Comprehensive Biochemistry*, Elsevier: 2002; Vol. 36, pp 181-204.
67. Dowhan, W.; Bogdanov, M., Chapter 1 Functional roles of lipids in membranes. In *New Comprehensive Biochemistry*, Elsevier: 2002; Vol. 36, pp 1-35.
68. Ferreri, C.; Pierotti, S.; Barbieri, A.; Zambonin, L.; Landi, L.; Rasi, S.; Luisi, P. L.; Barigelletti, F.; Chatgililoglu, C., Comparison of phosphatidylcholine vesicle properties related to geometrical isomerism. *Photochem Photobiol* **2006**, *82* (1), 274-80.
69. Cevc, G., *Phospholipids Handbook*. CRC Press.
70. Roach, C.; Feller, S. E.; Ward, J. A.; Shaikh, S. R.; Zerouga, M.; Stillwell, W., Comparison of cis and trans fatty acid containing phosphatidylcholines on membrane properties. *Biochemistry* **2004**, *43* (20), 6344-51.
71. Ferreri, C.; Samadi, A.; Sassatelli, F.; Landi, L.; Chatgililoglu, C., Regioselective Cis-Trans Isomerization of Arachidonic Double Bonds by Thiyl Radicals: The Influence of Phospholipid Supramolecular Organization. *Journal of the American Chemical Society* **2004**, *126* (4), 1063-1072.
72. Yang, X.; Sheng, W.; Sun, G. Y.; Lee, J. C. M., Effects of fatty acid unsaturation numbers on membrane fluidity and  $\alpha$ -secretase-dependent amyloid precursor protein processing. *Neurochemistry international* **2011**, *58* (3), 321-329.
73. Mihaljevic, B.; Tartaro, I.; Ferreri, C.; Chatgililoglu, C., Linoleic acid peroxidation vs. isomerization: a biomimetic model of free radical reactivity in the presence of thiols. *Org Biomol Chem* **2011**, *9* (9), 3541-8.
74. Heipieper, H. J.; Meinhardt, F.; Segura, A., The cis-trans isomerase of unsaturated fatty acids in *Pseudomonas* and *Vibrio*: biochemistry, molecular biology and physiological function of a unique stress adaptive mechanism. *FEMS Microbiol Lett* **2003**, *229* (1), 1-7.
75. Diefenbach, R.; Heipieper, H.-J.; Keweloh, H., The conversion of cis into trans unsaturated fatty acids in *Pseudomonas putida* P8: evidence for a role in the regulation of membrane fluidity. *Applied Microbiology and Biotechnology* **1992**, *38* (3), 382-387.
76. Ferreri, C.; Chatgililoglu, C., Geometrical trans Lipid Isomers: A New Target for Lipidomics. *ChemBioChem* **2005**, *6* (10), 1722-1734.

77. Chatgililoglu, C.; Ferreri, C.; Lykakis, I. N.; Wardman, P., Trans-fatty acids and radical stress: what are the real culprits? *Bioorg Med Chem* **2006**, *14* (18), 6144-8.
78. Ferreri, C.; Manco, I.; Faraone-Mennella, M. R.; Torreggiani, A.; Tamba, M.; Chatgililoglu, C., A biomimetic model of tandem radical damage involving sulfur-containing proteins and unsaturated lipids. *Chembiochem* **2004**, *5* (12), 1710-2.
79. Gardner, H. W., Oxygen radical chemistry of polyunsaturated fatty acids. *Free Radical Biology and Medicine* **1989**, *7* (1), 65-86.
80. Sprinz, H.; Adhikari, S.; Brede, O., Transformation of phospholipid membranes by thiyl radicals via cis-trans isomerization of fatty acid residues. *Advances in Colloid and Interface Science* **2001**, *89-90*, 313-325.
81. Yorihiro, Y.; Etsuo, N.; Yoshio, K.; Hiroyuki, S., Oxidation of lipids: 7. Oxidation of phosphatidylcholines in homogeneous solution and in water dispersion. *Biochimica et Biophysica Acta (BBA) - Lipids and Lipid Metabolism* **1984**, *795* (2), 332-340.
82. Porter, N. A.; Caldwell, S. E.; Mills, K. A., Mechanisms of free radical oxidation of unsaturated lipids. *Lipids* **1995**, *30* (4), 277-90.
83. Ascherio, A.; Willett, W. C., Health effects of trans fatty acids. *Am J Clin Nutr* **1997**, *66* (4 Suppl), 1006s-1010s.
84. Niki, E.; Yoshida, Y.; Saito, Y.; Noguchi, N., Lipid peroxidation: mechanisms, inhibition, and biological effects. *Biochem Biophys Res Commun* **2005**, *338* (1), 668-76.
85. Gutteridge, J. M. C.; Richmond, R.; Halliwell, B., Oxygen free-radicals and lipid peroxidation: inhibition by the protein caeruloplasmin. *FEBS Letters* **1980**, *112* (2), 269-272.
86. Birben, E.; Sahiner, U. M.; Sackesen, C.; Erzurum, S.; Kalayci, O., Oxidative stress and antioxidant defense. *World Allergy Organ J* **2012**, *5* (1), 9-19.
87. Schoneich, C.; Dillinger, U.; von Bruchhausen, F.; Asmus, K. D., Oxidation of polyunsaturated fatty acids and lipids through thiyl and sulfonyl radicals: reaction kinetics, and influence of oxygen and structure of thiyl radicals. *Arch Biochem Biophys* **1992**, *292* (2), 456-67.
88. D'Aquino, M.; Dunster, C.; Willson, R. L., Vitamin A and glutathione-mediated free radical damage: competing reactions with polyunsaturated fatty acids and vitamin C. *Biochem Biophys Res Commun* **1989**, *161* (3), 1199-203.
89. Shils, M. E., *Modern Nutrition in Health and Disease*. 10th Revised edition ed.; Lippincott Williams and Wilkins: Philadelphia, United States.

90. Wong-ekkabut, J.; Xu, Z.; Triampo, W.; Tang, I. M.; Tieleman, D. P.; Monticelli, L., Effect of Lipid Peroxidation on the Properties of Lipid Bilayers: A Molecular Dynamics Study. *Biophysical Journal* **2007**, *93* (12), 4225-4236.
91. Mylonas, C.; Kouretas, D., Lipid peroxidation and tissue damage. *In Vivo* **1999**, *13* (3), 295-309.
92. Barrera, G., Oxidative stress and lipid peroxidation products in cancer progression and therapy. *ISRN Oncol* **2012**, *2012*, 137289.
93. Strandberg, E.; Tiltak, D.; Ehni, S.; Wadhvani, P.; Ulrich, A. S., Lipid shape is a key factor for membrane interactions of amphipathic helical peptides. *Biochimica et Biophysica Acta (BBA) - Biomembranes* **2012**, *1818* (7), 1764-1776.
94. Deamer, D., The Role of Lipid Membranes in Life's Origin. *Life* **2017**, *7* (1), 5.
95. Yang, K.; Han, X., Lipidomics: Techniques, Applications, and Outcomes Related to Biomedical Sciences. *Trends Biochem Sci* **2016**, *41* (11), 954-969.
96. Zalba, S.; Ten Hagen, T. L., Cell membrane modulation as adjuvant in cancer therapy. *Cancer Treat Rev* **2017**, *52*, 48-57.
97. Chatgililoglu, C.; Ferreri, C.; Masi, A.; Melchiorre, M.; Sansone, A.; Terzidis, M. A.; Torreggiani, A., Free Radicals in Chemical Biology: from Chemical Behavior to Biomarker Development. *Journal of visualized experiments : JoVE* **2013**, (74), 50379.
98. Lipidomic Profiles and Intervention Strategies in Prevention and Diseases. In *Membrane Lipidomics for Personalized Health*.
99. Bangham, A. D.; Hill, M. W.; Miller, N. G. A., Preparation and Use of Liposomes as Models of Biological Membranes. In *Methods in Membrane Biology: Volume 1*, Korn, E. D., Ed. Springer US: Boston, MA, 1974; pp 1-68.
100. Maheux, S.; Frache, G.; Thomann, J. S.; Clément, F.; Penny, C.; Belmonte, T.; Duday, D., Small unilamellar liposomes as a membrane model for cell inactivation by cold atmospheric plasma treatment. *Journal of Physics D: Applied Physics* **2016**, *49* (34), 344001.
101. Breslow, R., Biomimetic chemistry: a frontier at the chemistry/biology interface. *Chemistry & Biology* **1998**, *5* (2), R27-R28.
102. Akbarzadeh, A.; Rezaei-Sadabady, R.; Davaran, S.; Joo, S. W.; Zarghami, N.; Hanifepour, Y.; Samiei, M.; Kouhi, M.; Nejati-Koshki, K., Liposome: classification, preparation, and applications. *Nanoscale Research Letters* **2013**, *8* (1), 102.
103. Martino, C.; deMello, A. J., Droplet-based microfluidics for artificial cell generation: a brief review. *Interface Focus* **2016**, *6* (4), 20160011.

104. Mendez, R.; Banerjee, S., Sonication-Based Basic Protocol for Liposome Synthesis. *Methods in molecular biology (Clifton, N.J.)* **2017**, *1609*, 255-260.
105. Hamilton, R. L., Jr.; Goerke, J.; Guo, L. S.; Williams, M. C.; Havel, R. J., Unilamellar liposomes made with the French pressure cell: a simple preparative and semiquantitative technique. *J Lipid Res* **1980**, *21* (8), 981-92.
106. Costa, A. P.; Xu, X.; Burgess, D. J., Freeze-Anneal-Thaw Cycling of Unilamellar Liposomes: Effect on Encapsulation Efficiency. *Pharmaceutical Research* **2014**, *31* (1), 97-103.
107. Vemuri, S.; Rhodes, C. T., Preparation and characterization of liposomes as therapeutic delivery systems: a review. *Pharm Acta Helv* **1995**, *70* (2), 95-111.
108. Wang, T.; Deng, Y.; Geng, Y.; Gao, Z.; Zou, J.; Wang, Z., Preparation of submicron unilamellar liposomes by freeze-drying double emulsions. *Biochimica et Biophysica Acta (BBA) - Biomembranes* **2006**, *1758* (2), 222-231.
109. Dimov, N.; Kastner, E.; Hussain, M.; Perrie, Y.; Szita, N., Formation and purification of tailored liposomes for drug delivery using a module-based micro continuous-flow system. *Scientific Reports* **2017**, *7* (1), 12045.
110. Ong, S. G. M.; Chitneni, M.; Lee, K. S.; Ming, L. C.; Yuen, K. H., Evaluation of Extrusion Technique for Nanosizing Liposomes. *Pharmaceutics* **2016**, *8* (4), 36.
111. Patil, Y. P.; Jadhav, S., Novel methods for liposome preparation. *Chemistry and Physics of Lipids* **2014**, *177*, 8-18.
112. Sercombe, L.; Veerati, T.; Moheimani, F.; Wu, S. Y.; Sood, A. K.; Hua, S., Advances and Challenges of Liposome Assisted Drug Delivery. *Frontiers in Pharmacology* **2015**, *6*, 286.
113. Lasic, D. D., Novel applications of liposomes. *Trends in Biotechnology* **1998**, *16* (7), 307-321.
114. Chatterjee, S. N.; Agarwal, S., Liposomes as membrane model for study of lipid peroxidation. *Free radical biology & medicine* **1988**, *4* (1), 51-72.
115. Jana, A. K.; Agarwal, S.; Chatterjee, S. N., The Induction of Lipid Peroxidation in Liposomal Membrane by Ultrasound and the Role of Hydroxyl Radicals. *Radiation Research* **1990**, *124* (1), 7-14.
116. Alavi, M.; Karimi, N.; Safaei, M., Application of Various Types of Liposomes in Drug Delivery Systems. *Advanced Pharmaceutical Bulletin* **2017**, *7* (1), 3-9.
117. Maeda, N.; Ikeda, K.; Matsumoto, M.; Namba, Y., Advanced lipid technology. *J Liposome Res* **2017**, *27* (3), 221-227.

118. Daraee, H.; Etemadi, A.; Kouhi, M.; Alimirzalu, S.; Akbarzadeh, A., Application of liposomes in medicine and drug delivery. *Artif Cells Nanomed Biotechnol* **2016**, *44* (1), 381-91.
119. Mishra, G. P.; Bagui, M.; Tamboli, V.; Mitra, A. K., Recent Applications of Liposomes in Ophthalmic Drug Delivery. *Journal of Drug Delivery* **2011**, *2011*, 863734.
120. Slator, C.; Molphy, Z.; McKee, V.; Long, C.; Brown, T.; Kellett, A., Di-copper metallodrugs promote NCI-60 chemotherapy via singlet oxygen and superoxide production with tandem TA/TA and AT/AT oligonucleotide discrimination. *Nucleic Acids Research* **2018**, *46* (6), 2733-2750.
121. Slator, C.; Barron, N.; Howe, O.; Kellett, A., [Cu(o-phthalate)(phenanthroline)] Exhibits Unique Superoxide-Mediated NCI-60 Chemotherapeutic Action through Genomic DNA Damage and Mitochondrial Dysfunction. *ACS Chem Biol* **2016**, *11* (1), 159-71.
122. Molphy, Z.; Slator, C.; Chatgililoglu, C.; Kellett, A., DNA oxidation profiles of copper phenanthrene chemical nucleases. *Front Chem* **2015**, *3*, 28.
123. Chatgililoglu, C.; Ferreri, C.; Guerra, M.; Samadi, A.; Bowry, V. W., The Reaction of Thiyl Radical with Methyl Linoleate: Completing the Picture. *J Am Chem Soc* **2017**, *139* (13), 4704-4714.
124. Ferreri, C.; Costantino, C.; Perrotta, L.; Landi, L.; Mulazzani, Q. G.; Chatgililoglu, C., Cis-Trans Isomerization of Polyunsaturated Fatty Acid Residues in Phospholipids Catalyzed by Thiyl Radicals. *Journal of the American Chemical Society* **2001**, *123* (19), 4459-4468.
125. Lipid Isomerization. In *Encyclopedia of Radicals in Chemistry, Biology and Materials*.
126. Ferreri, C.; Panagiotaki, M.; Chatgililoglu, C., Trans fatty acids in membranes: the free radical path. *Mol Biotechnol* **2007**, *37* (1), 19-25.
127. Maulucci, G.; Cohen, O.; Daniel, B.; Sansone, A.; Petropoulou, P. I.; Filou, S.; Spyridonidis, A.; Pani, G.; De Spirito, M.; Chatgililoglu, C.; Ferreri, C.; Kypreos, K. E.; Sasson, S., Fatty acid-related modulations of membrane fluidity in cells: detection and implications. *Free Radic Res* **2016**, *50* (sup1), S40-s50.
128. Pradenas, G. A.; Paillavil, B. A.; Reyes-Cerpa, S.; Perez-Donoso, J. M.; Vasquez, C. C., Reduction of the monounsaturated fatty acid content of Escherichia coli results in increased resistance to oxidative damage. *Microbiology* **2012**, *158* (Pt 5), 1279-83.

129. Godoy, C. A.; Valiente, M.; Pons, R.; Montalvo, G., Effect of fatty acids on self-assembly of soybean lecithin systems. *Colloids Surf B Biointerfaces* **2015**, *131*, 21-8.
130. Alves, A. C.; Ribeiro, D.; Nunes, C.; Reis, S., Biophysics in cancer: The relevance of drug-membrane interaction studies. *Biochim Biophys Acta* **2016**, *1858* (9), 2231-2244.
131. Beloribi-Djefafli, S.; Vasseur, S.; Guillaumond, F., Lipid metabolic reprogramming in cancer cells. *Oncogenesis* **2016**, *5*, e189.
132. Tremi, I.; Anagnostopoulos, D.; Spyratou, E.; Gkeka, P.; Georgakilas, A. G.; Chatgililoglu, C., Effect of 5-trans Isomer of Arachidonic Acid on Model Liposomal Membranes Studied by a Combined Simulation and Experimental Approach. **2018**, *251* (3), 475-489.
133. De Leo, V.; Ruscigno, S.; Trapani, A.; Di Gioia, S.; Milano, F.; Mandracchia, D.; Comparelli, R.; Castellani, S.; Agostiano, A.; Trapani, G.; Catucci, L.; Conese, M., Preparation of drug-loaded small unilamellar liposomes and evaluation of their potential for the treatment of chronic respiratory diseases. *Int J Pharm* **2018**, *545* (1-2), 378-388.
134. Ichihara, K. i.; Fukubayashi, Y., Preparation of fatty acid methyl esters for gas-liquid chromatography. *Journal of Lipid Research* **2010**, *51* (3), 635-640.
135. Eder, K., Gas chromatographic analysis of fatty acid methyl esters. *Journal of Chromatography B: Biomedical Sciences and Applications* **1995**, *671* (1), 113-131.
136. Funari, S. S.; Barcelo, F.; Escriba, P. V., Effects of oleic acid and its congeners, elaidic and stearic acids, on the structural properties of phosphatidylethanolamine membranes. *J Lipid Res* **2003**, *44* (3), 567-75.
137. Huston, P.; Espenson, J. H.; Bakac, A., Reactions of Thiyl Radicals with Transition-Metal Complexes. *Journal of the American Chemical Society* **1992**, *114* (24), 9510-9516.
138. Chatgililoglu, C.; Ferreri, C.; Ballestri, M.; Mulazzani, Q. G.; Landi, L., cis-trans Isomerization of Monounsaturated Fatty Acid Residues in Phospholipids by Thiyl Radicals. *Journal of the American Chemical Society* **2000**, *122* (19), 4593-4601.
139. Nagy, P., Kinetics and Mechanisms of Thiol-Disulfide Exchange Covering Direct Substitution and Thiol Oxidation-Mediated Pathways. *Antioxidants & Redox Signaling* **2013**, *18* (13), 1623-1641.
140. Chatgililoglu, C.; Ferreri, C.; Melchiorre, M.; Sansone, A.; Torreggiani, A., Lipid geometrical isomerism: from chemistry to biology and diagnostics. *Chem Rev* **2014**, *114* (1), 255-84.

141. Menounou, G.; Giacometti, G.; Scanferlato, R.; Dambruoso, P.; Sansone, A.; Tueros, I.; Amézaga, J.; Chatgialiloglu, C.; Ferreri, C., Trans Lipid Library: Synthesis of Docosahexaenoic Acid (DHA) Monotrans Isomers and Regioisomer Identification in DHA-Containing Supplements. *Chemical research in toxicology* **2018**, *31* (3), 191-200.
142. Siddiqui, R. A.; Harvey, K.; Stillwell, W., Anticancer properties of oxidation products of docosahexaenoic acid. *Chemistry and physics of lipids* **2008**, *153* (1), 47-56.
143. Armitage, B., Photocleavage of Nucleic Acids. *Chemical Reviews* **1998**, *98* (3), 1171-1200.
144. Opinion of the Panel on dietetic products, nutrition and allergies (NDA) on a request from the Commission related to scientific and technical guidance for the preparation and presentation of the application for authorisation of a health claim. *EFSA Journal* **2007**, *5* (7), 530.
145. Sanders, T. A., DHA status of vegetarians. *Prostaglandins Leukot Essent Fatty Acids* **2009**, *81* (2-3), 137-41.
146. Kemény, Z.; Recseg, K.; Hénon, G.; Kövári, K.; Zwobada, F., Deodorization of vegetable oils: Prediction of trans polyunsaturated fatty acid content. *Journal of the American Oil Chemists' Society* **2001**, *78* (9), 973-979.
147. Fournier, V.; Destailats, F.; Hug, B.; Golay, P. A.; Joffre, F.; Juaneda, P.; Semon, E.; Dionisi, F.; Lambelet, P.; Sebedio, J. L.; Berdeaux, O., Quantification of eicosapentaenoic and docosahexaenoic acid geometrical isomers formed during fish oil deodorization by gas-liquid chromatography. *J Chromatogr A* **2007**, *1154* (1-2), 353-9.
148. Sciotto, C.; Mjos, S. A., Trans isomers of EPA and DHA in omega-3 products on the European market. *Lipids* **2012**, *47* (7), 659-67.
149. Liu, X.-R.; Deng, Z.-Y.; Hu, J.-N.; Fan, Y.-W.; Liu, R.; Li, J.; Peng, J.-T.; Su, H.; Peng, Q.; Li, W.-F., Erythrocyte membrane trans-fatty acid index is positively associated with a 10-year CHD risk probability. *British Journal of Nutrition* **2013**, *109* (9), 1695-1703.
150. Anderson, A. K.; McDougald, D. M.; Steiner-Asiedu, M., Dietary trans fatty acid intake and maternal and infant adiposity. *Eur J Clin Nutr* **2010**, *64* (11), 1308-15.
151. Aung, T.; Halsey, J.; Kromhout, D.; Gerstein, H. C.; Marchioli, R.; Tavazzi, L.; Geleijnse, J. M.; Rauch, B.; Ness, A.; Galan, P.; Chew, E. Y.; Bosch, J.; Collins, R.; Lewington, S.; Armitage, J.; Clarke, R., Associations of Omega-3 Fatty Acid Supplement Use With Cardiovascular Disease Risks: Meta-analysis of 10 Trials Involving 77917 Individuals. *JAMA cardiology* **2018**, *3* (3), 225-234.

152. Ethan M Balk, M., MPH, Gaelen P Adam, MLIS, Valerie Langberg, ScM at al., *Omega-3 Fatty Acids and Cardiovascular Disease: An Updated Systematic Review*. Evidence Reports/Technology Assessments Agency for Healthcare Research and Quality (US), 2016 Aug; Vol. No. 223.
153. Bisgaard, H.; Stokholm, J.; Chawes, B. L.; Vissing, N. H.; Bjarnadottir, E.; Schoos, A. M.; Wolsk, H. M.; Pedersen, T. M.; Vinding, R. K.; Thorsteinsdottir, S.; Folsgaard, N. V.; Fink, N. R.; Thorsen, J.; Pedersen, A. G.; Waage, J.; Rasmussen, M. A.; Stark, K. D.; Olsen, S. F.; Bonnelykke, K., Fish Oil-Derived Fatty Acids in Pregnancy and Wheeze and Asthma in Offspring. *The New England journal of medicine* **2016**, *375* (26), 2530-9.
154. Sydne J Newberry, M., PhD, Mei Chung, MPH, PhD, Marika Booth, MS et al., *Omega-3 Fatty Acids and Maternal and Child Health: An Updated Systematic Review*. Evidence Reports/Technology Assessments: Agency for Healthcare Research and Quality (US), 2016 Oct.; Vol. No. 224.
155. Chatgililoglu, C.; Ferreri, C.; Melchiorre, M.; Sansone, A.; Torreggiani, A., Lipid geometrical isomerism: from chemistry to biology and diagnostics. *Chem Review* **2014**, *114* (1), 255-84.
156. Chatgililoglu, C.; Ferreri, C.; Guerra, M.; Samadi, A.; Bowry, V. W., The Reaction of Thiyl Radical with Methyl Linoleate: Completing the Picture. *Journal of the American Chemical Society* **2017**, *139* (13), 4704-4714.
157. Ferreri, C.; Faraone Mennella, M. R.; Formisano, C.; Landi, L.; Chatgililoglu, C., Arachidonate geometrical isomers generated by thiyl radicals: the relationship with trans lipids detected in biological samples. *Free radical biology & medicine* **2002**, *33* (11), 1516-26.
158. Zambonin, L.; Ferreri, C.; Cabrini, L.; Prata, C.; Chatgililoglu, C.; Landi, L., Occurrence of trans fatty acids in rats fed a trans-free diet: a free radical-mediated formation? *Free radical biology & medicine* **2006**, *40* (9), 1549-1556.
159. Ferreri, C.; Kratzsch, S.; Brede, O.; Marciniak, B.; Chatgililoglu, C., Trans lipid formation induced by thiols in human monocytic leukemia cells. *Free radical biology & medicine* **2005**, *38* (9), 1180-7.
160. Souabni, H.; Thoma, V.; Bizouarn, T.; Chatgililoglu, C.; Siafaka-Kapadai, A.; Baciou, L.; Ferreri, C.; Houée-Levin, C.; Ostuni, M. A., trans Arachidonic acid isomers inhibit NADPH-oxidase activity by direct interaction with enzyme components. *Biochimica et Biophysica Acta (BBA) - Biomembranes* **2012**, *1818* (9), 2314-2324.

161. Aoun, M.; Feillet-Coudray, C.; Fouret, G.; Chabi, B.; Crouzier, D.; Ferreri, C.; Chatgililoglu, C.; Wrutniak-Cabello, C.; Cristol, J. P.; Carbonneau, M. A.; Coudray, C., Rat liver mitochondrial membrane characteristics and mitochondrial functions are more profoundly altered by dietary lipid quantity than by dietary lipid quality: effect of different nutritional lipid patterns. *Br J Nutr* **2012**, *107* (5), 647-59.
162. Grandgirard, A.; Piconneaux, A.; Sebedio, J. L.; O'Keefe, S. F.; Semon, E.; Le Quère, J. L., Occurrence of geometrical isomers of eicosapentaenoic and docosahexaenoic acids in liver lipids of rats fed heated linseed oil. *Lipids* **1989**, *24* (9), 799-804.
163. Vendel Nielsen, L.; Krogager, T. P.; Young, C.; Ferreri, C.; Chatgililoglu, C.; Nørregaard Jensen, O.; Enghild, J. J., Effects of Elaidic Acid on Lipid Metabolism in HepG2 Cells, Investigated by an Integrated Approach of Lipidomics, Transcriptomics and Proteomics. *PLoS ONE* **2013**, *8* (9), e74283.
164. Ferreri, C.; Grabovskiy, S. A.; Aoun, M.; Melchiorre, M.; Kabal'nova, N.; Feillet-Coudray, C.; Fouret, G.; Coudray, C.; Chatgililoglu, C., Trans fatty acids: chemical synthesis of eicosapentaenoic acid isomers and detection in rats fed a deodorized fish oil diet. *Chemical research in toxicology* **2012**, *25* (3), 687-94.
165. Vatile, J.-M.; Doan, H. D.; Chardigny, J.-M.; Sébédio, J.-L.; Grandgirard, A., Synthesis of methyl (5Z, 8Z, 11Z, 14Z, 17E)-eicosapentaenoate and methyl (4Z, 7Z, 10Z, 13Z, 16Z, 19E)-docosahexaenoate. *Chemistry and Physics of Lipids* **1994**, *74* (2), 185-193.
166. Mjos, S. A., Properties of trans isomers of eicosapentaenoic acid and docosahexaenoic acid methyl esters on cyanopropyl stationary phases. *J Chromatogr A* **2005**, *1100* (2), 185-92.
167. Mjø, S. A.; Solvang, M., Geometrical isomerisation of eicosapentaenoic and docosahexaenoic acid at high temperatures. *European Journal of Lipid Science and Technology* **2006**, *108* (7), 589-597.
168. VanRollins, M.; Frade, P. D.; Carretero, O. A., Synthesis of epoxide and vicinal diol regioisomers from docosahexaenoate methyl esters. *J Lipid Res* **1989**, *30* (2), 275-86.
169. Jakobsen, M. G.; Vik, A.; Hansen, T. V., Concise syntheses of three  $\omega$ -3 polyunsaturated fatty acids. *Tetrahedron Letters* **2012**, *53* (44), 5837-5839.
170. Lucas, D.; Goulitquer, S.; Marienhagen, J.; Fer, M.; Dreano, Y.; Schwaneberg, U.; Amet, Y.; Corcos, L., Stereoselective epoxidation of the last double bond of polyunsaturated fatty acids by human cytochromes P450. *J Lipid Res* **2010**, *51* (5), 1125-33.

171. Kato, T.; Ishimatu, T.; Aikawa, A.; Taniguchi, K.; Kurahashi, T.; Nakai, T., Preparation of the enantiomers of 19-epoxy docosahexaenoic acids and their 4-hydroxy derivatives. *Tetrahedron: Asymmetry* **2000**, *11* (4), 851-860.
172. Zhang, G.; Kodani, S.; Hammock, B. D., Stabilized epoxygenated fatty acids regulate inflammation, pain, angiogenesis and cancer. *Prog Lipid Res* **2014**, *53*, 108-23.
173. Fer, M.; Dreano, Y.; Lucas, D.; Corcos, L.; Salaun, J. P.; Berthou, F.; Amet, Y., Metabolism of eicosapentaenoic and docosahexaenoic acids by recombinant human cytochromes P450. *Arch Biochem Biophys* **2008**, *471* (2), 116-25.
174. Albert, B. B.; Derraik, J. G.; Cameron-Smith, D.; Hofman, P. L.; Tumanov, S.; Villas-Boas, S. G.; Garg, M. L.; Cutfield, W. S., Fish oil supplements in New Zealand are highly oxidised and do not meet label content of n-3 PUFA. *Sci Rep* **2015**, *5*, 7928.
175. Srigley, C. T.; Rader, J. I., Content and composition of fatty acids in marine oil omega-3 supplements. *J Agric Food Chem* **2014**, *62* (29), 7268-78.
176. Samadi, A.; Andreu, I.; Ferreri, C.; Dellonte, S.; Chatgililoglu, C., Thiol radical-catalyzed isomerization of oils: An entry to the trans lipid library. *Journal of the American Oil Chemists' Society* **2004**, *81* (8), 753-758.
177. Gao, K.; Liang, Q.; Zhao, Z.-H.; Li, Y.-F.; Wang, S.-F., Synergistic anticancer properties of docosahexaenoic acid and 5-fluorouracil through interference with energy metabolism and cell cycle arrest in human gastric cancer cell line AGS cells. *World Journal of Gastroenterology* **2016**, *22* (10), 2971-2980.
178. Siddiqui, R. A.; Harvey, K. A.; Xu, Z.; Bammerlin, E. M.; Walker, C.; Altenburg, J. D., Docosahexaenoic acid: a natural powerful adjuvant that improves efficacy for anticancer treatment with no adverse effects. *BioFactors (Oxford, England)* **2011**, *37* (6), 399-412.
179. D'Eliseo, D.; Velotti, F., Omega-3 Fatty Acids and Cancer Cell Cytotoxicity: Implications for Multi-Targeted Cancer Therapy. *Journal of Clinical Medicine* **2016**, *5* (2), 15.
180. Park, M.; Kim, H., Anti-cancer Mechanism of Docosahexaenoic Acid in Pancreatic Carcinogenesis: A Mini-review. *Journal of Cancer Prevention* **2017**, *22* (1), 1-5.
181. Merendino, N.; Costantini, L.; Manzi, L.; Molinari, R.; D'Eliseo, D.; Velotti, F., Dietary n-3 Polyunsaturated Fatty Acid DHA: A Potential Adjuvant in the Treatment of Cancer. *BioMed Research International* **2013**, *2013*, 11.

182. de Aguiar Pastore Silva, J.; Emilia de Souza Fabre, M.; Waitzberg, D. L., Omega-3 supplements for patients in chemotherapy and/or radiotherapy: A systematic review. *Clinical nutrition (Edinburgh, Scotland)* **2015**, *34* (3), 359-66.
183. Morland, S. L.; Martins, K. J. B.; Mazurak, V. C., n-3 polyunsaturated fatty acid supplementation during cancer chemotherapy. *Journal of Nutrition & Intermediary Metabolism* **2016**, *5*, 107-116.
184. Newell, M.; Baker, K.; Postovit, L. M.; Field, C. J., A Critical Review on the Effect of Docosahexaenoic Acid (DHA) on Cancer Cell Cycle Progression. *International Journal of Molecular Sciences* **2017**, *18* (8), 1784.
185. Ng, Y.; Barhoumi, R.; B.Tjalkens, R.; Fan, Y.-Y.; Kolar, S.; Wang, N.; R.Lupton, J.; S.Chapkin, R., The role of docosahexaenoic acid in mediating mitochondrial membrane lipid oxidation and apoptosis in colonocytes. *Carcinogenesis* **2005**, *26* (11), 1914-1921.
186. Hawkins, R. A.; Sangster, K.; Arends, M. J., Apoptotic death of pancreatic cancer cells induced by polyunsaturated fatty acids varies with double bond number and involves an oxidative mechanism. *The Journal of pathology* **1998**, *185* (1), 61-70.
187. Folch, J.; Lees, M.; Sloane Stanley, G. H., A simple method for the isolation and purification of total lipides from animal tissues. *The Journal of biological chemistry* **1957**, *226* (1), 497-509.
188. Dais, P.; Misiak, M.; Hatzakis, E., Analysis of marine dietary supplements using NMR spectroscopy. *Analytical Methods* **2015**, *7* (12), 5226-5238.
189. Siddiqui, N.; Sim, J.; Silwood, C.; Toms, H.; A. Iles, R.; Grootveld, M., *Multicomponent analysis of encapsulated marine oil supplements using high-resolution 1 H and*. 2018.
190. Knothe, G.; Kenar, J. A., Determination of the fatty acid profile by 1H-NMR spectroscopy. *European Journal of Lipid Science and Technology* **2004**, *106* (2), 88-96.
191. Alexandri, E.; Ahmed, R.; Siddiqui, H.; Choudhary, M. I.; Tsiafoulis, C. G.; Gerothanassis, I. P., High Resolution NMR Spectroscopy as a Structural and Analytical Tool for Unsaturated Lipids in Solution. *Molecules* **2017**, *22* (10).
192. Ferreri, C.; Pierotti, S.; Barbieri, A.; Zamboni, L.; Landi, L.; Rasl, S.; Luisi, P. L.; Barigelletti, F.; Chatgililoglu, C., Comparison of Phosphatidylcholine Vesicle Properties Related to Geometrical Isomerism†. *Photochemistry and photobiology* **2006**, *82* (1), 274-280.

193. Chatgialiloglu, C.; Ferreri, C.; Lykakis, I. N.; Mihaljević, B., Biomimetic Thiyl Radical Chemistry by  $\gamma$ -Irradiation of Micelles and Vesicles Containing Unsaturated Fatty Acids. *Israel Journal of Chemistry* **2014**, *54* (3), 242-247.
194. Soubias, O.; Gawrisch, K., Docosahexaenoyl Chains Isomerize on the Sub-Nanosecond Time Scale. *Journal of the American Chemical Society* **2007**, *129* (21), 6678-6679.
195. Sherratt, S. C. R.; Mason, R. P., Eicosapentaenoic acid and docosahexaenoic acid have distinct membrane locations and lipid interactions as determined by X-ray diffraction. *Chemistry and Physics of Lipids* **2018**, *212*, 73-79.
196. Liu, H. K.; Sadler, P. J., Metal complexes as DNA intercalators. *Accounts of chemical research* **2011**, *44* (5), 349-59.
197. Lerman, L. S., Structural considerations in the interaction of DNA and acridines. *J Mol Biol* **1961**, *3*, 18-30.
198. Luzzati, V.; Masson, F.; Lerman, L. S., Interaction of DNA and proflavine: A small-angle X-ray scattering study. *Journal of Molecular Biology* **1961**, *3* (5), 634-639.
199. Lerman, L. S., THE STRUCTURE OF THE DNA-ACRIDINE COMPLEX. *Proceedings of the National Academy of Sciences of the United States of America* **1963**, *49* (1), 94-102.
200. K.R, S. G.; Mathew, B. B.; Sudhamani, C. N.; Naik, H. S. B., Mechanism of DNA Binding and Cleavage. *Biomedicine and Biotechnology* **2014**, *2* (1), 1-9.
201. Brana, M. F.; Cacho, M.; Gradillas, A.; de Pascual-Teresa, B.; Ramos, A., Intercalators as anticancer drugs. *Current pharmaceutical design* **2001**, *7* (17), 1745-80.
202. Baguley, B. C.; Wakelin, L. P.; Jacintho, J. D.; Kovacic, P., Mechanisms of action of DNA intercalating acridine-based drugs: how important are contributions from electron transfer and oxidative stress? *Current medicinal chemistry* **2003**, *10* (24), 2643-9.
203. Giese, B., Long-distance electron transfer through DNA. *Annual review of biochemistry* **2002**, *71*, 51-70.
204. Conwell, E. M.; Basko, D. M., Hole traps in DNA. *J Am Chem Soc* **2001**, *123* (46), 11441-5.
205. Prasher, P.; Sharma, M., Medicinal Chemistry of Acridine and its Analogues. *MedChemComm* **2018**.
206. Mancin, F.; Scrimin, P.; Tecilla, P., Progress in artificial metallonucleases. *Chemical Communications* **2012**, *48* (45), 5545-5559.

207. Chen, J.; Stubbe, J., Bleomycins: towards better therapeutics. *Nature reviews. Cancer* **2005**, *5* (2), 102-12.
208. Pitié, M.; Pratviel, G., Activation of DNA Carbon–Hydrogen Bonds by Metal Complexes. *Chemical Reviews* **2010**, *110* (2), 1018-1059.
209. Larragy, R.; Fitzgerald, J.; Prisecaru, A.; McKee, V.; Leonard, P.; Kellett, A., Protein engineering with artificial chemical nucleases. *Chemical Communications* **2015**, *51* (65), 12908-12911.
210. Komor, A. C.; Barton, J. K., The path for metal complexes to a DNA target. *Chemical Communications* **2013**, *49* (35), 3617-3630.
211. McC. Howell, J. G., J. M., *Copper in Animals and Man*. CRC Press: 1987; Vol. 1.
212. Boal, A. K.; Rosenzweig, A. C., Structural biology of copper trafficking. *Chem Rev* **2009**, *109* (10), 4760-79.
213. Cowan, J. A., Metal Activation of Enzymes in Nucleic Acid Biochemistry. *Chemical Reviews* **1998**, *98* (3), 1067-1088.
214. Cowan, J. A., Chemical nucleases. *Current opinion in chemical biology* **2001**, *5* (6), 634-42.
215. Yu, Z.; Han, M.; Cowan, J. A., Toward the Design of a Catalytic Metallodrug: Selective Cleavage of G-Quadruplex Telomeric DNA by an Anticancer Copper–Acridine–ATCUN Complex(). *Angewandte Chemie (International ed. in English)* **2015**, *54* (6), 1901-1905.
216. Sigman, D. S.; Graham, D. R.; D'Aurora, V.; Stern, A. M., Oxygen-dependent cleavage of DNA by the 1,10-phenanthroline . cuprous complex. Inhibition of Escherichia coli DNA polymerase I. *The Journal of biological chemistry* **1979**, *254* (24), 12269-72.
217. Chen, T.; Greenberg, M. M., Model Studies Indicate That Copper Phenanthroline Induces Direct Strand Breaks via  $\beta$ -Elimination of the 2'-Deoxyribonolactone Intermediate Observed in Eneidyne Mediated DNA Damage. *Journal of the American Chemical Society* **1998**, *120* (15), 3815-3816.
218. Sigman, D. S., Chemical nucleases. *Biochemistry* **1990**, *29* (39), 9097-9105.
219. Bales, B. C.; Pitié, M.; Meunier, B.; Greenberg, M. M., A Minor Groove Binding Copper-Phenanthroline Conjugate Produces Direct Strand Breaks via  $\beta$ -Elimination of 2-Deoxyribonolactone. *Journal of the American Chemical Society* **2002**, *124* (31), 9062-9063.

220. Bales, B. C.; Kodama, T.; Weledji, Y. N.; Pitié, M.; Meunier, B.; Greenberg, M. M., Mechanistic studies on DNA damage by minor groove binding copper–phenanthroline conjugates. *Nucleic Acids Research* **2005**, *33* (16), 5371-5379.
221. Molphy, Z.; Prisecaru, A.; Slator, C.; Barron, N.; McCann, M.; Colleran, J.; Chandran, D.; Gathergood, N.; Kellett, A., Copper phenanthrene oxidative chemical nucleases. *Inorganic chemistry* **2014**, *53* (10), 5392-404.
222. Molphy, Z.; Slator, C.; Chatgililoglu, C.; Kellett, A., DNA oxidation profiles of copper phenanthrene chemical nucleases. *Frontiers in Chemistry* **2015**, *3*, 28.
223. *Radiation-Induced and Oxidative DNA Damages* Frontiers in Chemistry 2015.
224. Chatgililoglu, C.; Ferreri, C.; Masi, A.; Melchiorre, M.; Sansone, A.; Terzidis, M. A.; Torreggiani, A., Free radicals in chemical biology: from chemical behavior to biomarker development. *Journal of visualized experiments : JoVE* **2013**, (74).
225. Dizdaroglu, M.; Jaruga, P., Mechanisms of free radical-induced damage to DNA. *Free Radical Research* **2012**, *46* (4), 382-419.
226. Khan, I.; Suhasini, A. N.; Banerjee, T.; Sommers, J. A.; Kaplan, D. L.; Kuper, J.; Kisker, C.; Brosh, R. M., Jr., Impact of Age-Associated Cyclopurine Lesions on DNA Repair Helicases. *PLOS ONE* **2014**, *9* (11), e113293.
227. Kropachev, K.; Ding, S.; Terzidis, M. A.; Masi, A.; Liu, Z.; Cai, Y.; Kolbanovskiy, M.; Chatgililoglu, C.; Broyde, S.; Geacintov, N. E.; Shafirovich, V., Structural basis for the recognition of diastereomeric 5',8-cyclo-2'-deoxypurine lesions by the human nucleotide excision repair system. *Nucleic Acids Research* **2014**, *42* (8), 5020-5032.
228. Brooks, P. J., The cyclopurine deoxynucleosides: DNA repair, biological effects, mechanistic insights, and unanswered questions. *Free radical biology & medicine* **2017**, *107*, 90-100.
229. Terzidis, M. A.; Chatgililoglu, C., An ameliorative protocol for the quantification of purine 5',8-cyclo-2'-deoxynucleosides in oxidized DNA. *Frontiers in Chemistry* **2015**, *3*, 47.
230. Krokidis, M. G.; Terzidis, M. A.; Efthimiadou, E.; Zervou, S.-K.; Kordas, G.; Papadopoulos, K.; Hiskia, A.; Kletsas, D.; Chatgililoglu, C., Purine 5',8-cyclo-2'-deoxynucleoside lesions: formation by radical stress and repair in human breast epithelial cancer cells. *Free Radical Research* **2017**, *51* (5), 470-482.

231. Jaruga, P.; Dizdaroglu, M., 8,5'-Cyclopurine-2'-deoxynucleosides in DNA: Mechanisms of formation, measurement, repair and biological effects. *DNA Repair* **2008**, 7 (9), 1413-1425.
232. (a) Haghdoost, S.; Czene, S.; Naslund, I.; Skog, S.; Harms-Ringdahl, M., Extracellular 8-oxo-dG as a sensitive parameter for oxidative stress in vivo and in vitro. *Free Radic Res* **2005**, 39 (2), 153-62; (b) Roszkowski, K.; Jozwicki, W.; Blaszczyk, P.; Mucha-Malecka, A.; Siomek, A., Oxidative damage DNA: 8-oxoGua and 8-oxodG as molecular markers of cancer. *Medical science monitor : international medical journal of experimental and clinical research* **2011**, 17 (6), Cr329-33.
233. (a) Wang, D.; Kreutzer, D. A.; Essigmann, J. M., Mutagenicity and repair of oxidative DNA damage: insights from studies using defined lesions. *Mutation Research/Fundamental and Molecular Mechanisms of Mutagenesis* **1998**, 400 (1), 99-115; (b) Krokidis, M. G.; Terzidis, M. A., Purine 5',8-cyclo-2'-deoxynucleoside lesions: formation by radical stress and repair in human breast epithelial cancer cells. **2017**, 51 (5), 470-482.
234. Slator, C.; Molphy, Z.; McKee, V.; Long, C.; Brown, T.; Kellett, A., Di-copper metallodrugs promote NCI-60 chemotherapy via singlet oxygen and superoxide production with tandem TA/TA and AT/AT oligonucleotide discrimination. *Nucleic Acids Res* **2018**, 46 (6), 2733-2750.
235. Terzidis, M. A.; Ferreri, C.; Chatgialloglu, C., Radiation-induced formation of purine lesions in single and double stranded DNA: revised quantification. *Front Chem* **2015**, 3, 18.
236. Terzidis, M. A.; Prisecaru, A.; Molphy, Z.; Barron, N.; Randazzo, A.; Dumont, E.; Krokidis, M. G.; Kellett, A.; Chatgialloglu, C., Radical-induced purine lesion formation is dependent on DNA helical topology. *Free Radic Res* **2016**, 50 (sup1), S91-s101.
237. Nitiss, J. L.; Soans, E.; Rogojina, A.; Seth, A.; Mishina, M., Topoisomerase Assays. *Current Protocols in Pharmacology* **2012**, CHAPTER, Unit3.3-Unit3.3.
238. Tabassum, S.; Al-Asbahy, W. M.; Afzal, M.; Arjmand, F.; Bagchi, V., Molecular drug design, synthesis and structure elucidation of a new specific target peptide based metallo drug for cancer chemotherapy as topoisomerase I inhibitor. *Dalton transactions (Cambridge, England : 2003)* **2012**, 41 (16), 4955-64.
239. Zhou, W.; Wang, X.; Hu, M.; Zhu, C.; Guo, Z., A mitochondrion-targeting copper complex exhibits potent cytotoxicity against cisplatin-resistant tumor cells through multiple mechanisms of action. *Chemical Science* **2014**, 5 (7), 2761-2770.

240. Molphy, Z.; Slator, C.; Chatgililoglu, C.; Kellett, A., DNA oxidation profiles of copper phenanthrene chemical nucleases. *Frontiers in Chemistry* **2015**, *3* (28).
241. Terzidis, M. A.; Prisecaru, A.; Molphy, Z.; Barron, N.; Randazzo, A.; Dumont, E.; Krokidis, M. G.; Kellett, A.; Chatgililoglu, C., Radical-induced purine lesion formation is dependent on DNA helical topology. *Free Radical Research* **2016**, *50* (sup1), S91-S101.
242. Slator, C.; Molphy, Z.; McKee, V.; Kellett, A., Triggering autophagic cell death with a di-manganese(II) developmental therapeutic. *Redox biology* **2017**, *12*, 150-161.
243. Peixoto, P.; Bailly, C.; David-Cordonnier, M. H., Topoisomerase I-mediated DNA relaxation as a tool to study intercalation of small molecules into supercoiled DNA. *Methods in molecular biology (Clifton, N.J.)* **2010**, *613*, 235-56.
244. *Drug-DNA Interaction Protocols* Second ed.; Humana Press: 2010; p IX, 311.
245. Hatahet, Z.; Kow, Y. W.; Purmal, A. A.; Cunningham, R. P.; Wallace, S. S., New substrates for old enzymes. 5-Hydroxy-2'-deoxycytidine and 5-hydroxy-2'-deoxyuridine are substrates for Escherichia coli endonuclease III and formamidopyrimidine DNA N-glycosylase, while 5-hydroxy-2'-deoxyuridine is a substrate for uracil DNA N-glycosylase. *The Journal of biological chemistry* **1994**, *269* (29), 18814-20.
246. Keller, W., Determination of the number of superhelical turns in simian virus 40 DNA by gel electrophoresis. *Proceedings of the National Academy of Sciences of the United States of America* **1975**, *72* (12), 4876-80.
247. Webb, M. R.; Ebeler, S. E., A gel electrophoresis assay for the simultaneous determination of topoisomerase I inhibition and DNA intercalation. *Analytical biochemistry* **2003**, *321* (1), 22-30.
248. Hadi, S. M.; Ullah, M. F.; Shamim, U.; Bhatt, S. H.; Azmi, A. S., Catalytic Therapy of Cancer by Ascorbic Acid Involves Redox Cycling of Exogenous/Endogenous Copper Ions and Generation of Reactive Oxygen Species. *Chemotherapy* **2010**, *56* (4), 280-284.
249. Chiou, S. H.; Chang, W. C.; Jou, Y. S.; Chung, H. M.; Lo, T. B., Specific cleavages of DNA by ascorbate in the presence of copper ion or copper chelates. *Journal of biochemistry* **1985**, *98* (6), 1723-6.
250. Kazakov, S. A.; Astashkina, T. G.; Mamaev, S. V.; Vlassov, V. V., Site-specific cleavage of single-stranded DNAs at unique sites by a copper-dependent redox reaction. *Nature* **1988**, *335* (6186), 186-8.

251. Galindo-Murillo, R.; García-Ramos, J. C.; Ruiz-Azuara, L.; Cheatham, I. I. I. T. E.; Cortés-Guzmán, F., Intercalation processes of copper complexes in DNA. *Nucleic Acids Research* **2015**, *43* (11), 5364-5376.
252. Lindahl, T., Instability and decay of the primary structure of DNA. *Nature* **1993**, *362*, 709.
253. Tchou, J.; Bodepudi, V.; Shibutani, S.; Antoshechkin, I.; Miller, J.; Grollman, A. P.; Johnson, F., Substrate specificity of Fpg protein. Recognition and cleavage of oxidatively damaged DNA. *The Journal of biological chemistry* **1994**, *269* (21), 15318-24.
254. Dizdaroglu, M.; Laval, J.; Boiteux, S., Substrate specificity of the Escherichia coli endonuclease III: Excision of thymine- and cytosine-derived lesions in DNA produced by radiation-generated free radicals. *Biochemistry* **1993**, *32* (45), 12105-12111.
255. Abner, C. W.; Lau, A. Y.; Ellenberger, T.; Bloom, L. B., Base Excision and DNA Binding Activities of Human Alkyladenine DNA Glycosylase Are Sensitive to the Base Paired with a Lesion. *Journal of Biological Chemistry* **2001**, *276* (16), 13379-13387.
256. Levin, J. D.; Johnson, A. W.; Demple, B., Homogeneous Escherichia coli endonuclease IV. Characterization of an enzyme that recognizes oxidative damage in DNA. *Journal of Biological Chemistry* **1988**, *263* (17), 8066-71.
257. Yao, M.; Hatahet, Z.; Melamed, R.; Kow, Y. W., *Purification and characterization of a novel deoxyinosine-specific enzyme, deoxyinosine 3' endonuclease, from Escherichia coli*. 1994; Vol. 269, p 16260-8.
258. Yao, M.; Kow, Y. W., Strand-specific cleavage of mismatch-containing DNA by deoxyinosine 3'-endonuclease from Escherichia coli. *Journal of Biological Chemistry* **1994**, *269* (50), 31390-6.
259. Yao, M.; Kow, Y. W., Cleavage of Insertion/Deletion Mismatches, Flap and Pseudo-Y DNA Structures by Deoxyinosine 3'-Endonuclease from Escherichia coli. *Journal of Biological Chemistry* **1996**, *271* (48), 30672-30676.
260. Yao, M.; Kow, Y. W., Further Characterization of Escherichia coli Endonuclease V: MECHANISM OF RECOGNITION FOR DEOXYINOSINE, DEOXYURIDINE, AND BASE MISMATCHES IN DNA. *Journal of Biological Chemistry* **1997**, *272* (49), 30774-30779.
261. Dianov, G.; Lindahl, T., Preferential recognition of I.T base-pairs in the initiation of excision-repair by hypoxanthine-DNA glycosylase. *Nucleic Acids Research* **1991**, *19* (14), 3829-3833.

262. Fantoni, N.; Lauria, T.; Kellett, A., *Genome Engineering with Synthetic Copper Nucleases*. 2015; Vol. 26.
263. Keane, P. M.; Hall, J. P.; Poynton, F. E.; Poulsen, B. C.; Gurung, S. P.; Clark, I. P.; Sazanovich, I. V.; Towrie, M.; Gunnlaugsson, T.; Quinn, S. J.; Cardin, C. J.; Kelly, J. M., Inosine Can Increase DNA's Susceptibility to Photo-oxidation by a RuII Complex due to Structural Change in the Minor Groove. *Chemistry – A European Journal* **2017**, *23* (43), 10344-10351.
264. Cadet, J.; Wagner, J. R., DNA base damage by reactive oxygen species, oxidizing agents, and UV radiation. *Cold Spring Harbor perspectives in biology* **2013**, *5* (2).
265. Bhattacharjee, S.; Deterding, L. J.; Chatterjee, S.; Jiang, J.; Ehrenshaft, M.; Lardinois, O.; Ramirez, D. C.; Tomer, K. B.; Mason, R. P., Site-specific radical formation in DNA induced by Cu(II)-H<sub>2</sub>O<sub>2</sub> oxidizing system, using ESR, immuno-spin trapping, LC-MS, and MS/MS. *Free radical biology & medicine* **2011**, *50* (11), 1536-45.
266. Loschen, G.; Azzi, A.; Richter, C.; Flohe, L., Superoxide radicals as precursors of mitochondrial hydrogen peroxide. *FEBS Lett* **1974**, *42* (1), 68-72.
267. Robert, C.; Rassool, F. V., Chapter Three - HDAC Inhibitors: Roles of DNA Damage and Repair. In *Advances in Cancer Research*, Grant, S., Ed. Academic Press: 2012; Vol. 116, pp 87-129.

## Acknowledgements

*Oscar Wilde once wrote*

*“There are only two tragedies in life: one is not getting what one wants, and the other is getting it.”*

*Inspired by this quote I always believed that there can be two tragedies in the life of a chemist; one is the experimental strategy not to work and the other is...to work! A strategy that works as planned can teach nothing, after all chemistry cannot be designed in papers and no doubt that it cannot be predicted. If that was the case then chemists would not need benches, but offices...not pipettes but pencils! That is exactly the beauty of chemistry that every experiment has a story to tell and all we have to do is be careful and respectful enough to listen...there is no greater joy than an experiment that leads to an ‘undesirable’ and an ‘unexpected’ result, in this way new questions arise and new pathways must be considered. The greatest blessing for a chemist is that during his experimental adventures he is not alone, on the contrary is a member of a group with ultimate goal to help and support each other. In my case I had the luck to become part of the ‘Bio Free Radicals’ Group at the National Council of Research in Bologna. I have no words to thank the group leaders Dr. Carla Ferreri and especially Dr. Chrissyostomos Chatgililoglu for the opportunity to join their group, the valuable advices and all the thoughtful discussions when experimental difficulties arose. I am particularly grateful to Professor Marinella Roberti for the guidance all these years, as well as on organizing the thesis. I would like to offer my special thanks to Dr. Annalisa Masi and Dr. Marios Krokidis. It was a pleasure collaborating with them and an educative experience I will never forget.*

*My sincere thanks also goes Dr. Andrew Kellett in Dublin City University, who provided me the opportunity to join his group during my secondment giving me access to his laboratory and to his projects. In his group I had the chance to be guided by Dr. Zara Molphy and Dr. Creina Slator. I am not sure if I am more grateful for all the knowledge, the access to new techniques, the sharing of their experience, the support and the time*

*these two young ladies dedicated on me or for the fact that I made two true friends that I will never forget. I am also grateful to Nicolo Fantoni for synthesizing and sharing the novel metallodrugs that were used in my studies.*

*I would like to thank my fellow labmates Maria Louka and Gianluca Toniolo for the stimulating discussions, the help, the support and most of all for all the sleepless nights sharing our thoughts and troubles. As Dr. Carla Ferreri used to say 'our group is international' and during these three years of hard work I had the unique opportunity to collaborate inside the lab and make friends people from all over the world. I hold a special place in my heart for Dr. Antonia Malenou, Dr. Tadhg Mcgivern, Giuseppe Avella, Vasilis Tsopanakis, Mohammed Fanokh, Aysegul Hanikoglu, Rebecca Anderson, Francesco Mastro and Anna Vita Larocca.*

*It would not feel right to not acknowledge the people who taught me what chemistry is in my earliest steps, what working on a chemical bench is, how to be part of a lab family and what respecting and loving your science truly means. I am referring to all my dear Professors from the University of Crete. Particularly, I always think of Professor Haralambos Katerinopoulos as my mentor in the beauty of synthetic organic chemistry and there are not enough words to express my gratitude for the education he provided me with, or to express what an inspiration he has been for me ever since.*

*In the pathway that a scientist follows apart from the difficulties on the research and his quest to balance things in the laboratory, it is absolutely necessary to balance his own life. In my case that would have been impossible without the support of my family, my beloved parents Maria Maravelaki and Marinos Menounos. I am truly grateful for the support, the guidance, the advices, the ethos, the honesty, the respect and all the moral values they nourished me with. I am also grateful because in this journey of PhD and specifically in the 'ClickGene Family' I met the love of my life Stefano Croce, who was always patient and supportive with me. Stefano was always there to hear my complaints and tolerate my difficult behavior due to stressful periods and honestly I do not know if I would have managed to achieve my goal without his unconditional love.*

*In addition, I would like to thank my family, maybe not by blood but definitely at heart, Sophia Sarpaki, Eirini Ieridou, Nikos Tsakiris and Thomas Themelis for hearing my thoughts, fears and feelings as well as for their support and love.*

*Last but not least, a very special gratitude goes out to Marie Skłodowska-Curie Innovative Training Network (ITN) ClickGene [H2020-MSCA-ITN-2014-642023] for providing the funding for my PhD.*